BEHAVIOR OF AXIALLY LOADED DRILLED SHAFTS IN BEAUMONT CLAY

PART TWO - SITE INVESTIGATION AND TEST SHAFT INSTRUMENTATION

BY

Michael W. O'Neill
Lymon C. Reese

Research Report Number 89-8

Soil Properties as Related to Load Transfer
Characteristics of Drilled Shafts

Research Project 3-5-65-89

conducted for

The Texas Highway Department

in cooperation with the
U. S. Department of Transportation
Federal Highway Administration

by the

CENTER FOR HIGHWAY RESEARCH
THE UNIVERSITY OF TEXAS AT AUSTIN

December, 1970

The opinions, findings, and conclusions expressed in this publication are those of the authors and not necessarily those of the Federal Highway Administration.

PREFACE

This report is the eighth in a series of reports from Research Project 3-5-65-89 of the Cooperative Highway Research Program. The principal aim of the report is to describe the results of axial load tests of full-scale, instrumented drilled shafts in the Beaumont Clay formation in Houston, Texas. The tests were conducted to measure side and base stresses in cylindrical and underreamed shafts, constructed by both wet and dry procedures. The distribution of shear stresses along the sides of the shafts was measured to provide an insight into the mechanism affecting the load transfer behavior of drilled shafts in clay. Maximum side shear stresses and base capacities have been correlated with the undrained shear strength of the soil as indicated by laboratory procedures and with results of Texas Highway Department cone penetration tests.

The report is issued in five separately bound parts:

Part One - "State of the Art" describes the historical development of drilled shafts, describes construction procedures, presents the mechanics of shaft behavior, outlines current methods of design, and presents a summary of the results of field tests reported in the technical literature.

Part Two - "Site Investigation and Test Shaft Instrumentation" gives details of the geotechnical investigation of the test site, describes the test shafts and anchorage systems, describes the various instrumentation

systems, and presents results of monitoring the instrumentation under no-load conditions.

Part Three - "Field Tests" describes the field test procedures and presents the detailed results of the tests.

Part Four - "Design Influences and Conclusions" presents criteria, obtained through the field tests and from the literature review, for designing drilled shafts in Beaumont Clay.

Part Five - "Appendices" gives supporting data and details not contained in the main body of Parts One through Four.

It is not intended that the reader read the entire report in order to obtain information on any particular subject. The report was separated into the various Parts, any of which can be consulted for specific details, for this reason. It is expected that most readers will desire to consult only Part Four, which briefly summarizes Parts One through Three, and then consicely presents design criteria for axially loaded drilled shafts in Beaumont Clay. The Chapters are numbered continuously from Part One through Part Five. Although some cross-referencing exists, the various Parts are written to be as independent as possible. The reference list is contained in Part Four.

This report is the manifestation of the efforts of many individuals. The technical contributions of Dr. Walter R. Barker, Mr. Harold H. Dalrymple, Mr. James N. Anagnos, Mr. Frederick E. Koch, and Mr. Olen L. Hudson merit special recognition. Mr. James Holmes skillfully made the drawings. Miss Mary Kern proficiently prepared the final copy. Thanks

are also due to Miss Pamela Terwelp, Miss Cheryl Johnson, and Mrs. Eddie B. Hudepohl for their assistance in preparing the report. The authors also acknowledge the valuable assistance and advice given by Mr. Horace Hoy, Mr. H. D. Butler, and Mr. Gaston Berthelot, all of the Texas Highway Department, and by the maintenance personnel of District 12.

Michael W. O'Neill

Lymon C. Reese

December 1970

LIST OF REPORTS

Report No. 89-1, "Field Testing of Drilled Shafts to Develop Design Methods," by Lymon C. Reese and W. Ronald Hudson, describes the overall approach to the design of drilled shafts based on a series of field and laboratory investigations.

Report No. 89-2, "Measurements of Lateral Earth Pressure in Drilled Shafts," by Lymon C. Reese, J. Crozier Brown, and H. H. Dalrymple, describes the development and evaluation of pressure gages to measure lateral-earth pressures on the drilled shaft.

Report No. 89-3, "Studies of Shearing Resistance Between Cement Mortar and Soil," by John W. Chuang and Lymon C. Reese, describes the overall approach to the design of drilled shafts based on field and laboratory investigations.

Report No. 89-4, "The Nuclear Method of Soil-Moisture Determination at Depth," by Clarence J. Ehlers, Lymon C. Reese, and James N. Anagnos, describes the use of nuclear equipment for measuring the variations of moisture content at the drilled shaft test sites.

Report No. 89-5, "Load Distribution for a Drilled Shaft in Clay Shale," by Vasant N. Vijayvergiya, W. Ronald Hudson, and Lymon C. Reese, describes the development of instrumentation capable of measuring axial load distribution along a drilled shaft, the development, with the aid of full-scale load testing, of a technique of analysis of observed data, and the correlation of observed data with the Texas Highway Department cone penetration test.

Report No. 89-6, "Instrumentation for Measurement of Axial Load In Drilled Shafts," by Walter R. Barker and Lymon C. Reese, describes the development and performance of various instrumentation systems used to measure the axial load distribution in field tests of full-scale drilled shafts.

Report No. 89-7, "The Determination of Soil Properties In Situ," by David B. Campbell and W. Ronald Hudson, describes the use of the Menard Pressuremeter, the Texas Highway Department cone penetrometer, and The University of Texas in situ device in estimating soil properties in situ and estimating load transfer values obtained from drilled shaft tests.

Report No. 89-8, "Behavior of Axially Loaded Drilled Shafts in Beaumont Clay," by Michael W. O'Neill and Lymon C. Reese, describes the results of axial load tests of instrumented drilled shafts having varying geometry and differing methods of installation and presents a tentative design procedure for drilled shafts in Beaumont Clay.

ABSTRACT

A drilled shaft is a foundation element formed by boring a cylindrical hole into the soil and backfilling the hole with concrete. The recent increase in the utilization of drilled shafts as foundations for major structures has created a need for systematic investigations of their behavior. One such investigation, in which four full-sized drilled shafts of varying geometries were loaded axially to failure, was conducted at a site in the stiff, fissured Beaumont Clay in Houston, Texas. The test shafts were constructed by both wet and dry procedures. They were fully instrumented for measurement of the distribution of axial load, thereby permitting a calculation of the distribution of developed side resistance and of base resistance.

Prior to and during the field tests, a careful site investigation was conducted, and a shear strength profile was developed based on unconsolidated, undrained triaxial test results and Texas Highway Department cone penetrometer soundings. The maximum side shear stresses developed during the load tests were compared to the shear strength profile and penetrometer results in order to arrive at shear strength reduction factors that could be relied upon in predicting design values for side friction.

The side shear stresses were observed to vary considerably from the tops of the shafts to the bottoms, generally being quite small at both ends. Overall, the shafts that were installed in dry boreholes developed an average maximum side shear stress of about one-half of the shear

strength of the clay. The single shaft installed in a processed borehole developed an average of only about one-third of the shear strength of the clay along its sides.

The load measurements indicated that bearing capacity equations used for ultimate base resistance for piles in clay were valid for both belled and cylindrical test shafts.

After the tests were completed, soil adjacent to the walls of three of the shafts was sampled in an attempt to determine the nature of the mechanism of shear strength reduction in soil immediately adjacent to the sides of drilled shafts. In the shafts installed in dry boreholes, some soil softening due to an increase in moisture content occurred, particularly near the bases. This softening, produced by water from the setting concrete, accounted for some, but not all of the measured strength reduction. Other reasons for shear strength reduction are reasoned to be the effects of remolding and opening of fissures as the boreholes were drilled and mechanical base-side interference. Samples taken adjacent to the shaft installed in a processed hole revealed pockets of trapped drilling mud between the sides of the borehole and the wall of the shaft.

Based upon the field study and a comprehensive review of related research conducted in similar soil formations, a tentative design procedure is suggested. That procedure includes criteria for providing an adequate factor of safety against plunging failure and for limiting immediate settlement at working load to an acceptable value.

KEY WORDS: piles, bored piles, drilled shafts, soil mechanics, undrained shear tests, cohesive soils, cone penetrometer, instrumentation, field tests, design criteria

SUMMARY

The purpose of this report is to describe the results of field tests of full-sized, instrumented drilled shafts in the Beaumont Clay formation. Drilled shafts with varying base geometry, length, and method of installation were load tested to obtain measurements of the distribution of axial load with depth and of base load-settlement characteristics in order to develop design criteria.

Pertinent soil parameters were obtained by various standard procedures, including the unconsolidated, undrained triaxial test and the T.H.D. cone penetrometer test to provide a basis for the correlation of test results.

The test shafts were observed to develop considerable resistance in side friction. Furthermore, side resistance was observed to develop much sooner than base resistance, with the result that side resistance predominated over base resistance at design load. The shafts installed in dry boreholes mobilized an average of one-half of the shear strength of the soil in side friction, while the side frictional stresses in the shaft installed in a processed borehole were significantly smaller. An investigation showed that the shafts installed in the dry were well-formed and bonded securely to the soil composing the borehole walls, while the shaft installed in a processed hole contained pockets of drilling mud between the concrete and natural soil. Based upon these observations, the numerical test results, and field tests of other investigators in similar soil formations, a tentative design procedure incorporating side resistance is formulated.

IMPLEMENTATION STATEMENT

The study indicated that considerable load was resisted in side friction in axially loaded drilled shafts in stiff clay with both straight sides and underreams, installed in dry boreholes and in boreholes processe with drilling mud. The possibility that considerably smaller frictional resistance occurs in shafts installed in processed holes was observed, however. The test results generally agree with those of other investigators in similar soils.

Measured side shear and base capacities were correlated with standard soil strength tests. It appears that side friction can be reliably estimated for shafts in dry boreholes, and to some extent for shafts installed in processed holes, from laboratory soil tests or from penetrometer soundings. Therefore, a new design procedure for drilled shafts is suggested that incorporates side friction, a resistance component heretofore omitted from consideration. The incorporation of side friction in the design of drilled shafts will undoubtedly result in considerable monetary savings in bridge foundation construction.

The suggested general design parameters are, of necessity, somewhat conservative, because of the limited number of tests that were conducted and because field testing was limited to short-term loading in one specific soil formation. Further savings can be realized by extending the research into long-term testing, into testing in other soil formations, and into reevaluating construction techniques for installation of shafts in processed boreholes. Such research would provide a better definition of the design parameters in all situations and would therefore permit the design of drilled shafts to be more rational and less conservative.

CONTENTS

Page

PART FIVE - APPENDICES

NOMENCLATURE

Symbol	Definition
A_B	area of base
A_c	transformed cross-sectional area of stem (including effects of reinforcing steel)
A_S	peripheral area of stem
A'_S	nominal peripheral area of the stem excluding sections at the top and bottom, each equal in height to twice the stem diameter
B	diameter of loaded area
$\bar{B}$	width of group of piles or shafts
C'	change in void ratio for increment of applied load
C_c	compression index
C_e	expansion index
c'	effective cohesion
c_{base}	average undrained cohesion of clay beneath base of shaft
c_{mean}	average undrained soil cohesion for fissured soil
c_{sides}	average undrained cohesion of clay along sides of shaft
c_u	undrained cohesion
c_v	coefficient of consolidation
D_r	relative density
d	diameter of shaft or pile
d_{stem}	diameter of stem
E_c	Young's modulus of concrete

Symbol	Definition
E_o	slope of initial tangent to nonlinear soil stress-strain curve; circuit output
$\frac{E_o}{c_u}$	ratio of E_o to half of maximum indicated undrained stress difference of clay
$e_{corrected}$	void ratio at beginning of loading increment of consolidation test corrected for elastic compression of consolidation apparatus
e_i	indicated void ratio at beginning of loading increment in consolidation test
e_o	void ratio of soil under overburden pressure, p_o
e'_o	void ratio after load increased to preconsolidation pressure, then decreased to overburden pressure in consolidation test
e_{50}	void ratio corresponding to t_{50}
e_{100}	void ratio corresponding to t_{100}
F.S.	factor of safety at working load
f_1, f_2	base shape factors
H	thickness of compressible layer
h	depth of base of shaft
I_ρ	settlement influence coefficient
K	gage factor
K_o	coefficient of lateral earth pressure, or the ratio of horizontal effective stress to vertical effective stress
L	unit length along shaft
L_S	length of stem

Symbol	Definition
l	length of shaft or pile
N	number of blows per foot for T.H.D. penetrometer
N_c, N_q, N_γ	bearing capacity factors
N_q^*	bearing capacity factor for sands
NMC	natural moisture content
P_i	point at center of i^{th} layer at which consolidation settlement is computed
p	factor relating penetrometer results to maximum unit side resistance
Δp	increment of applied pressure causing consolidation
p'	factor relating penetrometer results to unit base capacity
p_c	preconsolidation pressure
p_i	i^{th} point on load transfer or load distribution curve
p_o	overburden pressure, or initial effective vertical pressure at the center of the compressible layer
$Q(z)$	function relating load in the shaft to depth
Q_B	total amount of load taken by the base
Q_S	total amount of load removed by the sides in shear
Q_T	applied load
$(Q_B)_{ult}$	ultimate base load
$(Q_S)_{ult}$	ultimate side load
$(Q_T)_{ult}$	ultimate load at top of pile or shaft
q	contact pressure
$(q_B)_{ult}$	unit ultimate bearing stress on the base

Symbol	Definition
$(q_S)_{ult}$	unit ultimate side resistance
$(q_B)_{ult, net}$	net unit ultimate bearing stress on the base
r	stem radius
S	mean shear strength of clay soil
S_r	degree of saturation
S_0	shear strength of soil before softening
S_1	shear strength of soil after softening
S1, S2, S3, S4	abbreviations for Test Shaft No. 1, Test Shaft No. 2, Test Shaft No. 3, Test Shaft No. 4
S1T1, etc.	abbreviation for "Test No. 1 on Test Shaft No. 1," etc.
s	shear stress, spacing between piles in a group
T_z	tensile force at depth z
t_{50}	time required to develop 50 per cent of primary consolidation (logarithm of time plot)
t_{100}	time required to develop 100 per cent of primary consolidation (logarithm of time plot)
v	applied voltage
w	downward movement, moisture content
w_T	downward displacement of the butt
$w_{\bar{z}}$	downward displacement at depth $\bar{z}$
z	depth coordinate
$\bar{z}$	generic depth
α	shear strength reduction factor
α_{avg}	average shear strength reduction factor over a specified length of shaft

Symbol	Definition
α_{min}	minimum shear strength reduction factor from a laboratory test series
α_{peak}	α_{avg} corresponding to peak side load
α_{ult}	α_{avg} corresponding to ultimate load
α_z	shear strength reduction factor at depth z
α_1	ratio of shear strength of soil around shaft after placing concrete to that existing before placing concrete
α_{11}	that part of α_1 due to softening because of migration of water from concrete into soil
α_{12}	that part of α_1 due to the shear strength reduction not accompanied by moisture migration (remolding, opening of surface fissures)
α_{13}	that part of α_1 due to surface effects and base-side mechanical interference
α_2	adhesion coefficient
$\bar{\alpha}$	average shear strength reduction factor over entire stem excluding top and bottom two diameters
β	settlement correlation coefficient, settlement interaction factor
γ'	effective unit of weight of soil
δ	angle of friction between the soil and concrete
δ_S	elastic compression of stem
ϵ	strain, general
$\epsilon_{circuit}$	circuit strain
ϵ_1	axial strain in triaxial or unconfined compression test
$\epsilon_{1_{steel}}$	strain in steel in longitudinal direction

Symbol	Definition
$\epsilon_{2_{steel}}$	strain in steel in transverse direction
ϵ_{50}	strain corresponding to one-half of the principal stress difference at failure
μv	abbreviation for microvolts
ν	Poisson's ratio
ξ	settlement ratio
ρ_B	average settlement beneath loaded area
ρ_c	total compression of compressible layer
σ	normal stress
σ_v'	vertical effective stress in the soil adjacent to the shaft
σ_Δ	principal stress difference in a triaxial or unconfined compression test
σ_1	maximum principal stress
σ_3	minimum principal stress
ϕ	angle of internal friction
ϕ' $(=\phi_d)$	effective angle of internal friction
ϕ_u	undrained angle of internal friction
ψ	additional shear strength reduction factor for shafts installed in a processed hole
ω	bearing capacity reduction factor for fissured clay

CHAPTER VI

SCOPE AND OBJECTIVES OF PRESENT FIELD STUDY

Under the sponsorship of the Texas Highway Department and the Bureau of Public Roads, Department of Transportation, the Center for Highway Research of The University of Texas at Austin has undertaken a study to obtain information pertinent to a more economical design of drilled shafts in Texas and, hopefully, to contribute to the body of knowledge outlined in the previous chapters. The study of the behavior of drilled shafts under axial loading is being carried out by conducting load tests of full-scale, instrumented shafts constructed by standard methods. To date, results of load tests on cylindrical shafts in Austin and San Antonio have been reported (Reese and Hudson, 1968; Vijayvergiya, Hudson, and Reese, 1969).

In order to obtain information which will be useful to the designer, several project objectives have been established. They are:

1. To develop instrumentation capable of measuring load distribution along a drilled shaft.
2. To develop techniques for performing field load tests, and to perform such tests on instrumented shafts at sites having varied soil conditions.
3. To correlate results of field tests to appropriate laboratory and field procedures for determining soil properties.
4. To develop methods, on the basis of the results of the field studies, by which the bearing capacity of a drilled shaft can be predicted from the results of soil tests.

5. To develop analytical methods to predict the load-settlement relationship for a drilled shaft under load.
6. To develop the necessary design aids, charts, computer programs, and related materials to make the prediction method readily accessible to the practicing engineer.

One phase of the research is concerned with load tests on shafts of various configurations, installed both wet and dry, in Houston, Texas, in a formation known as the Beaumont Clay. This formation is exposed in a wide band along the Texas Gulf Coast, and many important structures are founded in it. Drilled shafts are used in many localities for bridge foundations and in some cases in foundations for buildings. Little direct information concerning their behavior in this formation, especially with respect to side-load transfer, has been accumlated. The purpose of this report is to describe the results of load tests on instrumented shafts at a test site on State Highway 225 and Old South Loop East, in Houston (designated SH225 Test Site). The location of the SH225 site is indicated in Fig. 6.1. This site was chosen because it had a typical Beaumont Clay soil profile. It was also on Texas Highway Department right-of-way, which eliminated land rental expenses and permitted easy accessibility. One additional instrumented, axially loaded shaft was tested in Beaumont Clay at a different location (HB&T Test Site), also shown in the figure. The details of the testing program for that shaft are presented by Barker and Reese (1970).

The general soil profile for the SH225 site is given in Fig. 6.2. Differentiation according to percentage of sand, silt, and clay sizes is also shown. The soil profile is a composite of classifications from

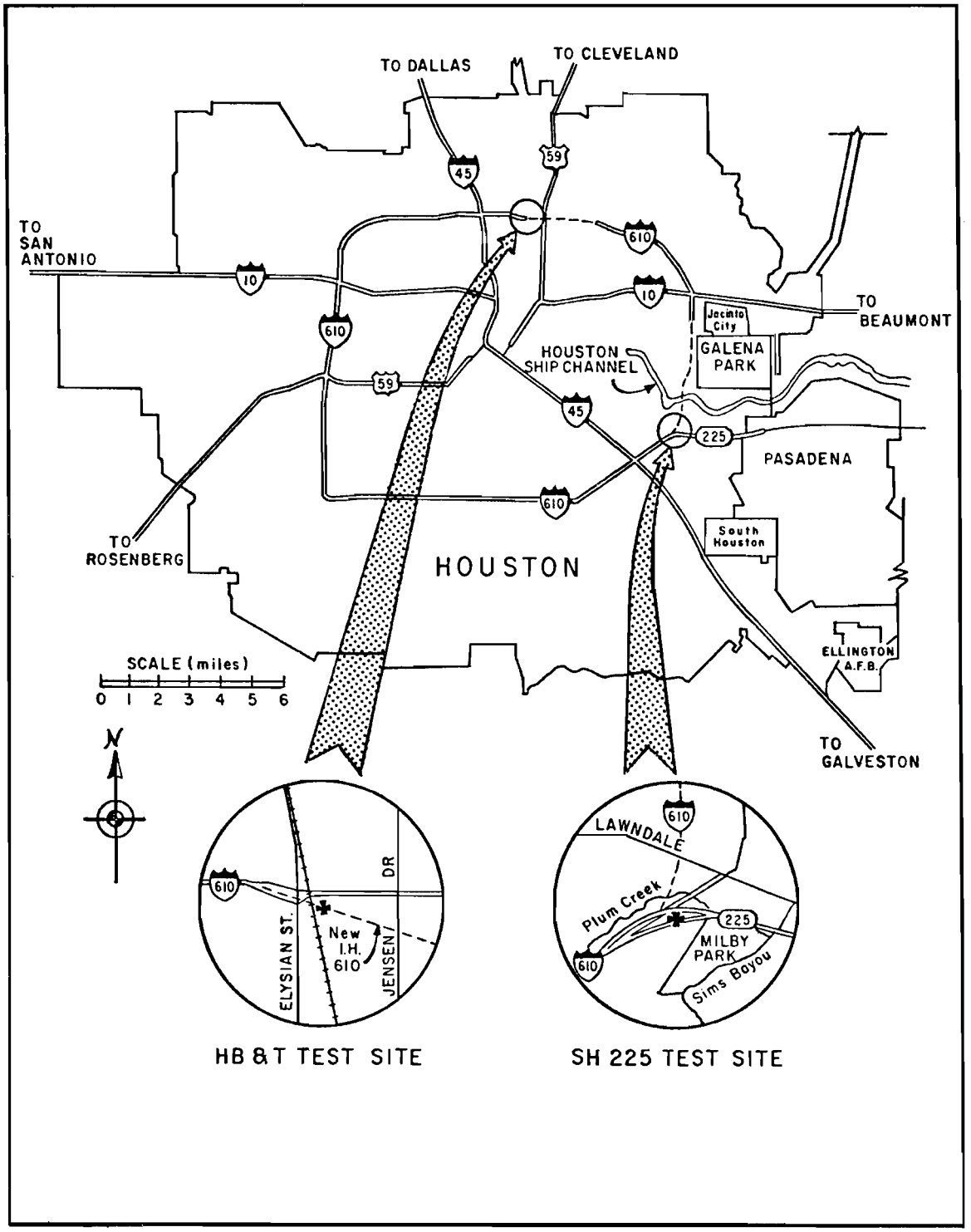

Fig. 6.1. Location Map for Houston Test Sites

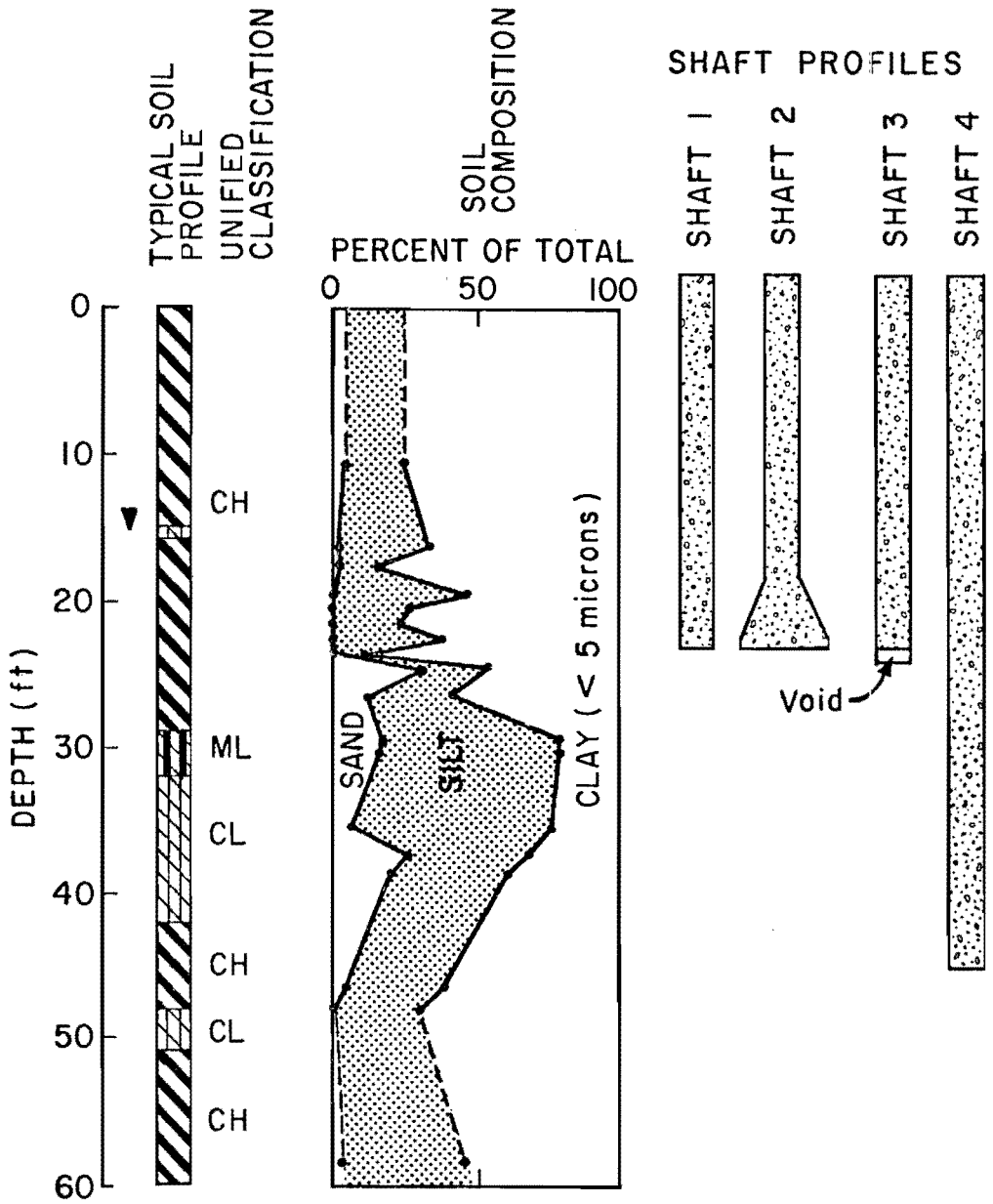

Fig. 6.2. Profiles of Soil Composition and Test Shafts, SH225 Test Site

six borings taken at various points on the site shown in Fig. 6.3. The soil is described in greater detail in the following chapters.

Four test shafts were installed and tested at the SH225 site. They are shown schematically along with their respective numerical designations (S1, S2, S3, and S4) in Fig. 6.2. All shafts had a nominal stem diameter of 30 inches, which is typical for bridge foundations in the Houston area. The bell in Shaft 2 was 7 1/2 feet in diameter, with the sides making a 60 degree angle with the horizontal. Shafts 1 through 3 were all embedded to a depth of 23 feet and were installed in the dry. Shaft 4 was 45 feet deep and was installed in a processed hole. The purpose of the test arrangement, in addition to facilitating measurement of load-settlement and load-transfer characteristics, was to permit investigation of the effects of the following parameters on the behavior of typical drilled shafts in Beaumont Clay:

1. Geometry of Base. Shafts 1 through 3 were identical, except that Shaft 1 was cylindrical, Shaft 2 had a belled base, and Shaft 3 was cast with a void beneath the base.
2. Length of shaft.
3. Method of installation (wet versus dry).
4. Large displacement.
5. Multiple loadings to failure.
6. Stratification of soil.

The effect of variation in shaft and bell diameter was not investigated. Studies of long-term stability, effects of variations in concrete properties, and possible effects of seasonal moisture variations were likewise excluded from the study. Since shaft diameters and concrete

properties do not deviate too greatly in practice from those taken in this study, their exclusion is not considered significant. Long-term stability under substantial load variations undoubtedly is an important topic, but it is beyond the scope of the present investigation.

The six parameters that were studied all have important design implications. The reason for including these particular parameters is that it was felt that they have the greatest influence on shaft behavior. For example, before planning the experiments it was expected that:

1. The geometry of the base possibly influences load transfer in the soil around the stem immediately above the base.
2. Long shafts may develop shearing resistances in a different pattern than do shorter shafts.
3. Large displacements and multiple loadings may tend to reduce the available side friction and promote load shedding in Beaumont Clay.
4. Different percentages of maximum shear strength mobilization may exist in different soil strata.
5. Shear strength mobilization may be different in shafts installed wet than in those installed in the dry.

The location of the test shafts, anchor shafts (used for jacking reaction), and nuclear monitoring point (used for obtaining subsurface moisture profiles) are shown in Fig. 6.3 in relation to the location of the test borings. "Grid North" is indicated in Fig. 6.3 for the purpose of describing positions of instruments in the test shafts. The average elevation of the ground surface is 34 feet above mean sea level.

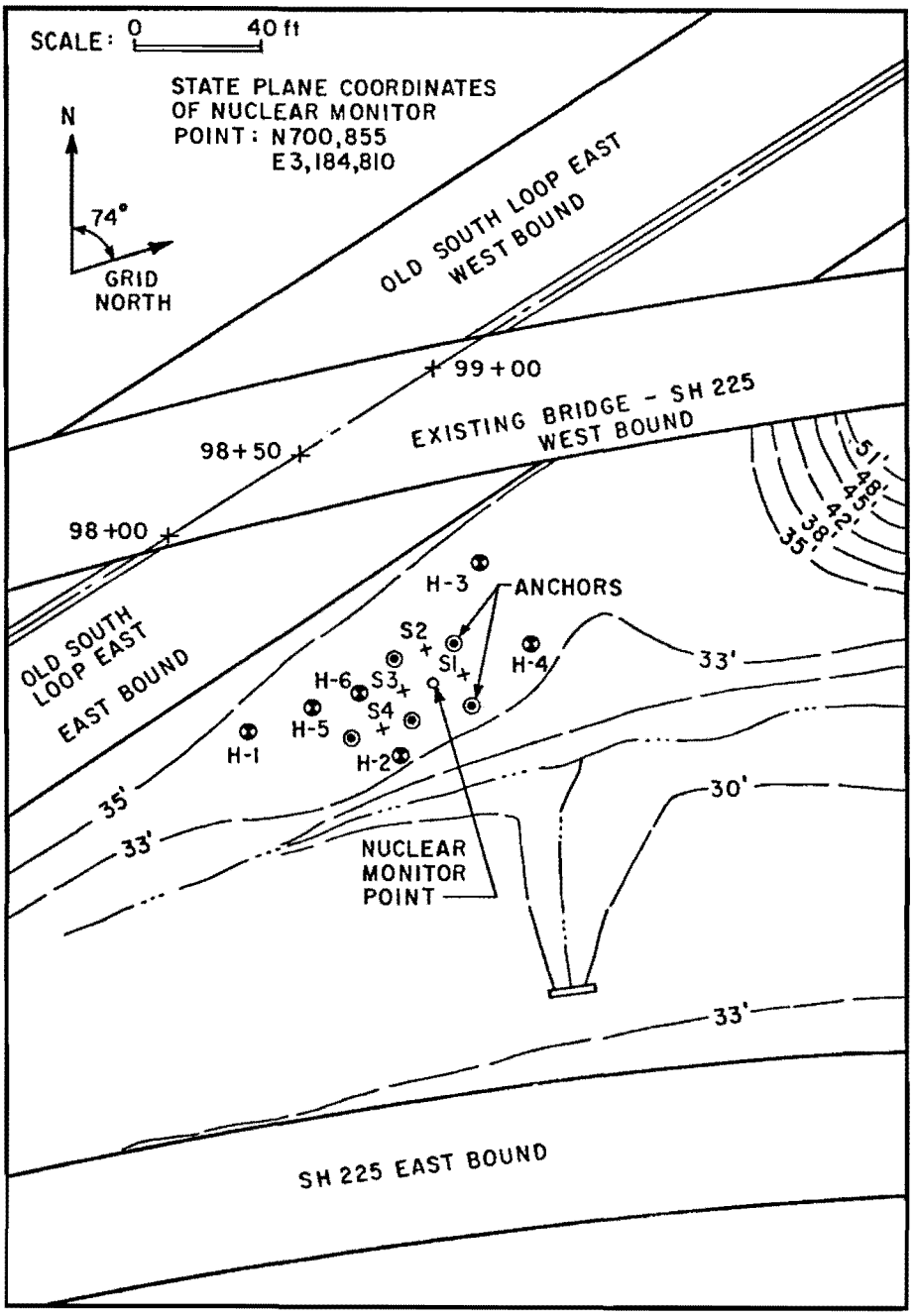

Fig. 6.3. Map of SH225 Test Site

Further details on site conditions, shaft installation, and instrumentation and test procedures are given in the following chapters.

CHAPTER VII

GEOTECHNICAL CONDITIONS

Geological Description of Beaumont Clay

Beaumont Clay is the name given to a geological formation, composed mainly of stiff clay, that is exposed in a band parallel to the Texas Gulf Coast from near the coastline to forty or fifty miles inland. Its surficial expression in Texas extends from the Sabine River on the east to southern Kleberg County on the south. Its present thickness is about 700 feet (Sellards, Adkins, and Plummer, 1932), and it dips southeastward beneath the Gulf of Mexico to the continental shelf at a rate of about three feet per mile. Such cities as Beaumont, Houston, and Corpus Christi are located on the Beaumont formation. The Beaumont Clay unconformably overlies the Lissie formation, which is primarily composed of sand. The Beaumont and Lissie formations, together with the deeper and older Willis formation, comprise the Houston Group. The Beaumont formation is sometimes referred to as the Prairie or Port Hudson formation.

The Beaumont Clay was deposited during the recession of the ice cap in the first Wisconsin Ice Age, approximately 75,000 to 100,000 years ago, which places it in the Pleistocene series (Bernard, LeBlanc, and Major, 1962). Beaumont sediments were deposited primarily in distributaries of rivers (deltas) and in shallow lagoons. It is presumed that the depositional environment resembled the Mississippi delta region of the present. The soil in the Houston area is non-marine, and appears to have been deposited by distributaries of the Brazos River, which took a more

northerly course at the time of deposition than it does today (Van Siclen, 1961).

The formation is somewhat heterogeneous, with inclusions of sand and silt being quite prevalent, as would be expected from the alluvial process of deposition. The clay portion typically presents a red or tan and gray mottled appearance. The mineralogical composition of the red, tan, and gray portions appears to be about the same. The clay generally has a liquid limit of around 70 and a plastic limit of about 20, although wide variations in both indices are common. A recent comprehensive study of the geotechnical properties of Beaumont Clay at a site in Baytown, Texas, (approximately 20 miles east of the SH225 site), has shown the clay fraction to be composed of montmorillonite (23-47 per cent), illite (28-55 per cent), kaolinite (7-18 per cent), and quartz (8-15 per cent) (Al-Layla, 1970). The principal montmorillonite cation is calcium. That part of the soil larger than two microns in diameter includes illite, kaolinite, quartz, feldspar, and calcite (Al-Layla, 1970). Beaumont Clay also contains some small amounts of organic detritis and calcareous nodules.

The Beaumont Clay has been preconsolidated by desiccation, with the indicated preconsolidation pressure being about 4 tons per square foot. Numerous wetting and drying cycles have also produced a network of randomly-oriented and closely-spaced fissures. Most of the fissures are small and discontinuous; however, a number of joints can be found which are larger in extent, and which appear to be old failure surfaces. The fissures are often slickensided. The fissure pattern strongly controls the mechanical behavior of the soil.

Soil Profile at SH225 Test Site

Prior to and during the field test program, six borings were made at the SH225 test site. Undistrubed samples for laboratory study were recovered using three-inch, thin-walled sampling tubes. Each sample was obtained by pushing a dry sampling tube into the soil, carefully measuring the depth, and extracting the tube by a combination rotary and lifting motion. Six-to-eight-inch long undisturbed samples were recovered for every foot of penetration. The soil was immediately extruded from the sampling tube and carefully preserved by wrapping it in aluminum foil, coating the foil with wax, placing the wax-coated specimen in a cardboard carton, and thoroughly waxing the exterior portion of the carton. The samples were returned directly to the laboratory in Austin in each case and placed in a 100 per cent humidity room until they were tested (except for Boring H-3, which was retained and tested by the Houston Urban Expressways Office Laboratory).

The complete individual boring logs for each of the six test holes are included in Appendix A. The nomenclature used in the Appendices to describe the samples contains first the boring designation and then the sample number. For example, Sample H-2-15 would be sample 15 from Boring H-2. This method of sample identification has been used throughout. The locations of the borings with respect to the test shafts are as given in Fig. 6.3. A simplified composite boring log for the test site has been presented in Fig. 6.2. The soil profile is reasonably uniform over the area covered by the test site. Boring H-4 was made for the purpose of conducting T.H.D. (Texas Highway Department) cone penetrometer tests, and no samples were recovered for testing.

Atterberg limits and natural moisture contents were routinely determined. The basic profile of liquid limit, plastic limit, and natural moisture content at the SH225 test site is shown in Fig. 7.1. The liquid limit is plotted against plasticity index on the plasticity chart in Fig. 7.2.

The soil at the site can be divided into six strata from ground level to a depth of 60 feet using the plasticity chart and visual classification as guides. The depth and unified soil classification of each stratum is given in Table 7.1.

TABLE 7.1. SOIL STRATA AT SH225 TEST SITE

Layer	Depth	Unified Classification
I	0-29'	CH
II	29-32'	ML
III	32-42'	CL
IV	42-48'	CH
V	48-51'	CL
VI	51-60'	CH

A four-to-six-inch thick seam of very silty clay was observed at a depth of about 15 feet. This seam was waterbearing on several occasions, but dry on others.

A profile of soil composition by per cent sand, silt, and clay, as determined by hydrometer tests, has been presented in Fig. 6.2. Sand is defined to be all material retained on a No. 200 sieve; silt is taken to

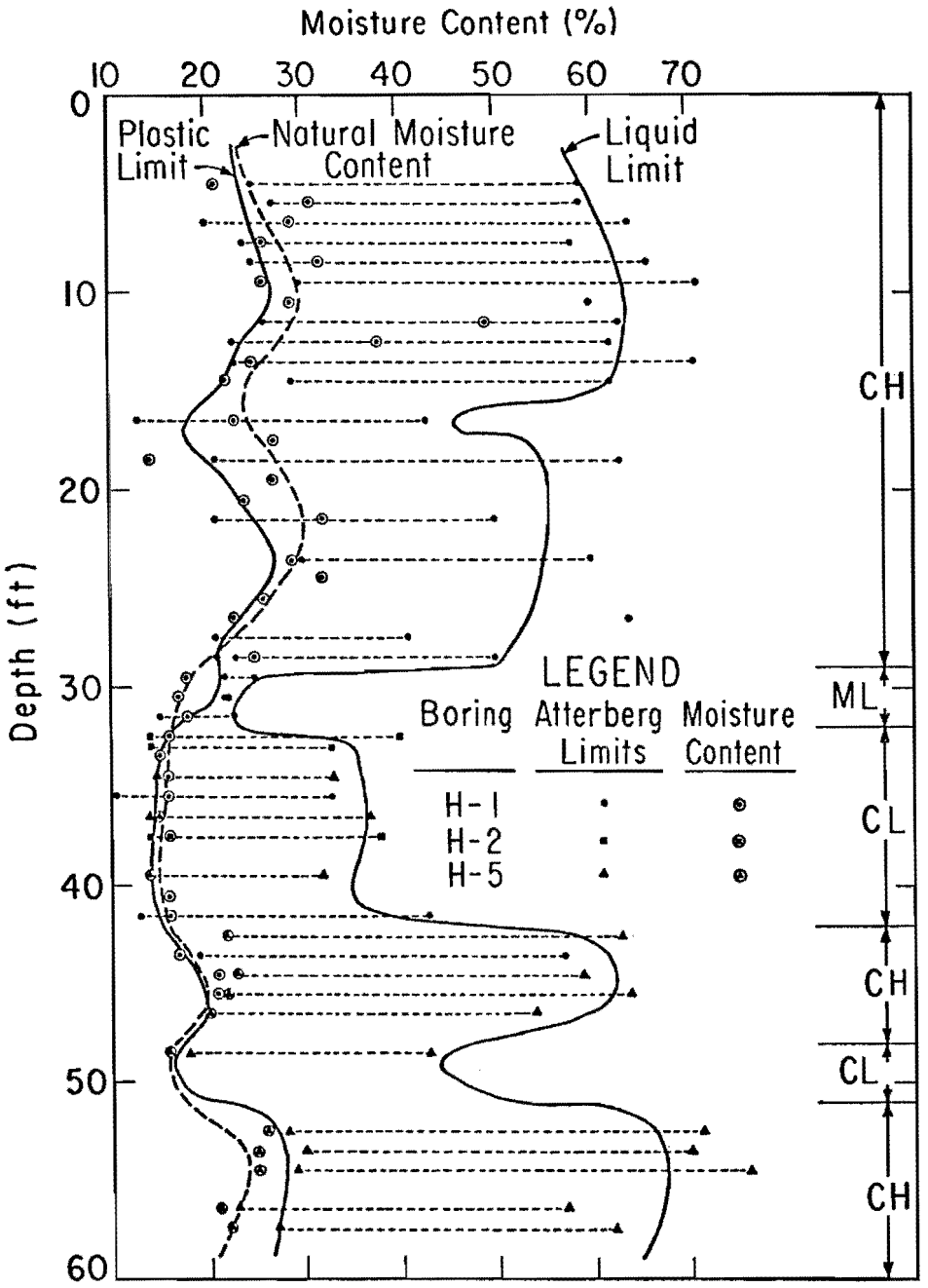

Fig. 7.1. Basic Profile of Atterberg Limits and Natural Moisture Contents

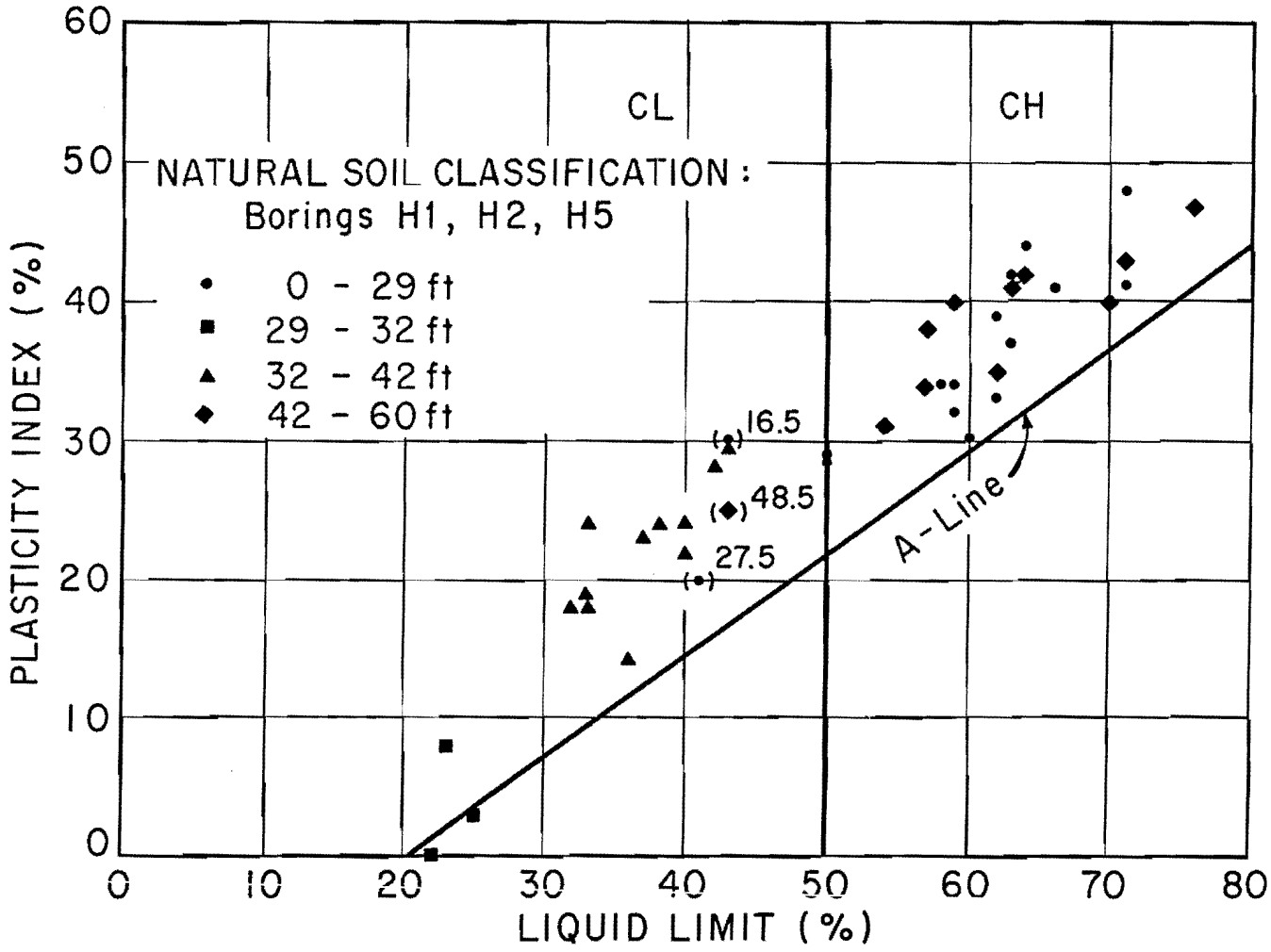

Fig. 7.2. Plasticity Chart

be all material passing a No. 200 sieve but larger than 5 microns in diameter; and the clay size embraces all material 5 microns or less in diameter. The definitions are those given by the American Society for Testing and Materials (ASTM), and the procedure used in the hydrometer analysis followed that specified by ASTM (American Society for Testing and Materials, 1970). A standard 152H hydrometer was used in all tests. A tabulation of hydrometer test results is given in Appendix B.

Photographs of typical three-inch-diameter specimens of Beaumont Clay taken from Layer I at the SH225 test site are shown in Fig. 7.3. The mottling is quite vivid. The specimen shown in the lower photograph was allowed to dry partially to show some of the cracks along the primary fissures.

Profiles for void ratio (e_o), degree of saturation (S_r), and compression index (C_c) are shown in Fig. 7.4. Numerical values were determined from consolidation tests, which will be described in detail later. It is observed that the soil is essentially saturated except at shallow depths.

An open piezometer installed at the test site indicated the water table to be located at a depth of 15 feet. The piezometer was installed in November, 1969, and was operative for only a few days. It is likely that some seasonal variation occurred in the level of the water table during the period of time the field study was being conducted (June, 1968-June, 1970).

The average wet density of the soil is about 125 pounds per cubic foot in the CH layers and about 135 pounds per cubic foot in the CL and ML layers. The activity of the CH layers varies from 0.5 to 1.0, which gives the soil at the site a "normal" activity classification.

a. Section Showing Mottled Structure

b. Partially Dried Section Showing Fissure Planes

Fig. 7.3. Typical Three-Inch-Diameter Specimens of Beaumont Clay

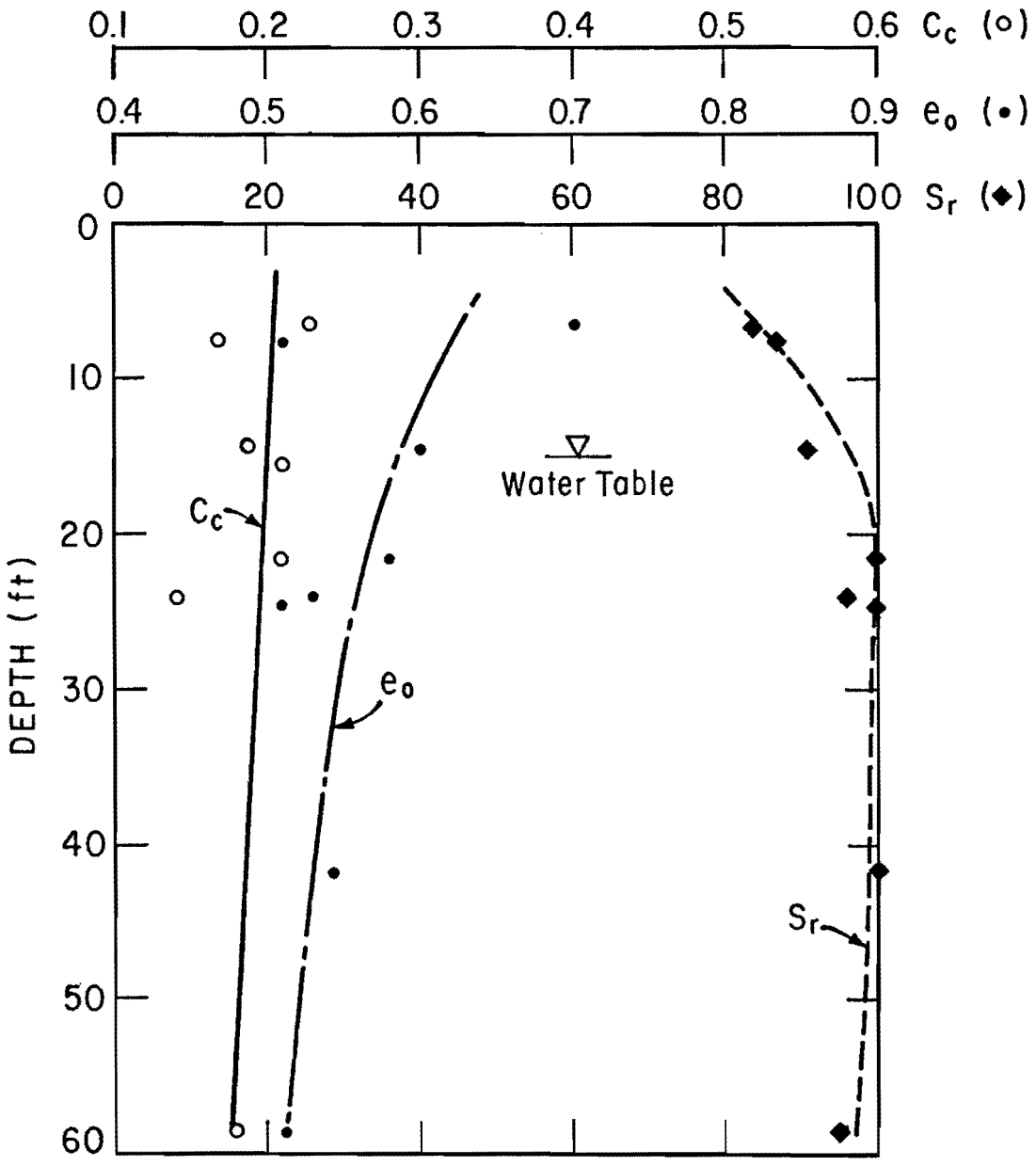

Fig. 7.4. Profiles of Void Ratio, Compression Index, and Degree of Saturation

Strength Tests

Two of the principal aims of the field testing program were to establish shear strength reduction factors and bearing capacity factors for drilled shafts in Beaumont Clay. In order to accomplish these objectives, it was necessary to obtain an accurate definition of the shear strength profile, to which the measured developed shear and bearing stresses could be referred. Two procedures can be followed in obtaining shear strengths. The first, direct in situ measurement of shear strength, is a desirable procedure because the in situ earth pressure is acting on the soil under test and because soil disturbance is minimized. The second, recovery of samples and subsequent laboratory testing, is ideally less desirable, since the soil under test has been subjected to a stress release, has been at least somewhat disturbed, and is probably not in the same condition of stress as it was in situ.

The latter procedure was selected for this study, however. It lacks the two desirable characteristics of the in situ method, but the procedures for obtaining samples and conducting soil tests are reasonably refined and yield repeatable results. Furthermore, practical devices for conducting accurate in situ shear strength measurements were either unavailable or had some inherent disadvantage (such as the vane shear device, which does not allow strains to be measured). It should be pointed out that the T.H.D. penetrometer test, which was conducted on the site and which is described later, is not considered to be an in situ test, since correlations of penetrometer blows to shear strength is done by employing graphs which were constructed by plotting numerous penetrometer results against laboratory shear strength values for the same soil. The recovery

and test procedure is employed by most design agencies, including the Texas Highway Department.

Soil strength testing is as important to the determination of the drilled shaft load transfer and bearing capacity factors as is the field testing of the shafts. Without a realistic shear strength profile, the value of the test results is diminished. In addition, since the measured shear stresses developed against the shafts are being compared to the shear strength of the soil, the soil profile should not indicate strength values which are too small, or the shear strength reduction and bearing capacity factors will be unconservative. This concept is opposite to that normally embraced in design. For this reason, care was taken in planning the laboratory test program to exclude procedures that would yield low strength values.

Tests conducted in the laboratory in support of the field study were all performed on a total stress basis. Therefore, effective stress parameters were not established. However, Al-Layla (1970) has presented typical effective stress parameters for Beaumont Clay. His results are summarized herein for completeness.

Al-Layla obtained a range of values of 15.5 to 19.5 degrees for the effective angle of internal friction from undrained triaxial tests and 12.5 to 13.0 degrees from drained tests. (This apparent anomaly was explained by minerological differences in test specimens and by the fact that drained specimens failed preferentially along fissures). The cohesion value from the drained tests was about 3.5 psi. The soil tested by Al-Layla had an A-parameter which varied from 0.6 at an overconsolidation ratio of unity to 0.2 at an overconsolidation ratio of ten. No negative

pore pressures were developed during shear except under very light confining pressures. Failure strains from 1.3 to 7.4 per cent were obtained in triaxial tests.

Al-Layla noted that the effective angle of internal friction did not vary with sample orientation in the triaxial test, but that the cohesion was somewhat greater when the sample was oriented such that the σ_1 axis coincided with the in situ horizontal plane than when it coincided with the vertical. He also measured higher values of Young's modulus for horizontal orientation than for vertical orientation. These results indicate that the soil has anisotropic mechanical properties. A coefficient of horizontal earth pressure of 1.5 was suggested.

Residual shear strength tests were also performed by Al-Layla. The residual strength was found to vary from 35 to 50 per cent of the peak strength. The sensitivity of the soil was found to vary from 1.0 to 1.3.

One final test of interest conducted by Al-Layla was the variation in remolded shear strength with water content. On the basis of a limited number of specimens tested, the relationship between initial shear strength S_0 and final shear strength S_1, after a moisture content change Δw, can be expressed as:

$$S_1 = S_0 \, 10^{-0.04(\Delta w)} \quad \ldots\ldots\ldots\ldots\ldots\ldots\ldots\ldots\ldots\ldots (7.1)$$

where Δw is in per cent. By contrast, undisturbed London Clay manifests the following relationship (derived from Skempton, 1959):

$$S_1 = S_0 \, 10^{-0.10(\Delta w)} \quad \ldots\ldots\ldots\ldots\ldots\ldots\ldots\ldots\ldots\ldots (7.2)$$

Considering again the present study, the undrained shear strength profile at the SH225 site was obtained by several different methods:

1. UU triaxial and unconfined tests using single-step shear
2. UU triaxial tests using multiple phase shear ("transmatic" procedure)
3. Direct shear
4. T.H.D. penetrometer
5. Pocket penetrometer

A description of the tests and presentation of results is given in the following sections.

UU Triaxial and Unconfined Compression Tests (Single-Step Shear - U.T.). Since the field load tests performed on the test shafts were conducted at a rate which produced failure before any appreciable drainage could occur in the soil, it was appropriate to conduct undrained strength tests for purposes of correlation. Specimens from Borings H-1, H-2, H-5, and H-6 were returned to The University of Texas at Austin (U.T.) soil mechanics laboratory for testing.

Boring H-1 was made in November, 1967, and samples recovered therefrom were used for conducting unconfined tests (along with Atterberg limits and moisture content determinations). Results from the tests were used for the purpose of obtaining design parameters for sizing the first test shaft and the anchor shafts. The unconfined compression tests were conducted on untrimmed (except for length) specimens, three inches in diameter by six inches in length. The tests were conducted under controlled strain conditions, with a strain rate of 0.75 per cent per minute. They were performed over a period of about eight weeks after sampling. Appendix C contains a

summary of the results of the unconfined tests. The results shown are grouped by "mean depth," which is a means of identifying groups of specimens with similar visual classification. In each test, the shear strength was defined to be half the peak unconfined strength. The quantity ϵ_{50} is the strain corresponding to one-half the maximum failure stress, which is a measure of the brittleness of the soil. Shear strength values indicated by the unconfined compression tests are plotted against depth, and a mean indicated shear strength profile is drawn in Fig. 7.5. The mean profile was fitted visually, as were the profiles for the other tests reported in this chapter.

The characteristic scatter for a fissured soil is evident in Fig. 7.5. Most of the specimens failed along irregular surfaces, with the failure plane often passing along fissures or joints as well as through blocks of intact soil. Intact soil blocks were about one-quarter to one-half inch in average dimensions. Many failure planes were slickensided. Specimens from Layer II were composed of light tan to gray clayey silt, but they possessed enough cohesion to allow unconfined tests to be run.

Unconsolidated Undrained triaxial tests were conducted on soil from Borings H-2, H-5, and H-6. The UU triaxial tests are commonly used procedures for determining shear strength in Beaumont Clay. In order to obtain shear strength values which did not approach the fissured strength, all triaxial specimens were trimmed to a 1.4-inch-diameter by 2.8-inch-long test size. As previously mentioned, the smaller specimens are expected to give higher strengths than the larger ones, since preferential failure through fissure planes is more probable in large samples of fissured clay. Since the soil is forced to fail along a plane parallel to

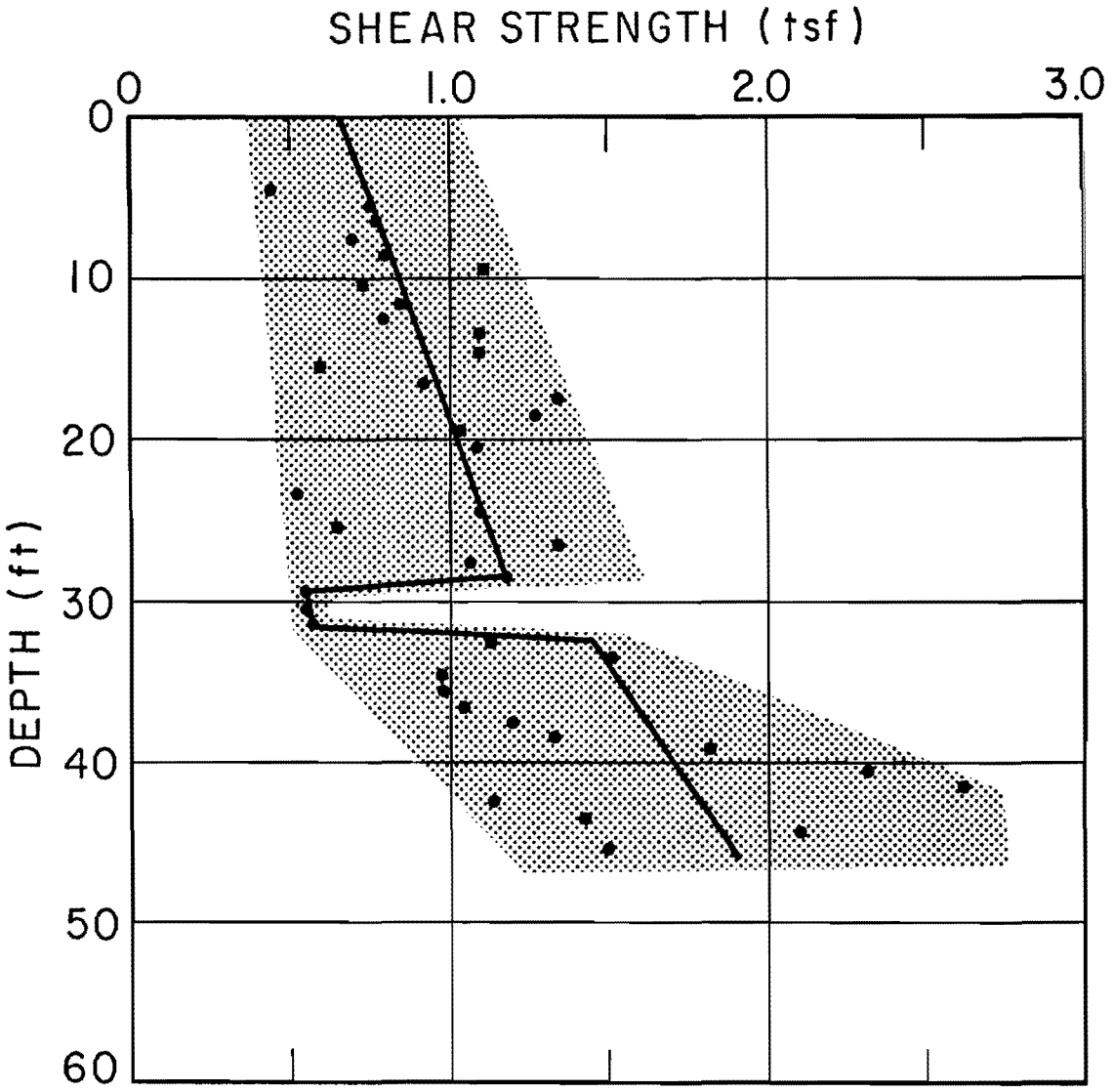

Fig. 7.5. Shear Strength Profile - Unconfined Compression Test

the surface of the walls of the shaft in a load test, preferential failure is unlikely to occur. Small specimens are, therefore, expected to give more representative operational strength values for purposes of side resistance correlation. The same may not be true for base failure, which may occur more readily along fissures or joints.

The UU triaxial tests were conducted by two procedures: controlled stress and controlled strain. The tests were performed over a period of several months after sampling. No significant differences were observed in the behavior of soil tested soon after sampling and soil tested several months after sampling. Soil from Boring H-2, recovered in November, 1967, was tested using a controlled stress procedure, which was chosen as the method best simulating the loading pattern which would occur in the field. The procedure employed was as follows:

1. The specimen was trimmed.
2. The specimen was placed in the triaxial cell between two thin teflon disks to reduce end friction.
3. End platens were placed.
4. The specimen was enclosed in a rubber membrane (single 0.002-inch-thick membrane sealed top and bottom with single O-rings).
5. The cell was sealed.
6. Cell fluid (glycerine) was pumped into the cell, and the cell pressure was applied.
7. Cell pressure was allowed to act on the specimen for 30 minutes.
8. The specimen was sheared by applying increments of five per cent of the expected failure load every five minutes.

Views of the controlled stress apparatus are shown in Fig. 7.6. Cell pressure was maintained by pressurizing glycerine in a reservoir outside the cell but freely communicating with it. Constant pressure in the glycerine reservoir was provided by compressed air, which was controlled by a diaphragm-type pressure regulator. Deviatoric stress was applied with dead weights through a hanger and yoke arrangement, which was initially counterpoised as shown in Fig. 7.6. The upward force on the piston due to the cell pressure was balanced by adding small weights to the hanger. Deformations were obtained by reading a dial indicator mounted to the loading frame, with its stem resting on the loading ball atop the piston. Each specimen was subjected to a confining pressure approximately equal to the computed in situ overburden stress. All specimens tested were in a vertical orientation. Commercial cells (Clockhouse) identical to the one pictured in Fig. 7.6 were used in the tests.

After completing the controlled stress tests, it was observed that strength values obtained from controlled strain tests conducted at an axial strain rate of 0.3 per cent per minute were almost identical to those obtained by the controlled stress method and that the stress-strain curves differed only slightly. Because of this fact, and because the controlled strain tests were easier to conduct, the controlled stress method was abandoned, and controlled strain was used for the remainder of the tests. Soil from Boring H-5, recovered in August, 1969, and Boring H-6, recovered in November, 1969, were tested under controlled strain. Apart from the method of applying load and length of time to failure (shorter for controlled strain), the only difference in the testing procedures was that air was used as the cell fluid in the controlled strain

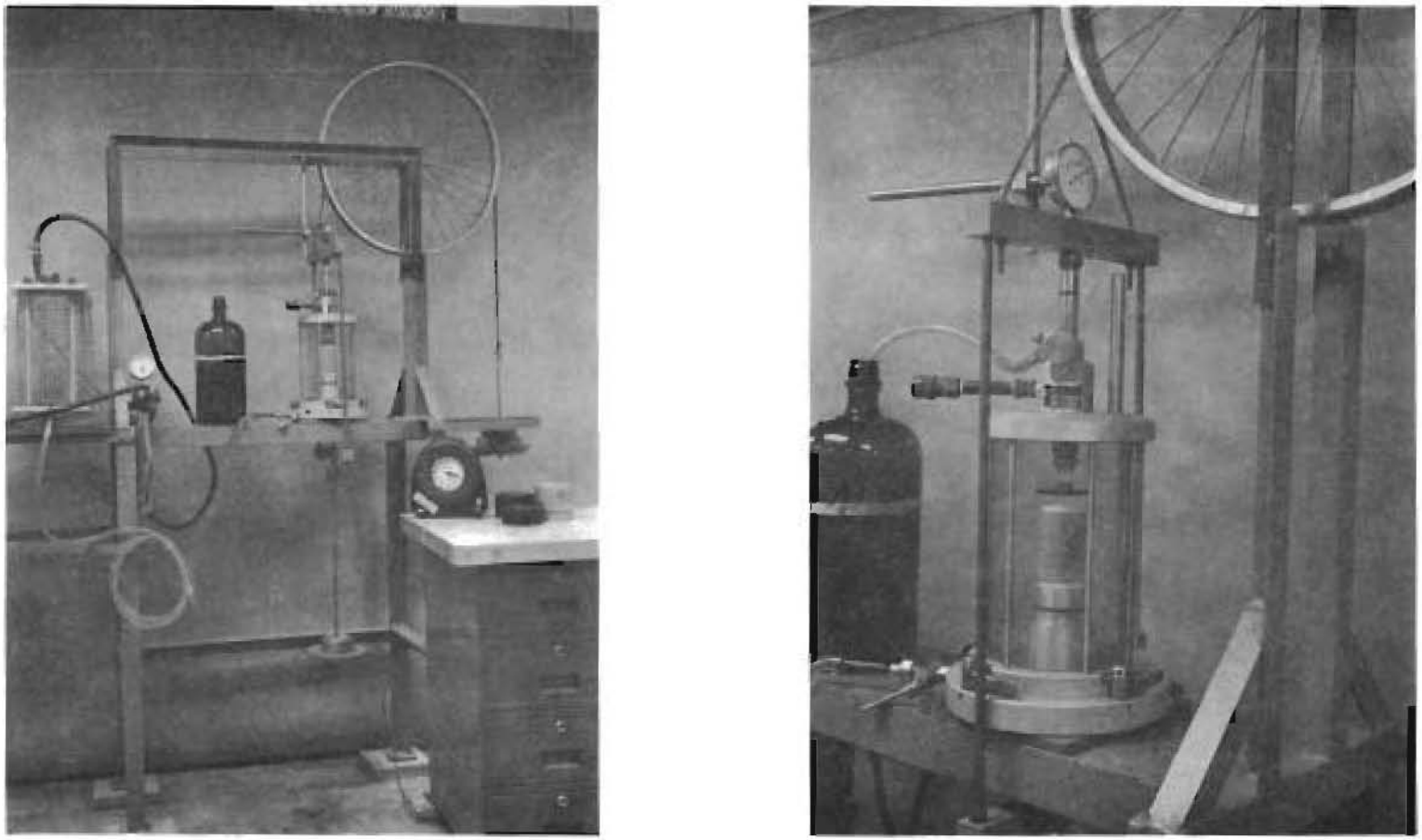

Fig. 7.6. Controlled Stress Triaxial Apparatus

tests to expedite testing. The load in the controlled strain tests was measured with a proving ring mounted between the loading head and the top of the piston.

The results of all of the triaxial tests are tabulated in Appendix C. In addition to showing shear strength values, the tabulation indicates the initial tangent modulus, E_o (slope of the stress difference-axial strain curve), the value of axial strain at one-half maximum principal stress difference, ϵ_{50}, and the ratio of E_o to the indicated shear strength, $\frac{E_o}{c_u}$. Shear strength is defined as half of the maximum stress difference. Corrections for changes in cross-sectional area were made assuming each specimen to be incompressible. Average values for these parameters are listed in Table 7.2.

Indicated shear strength is plotted against depth, and a visually-fitted shear strength profile is given in Fig. 7.7. The individual points are values of half the peak principal stress difference of each specimen. In obtaining the profile, no special weighting was given to either controlled-stress-tested or controlled-strain-tested specimens, although specimens from near the surface from Boring H-5 were discarded. Boring H-5 was recovered during an unusually dry period, and shallow specimens showed abnormally low moisture contents.

The fissured strength is expected to be represented by the lower strength bound. In Layer I, the fissured strength so indicated is about 55 per cent of the average strength.

It is of interest to note that the triaxial tests give consistently higher values of shear strength than do the unconfined tests because the

TABLE 7.2. AVERAGE VALUES FOR SOIL PARAMETERS

Layer	Initial Tangent Modulus, $E_o = \frac{\sigma_1-\sigma_3}{\epsilon_1}$ (psi)	One Half of Principal Stress Difference When Confined at Overburden Pressure, c_u (tsf)	$\frac{E_o}{c_u}$	Axial Strain at One-Half Maximum Stress Difference, ϵ_{50}
I	2,600	1.2	160	0.007
II	250	0.7	26	0.04
III	2,300	1.6	100	0.03
IV	6,500	2.3	200	0.012
V	2,500	2.3	80	0.018
VI	4,000	2.1	140	0.010

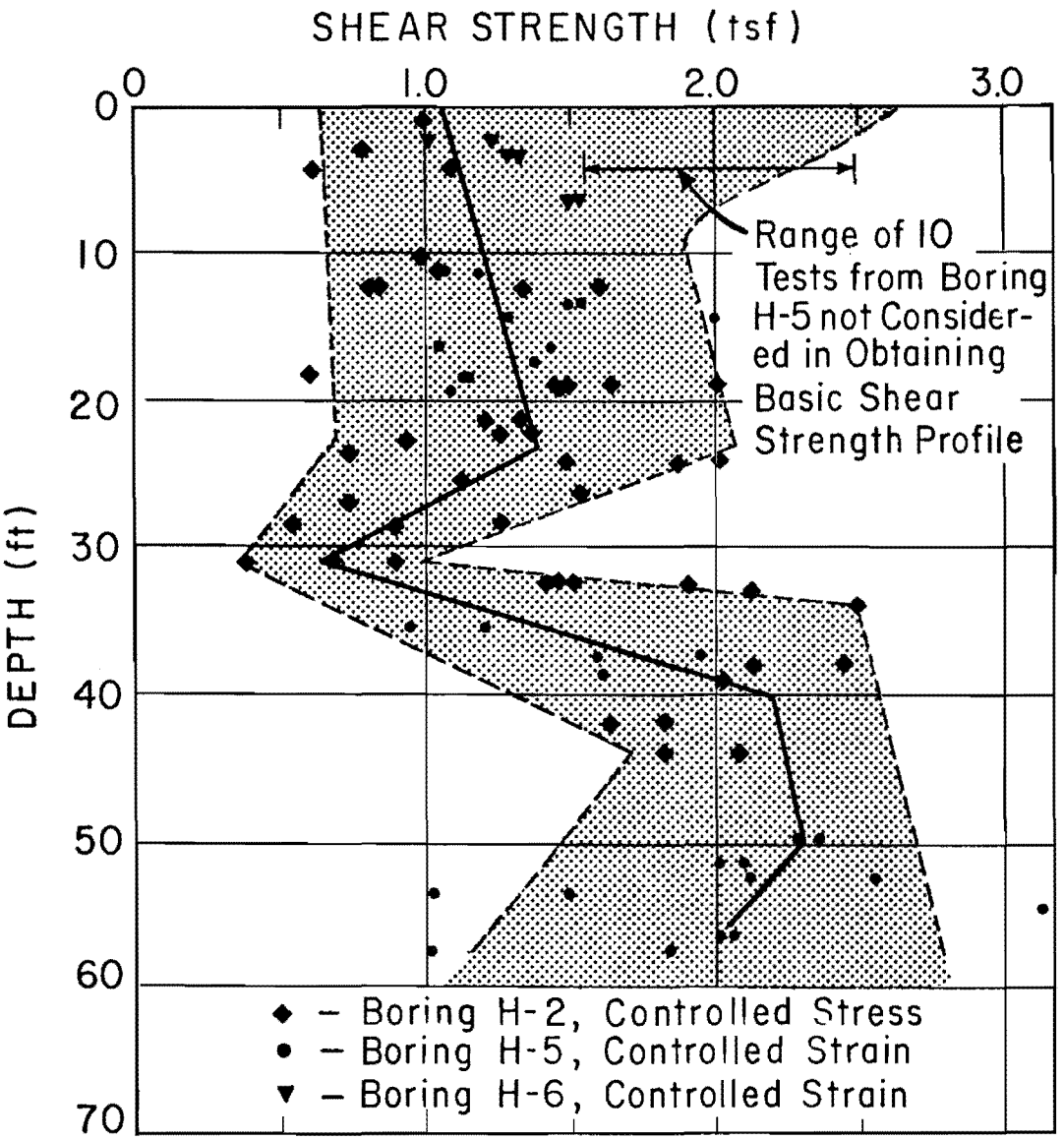

Fig. 7.7. Shear Strength Profile - U.T. Triaxial Test

confining pressure tends to close the fissures somewhat and because the soil as tested was not fully saturated.

The influence of the various sources of errors known to occur in triaxial testing have been ignored. Sample disturbance, nonuniform deformations in the test specimen, and use of values of confining pressure not truly representative of in situ conditions all contribute to the propagation of measured stress-strain curves which are somewhat in error when referred to in situ behavior. Likewise, the effects of soil anisotropy have not been considered in developing a strength profile. Undoubtedly, some effect of shear plane orientation does exist in Beaumont Clay, as indicated by Al-Layla (1970). The effects of these factors are not clearly understood in all cases, although their influence on estimated in situ properties is thought to be small for Beaumont Clay.

It is felt that the strength profile given in Fig. 7.7 and the modulus values given in Appendix C are reasonably representative of the in situ properties. The mean curve shown in Fig. 7.7, determined from the U.T. triaxial tests, is taken to be the correct field profile for all test shafts in all computations involving shear and bearing stress correlation.

Careful stress-strain measurements were taken during each unconfined and triaxial test. To indicate the scatter, the individual test results for Layer I for unconfined compression and triaxial compression at σ_3 = 10 psi (for both controlled stress and controlled strain) are included in Appendix C. Average stress-strain curves for the soil in each layer are plotted for the various values of confining pressure and testing procedures used in Figs. 7.8 through 7.20. The soil exhibited slightly different behavior under different testing techniques. For example, the

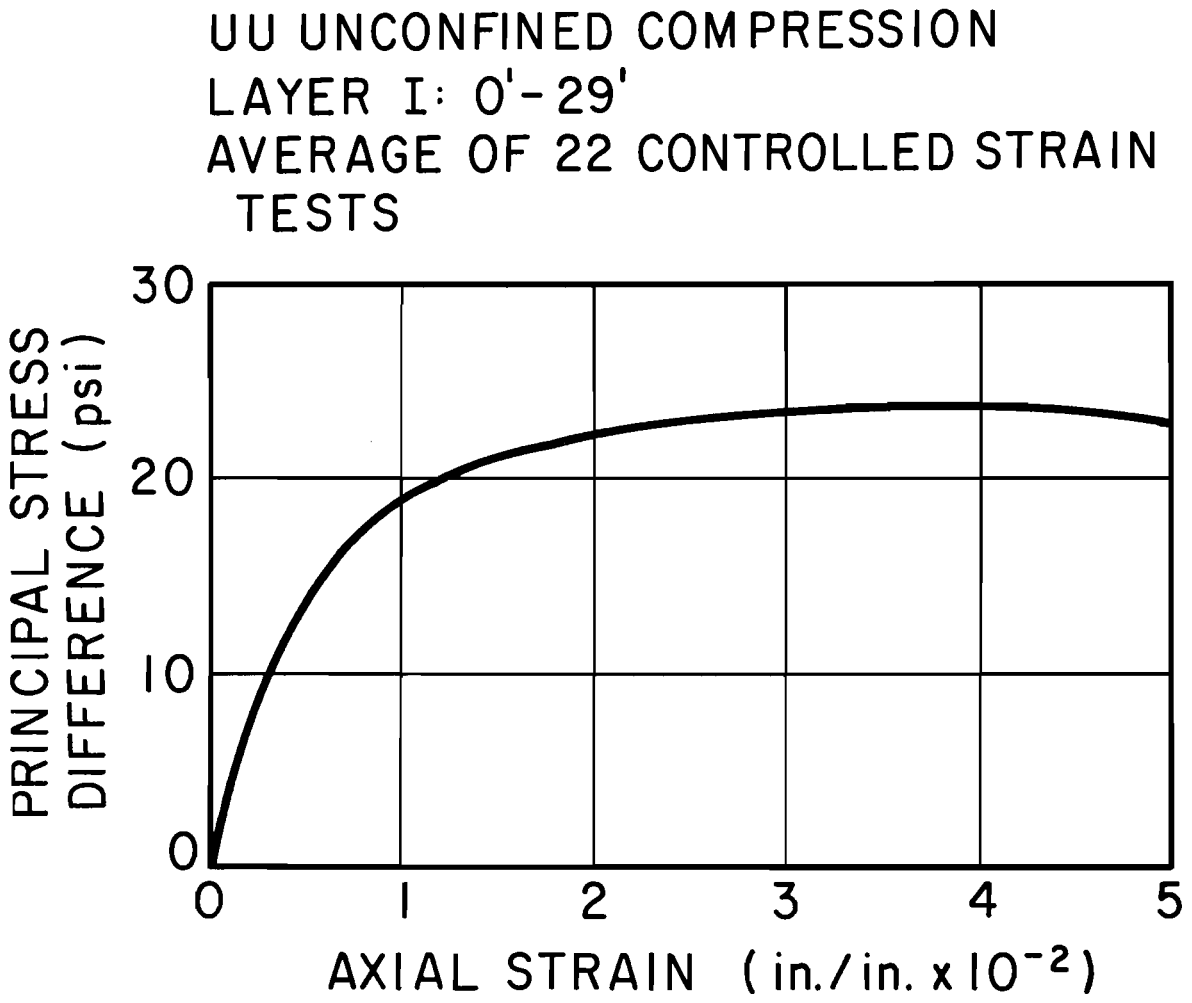

Fig. 7.8. Stress Versus Strain, Layer I, Unconfined Compression

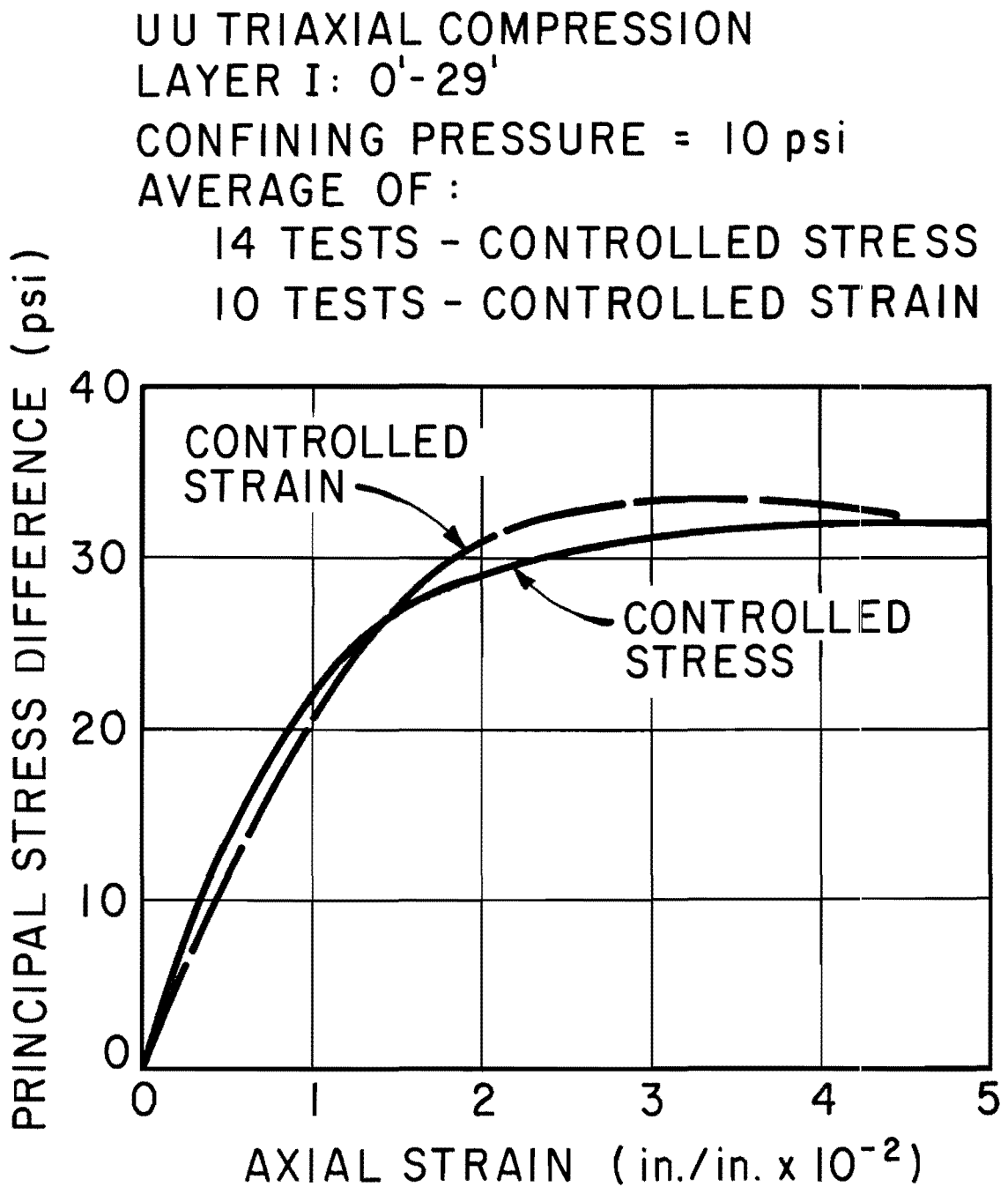

Fig. 7.9. Stress Versus Strain, Layer I, Triaxial Compression (10 psi)

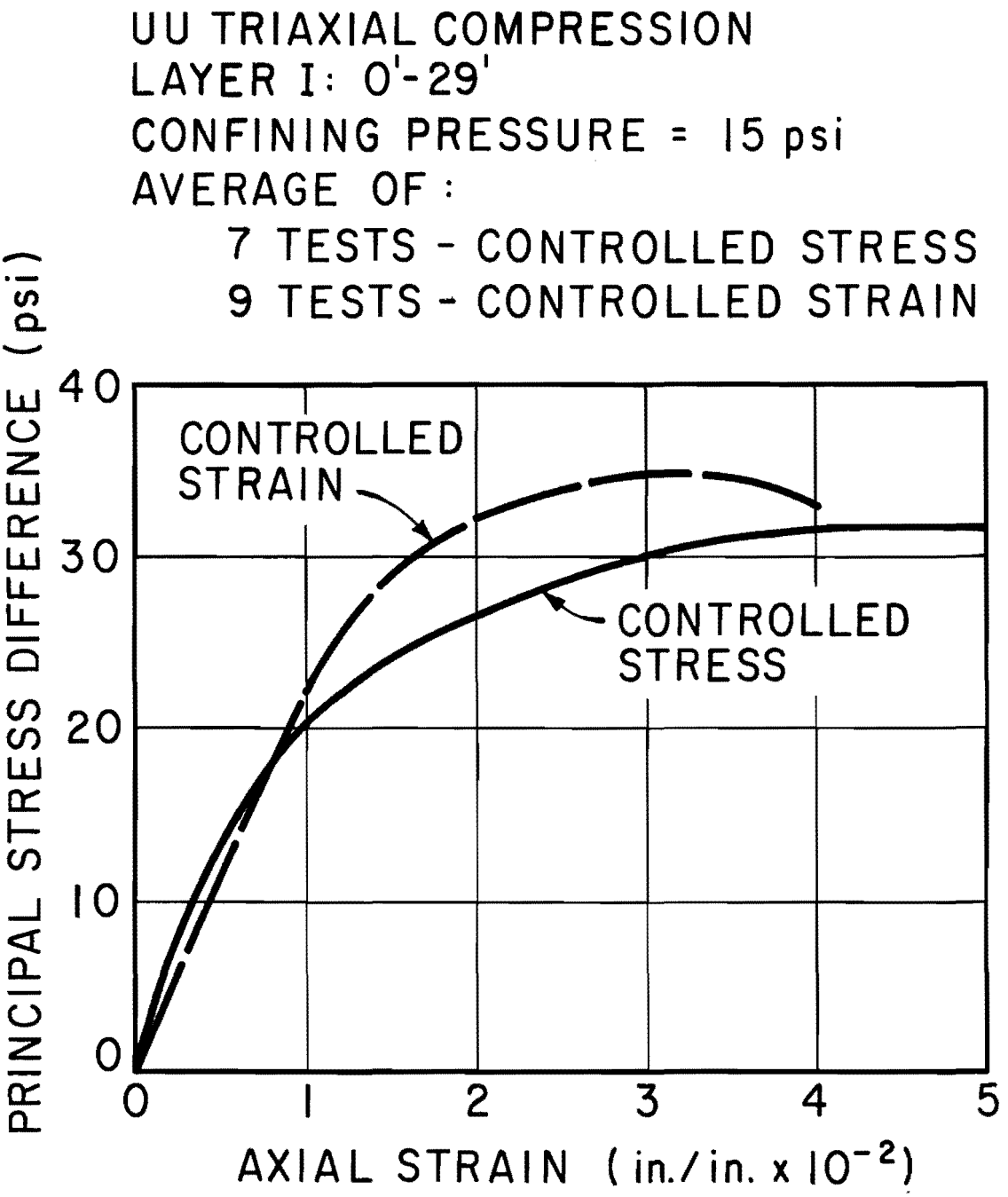

Fig. 7.10. Stress Versus Strain, Layer I, Triaxial Compression (15 psi)

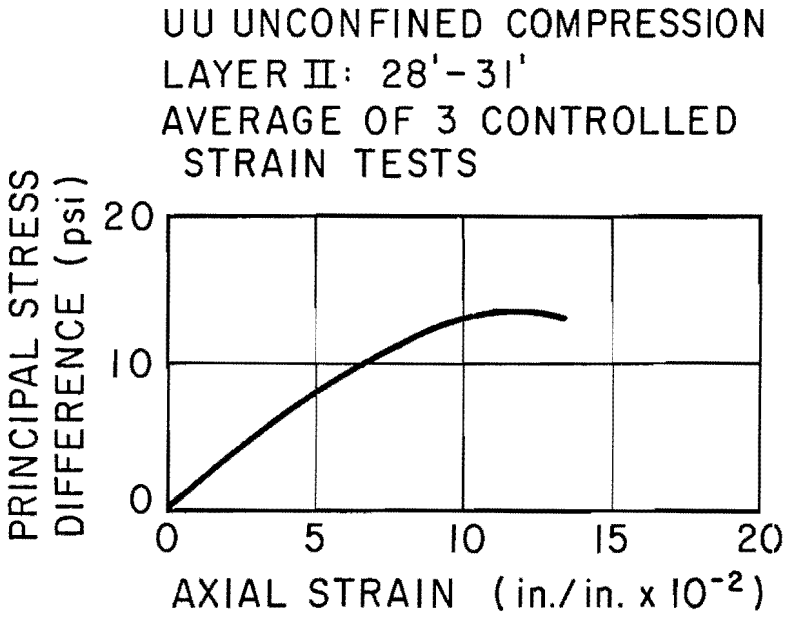

Fig. 7.11. Stress Versus Strain, Layer II, Unconfined Compression

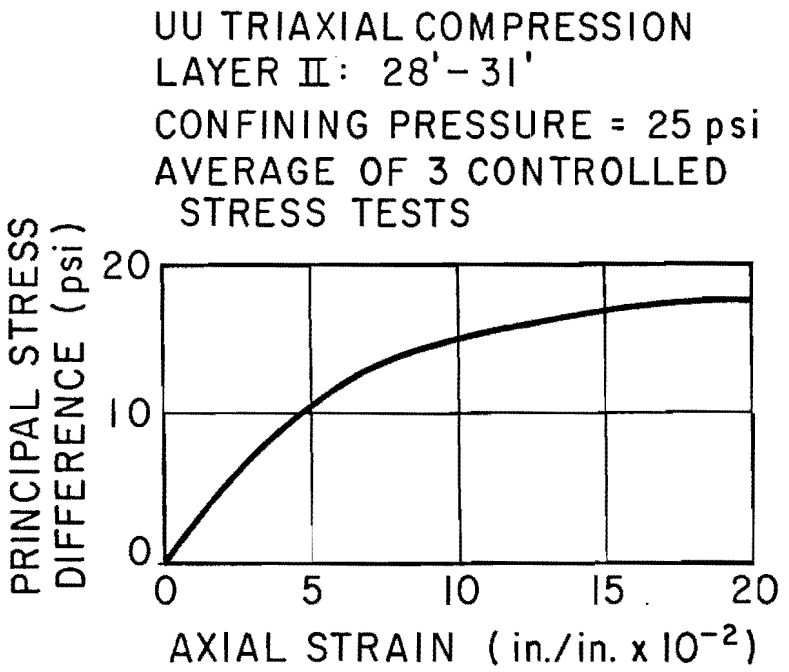

Fig. 7.12. Stress Versus Strain, Layer II, Triaxial Compression

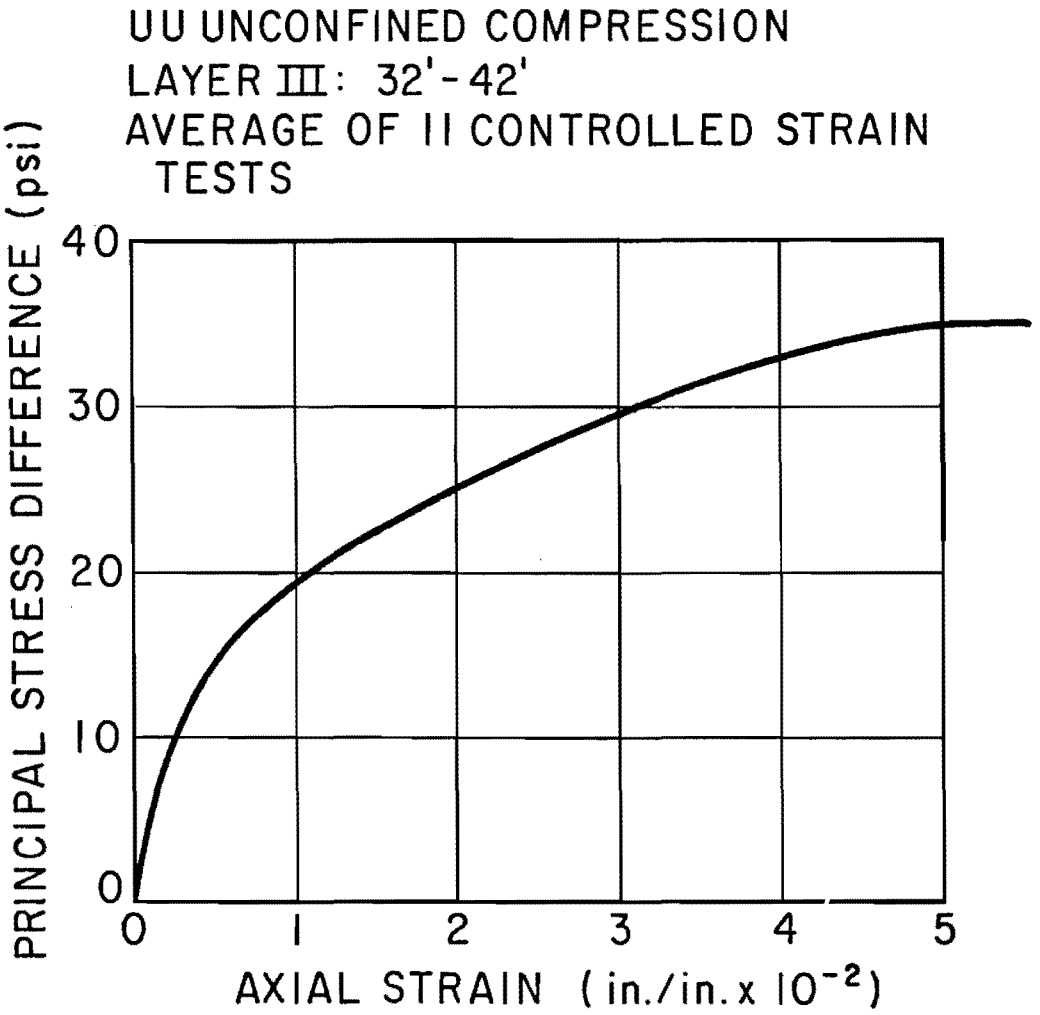

Fig. 7.13. Stress Versus Strain, Layer III, Unconfined Compression

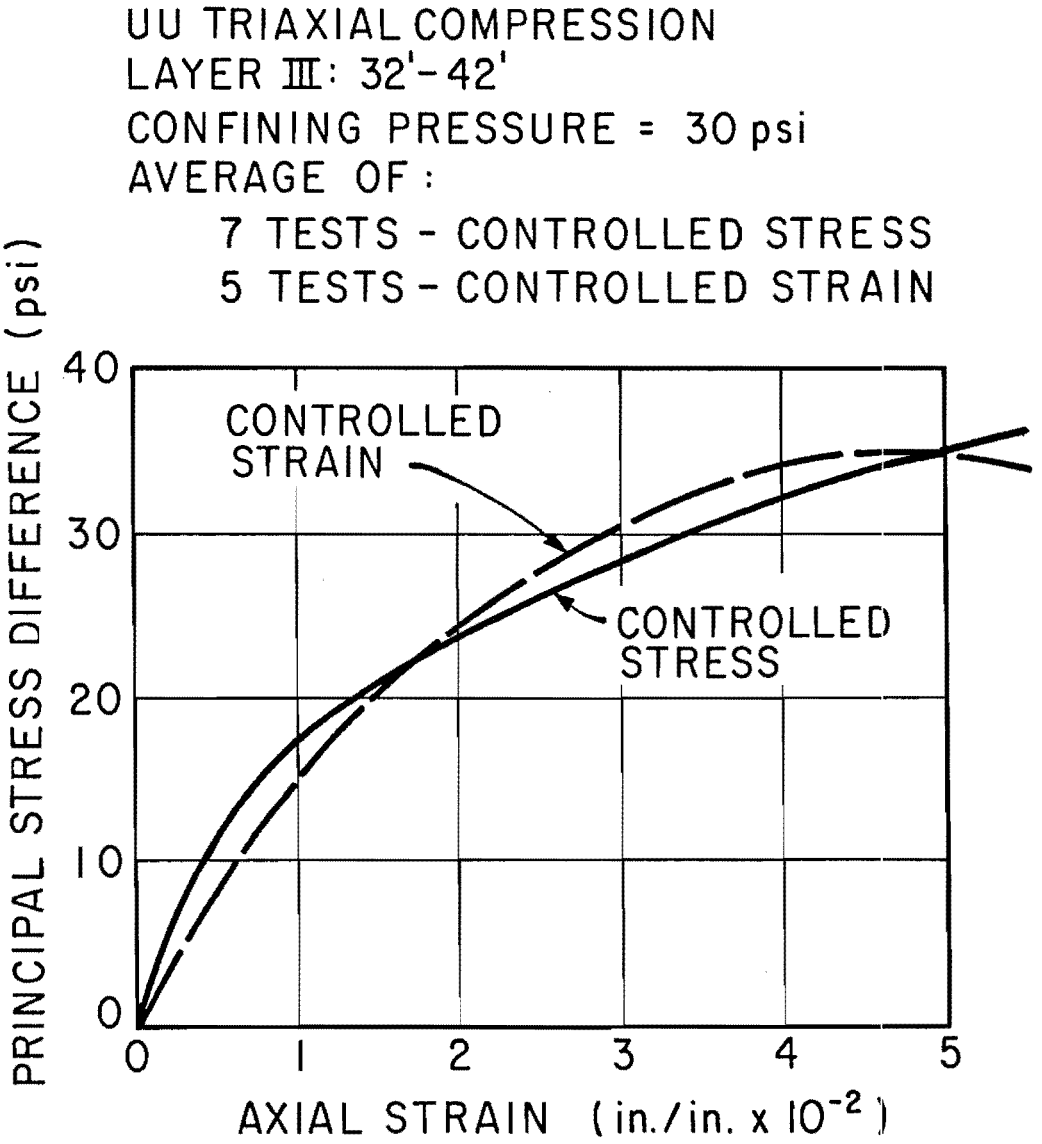

Fig. 7.14. Stress Versus Strain, Layer III, Triaxial Compression (30 psi)

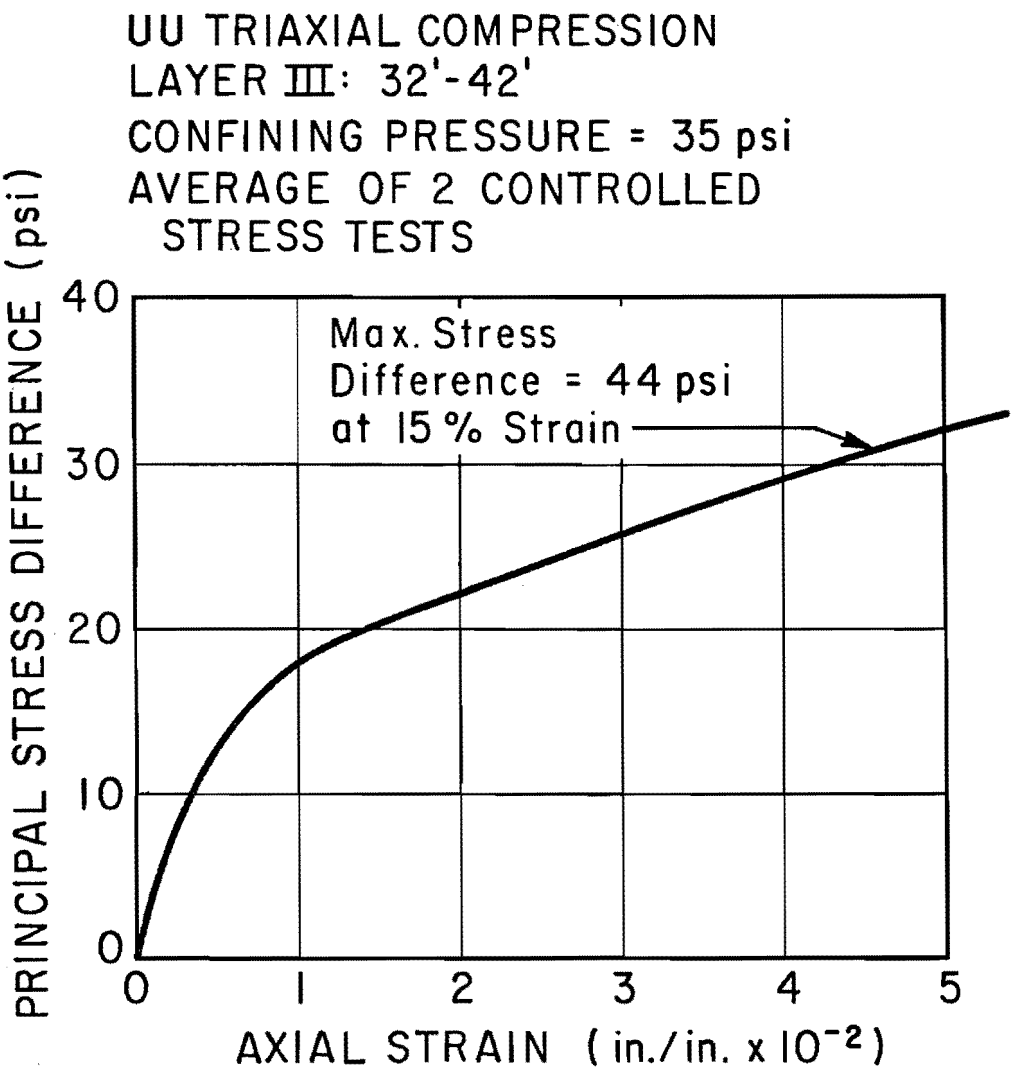

Fig. 7.15. Stress Versus Strain, Layer III, Triaxial Compression (35 psi)

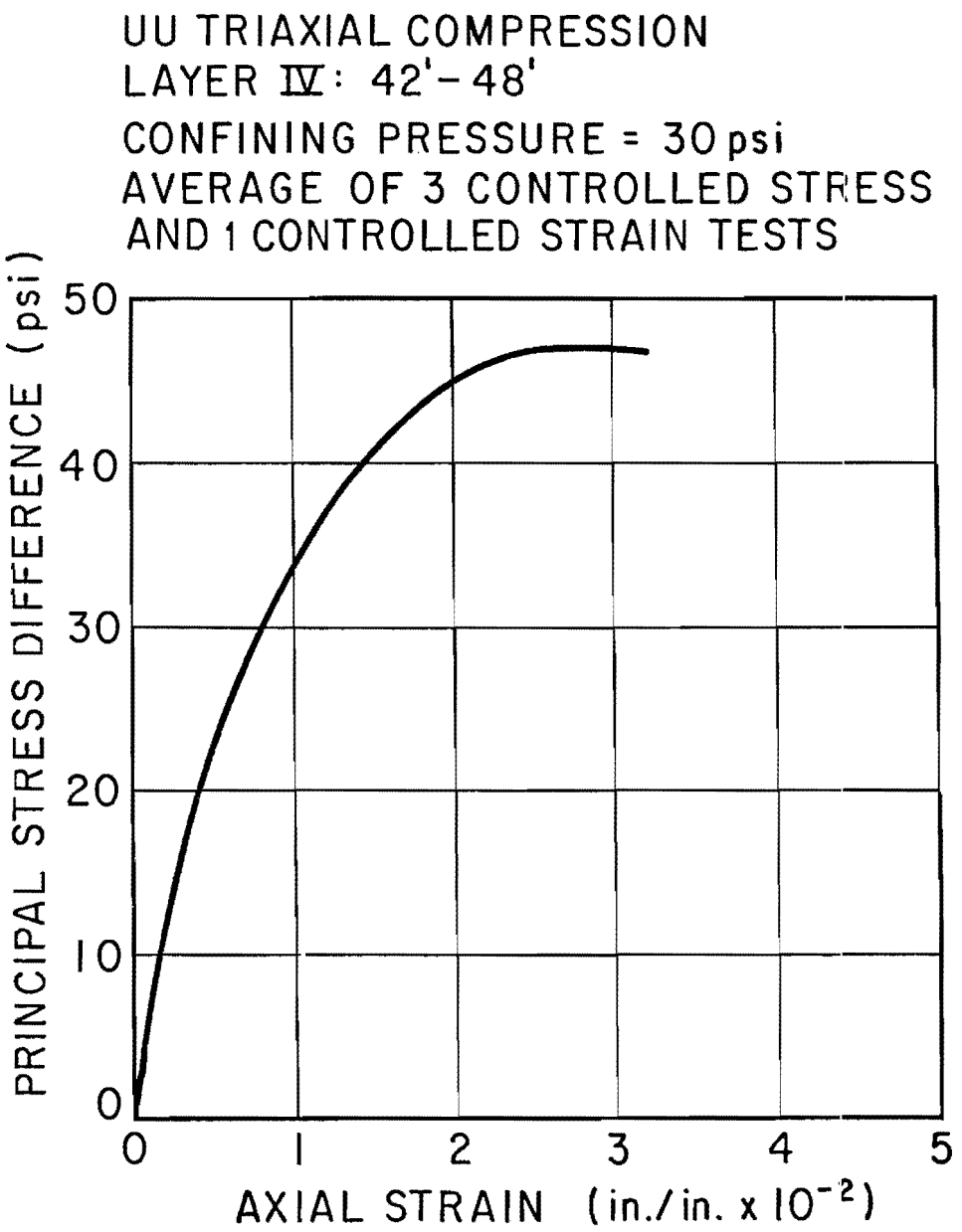

Fig. 7.16. Stress Versus Strain, Layer IV, Triaxial Compression (30 psi)

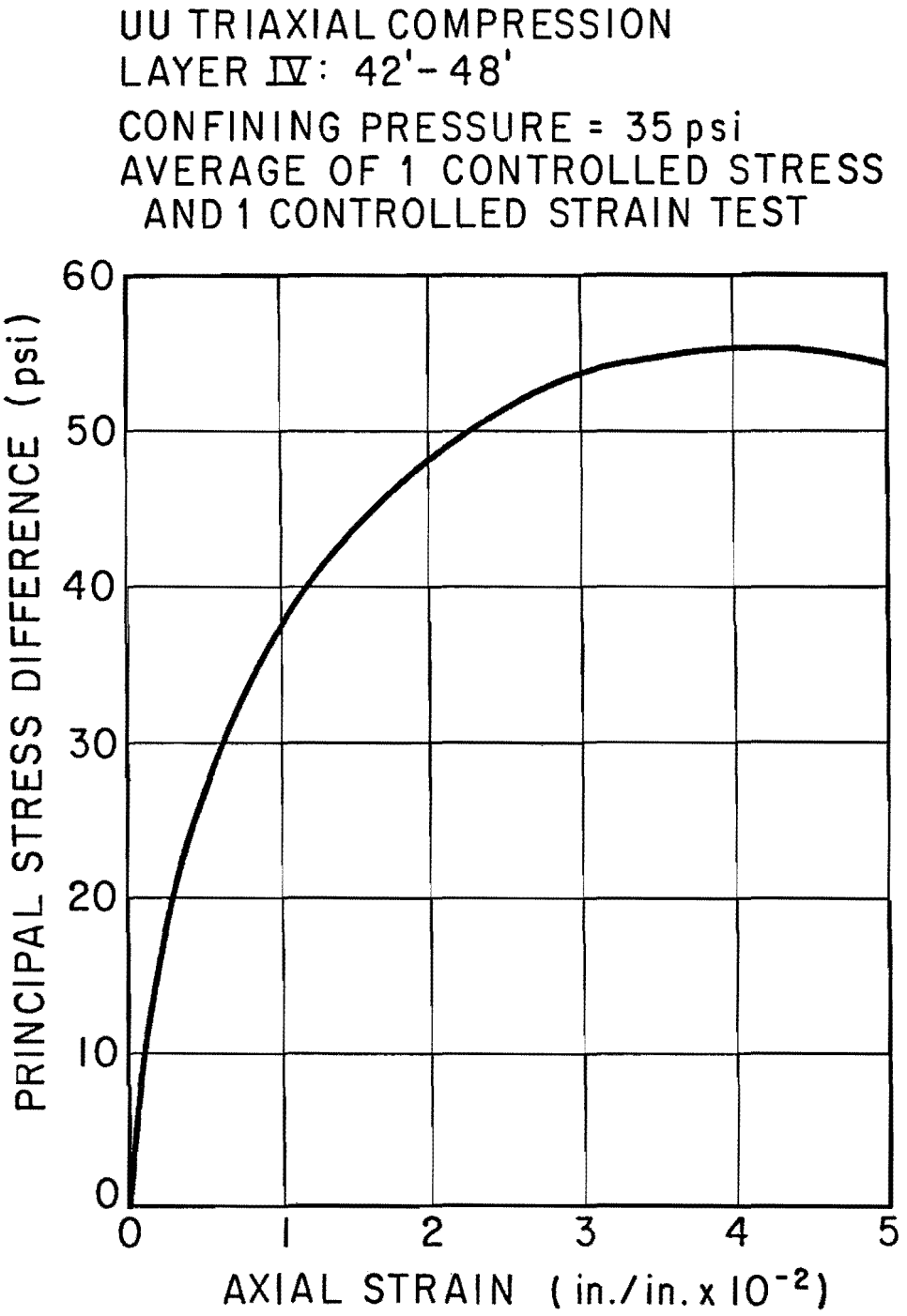

Fig. 7.17. Stress Versus Strain, Layer IV, Triaxial Compression (35 psi)

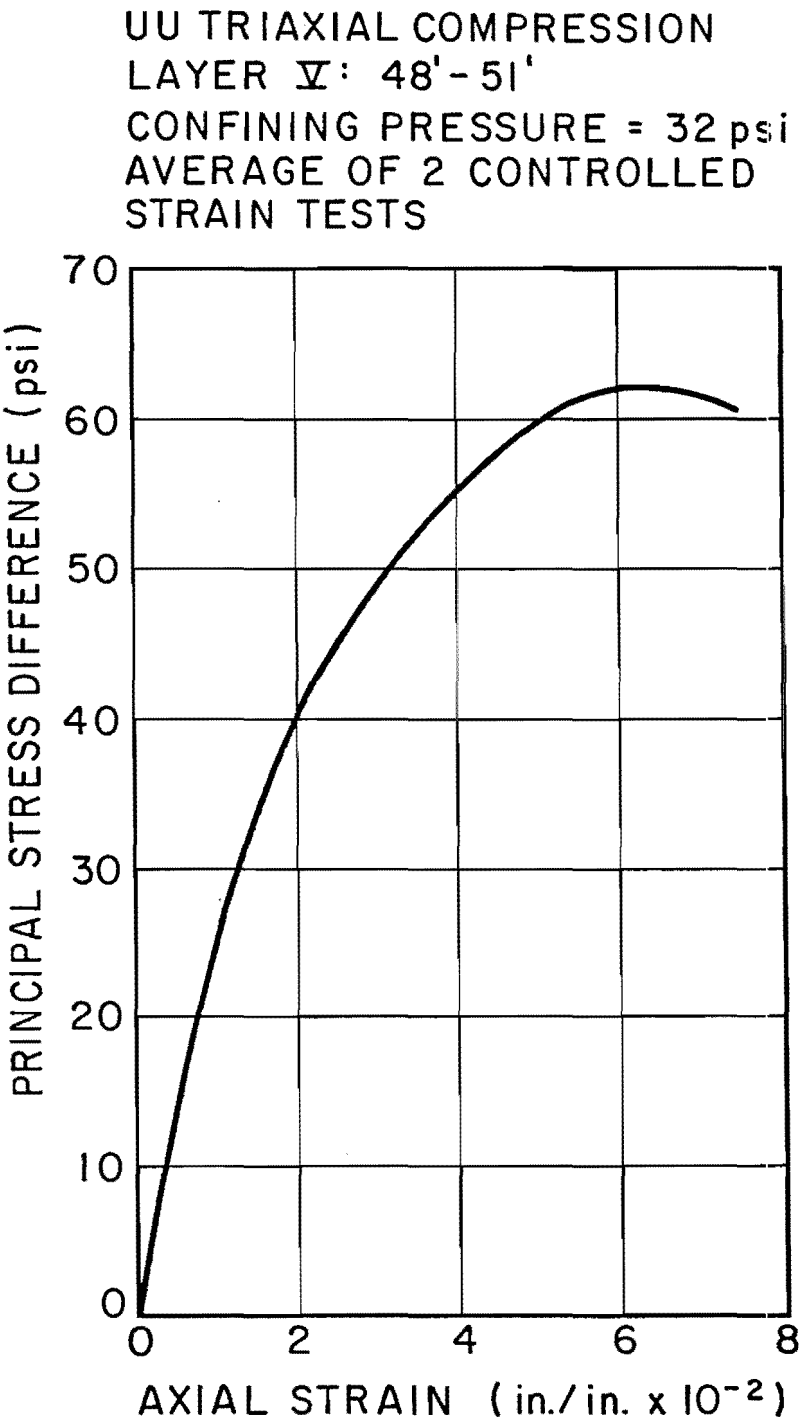

Fig. 7.18. Stress Versus Strain, Layer V, Triaxial Compression (32 psi)

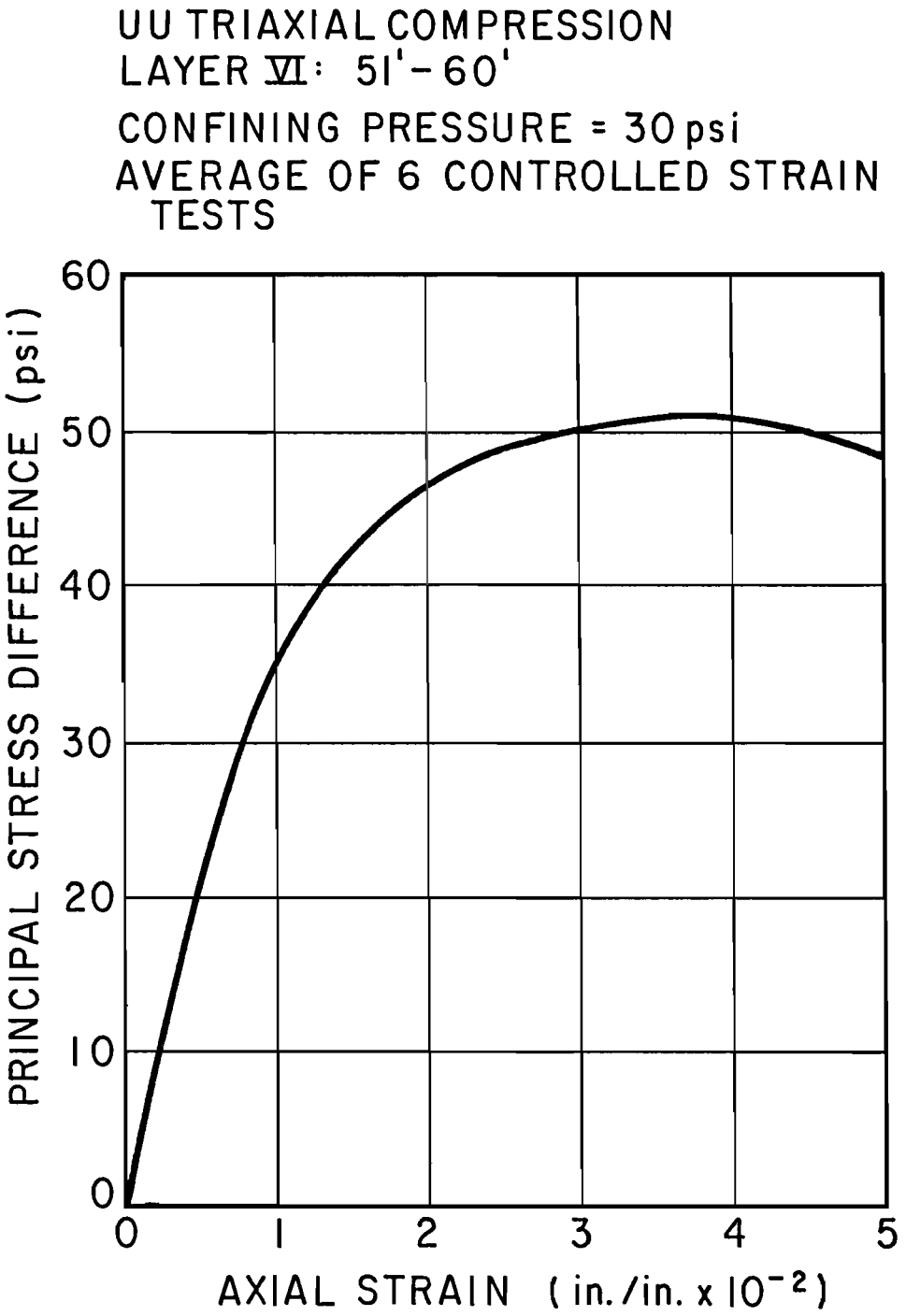

Fig. 7.19. Stress Versus Strain, Layer VI, Triaxial Compression (30 psi)

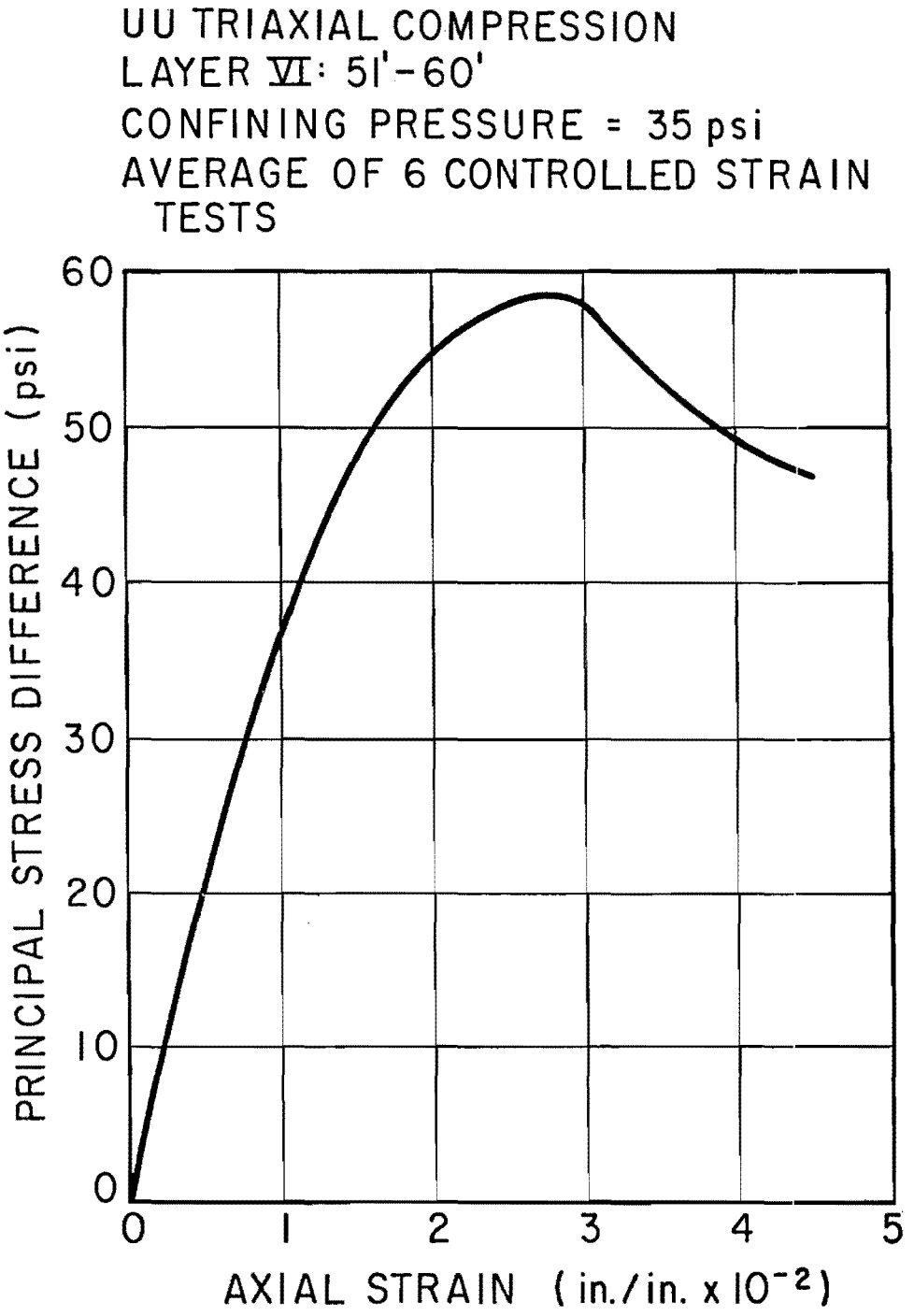

Fig. 7.20. Stress Versus Strain, Layer VI, Triaxial Compression (35 psi)

controlled stress relationships were more nonlinear than those for the controlled strain tests, as would be expected, but the initial tangent modulus, E_o, was slightly greater for the former. This difference in moduli can be explained at least partially by the fact that soil taken from different boreholes and taken at different times was used in the two testing sequences. In any event, the difference is not appreciable.

The unconfined tests yielded higher initial tangent moduli than did the triaxial tests in Layers I and III. This fact is possibly a reflection of the greater strain rate used in testing the unconfined specimens. No unconfined tests were conducted for specimens below Layer III.

The failure strains were approximately 3.5 per cent in Layers I, IV, and VI, 20 per cent in Layer II, and 6 per cent in Layer III and Layer V.

Mohr's circles have been drawn for each confining pressure and a Mohr-Coulomb failure envelope has been constructed for Layer I in Fig. 7.21. Considerable judgement is required in selecting a representative failure envelope. The apparent cohesion, c_u, was observed to be 10.5 psi, while the indicated angle of internal friction, ϕ_u, caused by fissures and partial saturation, was 14 degrees. Sufficient data were obtained from Layer III to allow a reasonably accurate establishment of values for c_u and ϕ_u, which were 15.4 psi and 10 degrees, respectively. Excessive scatter or lack of a sufficient number of different confining pressures did not permit an accurate appraisal of c_u and ϕ_u for other layers.

UU Triaxial Compression Tests (Multiple Phase Shear - T.H.D.). Soil from Boring H-3, recovered in November, 1967, was tested by the T.H.D. Houston Urban Expressways (H.U.E.) Office Laboratory. The "transmatic" triaxial cell was used in all tests. The transmatic cell is similar to a

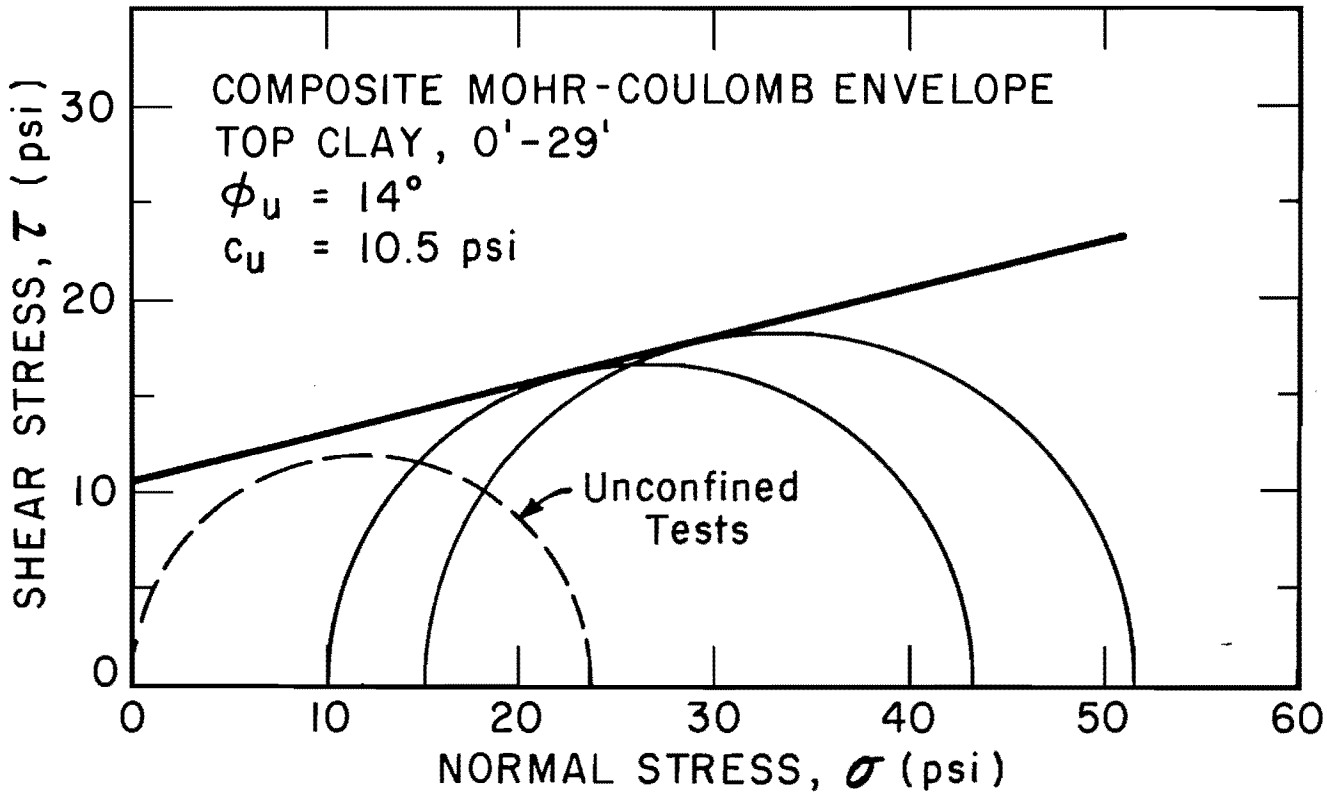

Fig. 7.21. Mohr-Coulomb Envelope for Layer I

usual triaxial cell in design, except that the proving ring is placed directly on top of the specimen inside the cell as shown in Fig. 7.22. Load is applied directly to the top part of the cell, which is free to move downward as the specimen deforms. This operation eliminates the need for a piston and consequently provides a more accurate means of measuring σ_1. The procedure used by H.U.E. was to test three-inch-diameter by six-inch-long specimens confined initially at a pressure somewhat less than the overburden pressure. The specimen was loaded at a constant strain rate until the loading rate was reduced to a small value (about 0.2 psi per 0.1 per cent strain). The stress at this loading rate was taken to be the failure stress corresponding to the applied confining pressure, and the confining pressure was increased. The specimen was again loaded until the loading rate was reduced to the same small value, and a failure stress was recorded. This process was repeated for a third confining pressure greater than the in situ overburden pressure. A Mohr-Coulomb envelope was drawn for the specimen, and the shear strength was then obtained from the envelope by taking the shear strength corresponding to the computed in situ overburden pressure.

A strength profile, similar to those for U.T. unconfined and triaxial tests, was plotted for the transmatic tests in Fig. 7.23. Less scatter was evidenced in the transmatic results, but the average shear strength was considerably less than the shear strength from the U.T. triaxial profile. The discrepancy can be explained by the difference in sample size, the difference in test procedure (for example, incomplete failure in multiphase tests), and possible differences in the soils tested. Figure 7.24 presents average rupture envelopes and relative values of the soil

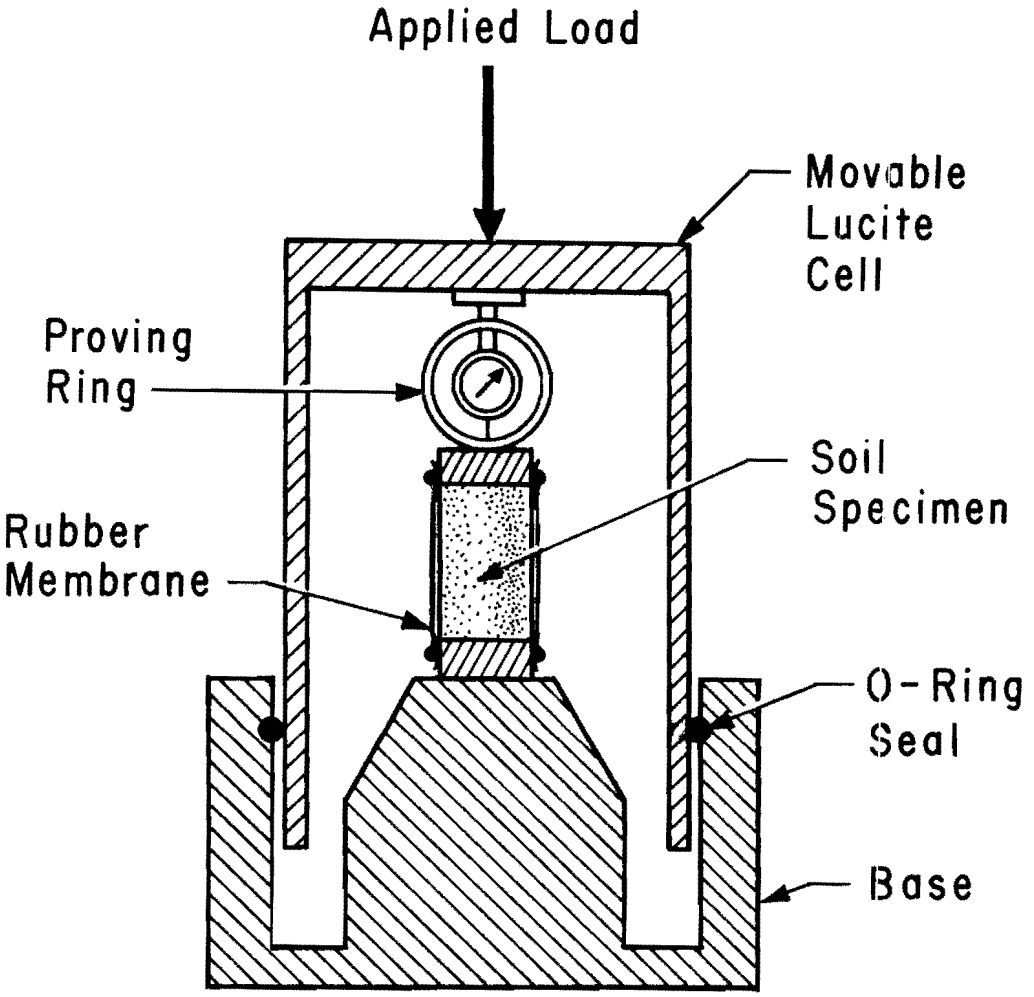

Fig. 7.22. Transmatic Triaxial Cell

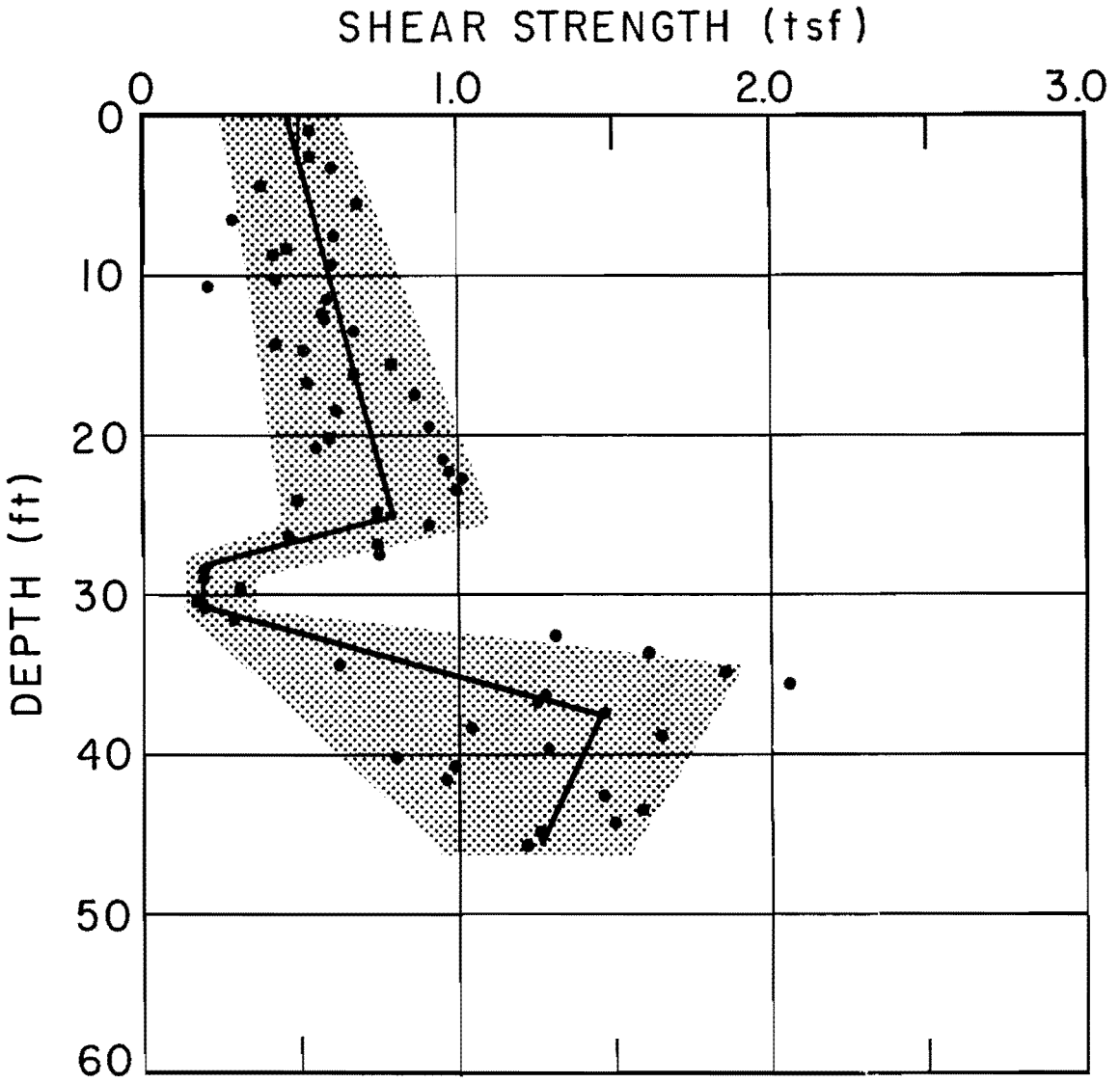

Fig. 7.23. Shear Strength Profile - Transmatic Triaxial Test

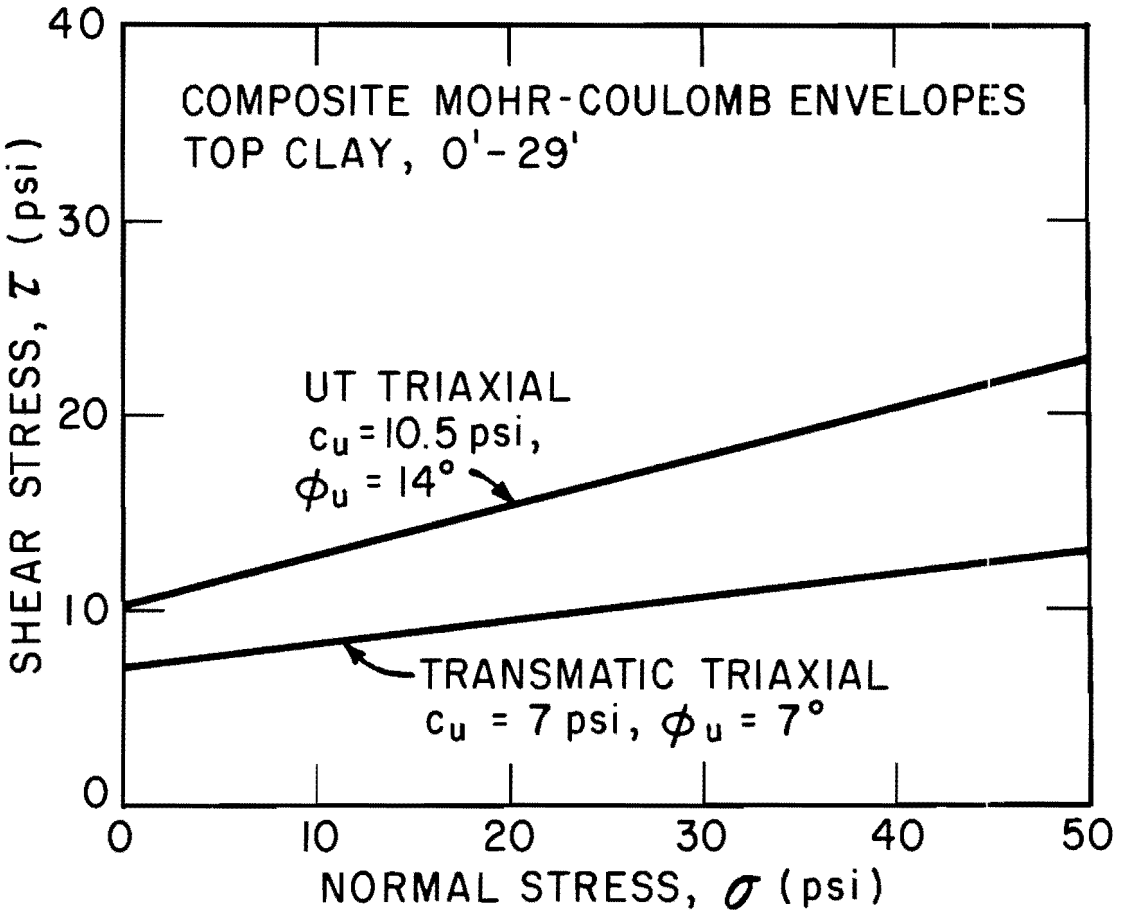

Fig. 7.24. Comparison of Failure Envelopes for Layer I

parameters c_u and ϕ_u indicated by the transmatic procedure as compared to the U.T. triaxial procedure for Layer I. Although the depth interval spanned by Layer I (0 to 29 feet) is perhaps too large to permit the values shown to be altogether meaningful, Fig. 7.24 is believed to be a valid indication of the real differences in the procedures, at least for the case reported herein. Such a comparison for an appropriately small depth interval within Layer I would be unwarranted because of the scatter in indicated shear strength and the lack of a number of tests sufficiently large to provide an adequate definition of the rupture envelopes in any reasonably small depth interval.

Direct Shear. Direct shear tests were performed on soil from Borings H-2 and H-5. Test specimens were trimmed from core samples to 2.8 inches in diameter by approximately one inch in height for testing. The cylindrical specimens were then sheared along the midplane at a constant rate of deformation of 0.04 inches per minute. Each test was completed in less than five minutes. Since the direct shear tests were performed in conjunction with the mortar migration studies (described later), the normal pressure employed was the estimated lateral pressure between the concrete in the shaft and the soil. This pressure was taken approximately as the overburden pressure or 21 psi, whichever was smaller. Since failure was forced through a predetermined horizontal surface, the strength measured in direct shear is expected to lie between the intact and fissured strength for Beaumont Clay, whose fissure pattern appears to be random. Test results are tabulated in Appendix C. Stress-displacement curves are given in the section on mortar migration studies under the designation "plain soil." The strength profile obtained from the direct shear tests is

presented in Fig. 7.25. No attempt was made to cycle the load or otherwise to develop the residual strength of the soil in these tests because suitable equipment was unavailable.

T.H.D. Penetrometer. The T.H.D. penetrometer is a dynamic device commonly used by the Texas Highway Department for assessing the strength of soil when more elaborate procedures are not justified or when subsurface conditions do not permit recovery of undisturbed specimens. The penetrometer, described in detail by Vijayvergiya, Hudson, and Reese (1969), is a three-inch diameter cone with a point angle of about 60 degrees. In its operating position, it is attached to the end of a drill stem and set at the bottom of a borehole. After the cone is seated, readings are obtained by dropping a 170 pound hammer through a distance of two feet onto the top of the drill stem. The number of blows required to advance the penetrometer six inches is recorded. This process is routinely repeated for a second six-inch penetration. In clays, the readings for the first and second six inches are about the same, while more blows are usually required for the second six inches in granular soils. By taking penetrometer readings at a number of depths, a strength profile can be established for clay soils with the aid of the cone penetrometer correlation curve given in Fig. 1, p. 4-43, of the T.H.D. Foundation Manual (Texas Highway Department, 1964). That curve, obtained by correlating results of triaxial tests with cone penetrometer values in a number of Texas soils, is almost linear over a wide range of penetrometer values. Shear strength in tons per square foot is obtained approximately by dividing the number of penetrometer blows per foot by 38 (up to 100 blows per foot). The correlation given in the aforementioned manual is a conservative one, since it is

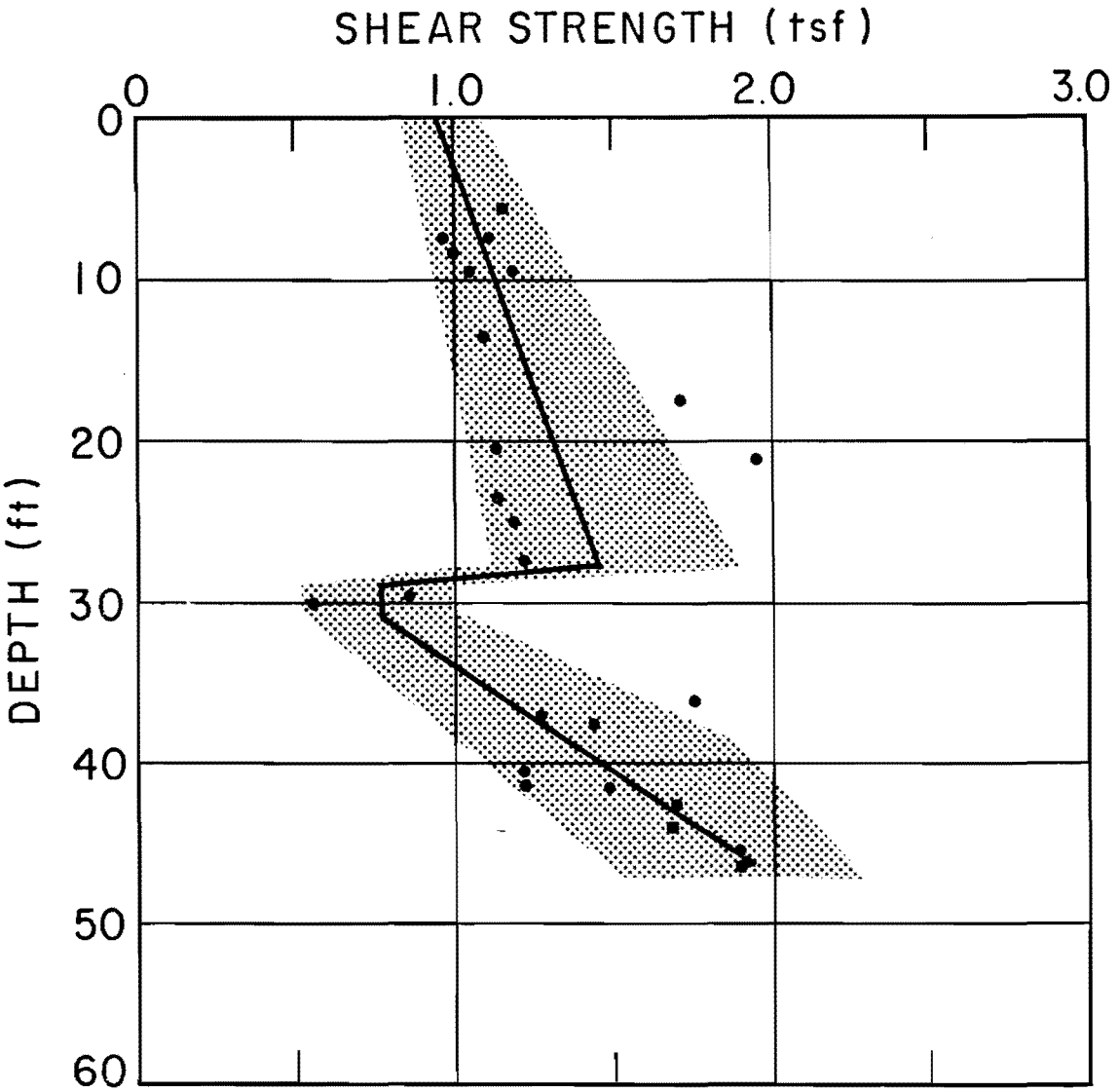

Fig. 7.25. Shear Strength Profile - Direct Shear Test

intended for routine use in the design office. In reality, the shear strength so obtained is probably a lower limit to the true shear strength profile.

Penetrometer readings were taken in Boring H-4 in November, 1967, and in Boring H-5 in August, 1969. The results are tabulated in Appendices A and C, and a shear strength profile as indicated by the T.H.D. penetrometer is shown in Fig. 7.26.

Although comprehensive studies of correlation of T.H.D. penetrometer results with the standard penetration test (split spoon penetrometer) have not been reported, the standard penetration test appears to require almost exactly half as many blows to advance the split spoon penetrometer the same distance as the T.H.D. cone penetrometer in the range of 8 to 80 blows per foot for the T.H.D. penetrometer.

Pocket Penetrometer. Pocket penetrometer tests were run on reasonably intact chunk samples of soil taken from end trimmings of test samples at the test site immediately after recovery. While the reliability of this method of measuring shear strength is questionable, the pocket penetrometer did provide a more direct measurement of the strength of the intact, or unfissured, soil. The strength profile indicated by the pocket penetrometer is shown in Fig. 7.27.

Comparison of Results of Strength Tests

Strength profiles obtained by the various methods are replotted in Fig. 7.28 for purposes of comparison. It is readily apparent that vastly different results were obtained from the several testing methods employed. The manner in which the strengths are ordered is not unreasonable, but

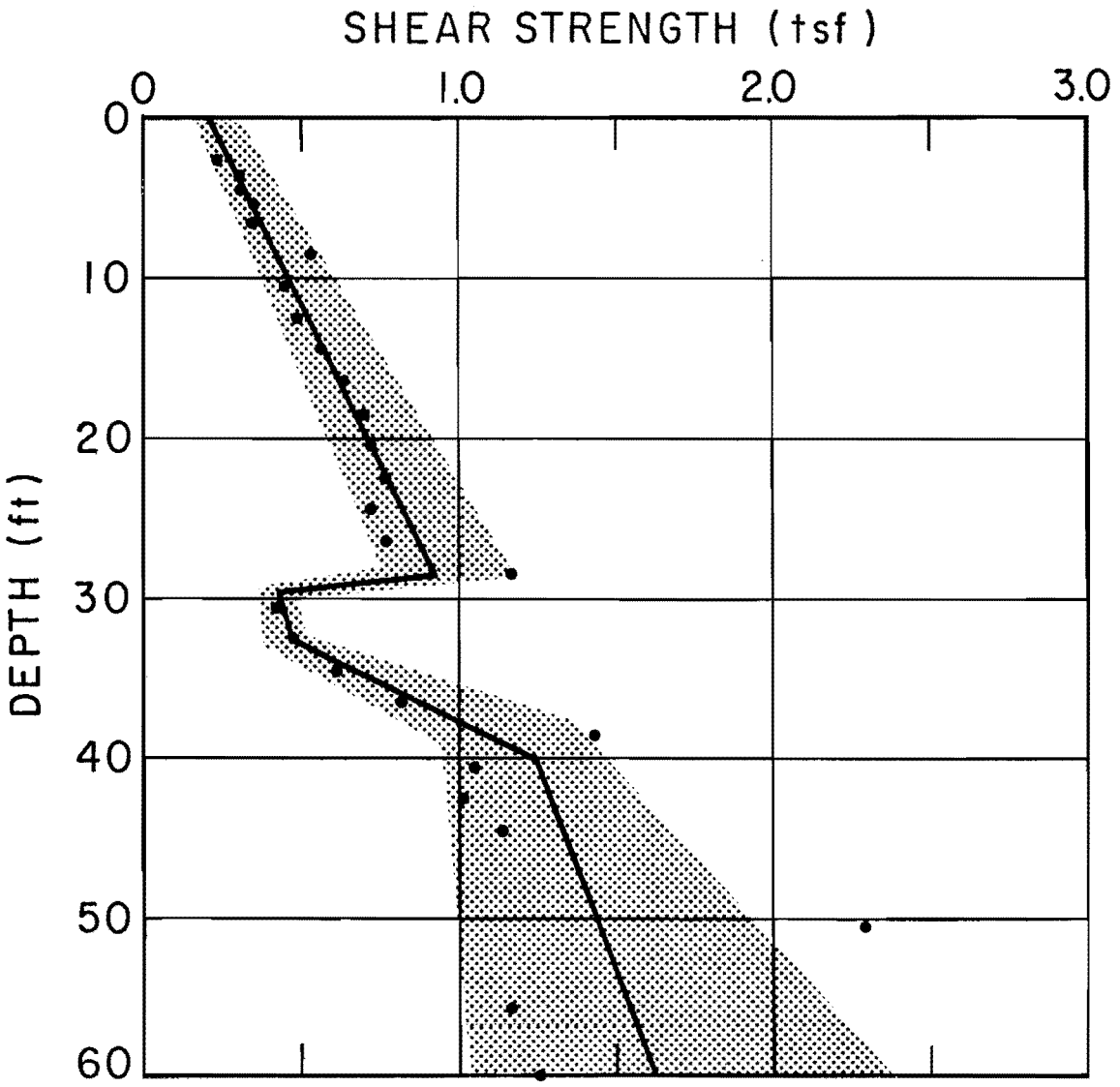

Fig. 7.26. Shear Strength Profile - T.H.D. Cone Penetrometer

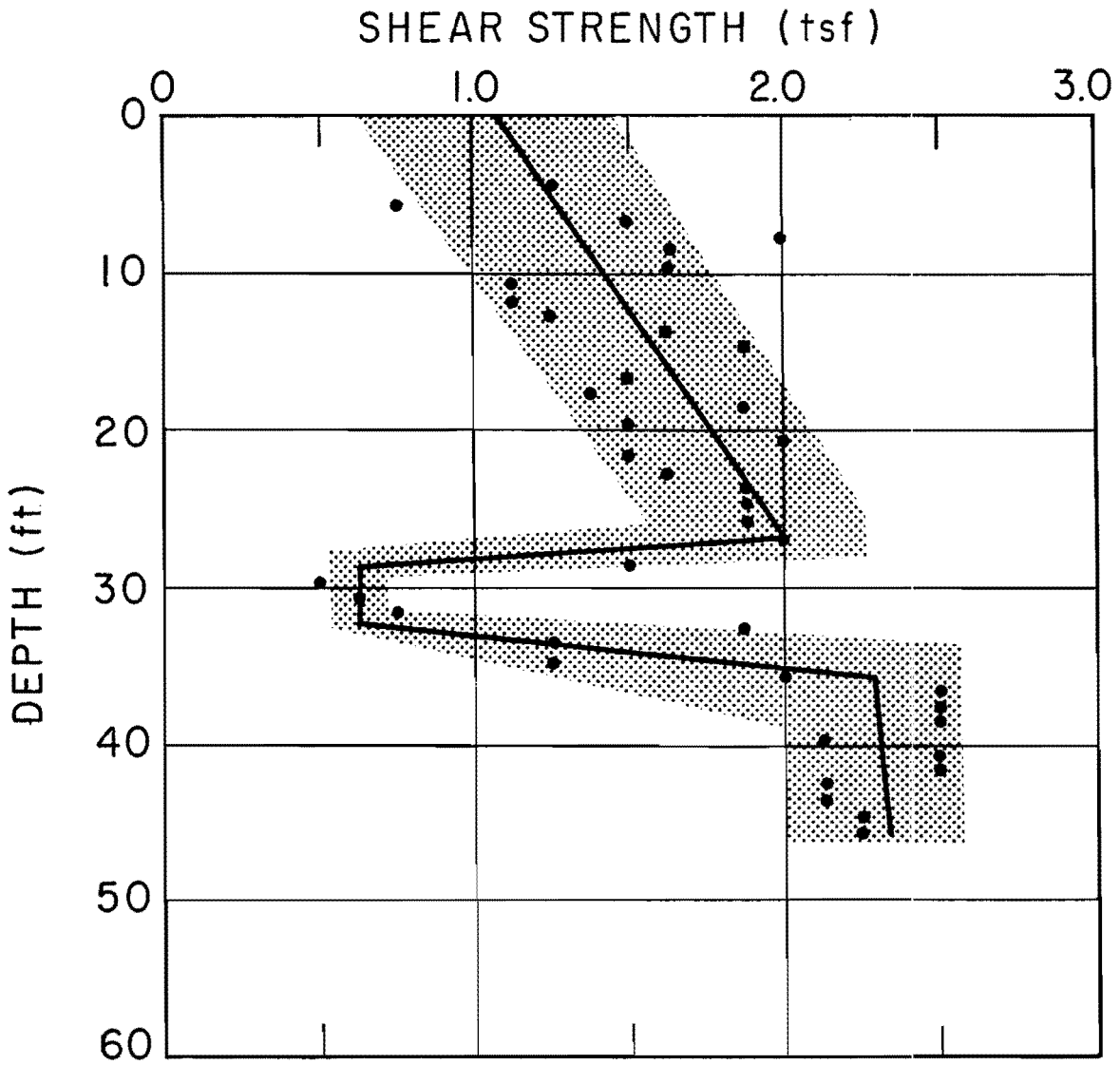

Fig. 7.27. Shear Strength Profile - Pocket Penetrometer

the differences in magnitudes are surprising. The highest strength values were obtained from pocket penetrometer tests on chunk samples, while the lowest were obtained from the T.H.D. penetrometer and transmatic triaxial tests. Some of the possible reasons for measuring lower strengths in the transmatic procedure compared to the U.T. triaxial method have been mentioned. The T.H.D. penetrometer is purposely conservative. Unconfined test results are undoubtedly lower than the U.T. triaxial test results because of differences in sample size and other problems related to fissuring. Finally, indeterminate stress conditions in the soil in the shear box and the possibility of progressive failure in the direct shear specimens make meaningful comparisons between the direct shear and triaxial tests difficult. The direct shear tests did, however, give smaller shear strength values than did the U.T. triaxial tests, except in Layer II.

Figure 7.28 should serve as a reminder that the soil testing procedure used to obtain a strength profile to which measured stresses from drilled shaft load tests are referred is extremely important. All values of the various factors reported in Chapter XII are based on the shear strength profile designated "U.T. Triaxial." It is felt that this profile is a realistic representation of a value of shear strength between the fissured strength and the intact strength, which approximates that strength effective in affording side resistance. Furthermore, it gives generally greater strengths than the other standard procedures, which makes it desirable from the standpoint of conservatism in reported values of shear strength reductions and bearing capacity factors.

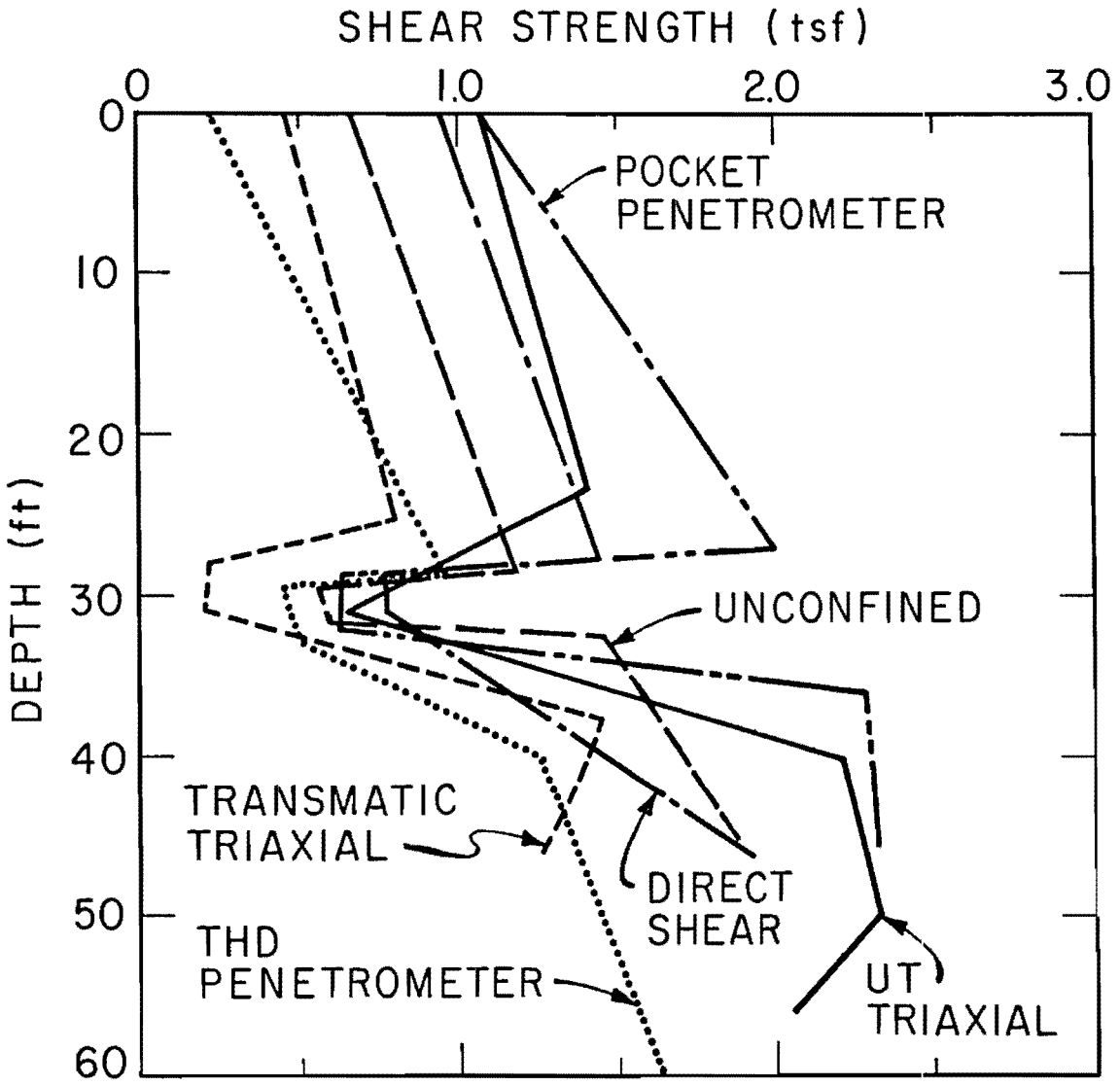

Fig. 7.28. Comparison of Shear Strength Profile Obtained by Various Methods

Mortar Migration Studies

The second principal laboratory effort was to attempt to determine the effect of placing wet concrete against soil on the shear strength of the soil. Generally, concrete used in drilled shaft construction contains considerably more water than is required for hydration of the cement, excess water being provided to enhance workability. It has been suggested (Meyerhof and Murdock, 1953) that water not required for hydration tends to migrate into the soil forming the borehole walls and softens it. This softening action causes a strength reduction, which can be evaluated numerically by employing Eq. 7.1 or Eq. 7.2, provided numerical values of moisture content increase in the soil are known. If the pore size is great enough, mortar will also migrate some distance into the soil, with the tendency that strengthening may occur in the soil adjacent to the concrete.

The problem of shear strength reduction due to migration of water from wet concrete into the soil has been analyzed by Chuang and Reese (1969). Those investigators cast specimens of concrete mortar against specimens of soil and monitored moisture content and shear strength changes in the soil. Numerous tests on soils with various properties showed that several parameters controlled the magnitude of softening that occurred:

1. Soils with very low initial moisture content imbibe water much more freely than those at higher initial moisture content. For example, a remolded clay of high plasticity (CH) with initial moisture content of 10.5 per cent increased in moisture content by 6 per cent when wet concrete was cast against it, whereas the same soil molded at 21 per cent initial

moisture content increased by only about 0.5 per cent. Type I cement was used to make the concrete mortar, which had a water-cement ratio of 0.6 (by weight) and which was pressed against the soil for several days under 5 psi surcharge pressure. Some specimens were allowed to cure under atmospheric pressure. These results confirmed, at least qualitatively, the tests of DuBose (1956).

2. The average moisture content increase diminishes as the mean grain size of the soil becomes smaller.
3. The average moisture content increase is greater by 10 to 20 per cent for surcharge pressures of 5 psi than for zero surcharge pressures.
4. Water-cement ratio has a very significant influence on moisture migration. For example, for a CH material with an initial moisture content of 13 per cent, a water-cement ratio of 0.5 caused an increase in moisture content of 3.8 per cent in the soil in the one-inch nearest the concrete. When the water-cement ratio was increased to 0.9, the corresponding moisture content increase was 10.1 per cent. (The water-cement ratio specified by the Texas Highway Department for drilled shaft concrete is 0.6.)
5. Approximately one-third more water migrated out of mortar made with Type I cement than that made with Type III cement.

Chuang and Reese also made the following observations concerning the effect of migration of moisture and mortar on the shear strength of soils against which mortar was cast:

1. For soils with pore spaces larger than cement grain size, both cement and water migrate into the soil, possibly causing an increase in shear strength. For clay, only water penetrates the soil, however.
2. For clay and sandy clay specimens, in which mortar having a water-cement ratio of 0.6 was cast against soil with a surcharge of 10 psi and allowed to cure for seven days, the weakest plane occurred at one-fourth inch away from the concrete-soil interface. Depending on initial moisture content, the ratio of softened shear strength to original shear strength (that is, α , the shear strength reduction factor) was observed to vary from about 0.4 (initial moisture content about 8 per cent) to 0.7 (initial moisture content about 22 per cent).

Chuang and Reese concluded that the most significant parameters influencing migration of water and cement mortar from concrete to soil were soil type (for example, unified classification types CL, CH, or SC), the initial moisture content of the soil, and the water-cement ratio of the concrete. The surcharge pressure was also thought to have an important influence on the shear strength reduction factor.

In the present study soil from Borings H-2 and H-5 was subjected to mortar migration tests to attempt to determine the effect of casting wet concrete against soil from the SH225 site, using a laboratory procedure suggested by Chuang and Reese. Specimens were trimmed to 2.8 inches in diameter and placed in the bottom half of a direct shear box, with a prescribed amount of soil protruding above the shear plane, as shown

schematically in Fig. 7.29. After the top of the shear box was set in place, mortar mixed with Type I cement at a water-cement ratio of 0.6 and sand-cement ratio of 3 (by weight) was cast on top of the soil. Mortar with these components is assumed to cause the soil to undergo the same moisture changes as would occur with the concrete mix generally used to construct drilled shafts. The distance between the shear plane and the top of the protruding soil was made equal to the distance from the soil-mortar interface at which the specimen was to be later sheared. The inside periphery of the top of the box was coated with grease to impede bonding between the mortar and the box. Generally the specimens could be easily removed from the box after testing, although some force was occasionally required to extract the mortar blocks.

A normal pressure, predetermined by a method explained later to be equal to the estimated lateral pressure between soil and concrete in a drilled shaft, was then applied to the mortar, and the specimen was allowed to cure for one week. Soil-mortar specimens were kept moist during the curing period by wrapping the shear boxes in which they were cured with damp rags.

Each test series consisted of several specimens cut from the same six-inch sample and cast identically, except that the failure plane was established at the soil-mortar interface as well as at various distances therefrom, up to one-half inch away. The top of the soil specimen, which became the soil-mortar interface, was leveled and smoothed by trimming it with a sharp straight edge. Watt, Kurfurst, and Zeman (1969) suggest that trimming the specimen in this manner causes a disturbance comparable to that produced by the action of the mechanical auger when the borehole is cut.

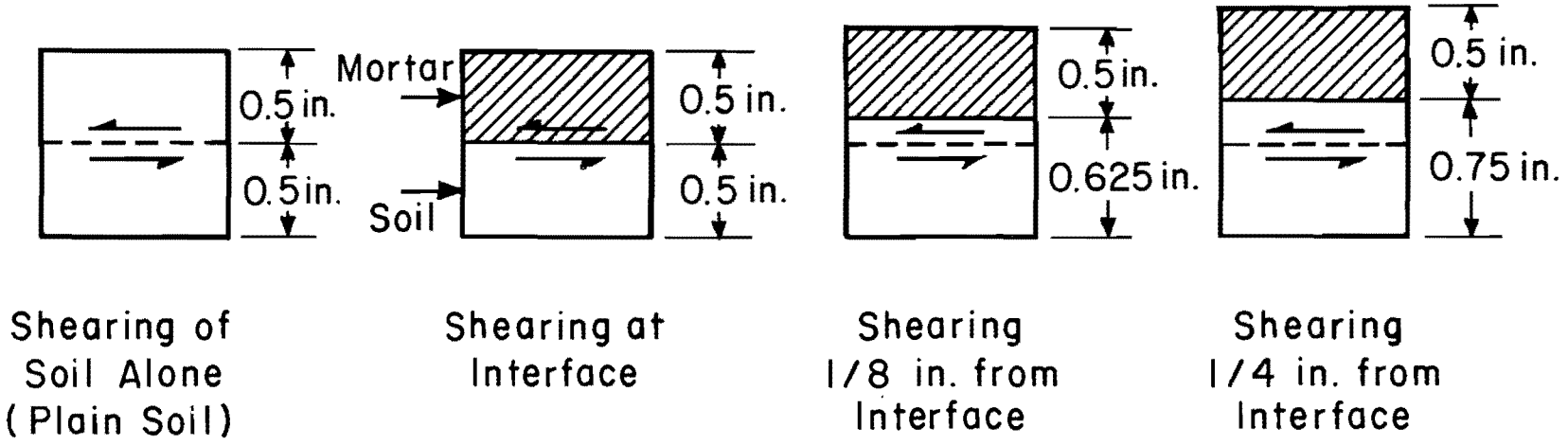

Fig. 7.29. Mortar Migration Test

After the seven-day cure period, the soil-mortar samples were sheared along a horizontal plane using a 0.04 inch per minute displacement rate. During shear, the normal stress which was imposed during curing was maintained. In addition, one specimen of plain soil was sheared immediately after trimming. All specimens were tested at the same normal pressure in a given test series, including the plain soil specimen. Specimens were sheared with an M.I.T. direct-shear testing machine, which operates by jacking the bottom half of the shear box away from the top half at a constant rate of deflection. The top half of the box was held in place by a horizontal yoke supported on a proving ring, which was used to measure load. Shearing displacement between top and bottom sections of the box was read directly with dial indicators. After each specimen was sheared, moisture contents at various distances from the interface were obtained.

The ratio of the maximum shear strength of each soil-mortar specimen to the shear strength of the plain soil was calculated in each test series. This provided a relationship for α as a function of distance from the interface for a sample of soil at a given depth. The minimum value obtained from that relationship was taken to be the α factor for the soil being tested. The distance from the interface at which that minimum value occurred is the weakest plane, and is the plane along which shearing would be predisposed to occur in soil immediately adjacent to the concrete in a drilled shaft if the laboratory test is truly representative of <u>in situ</u> behavior.

Horizontal surfaces were selected as shear planes for a matter of convenience. Although the shear strength of a specimen sheared along such a plane is possibly different from that of a specimen sheared vertically as

in the case of the prototype drilled shaft, the ratios of softened shear strength to plain soil shear strength are assumed to be invariants of the orientation of the shear plane.

The magnitude of normal pressure used undoubtedly has some effect on the migration of mortar and water. The lateral pressure which exists between the concrete and soil in the field is the appropriate value to be employed. Unfortunately, this is a variable, indeterminate quantity. Experimentation with lateral earth pressure gages to determine lateral earth pressure against drilled shafts (Reese, Brown, and Dalrymple, 1968) has been largely inconclusive. Consequently, the assumption has been made that the lateral earth pressure remains equal to the hydraulic pressure of the wet concrete against the sides of the borehole. This assumption appears to be justified, at least at the SH225 test site, because strain gages inside the shaft indicated a net expansion of the concrete during curing instead of the expected contraction. Furthermore, it is expected that a gradual increase in lateral earth pressure may occur as a result of creep in the soil. Thus, the horizontal fluid concrete pressure would be a lower limit to the lateral pressure existing between the concrete and soil.

The value of lateral pressure from the concrete at the time of pour was estimated from the A.C.I. procedure for computing lateral pressure against formwork (American Concrete Institute, 1963). For the rapid rates of placement employed in constructing the test shafts, that procedure indicates that the lateral pressure is hydrostatic up to the depth at which the pressure is 21 psi and remains constant at 21 psi below that depth. Since the hydrostatic pressure of the concrete is nearly equal to the overburden pressure of the soil, the form pressure, or value of the

normal pressure, was taken to be approximately the overburden pressure in the soil at the depth from which the soil sample was extracted or 21 psi, whichever was smaller. Occasional exceptions were made to this rule to attempt to gain some insight into the effect of normal pressure on α. Insufficient data were accumulated concerning this point to allow conclusions to be drawn, however.

The results of the mortar migration tests are summarized in Tables 7.3 through 7.6. Atterberg limits were estimated from the basic curve, Fig. 7.1. Each value of moisture content tabulated is actually an average value obtained from two to four shear tests for the sample of soil under test. In the test on sample H-5-6 all soil-mortar specimens were sheared at three-eighths inch from the interface. The α values from the tests on specimens H-2-9, H-2-10, and H-2-28 were excluded when computing the average α values for various distances from the interface because the specimens appeared quite heterogeneous. The average moisture content and α values recorded at the end of each table for each layer are numerical averages of the tabulated individual values, except those noted to be excluded. The value α_{min} is the average of the minimum values for each specimen. It is observed that this average is not necessarily equal to the smallest value from the average α-versus-distance from interface profile. Weighted averages are also shown for α_{min} where they differ from the numerical averages. The weighted averages take account of the length of shaft each test specimen represents in computing the average. In a few cases, an error in procedure was discovered. Results in such cases were not reported, but the word "error" has been entered in the table instead.

TABLE 7.3. SUMMARY OF MORTAR MIGRATION RESULTS, LAYER I

Class.	Sample	Depth (feet)	Description	Nat.M.C.* (%)	P.L. **	L.L. **	Moisture Content After Test Distance from Interface (ins.)				α - Values				α_{min}	Remarks
							0-1/8	1/8-1/4	1/4-3/8	3/8-1/2	0"	1/8"	1/4"	3/8"		
CH	H-2-1	5.5	Tan & gray clay	26.4	24	60	27.0	27.6	27.5	27.2	1.01	0.52	0.59	0.63	0.52	Form pressure
CH	H-5-6	7.5	Tan & gray clay	20.3	26	62	21.8	22.2	22.1	22.1	----	----	----	0.93 1.01 0.93	0.93	Form pressure
CH	H-2-3	7.5	Tan & gray clay	22.8	26	62	22.7	20.4	21.9	----	0.76	0.81	0.86	0.79	0.76	Form pressure
CH	H-5-7	8.5	Tan & gray clay, stiff	28.0	26	63	26.0	26.2	26.7	26.2	1.07	----	Error	----	1.07	Form pressure
CH	H-2-5	9.5	Yellow & gray clay	28.2	27	63	30.1	30.8	30.9	----	0.90	0.98	0.88	0.47	0.47	Form pressure
CH	H-5-8	9.5	Tan & gray clay; calcareous material	29.3	27	63	28.2	28.5	28.1	27.9	1.03	0.95	0.88	----	0.88	20 Psi
CH	H-2-9	13.5	Tan & gray clay with sand pockets	----	23	63	17.9	17.5	18.5	----	1.15	1.22	1.63	0.90	0.90	Form pressure[1]
CH	H-2-10	14.5	Tan & gray clay with sand pockets	19.2	22	62	18.2	17.5	17.3	----	1.15	1.09	0.94	1.09	0.94	Form pressure[1]
CH	H-2-13	17.5	Tan clay	23.3	18	54	20.2	20.1	19.7	----	0.91	1.28	0.87	0.88	0.87	Form pressure
CH	H-5-17	20.5	Stiff red silty clay	23.1	23	56	22.7	22.9	22.9	22.8	1.09	----	1.00	0.99	0.99	Form pressure
CH	H-2-18	21.0	Tan clay	24.8	23	56	22.2	22.8	21.8	----	1.06	0.66	0.72	0.61	0.61	Form pressure
CH	H-5-20	23.5	Stiff red clay	25.6	27	55	24.7	25.4	25.4	25.6	0.97	----	1.02	0.95	0.95	Form pressure
CH	H-2-24	25.0	Tan clay, slightly silty	24.1	26	54	24.4	24.6	24.6	----	1.00	0.98	1.11	0.98	0.98	Form pressure
CH	H-2-28	27.5	Tan clay with silt lenses	22.4	21	52	23.1	24.0	24.7	----	1.23	1.09	----	----	1.09	Form pressure[1]
	Average Layer I			24.0[2]	24	59	23.5	23.6	23.7	25.3[3]	0.98	0.88	0.88	0.83	0.83 0.77	Numerical aver. using $\alpha > 1 = 1$ Weighted aver.

* Average moisture content on trimmings taken before test.
** Atterberg Limits from Basic Curve, Fig. 7.1.

1 α values excluded from grand average.
2 Assuming Natural Moisture Content of 18.0% for H-2-9.
3 Not enough data.

TABLE 7.4. SUMMARY OF MORTAR MIGRATION RESULTS, LAYER II

Class.	Sample	Depth (feet)	Description	Nat.M.C.* (%)	P.L. **	L.L. **	Moisture Content After Test Distance from Interface (ins.)				α - Values				α_{min}	Remarks
							0-1/8	1/8-1/4	1/4-3/8	3/8-1/2	0"	1/8"	1/4"	3/8"		
ML	H-5-26	29.5	Clayey silt	16.3	21	25	16.6	16.3	16.5	15.7	1.31	----	1.50	1.22	1.22	Form pressure
ML	H-2-32	30.0	Clayey silt	29.3	21	24	31.4	30.5	29.6	----	1.10	----	1.29	1.07	1.07	Form pressure
	Aver. Layer II			22.8	21	25	24.0	23.4	23.1	----	1.20	----	1.40	1.15	1.00	

* Average moisture content on trimmings taken before test.
** Atterberg Limits from Basic Curve, Fig. 7.1.

TABLE 7.5. SUMMARY OF MORTAR MIGRATION RESULTS, LAYER III

Class.	Sample	Depth (feet)	Description	Nat.M.C.* (%)	P.L. **	L.L. **	Moisture Content After Test Distance from Interface (ins.)				α - Values				α_{min}	Remarks
							0-1/8	1/8-1/4	1/4-3/8	3/8-1/2	0"	1/8"	1/4"	3/8"		
CL	H-2-38	36.0	Gray, yellow, black sandy clay	15.0	15	36	17.1	15.5	14.4	----	1.25	1.15	0.94	1.11	0.94	Overburden pressure
CL	H-2-39	37.0	Gray, yellow, black slightly sandy clay	19.4	14	36	21.6	20.8	19.6	----	1.26	----	1.05	Error	1.05	Form pressure
CL	H-2-40	37.5	Gray, yellow, black sandy clay	17.4	14	36	14.5	16.6	16.9	----	1.13	1.07	1.11	1.05	1.05	Overburden pressure
CL	H-2-44	40.5	Gray, yellow, tan clay; calcareous material	21.6	14	35	21.7	21.5	20.7	----	1.16	1.27	1.38	Error	1.16	Overburden pressure
CL	H-2-45	41.5	Gray, yellow, tan clay; calcareous material	22.1	15	40	23.6	24.8	20.9	----	0.89	----	0.94	0.90	0.89	Form pressure (α = 0.89 at 1/2")
	Aver. Layer III			19.1	14	37	19.7	19.8	18.5	----	1.14	1.16	1.10	1.03	0.96	Numerical and Weighted averages (Using $\alpha > 1 = 1$)

* Average moisture content on trimmings taken before test.
** Atterberg Limits from Basic Curve, Fig. 7.1.

TABLE 7.6. SUMMARY OF MORTAR MIGRATION RESULTS, LAYER IV

Class.	Sample	Depth (feet)	Description	Nat.M.C.* (%)	P.L. **	L.L. **	Moisture Content After Test Distance from Interface (ins.)				α - Values				α_{min}	Remarks
							0-1/8	1/8-1/4	1/4-3/8	3/8-1/2	0"	1/8"	1/4"	3/8"		
CH	H-5-39	42.5	Very stiff tan & gray mottled clay	20.3	16	59	23.1	22.3	23.0	22.7	----	0.92	0.95	1.09	0.92	Form pressure
CH	H-5-40	43.5	Very stiff red & gray mottled clay	21.2	18	62	21.2	21.3	21.0	21.7	0.70	1.22	0.66	----	0.66	Form pressure
CH	H-2-48	44.0	Gray & tan clay; some calcareous material	20.1	19	62	23.0	20.9	20.3	----	0.95	----	0.97	0.95	0.95	Form pressure (α = 0.95 at 1/2")
CH	H-5-42	45.5	Very stiff red & gray clay; calcareous	18.3	20	62	21.0	20.6	21.0	20.8	0.62	0.62	1.16	----	0.62	Form pressure
CH	H-5-43	46.5	Very stiff red & gray clay; fissures	20.6	19	59	21.5	22.4	23.0	22.6	0.57	0.55	0.97	----	0.55	Form pressure
	Aver. Layer IV			20.1	18	61	22.0	21.5	21.7	----	0.71	0.83	0.94	1.02	0.74	Numerical aver.

* Average moisture content on trimmings taken before test.
** Atterberg Limits from Basic Curve, Fig. 7.1.

Since the deepest test shaft penetrated to a depth of 45 feet, only samples from Layers I through IV were subjected to mortar migration tests.

The minimum value of α for each test series is plotted as a function of the sample depth in Fig. 7.30. The variation in α with depth suggested therein would be the expected variation of α at failure in the test shafts, provided only mortar and moisture migration governed the maximum mobilized shear strength and provided that the laboratory mortar migration studies correctly simulate mortar-moisture migration in the field.

To aid in visualizing the moisture content gradients obtained in the laboratory study, values of moisture content have been plotted against distance from interface in Figs. 7.31 through 7.34. The individual tests indicate rather erratic moisture content gradients, particularly in the top layer. Some specimens were wetter near the concrete interface, while others were drier. The values plotted for one inch from the interface are the natural moisture contents, which were assumed to be unaffected by the presence of mortar at that distance.

To obtain a meaningful picture of the phenomenon of mortar-moisture migration, the average (numerical) moisture content and α values were plotted for each of the four layers of soil tested in Figs. 7.35 through 7.38.

From Fig. 7.35 it is observed that no significant moisture changes took place in the soil in Layer I. If anything, a slight drying gradient occurred. That is, the soil appeared slightly drier near the interface than at some distance away. The explanation for this action is not clear. Possibly some reverse water migration occurred (from soil to concrete) at the relatively low normal pressures employed in the CH material. There was, however, a significant variation of α with distance from the interface, with the highest and lowest values occurring at the interface and

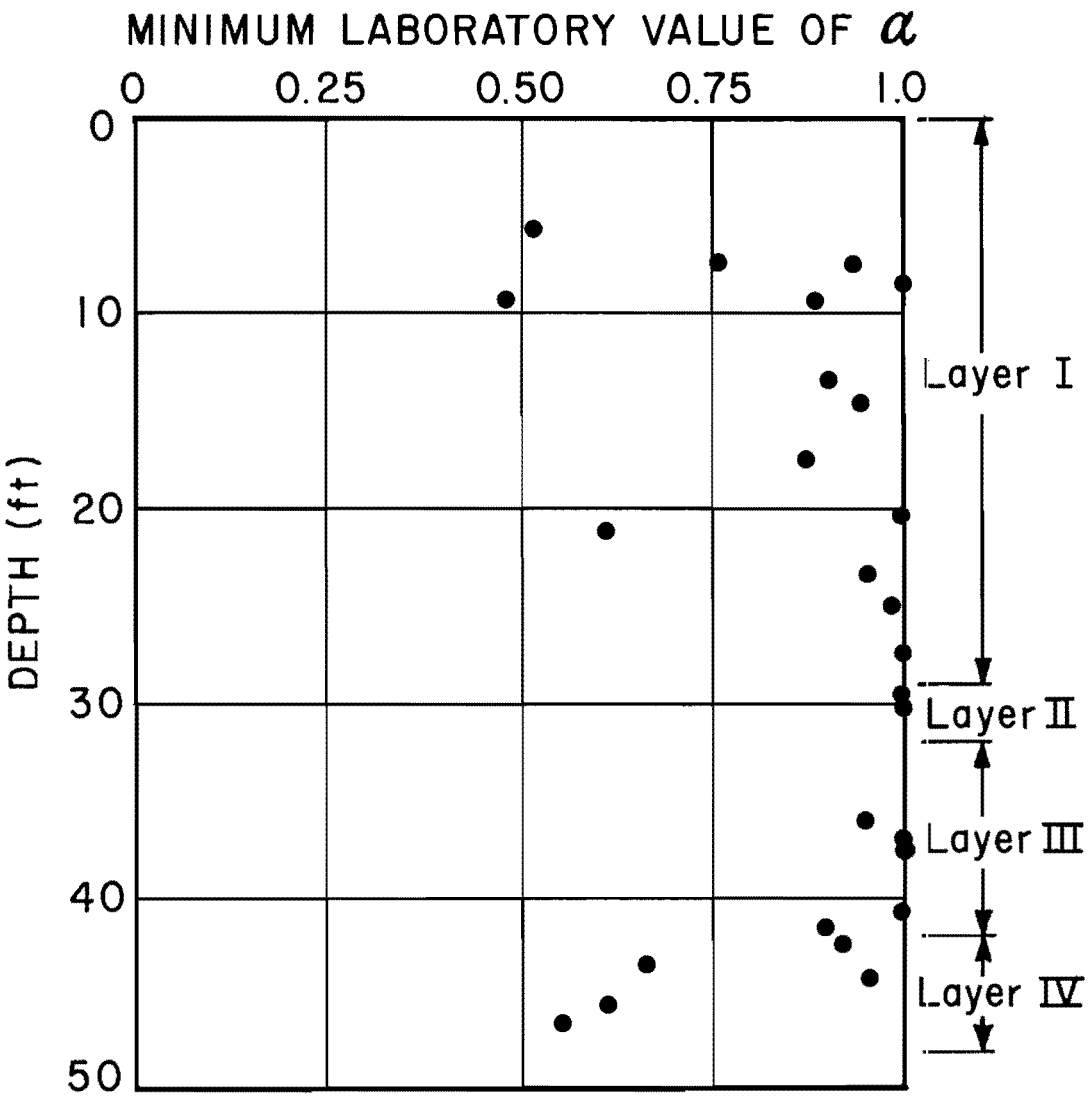

Fig. 7.30. Variation of Minimum Laboratory α Value with Depth

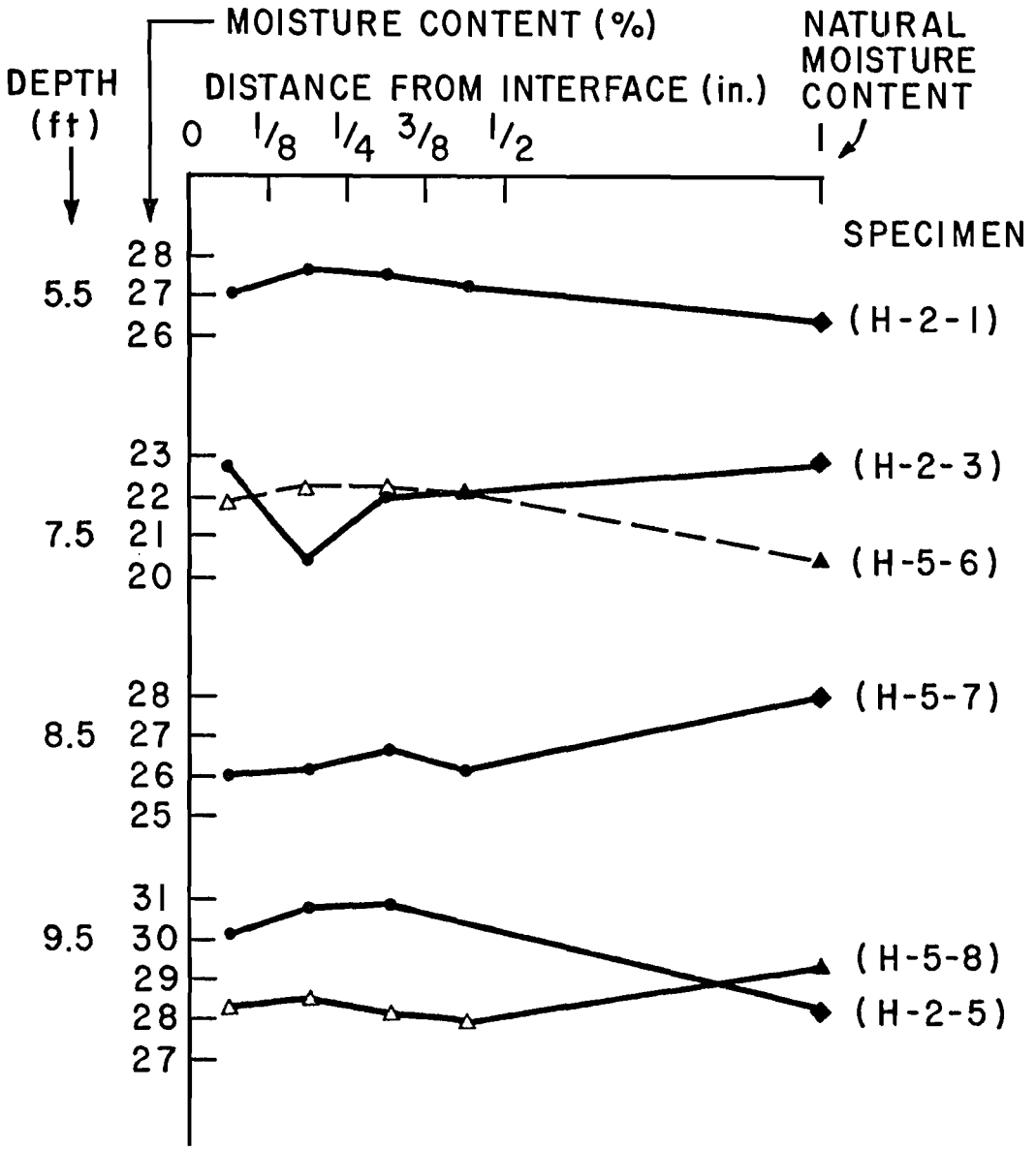

Fig. 7.31. Variations in Soil Moisture, Mortar Migration Study, Layer I

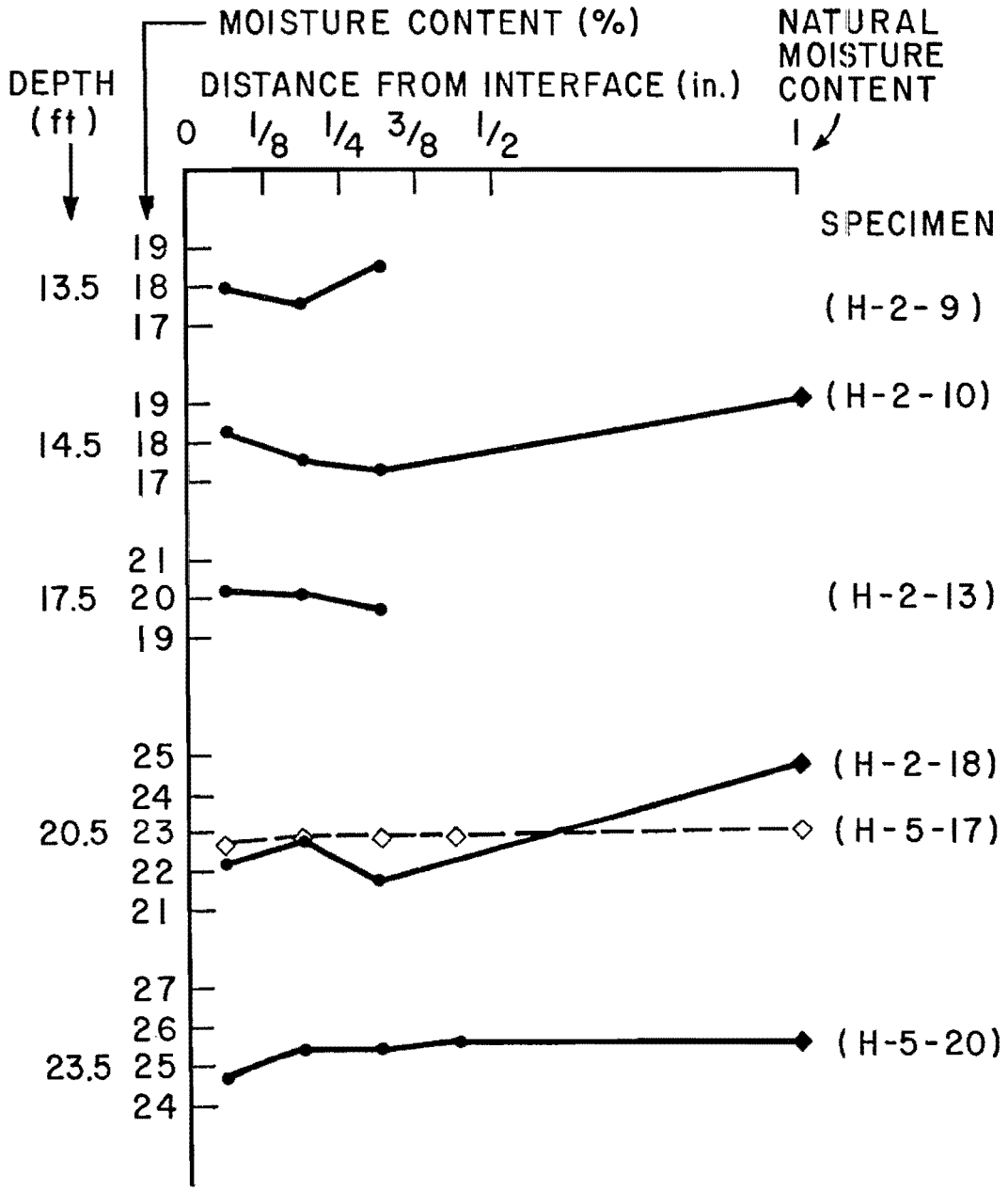

Fig. 7.31. Continued

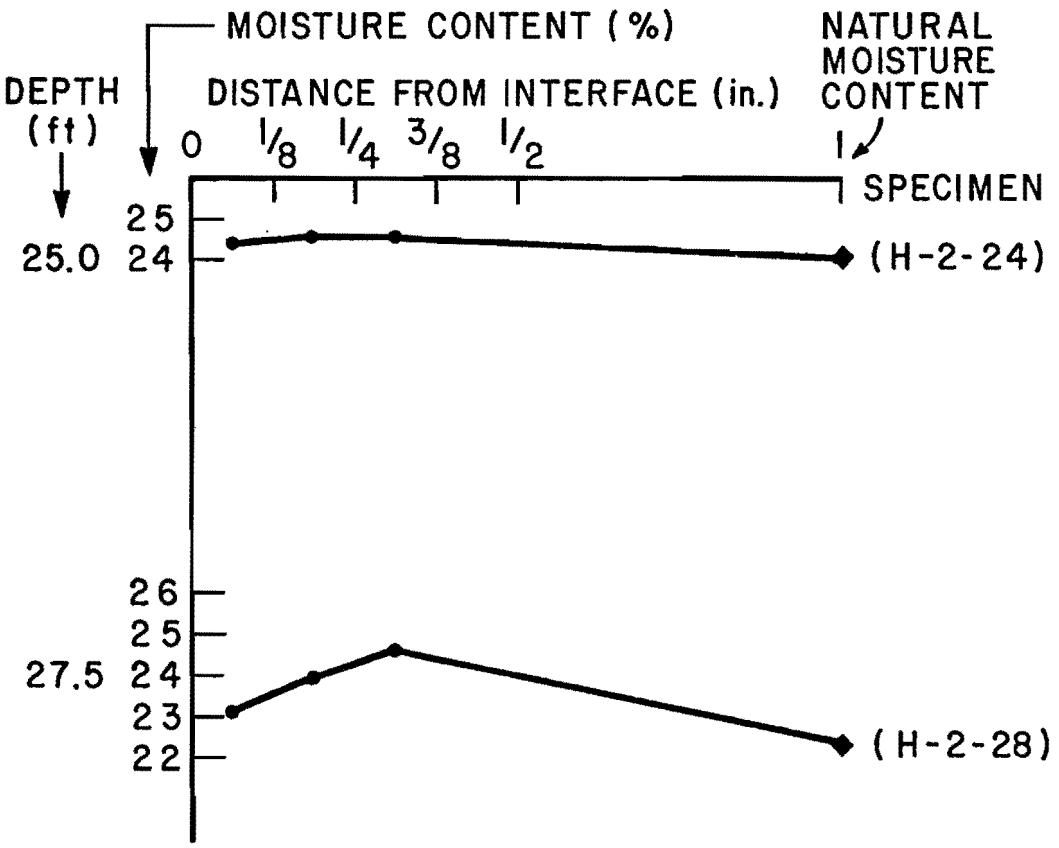

Fig. 7.31. Continued

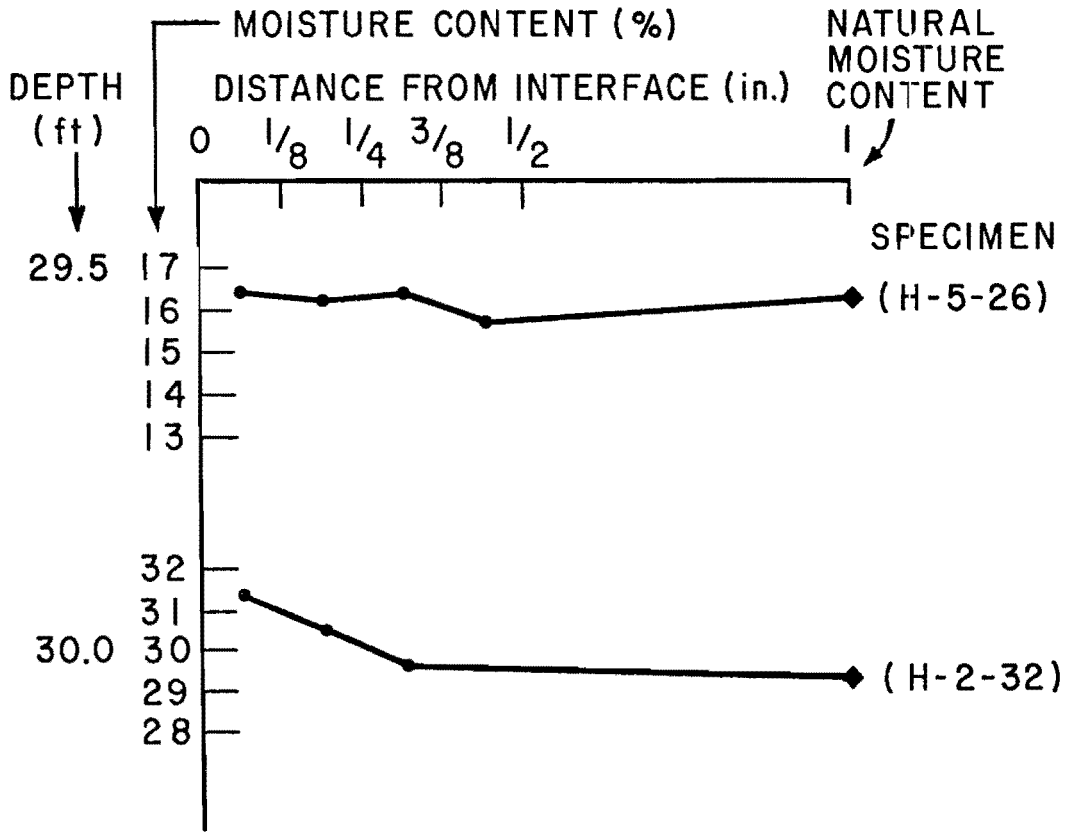

Fig. 7.32. Variations in Soil Moisture, Mortar Migration Study, Layer II

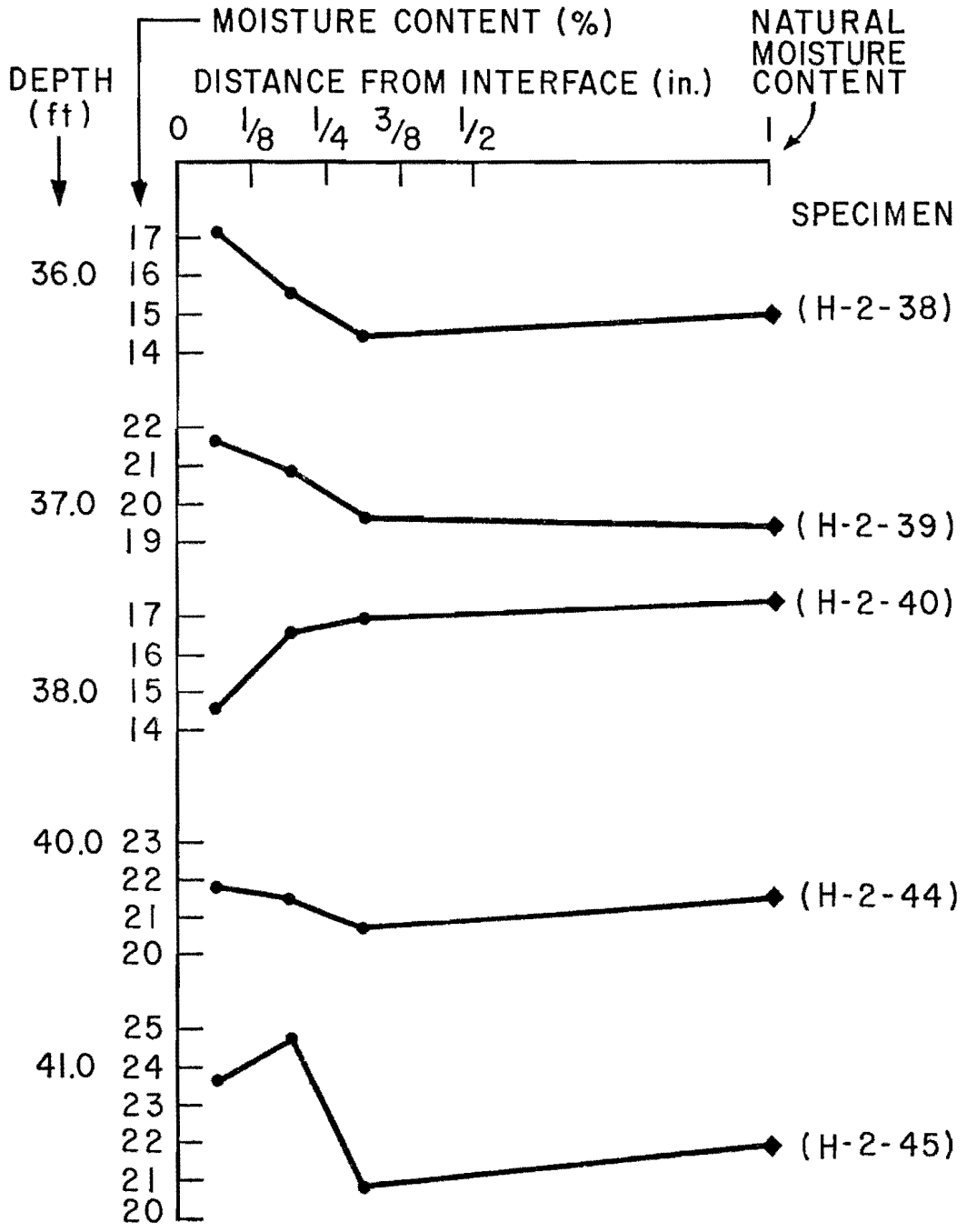

Fig. 7.33. Variations in Soil Moisture, Mortar Migration Study, Layer III

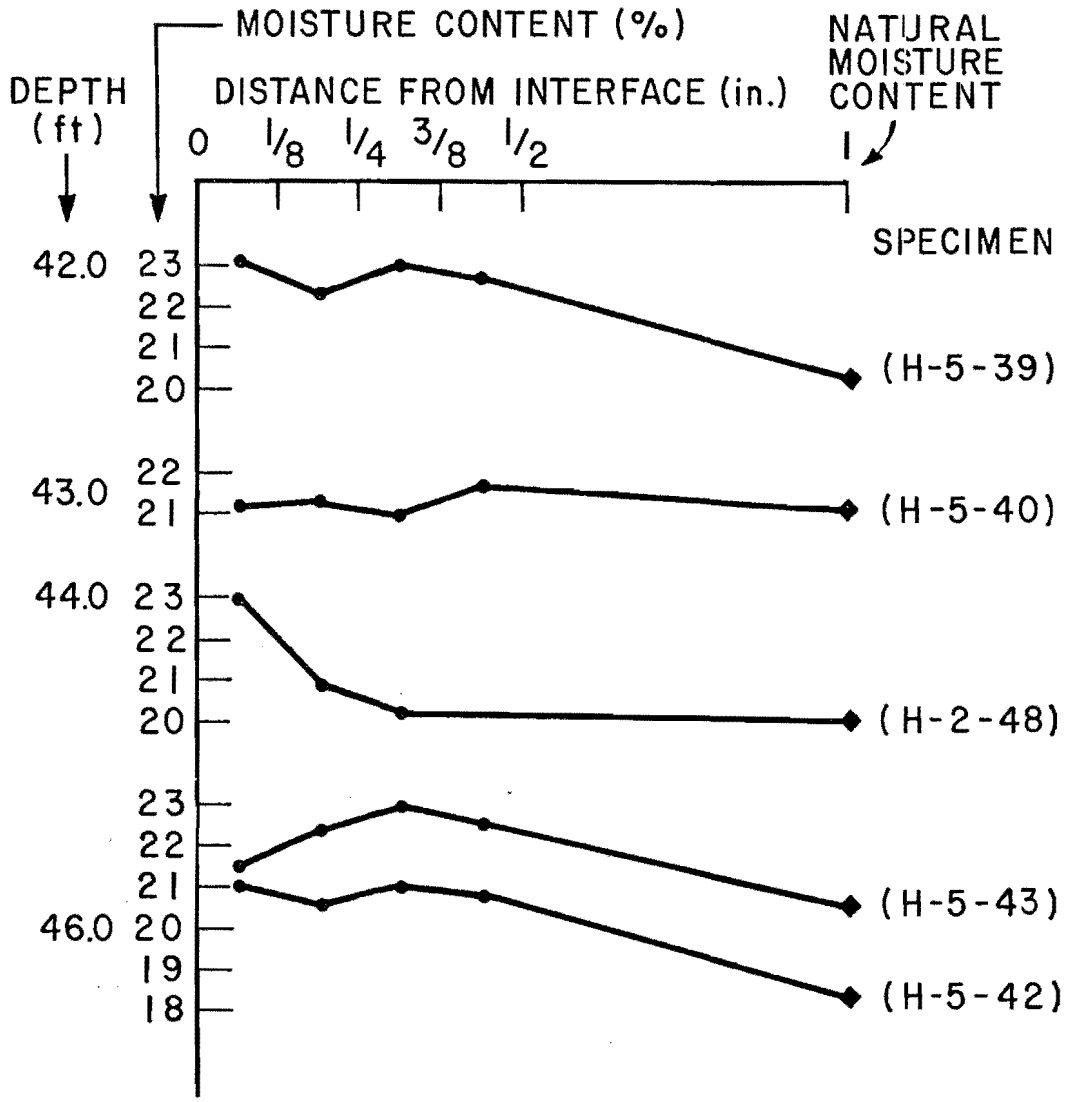

Fig. 7.34. Variations in Soil Moisture, Mortar Migration Study, Layer IV

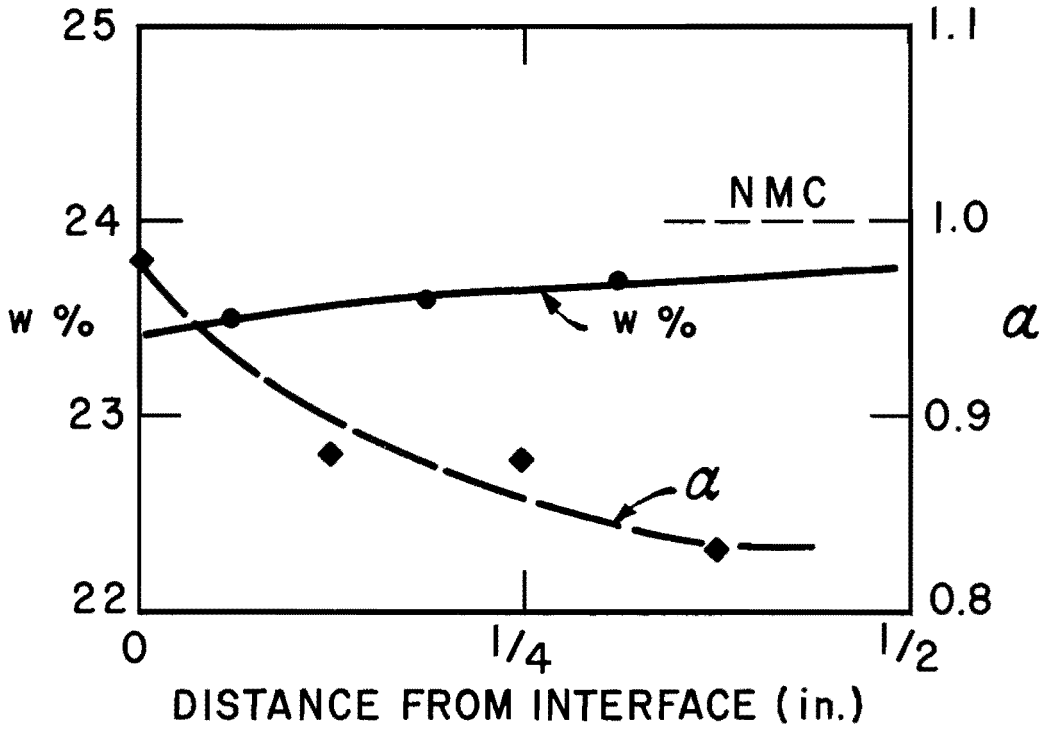

Fig. 7.35. Average Moisture Content and Shear Strength Reduction Profiles, Layer I

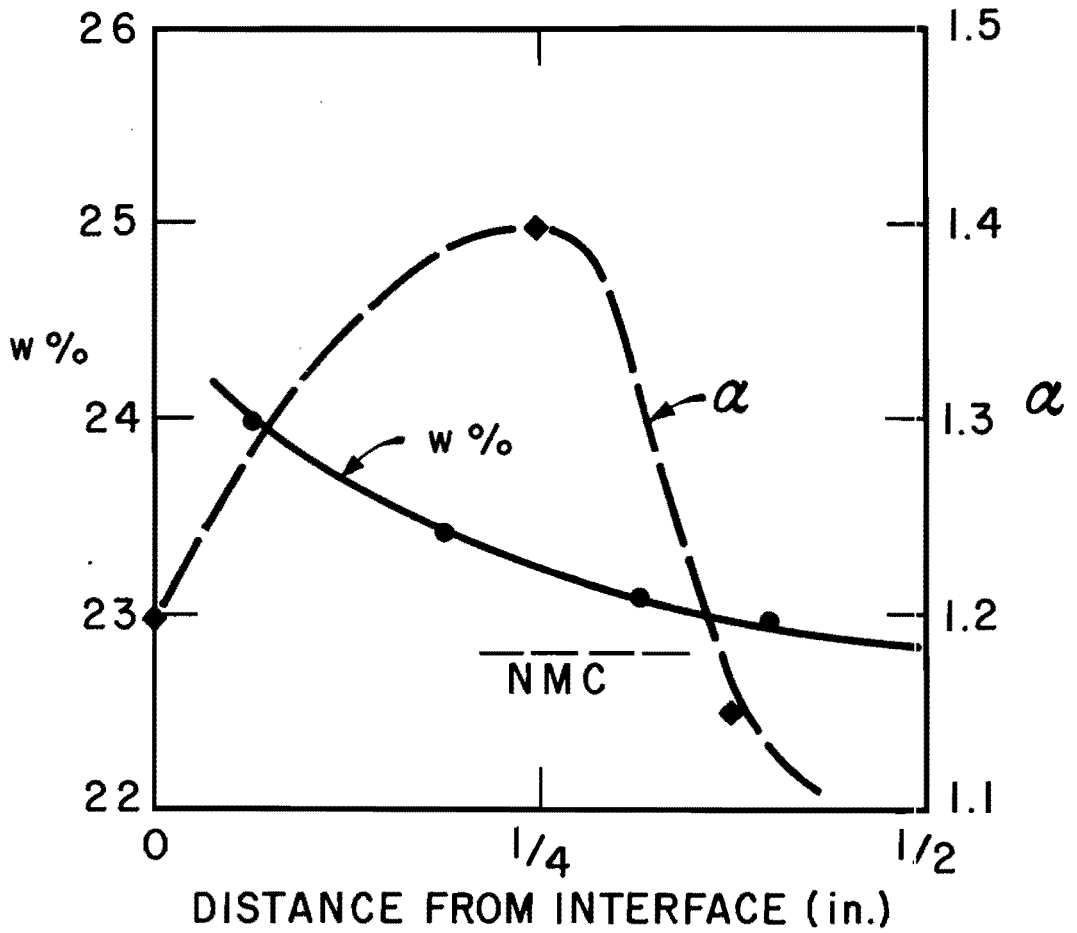

Fig. 7.36. Average Moisture Content and Shear Strength Reduction Profiles, Layer II

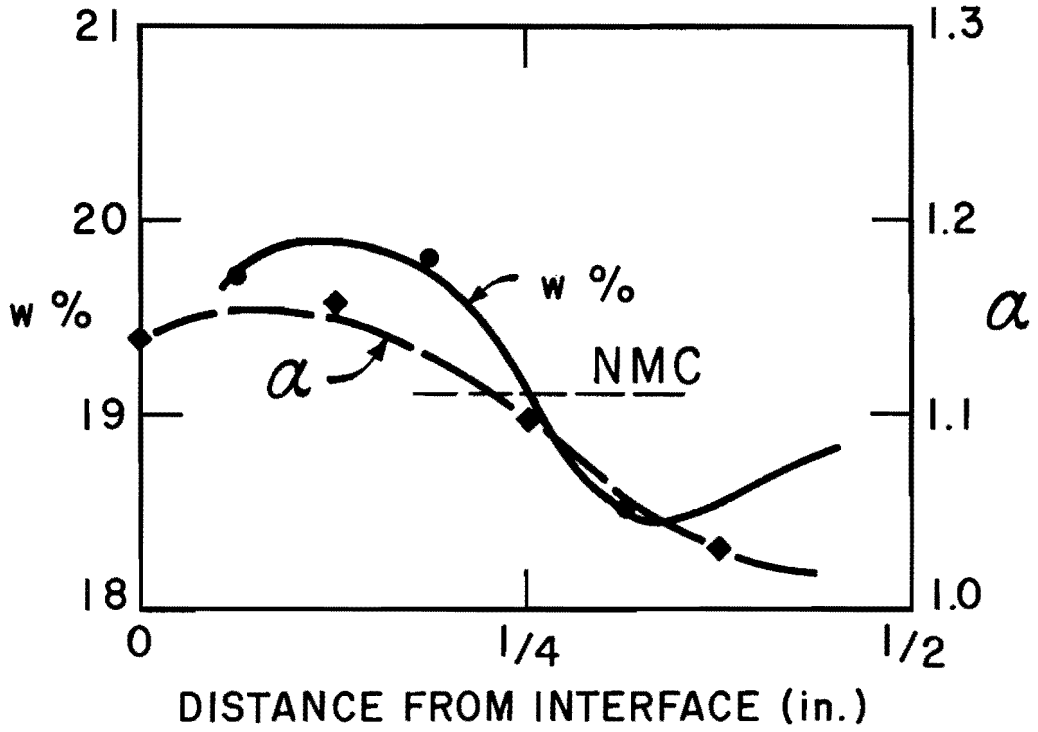

Fig. 7.37. Average Moisture Content and Shear Strength Reduction Profiles, Layer III

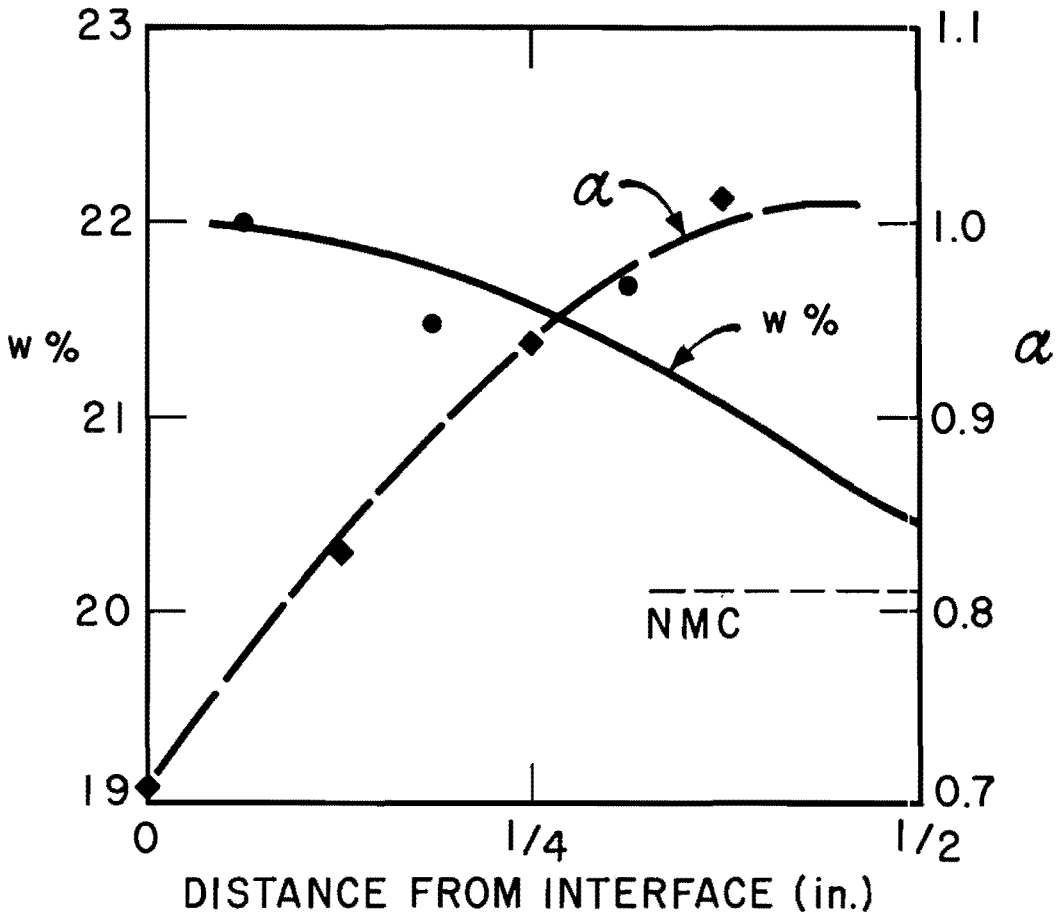

Fig. 7.38. Average Moisture Content and Shear Strength Reduction Profiles, Layer IV

three-eighths inch from the interface, respectively. The high value at the interface may have been caused by capillary forces in the pores of the soil, chemical bond between the soil and concrete, the interference of the presence of the concrete on shearing distortions in the soil, or a combination of these factors. Soil was actually observed to shear at a slight distance from the interface whenever the failure plane was established at the interface. No evidence of migration of cement was seen.

A few tests were conducted in which the shear plane was established at one-half inch from the interface in order to check whether the minimum value of α occurred within the distance zero to three-eighths inch from the interface. The one-half-inch tests yielded values at least as great as the three-eighths-inch tests, indicating that shear planes need not be created at distances greater than three-eighths inch from the interface in Layers I and IV.

It appears that the shear strength reduction which occurred some distance from the interface is not due to softening by the action of water migrating from the mortar into the soil in the material from Layer I, but to some other phenomenon. One explanation for this occurrence is the possibility that shrinkage and bonding to the upper half of the shear box occurred simultaneously in the mortar as it set up, causing a reduction in normal pressure against the soil in the specimens containing mortar blocks, whereas no such pressure reduction occurred in the plain soil samples. Thus, smaller shear strength values would have been indicated for the specimens containing mortar blocks whether or not moisture migration occurred. This speculation is supported by Fig. 7.30, which indicates a frictional effect on α in Layer I. That is, higher α factors for higher normal pressures

are seen to exist. The phenomenon of decreasing indicated shear strength without corresponding moisture content increase, illustrated in Fig. 7.35, was evidenced most graphically in the lightly pressured specimens.

On the basis of the laboratory tests, an average α factor on the order of 0.8 is predicted for the soil in Layer I.

The saturated silty soil from Layer II behaved in a more predictable fashion. Figure 7.36 shows a definite moisture gradient from the interface into the soil. A moisture content increase of about 1.5 per cent is indicated at the interface. Specimens for which the shear plane was fixed at the interface actually sheared in the soil along a dish-shaped failure surface through the soil. Hence, the α factor plotted for the interface is undoubtedly too low. Despite the fact that water content increased near the interface, the α factor was also higher (in fact, greater than unity) near the interface because some cement also migrated along with the water. Migration of cement mortar was limited to about one-fourth inch. Beyond that distance the shear strength rapidly approached that of the natural soil. It is concluded from the tests on the soil from Layer II that, under the surcharge pressures predicted from the A.C.I. formwork expression, the tendency for softening is overridden by the migration of mortar. Consequently, no shear strength reduction is expected to take place due to placing wet concrete against the soil from that stratum.

As seen in Fig. 7.37, Layer III behaved somewhat the same as Layer II, except that the moisture content increased in the one-fourth inch nearest the interface, but decreased in the next one-fourth inch. Some increase was observed in shear strength near the interface, possibly due to the same

phenomenon suggested for the shearing behavior of soil from Layer I. For all practical purposes, the α factor was unity for Layer III.

The soil in Layer IV (Fig. 7.38) exhibited the moisture and shear strength variations predicted qualitatively by Chuang and Reese. That is, the moisture content increased monotonically in the one-half inch nearest the interface, while the α factor decreased monotonically in the same zone. An average α factor in the order of 0.7 is indicated in Layer IV. The laboratory study predicts that failure would occur at the soil-mortar interface in Layer IV.

The average shear stress-displacement curves for the four levels for which mortar migration tests were carried out are given in Figs. 7.39 through 7.42. Individual stress-displacement results are tabulated in Appendix D. The stress-displacement curves have been plotted from average values. Since the various tests terminated at different displacements, the average curves could not be reliably plotted to failure, except at the interface, in Layers I, III, and IV. In addition, tests on six specimens included in Tables 7.3, 7.5, and 7.6 were excluded from consideration in plotting the stress-displacement curves either because the sample was not reasonably homogeneous or because displacement readings were not taken. Therefore, the maximum values shown in Figs. 7.39 through 7.42 do not necessarily reflect the tabulated α values. Figures 7.39 through 7.42 do, however, provide some insight into the behavior of soil-mortar specimens in direct shear. Of particular interest is the fact that the failure at the interface was more brittle than the failure at some distance away in every type of soil tested.

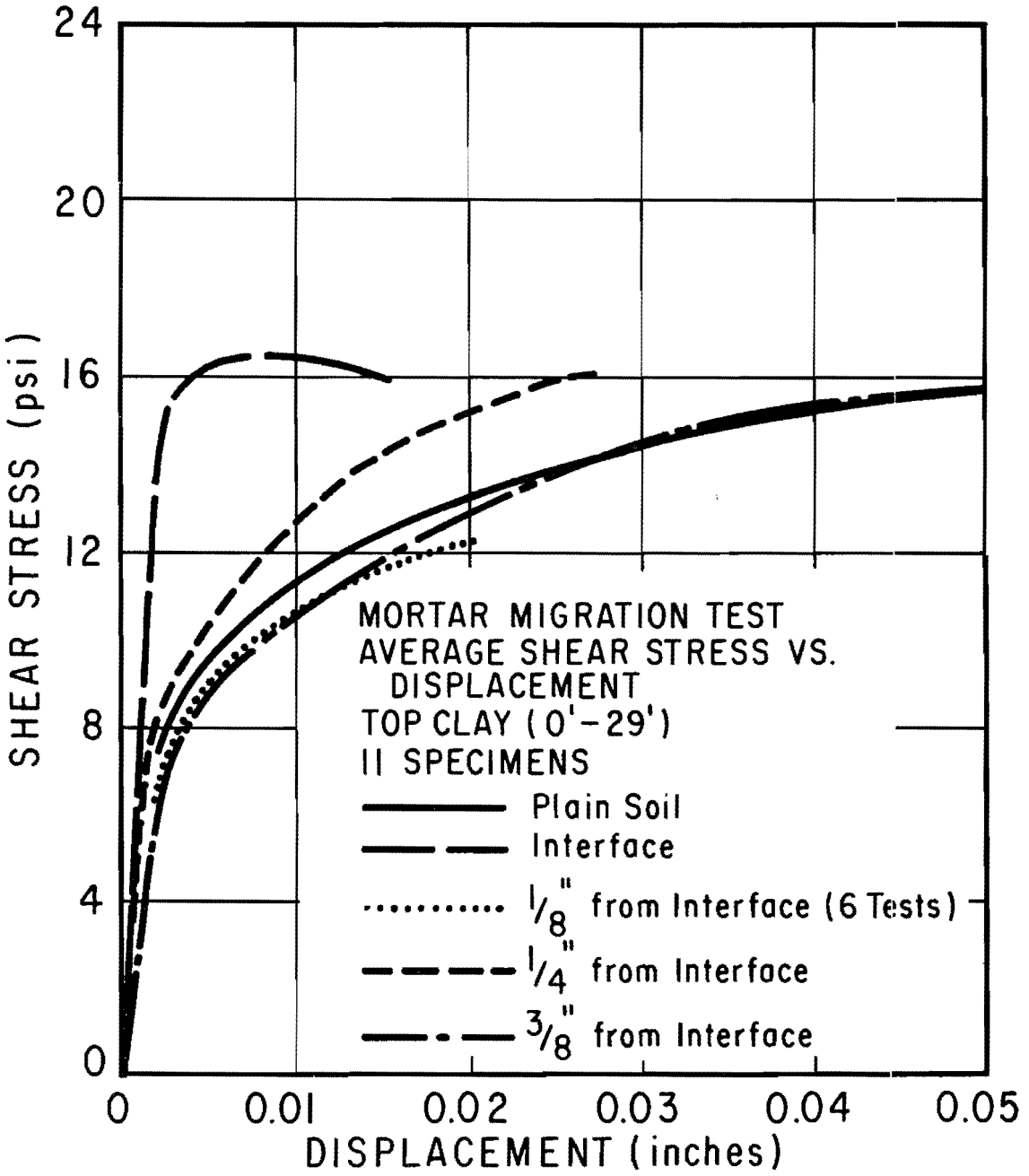

Fig. 7.39. Stress Versus Displacement, Mortar Migration Study, Layer I

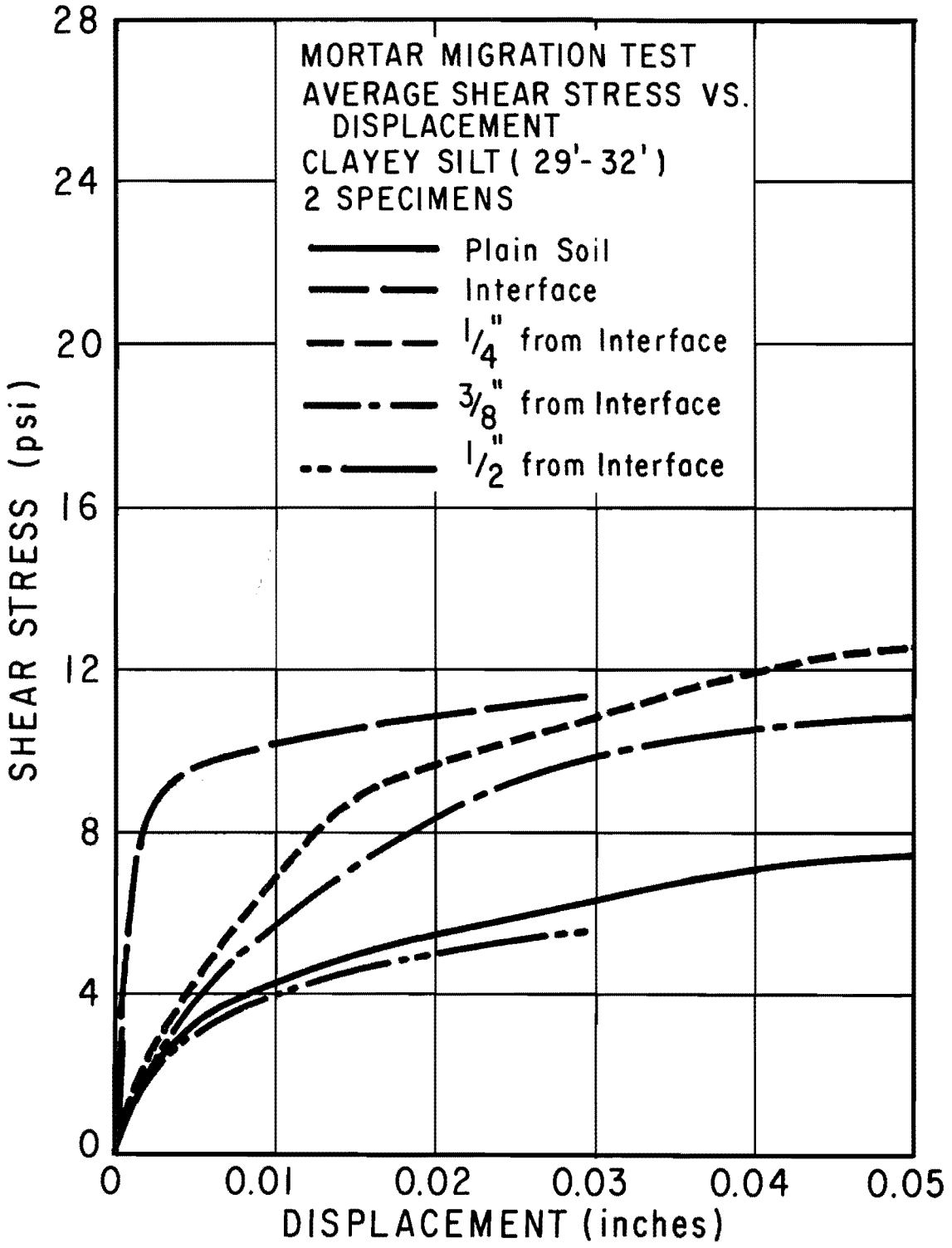

Fig. 7.40. Stress Versus Displacement, Mortar Migration Study, Layer II

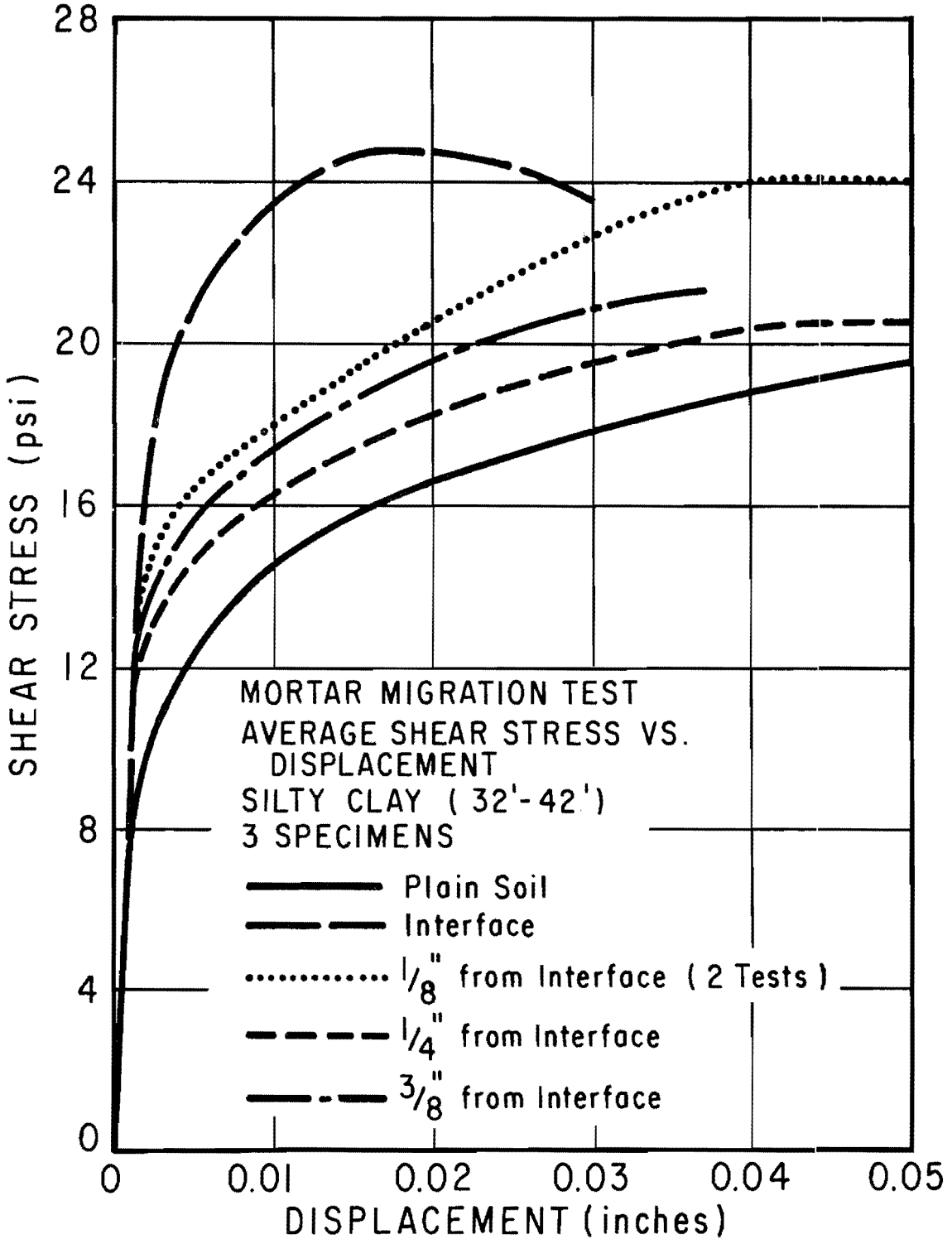

Fig. 7.41. Stress Versus Displacement, Mortar Migration Study, Layer III

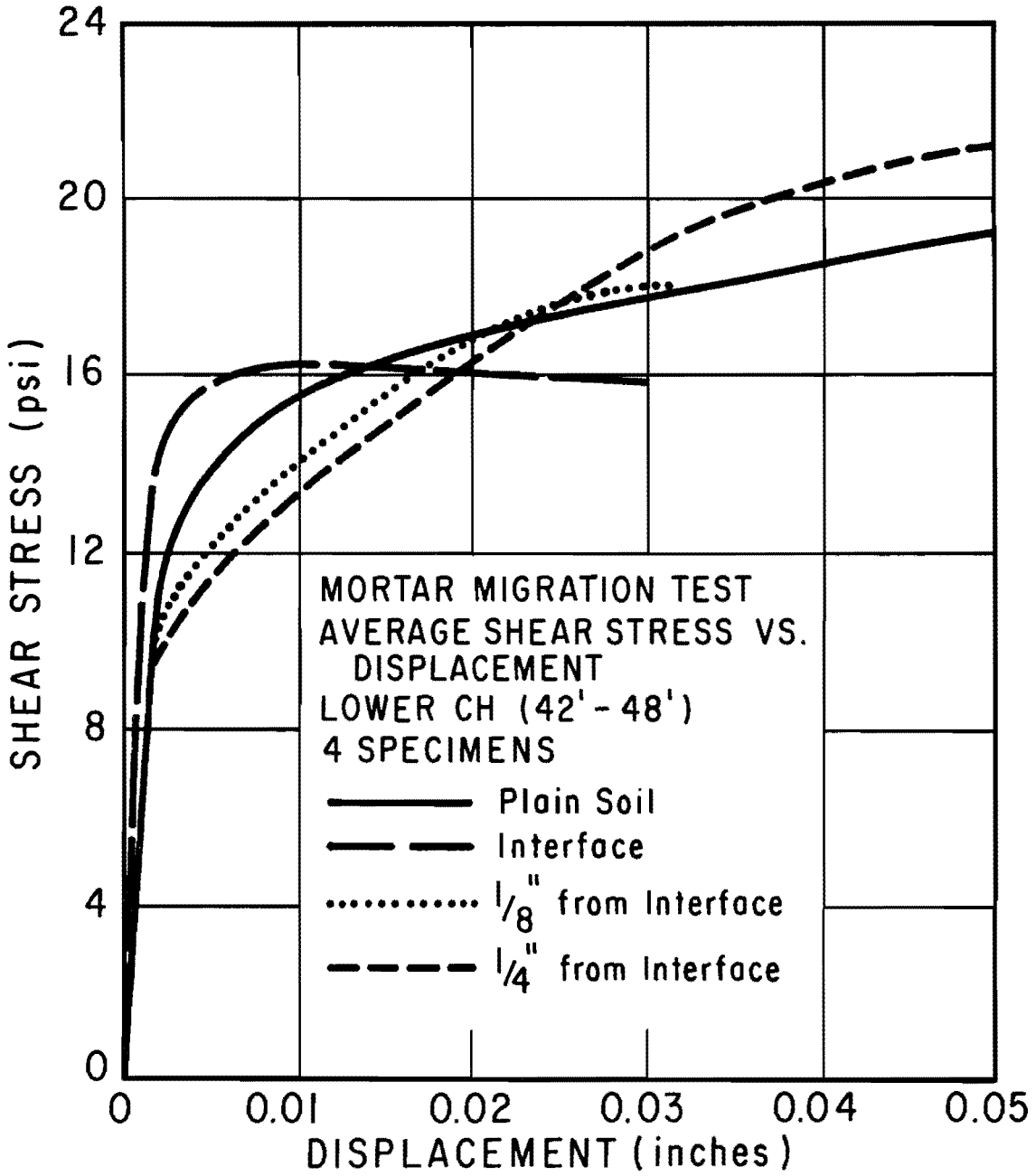

Fig. 7.42. Stress Versus Displacement, Mortar Migration Study, Layer IV

In summary, the migration of cement and water between concrete and soil appears to be a complex phenomenon. The possibility exists that moisture may migrate either toward or away from the soil, depending on the properties of the soil. The plasticity index appears to have a major influence on the shear strength reduction factor. The average minimum α factor is plotted against the average plasticity index for each layer in Fig. 7.43, without regard for other factors such as normal pressure. (The average normal pressures for Layers II, III, and IV were approximately the same, i.e. 21 psi, while the average normal pressure for Layer I was about 15 psi.) A definite trend toward lower α factors for higher plasticity index is indicated.

The laboratory tests reported herein suggest that moisture migration may not account for the entire amount of shear strength reduction reported in field tests or that factors neglected in the laboratory simulation may have an important effect on shear strength reduction. The presence of drilling mud has not been considered in this study, although a further reduction in α, particularly in clay soils, may occur if a layer of mud becomes entrapped between the concrete and borehole walls. This subject is treated by Barker and Reese (1970).

Consolidation Tests

One-dimensional consolidation tests were performed on several samples of soil from Borings H-2 and H-5 for the purpose of gaining further information about the characteristics of the soil at the test site. Results of the tests are reported herein to provide the reader with an additional description of the properties of the soil at the SH225 site. Consolidation specimens were 2.83 inches in diameter by 0.75 inches in height. Both

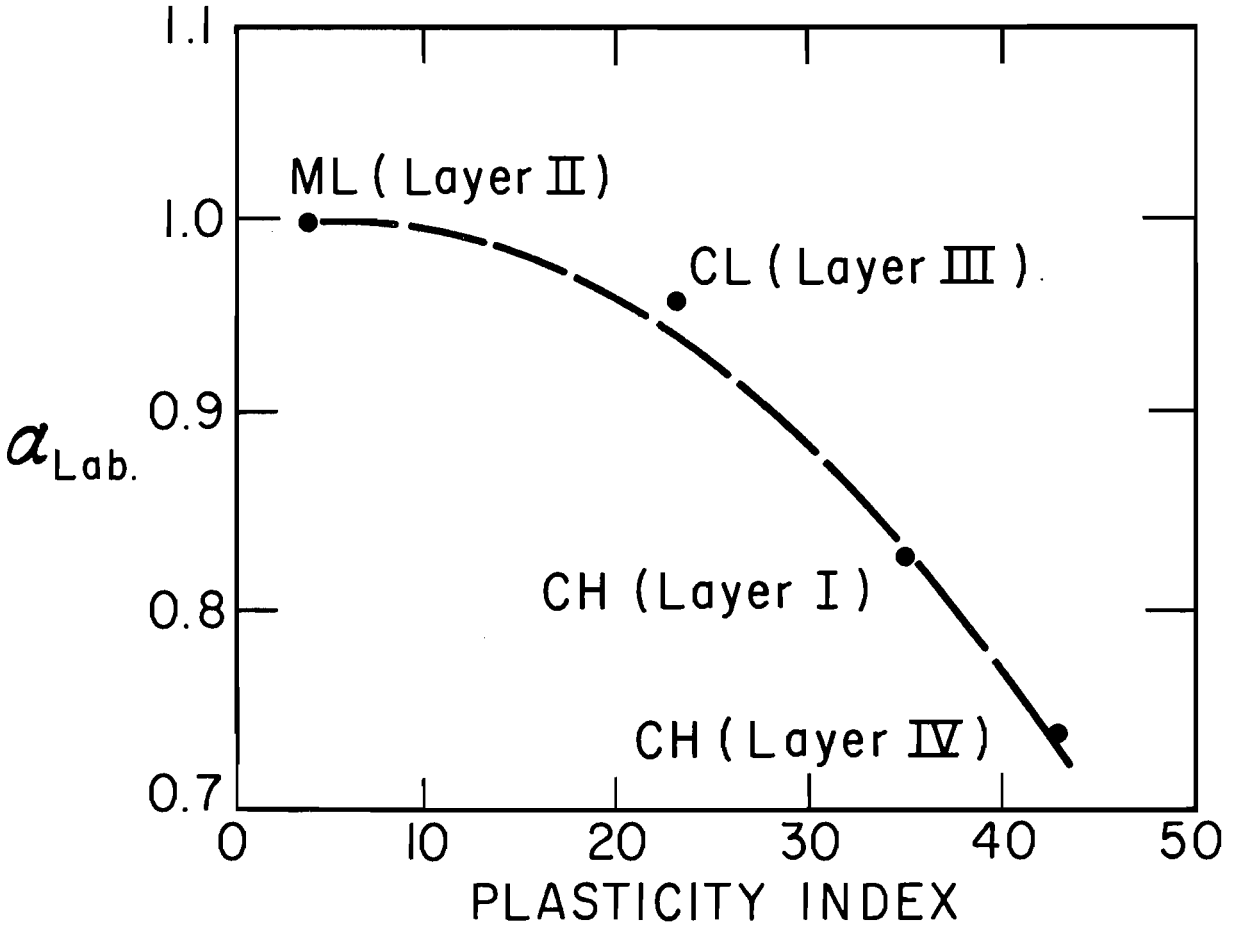

Fig. 7.43. α_{min} Versus Plasticity Index for SH225 Site Soil

sealed tests, in which no additional moisture is allowed to enter the test specimen, and submerged tests, in which the test specimen is allowed to absorb demineralized water freely, were performed. Swell pressure was obtained by measuring the force required to keep the specimen from expanding. Small values of swell pressure were observed for the sealed tests because the specimens tended to imbibe a small amount of water from the porous stones, which were moistened prior to beginning the tests. The two types of tests were performed to investigate the differences in consolidation behavior between specimens initially in normal condition (sealed tests) and those in a completely saturated condition in which the maximum swell pressure was acting (submerged test). Other than the expected fact that submerged specimens yielded higher swell pressures than sealed specimens, test results did not differ appreciably with testing methods.

The consolidation test results are summarized in Table 7.7. Preconsolidation pressure was estimated using the method of Casagrande. Based on the work of Brooker and Ireland (1965), in situ at rest earth pressures were estimated from the consolidation test results. An average value of K_o of 1.2 to 1.3 is indicated, with somewhat higher values occurring near the surface. The soil was found to have an overall average compression index, C_c, of 0.20 and an expansion index, C_e, of 0.10, excluding results from Sample H-2-45, which contained a large amount of calcareous material.

Values of compression index, C_c, initial void ratio, e_o, and initial degree of saturation, S_r, obtained from these tests have been plotted against depth in Fig. 7.4. Complete e-log p curves are given in Appendix E. The test on Sample H-2-11 is excluded from the Appendix

TABLE 7.7. SUMMARY OF CONSOLIDATION TESTS - HOUSTON SH225 SITE

Sample	Depth (Ft.)	Description	Type Test	C_c	C_e	Swell Pressure (Tsf)	Initial Degree of Saturation (%)	Initial Void Ratio e_o	P.I.*	Preconsolidation Pressure (Tsf)	Effective Overburden Pressure (Tsf)	Overconsolidation Ratio	K_o**
H-2-2	6.5	Tan and gray slickensided clay with calcareous material	Sealed	0.23	0.14	0.4	84	0.70	36	4.0	0.41	9.8	1.6
H-2-3	7.5	Same as above	Submerged	0.17	0.10	3.0	87	0.51	36	5.8	0.47	12.3	1.7
H-2-10	14.5	Tan clay with sand pockets	Submerged	0.19	-	0.5	91	0.60	40	3.3	0.91	3.6	1.0
H-2-11	15.5	Tan clay with some gray clay - slickensided	Sealed	0.21	0.09	-	-	-	35	4.6	0.96	4.8	1.1
H-5-18	21.5	Stiff red silty clay	Submerged	0.21	0.11	1.3	100	0.58	31	6.5	1.16	5.6	1.2
H-2-22	24.0	Slightly sandy tan clay with gray clay	Sealed	0.14	0.07	0.2	96	0.53	28	3.3	1.24	2.7	0.8
H-5-21	24.5	Stiff red clay; some silt	Submerged	0.21	0.08	0.6	100	0.51	28	8.0	1.26	6.3	1.2
H-2-45	41.5	Tan, gray & yellow clay; sandy with calcareous material	Sealed	(0.45)	0.14	0.4	100	0.54	25	(19.0)	1.74	10.9	1.5
H-5-53	58.5	Very stiff red clay with calcareous nodules	Submerged	0.18	0.09	1.8	95	0.51	35	8.0	2.32	3.4	1.0

* From Basic Curve, Fig. 7.1
**Determined from Brooker and Ireland (1965)

because of a blunder in obtaining swell pressure and final dry weight. The test on Sample H-2-10 was terminated at the load shown because the loading head cracked when an attempt was made to increase the load.

Typical log time-consolidation results are shown in Fig. 7.44. The sample and effective stress chosen for display represents the soil immediately below the bottom of Test Shaft Nos. 1 and 2 (24 feet) loaded to a stress approximately equal to a typical design bearing pressure (3.2 tsf). The coefficient of consolidation, c_v, for that value of imposed load was 4.2×10^{-4} square centimeters per second (0.65×10^{-4} square inches per second). The variation of c_v with effective pressure for Sample H-2-22 (depth of 24 feet) is given in Fig. 7.45.

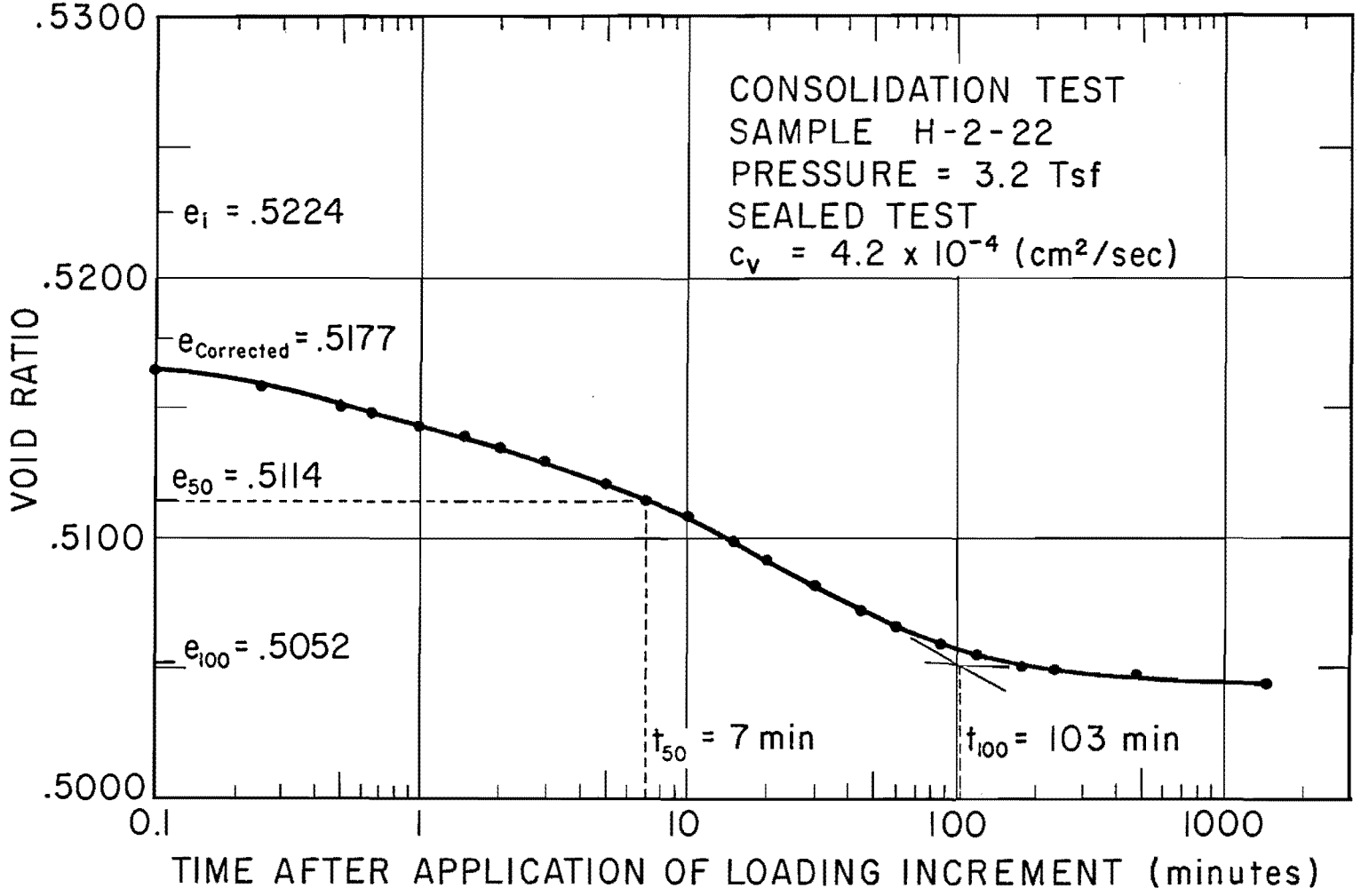

Fig. 7.44. Time-Consolidation Relationship, Sample H-2-22

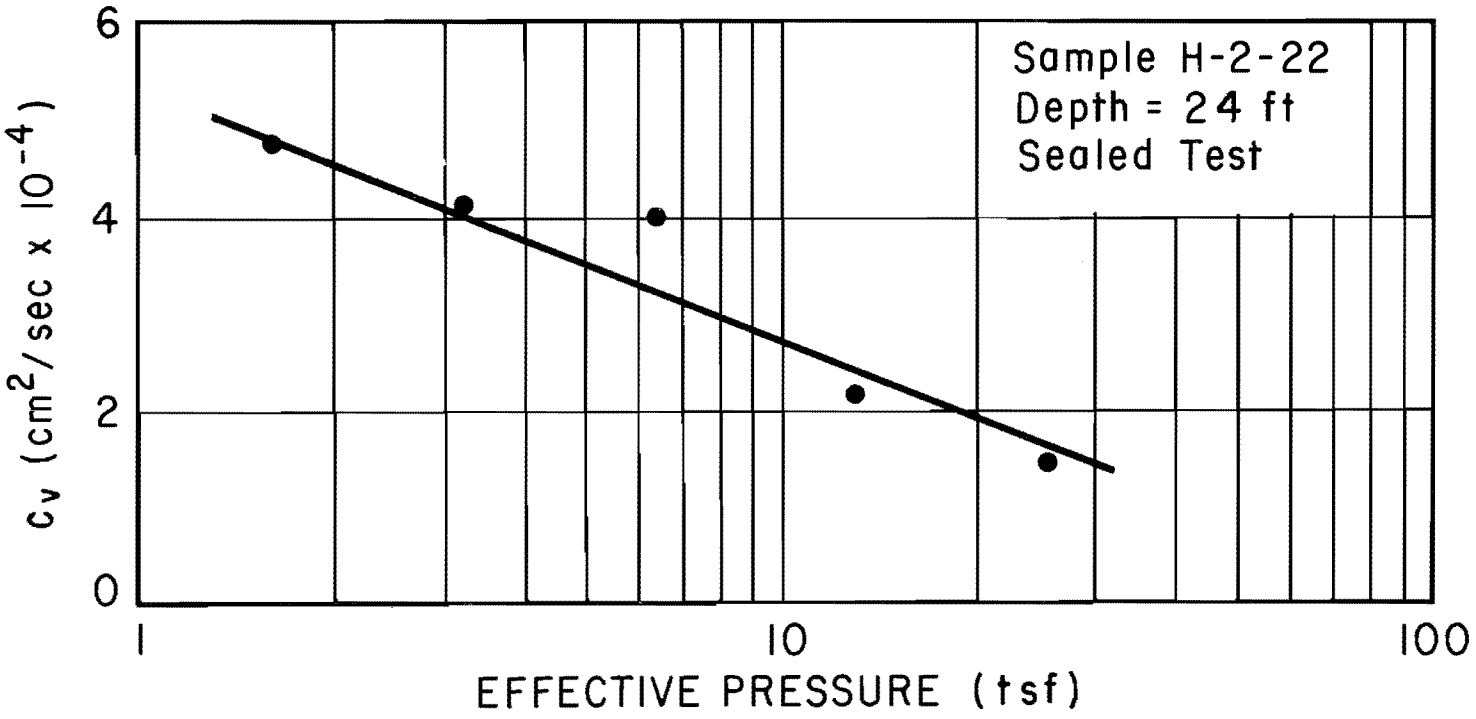

Fig. 7.45. c_v Versus Effective Pressure, Sample H-2-22

CHAPTER VIII

FIELD INSTALLATION PROCEDURES

Installation Schedule

Following the acquisition and preliminary testing of soil from Borings H-1, H-2, and H-3, tentative designs were made for the test shafts and anchors based on results of unconfined compression tests. It was decided that shafts with a 30-inch-stem-diameter were representative of the size used for bridge foundation construction in Beaumont Clay; consequently, all stem diameters were set at that value. It was also decided to install and test the shafts one at a time in order to analyze the data from a shaft of one design before proceeding to install the next shaft. This procedure allows each shaft to be constructed in such a way as to permit the investigation of the most important factors affecting behavior under load, including any that might be discovered during the testing program.

The test shafts were installed in numerical order. After the first two shafts had been installed and tested, it was decided to procede with the simultaneous design and installation of the final two shafts.

Shafts 1 through 3 were installed in the dry, whereas Shaft 4 was installed with drilling mud and casing. It was intended that the cylindrical test shafts have a length-to-diameter-ratio of at least 10 (length of 25 feet). This depth ratio was compromised slightly because it was felt that boring the hole to a depth of 25 feet might allow fissures to open, permitting water to infiltrate the borehole from the waterbearing silty soil from Layer II. Since placement of shafts terminating in Layer I

was programmed to be carried out completely in the dry, the design lengths for all such shafts were reduced to 23 feet. However, some water still infiltrated the borehole for Shaft 1.

The profiles of the four test shafts installed and tested are shown in Fig. 6.2, while the nominal and measured diameters and lengths are tabulated in Table 8.1. A discussion of the design and placement of instrumentation will be given in the next chapter. The test shafts are shown schematically, together with the location of instruments, in Fig. 9.21 through Fig. 9.28.

The schedule of shaft installation and testing is given in Table 8.2. Foundation construction at the test site was performed by the following drilling contractors, all of Houston, Texas: Layne-Texas Company, Inc. (original four anchors, Test Shaft No. 1), Griffin Foundation Drilling Corp. (Test Shaft No. 2), Farmer Foundation Company (fifth anchor, Test Shaft No. 3, Test Shaft No. 4). The first shaft installed at the site was Test Shaft No. 1. Next, four reaction anchors, placed in a square grid 20 feet on a side, were constructed in the locations indicated in Fig. 6.3. The test shafts were programmed to be installed at the centers of the sides of the grid. (Test Shaft No. 1 was already in place on one side.) The two anchors at adjacent corners of the grid were to be used as jacking reactions for each test shaft. This scheme was in fact followed for the first three test shafts, with Test Shaft No. 1 (hereafter abbreviated S1) at grid North, Test Shaft No. 2 (S2) at grid West, and Test Shaft No. 3 (S3) at grid South (see Fig. 6.3). However, Test Shaft No. 4 (S4) could not be installed properly at grid East, so a fifth anchor shaft had to be constructed 20 feet south of the original southeast anchor to accommodate

TABLE 8.1. TEST SHAFT GEOMETRIES, SH225 TEST SITE

Shaft Number	Stem Diameter (inches)	Bell Diameter at Base (inches)	Length (Measured)
1	30* (30.7)**	---	23' 1 1/2" (to bottom of load cell)
2	30* (31.1)**	90* (90.5)**	23' 0" (23' 6" to bottom of seating hole for belling tool)
3	30* (31.0)**	---	23' 0"
4	30*	---	45' 0"

*Design Value

**Measured Value

TABLE 8.2. SCHEDULE OF DRILLED SHAFT INSTALLATION, SH225 SITE

Shaft	Installation Method	Date Cage Instrumented	Date Shaft Installed	Dates Tested
Test Shaft No. 1	Dry augering	6-7 June 68	27 June 68	29 August 68 (Test 1, Test 2) 10 December 68 (Test 3)
Northeast Anchor	Wet rotary, with casing	---	15-17 July 68	---
Northwest Anchor	"	---	18 July 68	---
Southeast Anchor	"	---	19 July 68	---
Southwest Anchor	"	---	22 July 68	---
Test Shaft No. 2	Dry augering, with belling	5 December 68	6 January 69	4 March 69 (Test 1) 18 June 69 (Test 2)
Test Shaft No. 3	Dry augering	7 July 69	8 July 69	3 October 69 (Test 1)
Test Shaft No. 4	Wet rotary, with casing	7 July 69	9 July 69	4 December 69 (Test 1) 16-17 December 69 (Test 2) 17 June 70 (Test 3)
Anchor Shaft No. 5	"	---	5 September 69	---

testing of S4, which finally was installed ten feet grid South of the southeast anchor.

A typical anchor design is shown schematically in Fig. 8.1. The anchors were themselves drilled shafts three feet in diameter and belled to a nine-foot diameter at 62 feet. They were installed using the drilling fluid and casing technique described earlier. The size and depth shown were chosen to give a minimum uplift capacity of 500 tons per anchor and also to place the anchor bells at a distance below the elevation of the bases of the test shafts that would minimize their effect on test shaft behavior. Construction of a test underream at the site had shown belling to be feasible at 62 feet. The grid spacing gave an average ratio of spacing between test shaft and anchor shaft to anchor shaft diameter of 3.3, which was expected to be sufficient to minimize anchor shaft interference.

All anchors and test shafts were constructed with Class C concrete, in accordance with Item 421 in the Texas Highway Department Standard Specifications (Texas Highway Department, 1962). Class C concrete is mixed with 6 sacks of cement per cubic yard and a water-cement ratio of 6.5 gallons of water per sack (0.6 weight ratio). A maximum coarse aggregate size of one inch was specified. Additionally, the concrete mix for the test shafts was adjusted to give an approximate slump of six inches by adding water, cement, and retarder (Pozzolith). The same water-cement ratio as in standard Class C concrete was maintained. Mechanical vibration was employed only in S2.

The original four anchors were installed essentially as designed (Fig. 8.1), except that the northeast anchor was finally finished at a

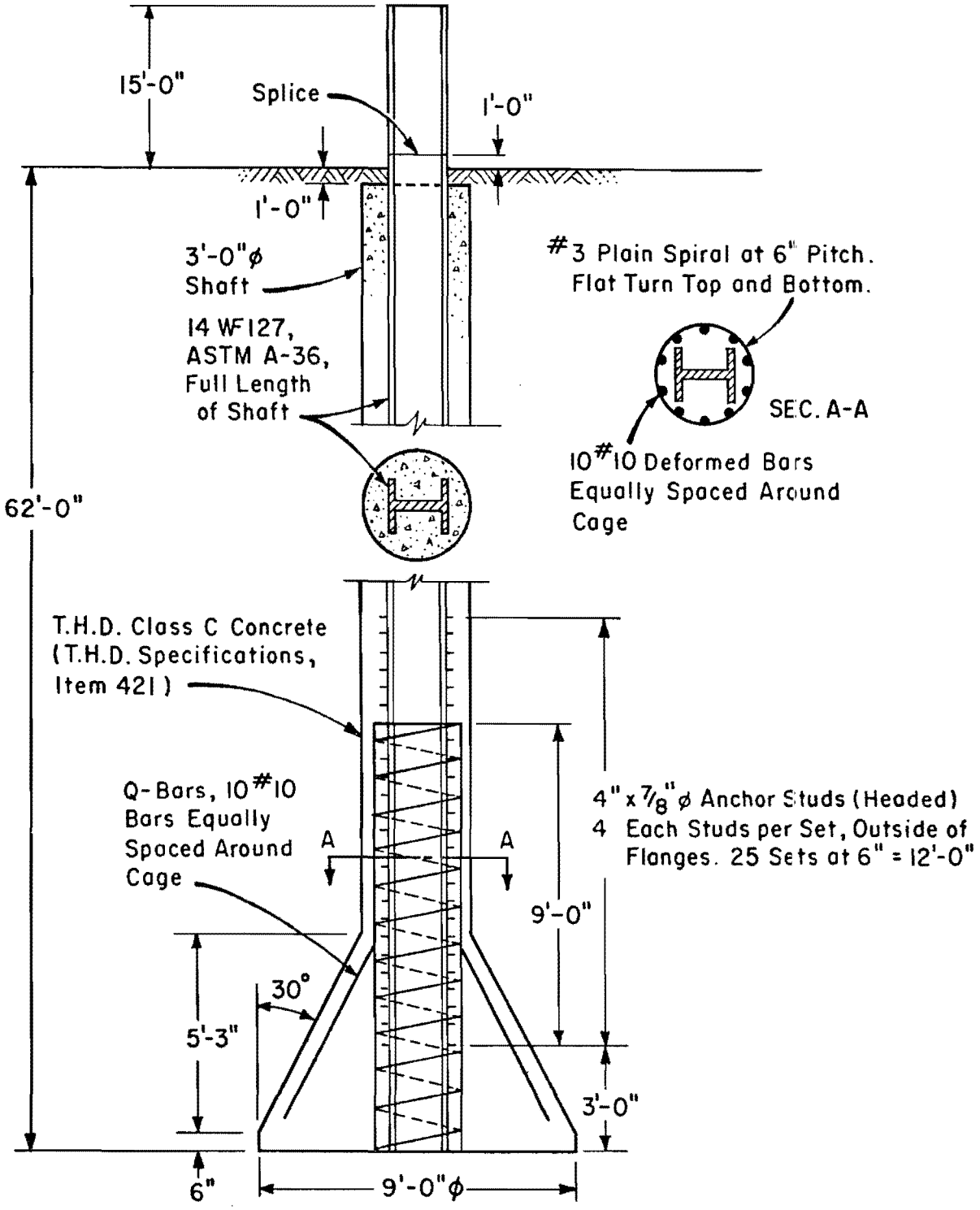

Fig. 8.1. Typical Anchor Shaft

90-foot depth because of problems with collapsing bells. The fifth anchor shaft, installed over a year after the completion of the original four, was designed to take advantage of the side resistance measured in the load tests on S1 and S2. It was 3 feet in diameter and 75 feet deep, with no bell, and was placed in a processed hole.

The anchors were reinforced as indicated in Fig. 8.1. The principal reinforcement was the central flange section, which was studded to effect adequate bonding between steel and concrete. After the shaft was cast, a section of wide flange was butt-welded to the core reinforcement section just above ground level, as shown, to provide an attachment for the reaction frame. The wide-flange member, shown pictorally in Fig. 8.2a, was kept plumb during concrete placement, which was carried out inside the casing by means of a double pipe tremie, as shown in Fig. 8.2b. The tremie served the dual purpose of steadying the wide-flange section and dispensing concrete uniformly. Once the fluid height of concrete was sufficient to provide adequate lateral support to the wide flange, the tremie was removed. The casing was then pulled upward and completely filled with concrete, as shown in Fig. 8.2c, to provide enough hydraulic head to displace the drilling mud trapped between the casing and soil as the casing was pulled (Fig. 8.2d).

The section of cage at the bottom of the anchor shafts was provided as a means of attachment for the Q-bars, which were included to prevent possible shear failure in the bell.

The fifth anchor shaft had a reinforcement scheme composed of a steel cage spanning the entire length of the shaft and a wide-flange section penetrating about 15 feet below ground level. This length of embedment

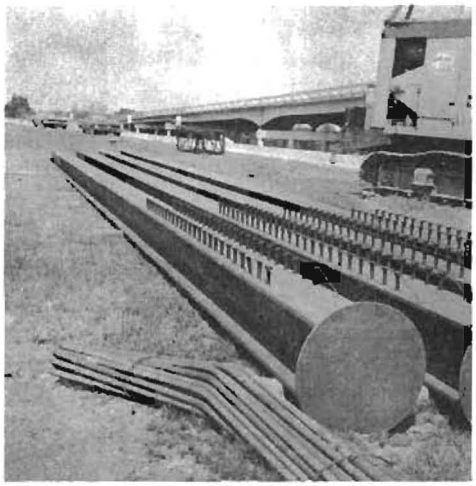

a. Studded Core Sections

b. Double Pipe Tremie

c. Placing Concrete Inside Partially Extracted Casing

d. Drilling Mud Flowing Up from Around Casing

Fig. 8.2. Installation of Anchor Shafts

was adequate for proper shear development for the ultimate load expected for S4. However, difficulty was experienced in keeping this short section aligned during the extraction of the casing, and a special offset connection had to be built to allow the reaction frame to be erected in the proper position.

Reaction System

A portable steel frame was used as the jacking reaction for the tests on S2 and S4. The reaction frame was designed to be bolted between any two adjacent anchor uprights. The frame, shown schematically in Fig. 8.3, consisted of two pairs of stacked 36 WF 230 beams, with each pair welded together as shown. The stacked pairs were bolted together laterally through diaphragm plates located over the loading box, which was used to transmit the applied load equally to the two sets of beams. The reaction frame was connected to the uprights by means of angle plates. Bearing and shear stiffeners were provided as shown.

Since the frame was designed to be assembled by bolting the components together, a minimum effort was required to reposition the frame, once tests on a particular shaft had been completed. The reaction frame was purposely designed to be as rigid as possible under the expected test loads, since flexing and twisting of the reaction beams can induce eccentric loads in the jacks. Eccentric loading results in a poor estimation of load from jack-pressure readings, in addition to imparting a bending moment to the butt of the test shaft. The bottom of the loading box was leveled as accurately as possible each time the frame was erected over a test shaft. Safety plates, shown in Fig. 8.3, were provided as erection aids and as safety stops in case of a connector failure during a load test.

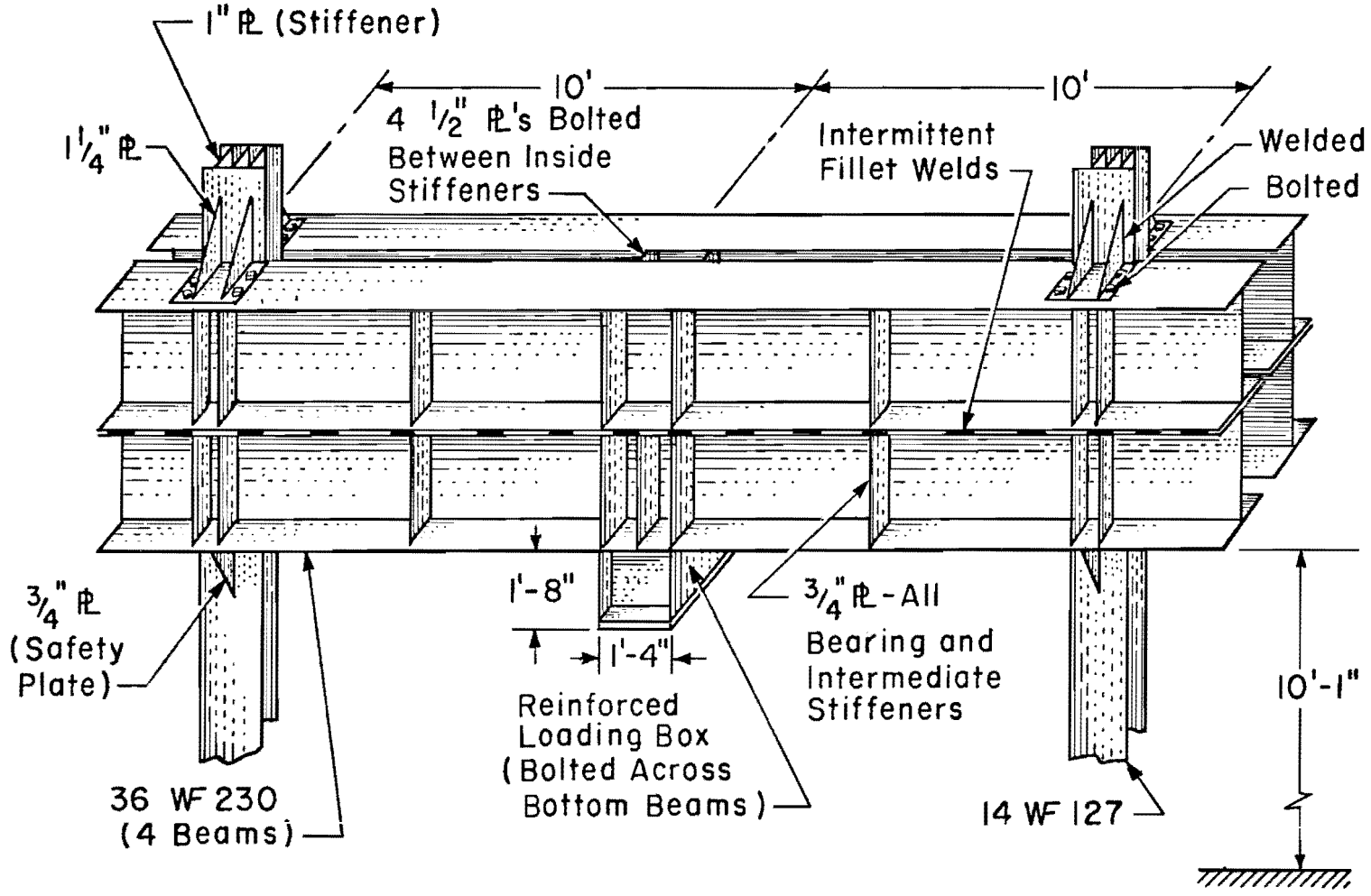

Fig. 8.3. Reaction Frame for S2 and S4

A second reaction frame was used for tests on S1 and S3. It was similar in design to the one shown in Fig. 8.3, with the exception that only a single level of beams was employed. This lighter frame was sufficiently rigid for the tests on S1 and S3, which were designed for relatively small failure loads.

Test Shaft Construction

The test shafts were installed using the standard procedures described in Chapter II. No special drilling techniques were used, except that care was taken to make the boreholes as smooth and cylindrical as possible. Each test shaft had a reinforcing cage composed of eight No. 8 vertical deformed rebars, with No. 3 horizontal circular ties at a 6-inch vertical spacing (S1) or a No. 2 or No. 3 spiral at a 6-inch pitch (S2, S3, S4), interrupted by horizontal ties at the locations where instruments were placed. Nearly all of the instruments were attached to the reinforcing cages prior to construction, and each instrumented cage was placed in the borehole as a single package. Each cage was uniform with depth and extended two feet out of the ground. The instrumentation systems and methods of placement are described fully in the next chapter. In all cases, the lateral steel was welded to the vertical reinforcement, and additional welded horizontal steel hoops were provided for S3 and S4. This was done to obtain near-rigid cages in order to prevent damage to instrumentation during handling. The outside diameter of each cage was 27 inches. The annular space allowed enough room for the concrete to flow between the outer reinforcement and the borehole wall. Also, there was ample clearance between the various gages, which were mounted on the inside of the reinforcing cage, and the tremie, which was used to deposit the concrete in

each test shaft. Each cage was provided with centralizing blocks to aid in setting the cage in the center of the borehole.

Each test shaft protruded one diameter (30 inches) out of the ground. Calibration gages (described in the next chapter) were at ground level and far enough from the applied load to minimize nonuniformities in the stress distribution. The shaft above ground was formed by placing a piece of sonotube form around the protruding part of the cage (nominally 24 inches above ground) and securing it so that the top plane was level and also concentric with the cage. The bottom of the sonotube section was set about one foot below ground. This was done to keep as much concrete as possible out of the enlarged section which invariably occurred at the top of the borehole. The concrete was placed monolithically in the borehole and up to the top of the sonotube form. Some concrete did flow around the bottom of the sonotube in S2 and S4, causing a slightly enlarged section of stem near the surface. The enlargement was minor in S2, and no remedial measures were taken. A large surface collar was formed in S4, however. It was later trimmed off to a depth of two feet with the use of air hammers.

Observations of details of the construction of the test shafts, considered to be pertinent to the behavior of the shafts under load, are presented in the following paragraphs. A full transcription of the field notes taken during construction operations is given in Appendix F.

S1. Test Shaft No. 1 was installed in the dry on June 27, 1968, with a light, truck-mounted auger rig. The borehole was initially drilled slightly undersized and was enlarged to the proper diameter by using a side-cutter on the auger. The final hole was quite smooth, with no

indications of sloughing. A one-inch blanket of sand was placed at the bottom of the hole after removal of drilling crumbs to provide a seat for the bottomhole load cell (described in the following chapter). By the time the load cell was placed and leveled, water had started to infiltrate into the hole from the bottom, but the sides remained dry. The instrumented reinforcing cage was then positioned and centered, as shown in Fig. 8.4a. As soon as the cage was placed, the concrete pour began, with water in the bottom about one to two inches over the top of the bottomhole cell (Fig. 8.4b). The elapsed time from beginning of drilling to completion of concrete placement was 4 1/2 hours. S1 was removed from the ground about 14 months after installation for inspection of its condition. That subject is treated in detail in Chapter XII. However, the shaft was well formed and almost perfectly cylindrical.

S2. Test Shaft No. 2 was installed in the dry on January 6, 1969, with a heavy, truck-mounted auger rig. S2 had a 60-degree-to-horizontal bell with a 6-inch cylindrical base section set at a depth of 23 feet. The top of the bell was at a depth of 18.5 feet and was sharply defined. The construction procedure was nominal, with smooth-sided stem walls and a well-formed bell. The bottom of the bell was "cleaned up" using the belling tool, as is normal practice. No hand cleaning was performed, although the bell was entered for inspection. The stem portion of the borehole was cylindrical, except for the top two to three feet, where it tapered out to about three inches oversize. This tapering occurred during the numerous insertions and extractions of the auger and belling tool. The hole was completely dry. Following the positioning of the cage, concrete was placed using vibration as an aid. However, one gage was struck and damaged by

a. Placing Instrumented Cage in Borehole

b. View of Cage and Borehole from Top

Fig. 8.4. Installation of S1

the vibrator, and the process of vibration was thereafter discontinued in the test shafts. The elapsed time from beginning of drilling to completion of concrete placement was 3 hours and 20 minutes.

S3. Test Shaft No. 3 was installed in the dry on July 8, 1969, with a heavy truck-mounted auger rig. The borehole was smooth, cylindrical, and cut to a depth of 24 feet. To provide a cavity beneath the shaft, a one-foot pad of styrofoam, shown in Fig. 8.5a, was attached to the bottom of the instrumented cage. A coil of copper tubing with numerous small spray-holes, shown in Fig. 8.5b, was embedded in the styrofoam. The coil was connected to the surface through a second copper tube. A vent tube, to allow pressure relief during loading, was also provided. The cage was fitted with a quarter-inch-thick plate, welded to the bottom of the vertical rebars on which the bottom instrumentation was mounted. The styrofoam pad was of such a diameter to allow it to be placed in the hole with a minimum of side clearance to prevent concrete from getting underneath the bottom of the cage. The hole was not entered for inspection, but it was calipered from the surface. The bottom was cleaned up only with the auger. The cage and pad were then set in the hole in the configuration shown in Figs. 8.5c and d, and the concrete was then placed. The hole was completely dry during the entire operation, which was completed in 1 hour and 40 minutes. No compression of the styrofoam was indicated during the placement of the concrete. Nine days after construction, three gallons of technical grade acetone were siphoned down the tube to the coil embedded in the styrofoam to dissolve the pad and allow the shaft to be supported only in side friction. Gage readings during the load test indicated that this operation was successful. A water-acetone mixture was expelled from

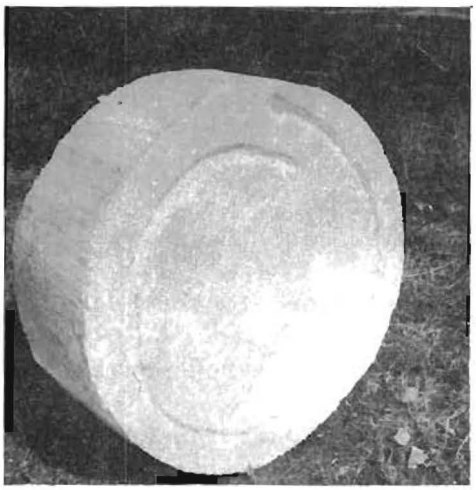

a. Styrofoam Pad

b. Copper Tube Coil

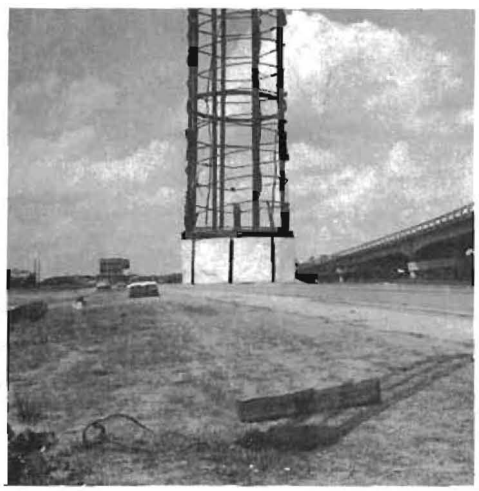

c. Pad in Place

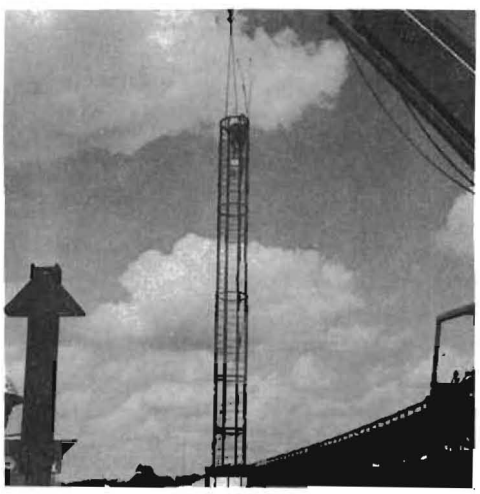

d. Cage in Position Over Borehole

Fig. 8.5. Instrumented Reinforcing Cage for S3

the vent tube during loading, indicating that some groundwater had entered the cavity beneath the shaft and that all acetone had not chemically reacted with the styrofoam.

S4. An attempt was made to install Test Shaft No. 4 at the grid East position on July 8, 1969, but, although drilling mud was used, the hole sloughed in Layer II and had to be abandoned. S4 was installed in the position indicated in Fig. 6.3 on July 9, 1969. The hole was augered with a large, truck-mounted rig, and was installed with the aid of drilling mud, composed of cuttings from the hole and several bags of bentonite, as described in Chapter II. Mud was introduced at the time Layer II was encountered and was present for the full length of the hole as drilling progressed from 29 feet to 40 feet. The casing was set and sealed at 40 feet, the mud inside the casing was bailed out, and the final 5 feet was completed in the dry. The bottom of the hole was cleaned up with the auger. The hole was not entered and could not be calipered after drilling mud was introduced. Some irregularities were observed in the sides of the hole near the surface, possibly caused from erosion by the drilling mud. The bottom of the hole was dry, except for a small amount of water contained in the pilot hole made by the auger. The instrumented cage, which was fitted with a bottom plate similar to that for S3, was set on a three-inch-thick plug of concrete to seat the bottom gages. The concrete placement operation was nominal, although a uniform flow of drilling mud from around the casing was not observed until the casing had been almost completely extracted, indicating possible entrapment of drilling mud between the concrete and soil at some point. The entire operation required 4 hours and 35 minutes.

Concrete Control

Concrete used in construction of the tests shafts was provided by ready-mix contractors. The entire shaft was poured from the same truck where possible. The quality of concrete used in the test shafts was checked by continually running slump tests and by taking standard cylinder samples as each pour progressed. Compressive strengths and elastic moduli were obtained on the cylinders. The concrete had reasonably uniform properties with depth in each test shaft and varied only slightly among all shafts. The average 28-day compressive strength was about 5000 psi, with an average initial modulus value of 5.9×10^6 psi. Modulus values were not obtained for S1, but it is assumed that the average modulus is about the same as for the other shafts. Results of the cylinder tests, conducted by Shilstone Testing Laboratory, of Houston, are contained in Appendix G.

Six-inch-slump concrete was specified to insure that all instrumentation was properly embedded. Care was taken during each pour to provide complete embedment for every gage.

CHAPTER IX

TEST SHAFT INSTRUMENTATION

Method of Obtaining Load Distribution Information from Instrumentation

In order to achieve the objectives of the study, the distribution of axial load along the test shafts was measured. This was accomplished, in principle, by applying a load, measuring the load remaining in the shaft at several levels, either directly or indirectly, and passing a smooth, best-fit load distribution curve through the data points. This procedure was repeated for each value of applied load.

It is felt that the technique of fitting a smooth curve to the discrete data points, which define load at various positions in the stem, is more desirable than merely connecting the points with a series of straight lines, at least from the standpoint of obtaining representative load transfer curves. The data scatter is great enough to cause the load transfer obtained from the slope of a straight line connecting adjacent data points to be considerably in error. The smoothing operation provided by the curve-fitting procedure reduces that error significantly. However, curve fitting has the disadvantage that it may cause real effects, such as an abrupt change in load transfer between two zones of the stem, to be attenuated in the final results.

The curve fitting was accomplished automatically on a digital computer using third, fourth, and fifth degree polynomial least-squares regression lines, and the polynomials producing load distribution curves that appeared to give the best visual representation were chosen from among the three

sets. Visual determination of the proper degree for the regression lines for each test was accomplished by instructing the computer to plot the data points together with each trial polynomial on microfilm, which was then viewed to select the proper degree. Careful selection of the proper degree was necessary because polynomials of a given degree may be ill-conditioned to represent the data, while those of a different degree may be well-conditioned. For example, data points that appear to define a load distribution curve with two points of contraflexure cannot be well-represented by a third degree polynomial, and the load transfer relationships derived from such a curve would be misleading. Instead, a fourth, or possibly fifth, degree curve would be required. An even higher degree polynomial may, however, begin to be unduly influenced by the data scatter, again giving misleading results. In general, therefore, indiscriminate use of polynomials of any given degree, without a visual check of the precision of fit, is to be avoided. The least-squares procedure was used in preference to fitting the data graphically in this study only because it permitted the process of curve fitting and determination of load transfer relationships to be programmed to be carried out automatically on the computer, whereas graphical curve fitting requires time-consuming construction for production of load transfer curves.

Special boundary conditions were imposed on the regression lines at the ground surface:

1. The load transfer was zero at the surface
2. The value of applied load was known exactly.

Hence, the regression line always passed through the data point representing applied load. The first boundary condition was established to be consistent

with the observation that generally poor contact existed between the shaft and soil for the top two or three feet. The curve fitting procedure is illustrated in Fig. 9.1 and is explained more fully by Barker and Reese (1970). The load distribution curve obtained by this procedure is expected to be a good representation of the true load distribution curve discussed in Chapter III. From a set of these regression curves, the load transfer curves were developed for various depths as described in Chapter III. Specifically, discrete values of load transfer and movement were computed at each level where the relationship was desired from a number of load distribution curves embracing the spectrum of applied loads. The results were then plotted, and a curve was fitted to the points visually. The single-order smoothing operation, conducted only on the load distribution data, led to well-defined load transfer relationships not requiring further statistical fitting in any instance.

The usual procedure for obtaining load at a particular level in a pile or drilled shaft is to measure the vertical strain in the concrete, convert strain to stress on the cross section, and finally, compute the load by multiplying stress by the cross-sectional area. A variation of this approach, explained later, was used in the present study. Since cross-sectional area and modulus of elasticity were needed in data reduction, the borehole diameter and concrete properties were controlled as closely as possible during construction.

Previous Attempts at Measurement of Axial Load Distribution in Driven Piles and Drilled Shafts

Procedures for measuring loads at various levels beneath the ground surface in loaded driven piles have been established for many years.

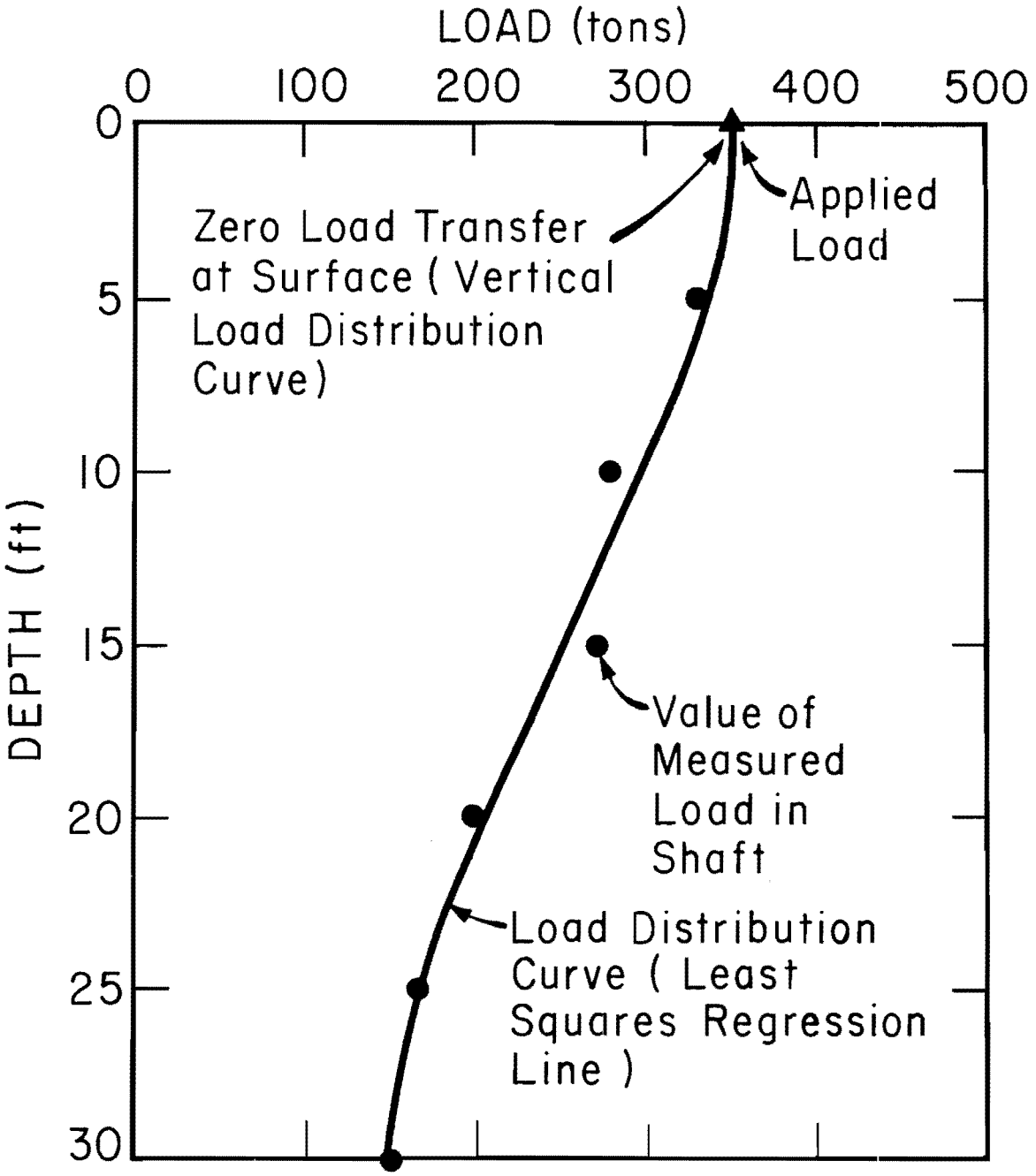

Fig. 9.1. Fitting a Load Distribution Curve Through Data Points

Hansen and Kneas (1942) reported using strain rods (telltales) situated at different depths in cast-in-place concrete shell piles as early as 1941 to obtain the variation in downward displacement with depth in piles. Sufficient information was available for computation of load distribution, although no load distribution relationships were reported. The Hansen and Kneas paper marked a notable achievement in pile testing, since, according to the editors of Civil Engineering magazine (Hansen and Kneas, 1942), it contained the first published results in the United States of distribution of displacements along a pile.

Electrical resistance strain gages have also been used for measuring load distribution in piles. Crandall (1948) reported an early application of bonded and unbonded wire gages to the measurement of strain distribution (and thereby load distribution) in cast-in-place concrete shell piles. Strain gages were aligned vertically and cemented at several levels to a central steel pipe which was subsequently cast inside the shell. During testing, the gages were read to give values of strain at the various gage levels. Strain values were converted to stress and then to load to obtain values of load remaining in the pile at the gage levels. Numerous applications of this basic procedure for obtaining load distribution have since been reported in connection with experimental studies of driven piles.

It should be pointed out that instrumentation of driven piles for load distribution has been much more successful than that for drilled shafts, and indicated load values have been much less scattered. Many problems mentioned in the following paragraphs contribute to data scatter in drilled shafts but are not encountered with driven piles. In particular, the material properties and cross-sectional areas are known accurately for

H-piles or pipe piles. Pipe piles have the additional advantage that strain gages can be mounted to the inside of the pipe, which, in addition to protecting the gages during driving, allows the gages to be kept dry and stable. Precast concrete piles can be gaged and precalibrated before installation. Cast-in-place concrete shell piles do have some of the same disadvantages of drilled shafts in regard to instrumentation, except that the cross-sectional areas are accurately known unless shell distortions occur before concrete placement.

There have been few reports of attempts at measurement of load distribution in drilled shafts. As mentioned in Chapter V, several investigators (DuBose, 1956; Whitaker and Cooke, 1966; Bhanot, 1968) installed load cells at the bases of drilled shafts to measure the total load transferred to the soil between the butt and base. The design of such a load cell, constructed with foil-type electrical strain gages and intended for use in a full-sized shaft, is described by Whitaker, Cooke, and Clarke (1962). A similar type of bottomhole load cell employing vibrating wire strain gages has been recently developed (Osgerby and Taylor, 1968). Bottomhole load cells constructed with the vibrating wire gage hold considerable promise for providing better long-term stability than can be achieved with bonded electrical resistance strain gages. Generally, the electrical load cell has been a reliable device for obtaining the load on the base (or at the top of the bell) of a drilled shaft under short-term static loading.

However, attempts to place instrumentation along the stem of a drilled shaft for the purpose of measuring load distribution have met with varying degrees of success (Cambefort, 1953; DuBose, 1956; Frischmann and Fleming, 1962; Van Doren et al., 1967; U.S. Army Engineer District, Fort Worth,

Texas, 1968; Reese, Hudson, and Vijayvergiya, 1969). In general, loads at depths intermediate between butt and base have not been measured as reliably as base loads measured with bottomhole load cells.

Some of the problems encountered in attempting to obtain usable load readings in the stem are enumerated below.

1. Axial load-measuring devices embedded in a concrete shaft are subjected to a wet, corrosive environment. Unlike above-ground installations, the concrete in a drilled shaft will remain moist for a prolonged period, perhaps permanently, unless the shaft is installed in a dry, permeable soil. Any device made with electrical resistance strain gages, such as a gaged reinforcing bar, is subject to instability resulting from the collection of moisture, even microscopic amounts, on the grid of the gage. Even when electrical resistance gages are thoroughly waterproofed by conventional methods, such as by covering the gage with several coats of waterproofing compound, water can still migrate onto the grid and cause significant resistance changes. These resistance changes are reflected in false indicated strains. Further instability can be caused by the presence of moisture, which can give a variable path to ground. Moisture-related stability problems apply to lead wire and connections, as well. The moisture problem can be circumvented by more elaborate waterproofing or by using gages which do not operate on the electrical resistance principle, such as strain rods, hydraulic pressure cells (described later), and vibrating wire electrical gages.

2. Any gage embedded in concrete is subject to damage or displacement during construction of the shaft.
3. Even if axial strain can be measured reliably, the conversion to stress is uncertain if the stress-strain characteristics of the concrete at the gage level are not known accurately.
4. Uncertainties arise in conversion of stress to load at a particular level because the exact cross-sectional area may be unknown (particularly in a shaft installed in a processed hole) and because the stress distribution may not be uniform across the section.
5. Problems related to construction (concrete separation, segregation, or necking) may cause gages to be inadequately embedded.
6. Poor gaging techniques, such as failure to provide proper temperature compensation for electrical gages or bad alignment of strain rods, can lead to errors in indicated load.

In principle, a drilled shaft could be segmented with properly sealed load cells. This would eliminate most of the problems listed herein, but because of practical problems of installation, new uncertainties would probably be introduced. Specifically, the extended period of time required for correct load cell placement could allow changes to occur in the soil composing the borehole walls, such as extreme wetting or drying, sloughing, or creep resulting in loss of ground. Placement of load cells would be troublesome in a dry hole. Satisfactory segmentation of a shaft installed in a processed hole would be an extremely difficult operation.

Experience has shown that the error involved in measuring load at any level in the stem of a drilled shaft is approximately a fixed percentage of the magnitude of load present. The load distribution data for the field

tests at the SH225 site (Chapter XII) reflect this fact by exhibiting more apparent scatter at higher values of applied load. For this reason, it is difficult to measure accurately the load transfer in a shaft in which the magnitude of load is high all along the stem, such as a belled shaft near its failure load.

Load Measurement Procedures Used in Present Study

Load distribution was measured in the present study in order to investigate the effects of base geometry on load transfer (possibility of reduction of load transfer near base), to determine the location of zones of ineffective load transfer, to obtain information concerning the depth at which load transfer effectively begins, and to measure the location and magnitude of the maximum developed shear stresses. Knowledge of the actual shape of the load distribution curves is useful in gaining insight into the manner in which a drilled shaft transfers load to the soil, in order to develop rational design procedures.

According to Barker and Reese (1969), an ideal load distribution instrumentation system should possess the following characteristics:

1. A degree of accuracy compatible with the objectives of the test.
2. A sensitivity such that the desired resolution is obtained.
3. Enough durability to remain operational during the testing period.
4. Adequate stability.
5. A cost which will not be prohibitively high.
6. A method of readout compatible with the testing procedure.
7. A relatively easy method of installation.

The system to be used in the tests at the SH225 site had to be quite sensitive, since concrete strains were expected to be small. In fact, to

read a load to the nearest ton, gages had to be able to resolve concrete strains of about 0.5 microinches per inch. One of the systems employed (the system composed of Type 1 Mustran cells, described later), actually had a reliable concrete strain resolution that was limited only by the accuracy of the readout equipment.

The primary instrumentation system (Mustran) was constructed to meet the other requirements outlined by Barker and Reese, as well.

All shafts were programmed to be loaded by the QL procedure for purposes of obtaining better correlation of measured shear stresses with undrained shear strength. It was imperative, therefore, that the instrumentation and data acquisition systems be designed in a manner to obtain data from all gages as nearly simultaneously as possible. This provides an accurate definition of load distribution curves as the shaft approaches failure, where distribution of load is possibly changing rapidly.

Load at various depths in test shafts was measured in the testing program in the following manner:

1. Gages of various designs, described later, were embedded in the concrete at several levels in the test shaft. Each level contained two, three, or four gages of the same design, placed around the centered reinforcing cage to permit cancellation of strain due to bending.
2. A similar set of each type of gage was placed at the ground surface.
3. Readings from the set of gages at the ground surface (calibration level) were obtained as a function of applied load as the load increased. The method of applying and reading butt loads is described in Chapter XI.

4. A plot of average readings of calibration gages was made against corresponding values of applied load. The resulting points were fitted with a third degree least-squares polynomial, as shown in Fig. 9.2.

5. The load-reading curve developed in such a manner was then assumed to be applicable at all levels. Inherent in this assumption is the supposition that the stress-strain properties, cross-sectional area of the shaft, gage sensitivity, and gage alignment were the same at the calibration level and at the level for which the load reading was desired. It is felt that these suppositions were valid for S1, S2, and S3, which were installed in the dry, but that the assumption of constant cross-sectional area was in error for S4, which was installed in a processed hole. (Removal and inspection of S1 revealed a well-formed cylindrical shaft, while excavation to a depth of 24 feet around S4 indicated an irregularly-shaped stem. See Chapter XII). Therefore, after the load tests, individual calibration curves were obtained for levels of instrumentation in S4 to a depth of 24 feet by cutting soil away from the sides of the shaft, thereby exposing the shaft to that depth, and subsequently loading the free-standing section to obtain direct load-reading curves. Test Shaft No. 2 was also calibrated in a slightly different manner, as explained in Chapter XII. The stresses developed in the concrete were rather low in all tests; therefore, the concrete stress-strain relationships were essentially linear in all cases. Since the response of the gages themselves was linear, calibration curves were nearly linear.

6. The calibration curve, Fig. 9.2, was entered with the average gage

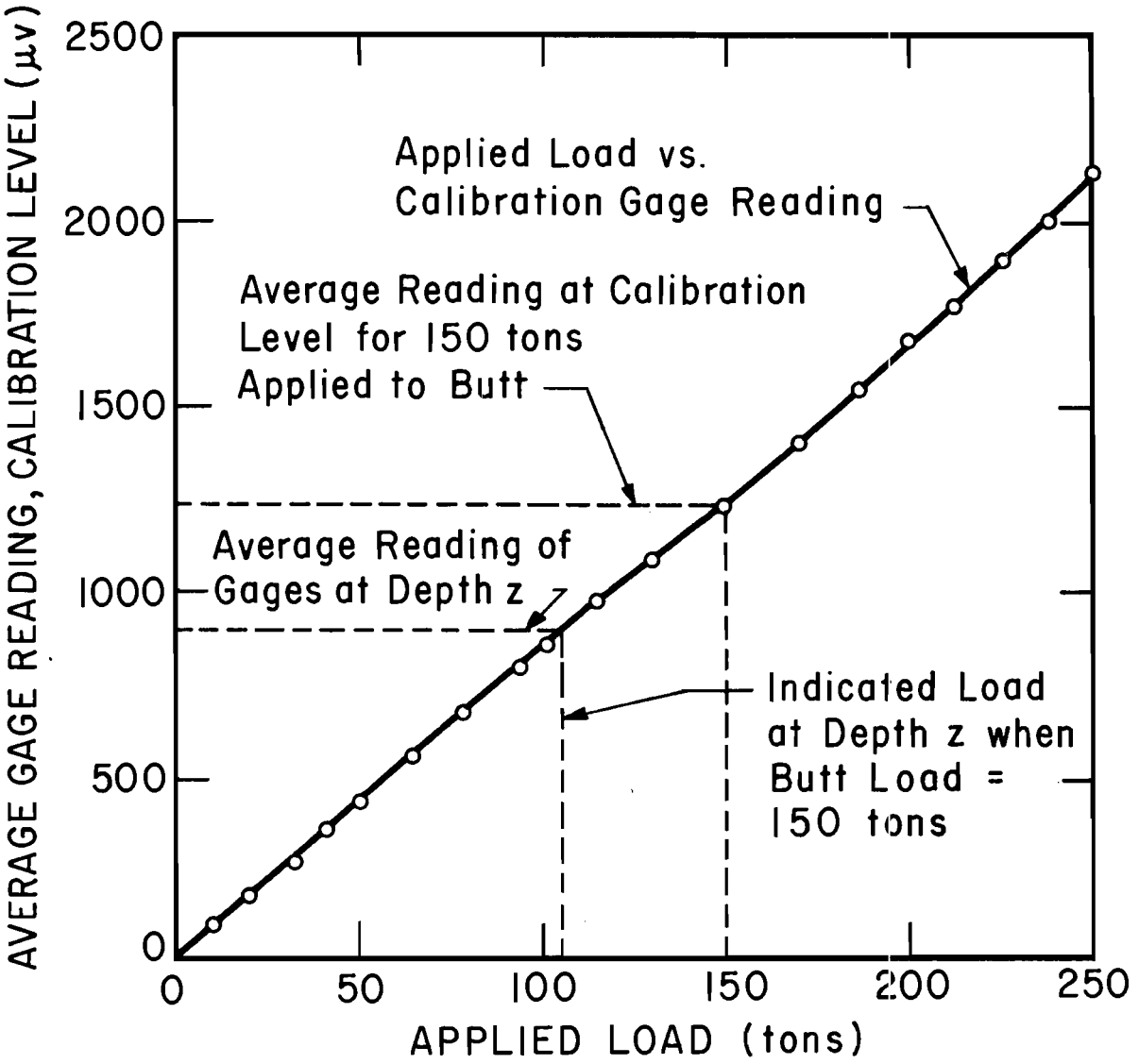

Fig. 9.2. Shaft Calibration Curves

reading, and the load value was read as illustrated to obtain a value of load corresponding to the particular average gage reading at a level.

7. The procedure outlined in Steps 1 through 6 was repeated for every level of gages, and a load distribution curve was fitted to the data. Similarly, load distribution curves were obtained for each value of applied load. Bottomhole load cell data were also included where applicable and were treated in the same way statistically as the data from embedded gages in constructing the load distribution curves (see description of cell later in this chapter).

Instrumentation Systems Used in Tests

Six types of instrumentation were used in the SH225 tests. Three types were intended as primary instrumentation, and three types were installed for purposes of evaluation. The primary instrumentation systems were:

1. Mustran cells,
2. Concrete embedment gages,
3. Bottomhole load cell.

Other instrumentation systems evaluated were:

4. Strain rods,
5. Hydraulic pressure cell,
6. Weldable strain gages.

Barker and Reese (1969) discuss in detail the first five types of instrumentation. The Mustran cell system proved to be the most reliable, and together with the bottomhole cell, is the system by which almost all load distribution data were obtained. The first three types and the last type can be described as electrical gages and the others as mechanical

gages. The bottomhole cell and hydraulic pressure cell provide a direct reading of load or stress. The other systems provide indirect readings since they measure concrete strains, which are then converted into loads in the manner outlined previously.

The instrumentation systems are briefly described in the following pages.

Mustran System. The Mustran cell is an electrical gage developed and constructed at The University of Texas at Austin specifically for use in load testing of drilled shafts (Barker and Reese, 1969). The word "Mustran" is an acronym for "multiplying strain transducer." The complete cost of a single cell is approximately seventy dollars. The cell has all of the seven characteristics desired of load distribution instrumentation listed earlier. The sensitivities of the individual cells were tailored to measure the expected strains with the desired degree of load resolution (about 0.5 per cent of the expected maximum applied load). The Mustran cell is designed to be embedded in the concrete and to respond to concrete strains. It does not measure concrete strains directly, but instead performs as a load indicator device, used in connection with the in-shaft calibration procedure explained earlier. The cell is designed to have the same stiffness as that of the concrete which it displaces.

Two basic types of Mustran cells, denoted Type 1 and Type 2, were constructed. The Type 1 cells were more sensitive and were used in S1, S3, and S4, in which the concrete strains were relatively small. The Type 2 cell was used in S2, in which the concrete strains were higher. The design of the Type 1 cell is shown in Fig. 9.3. Some very minor as-built differences in the details of individual cells existed within each type. They are mentioned only where warranted.

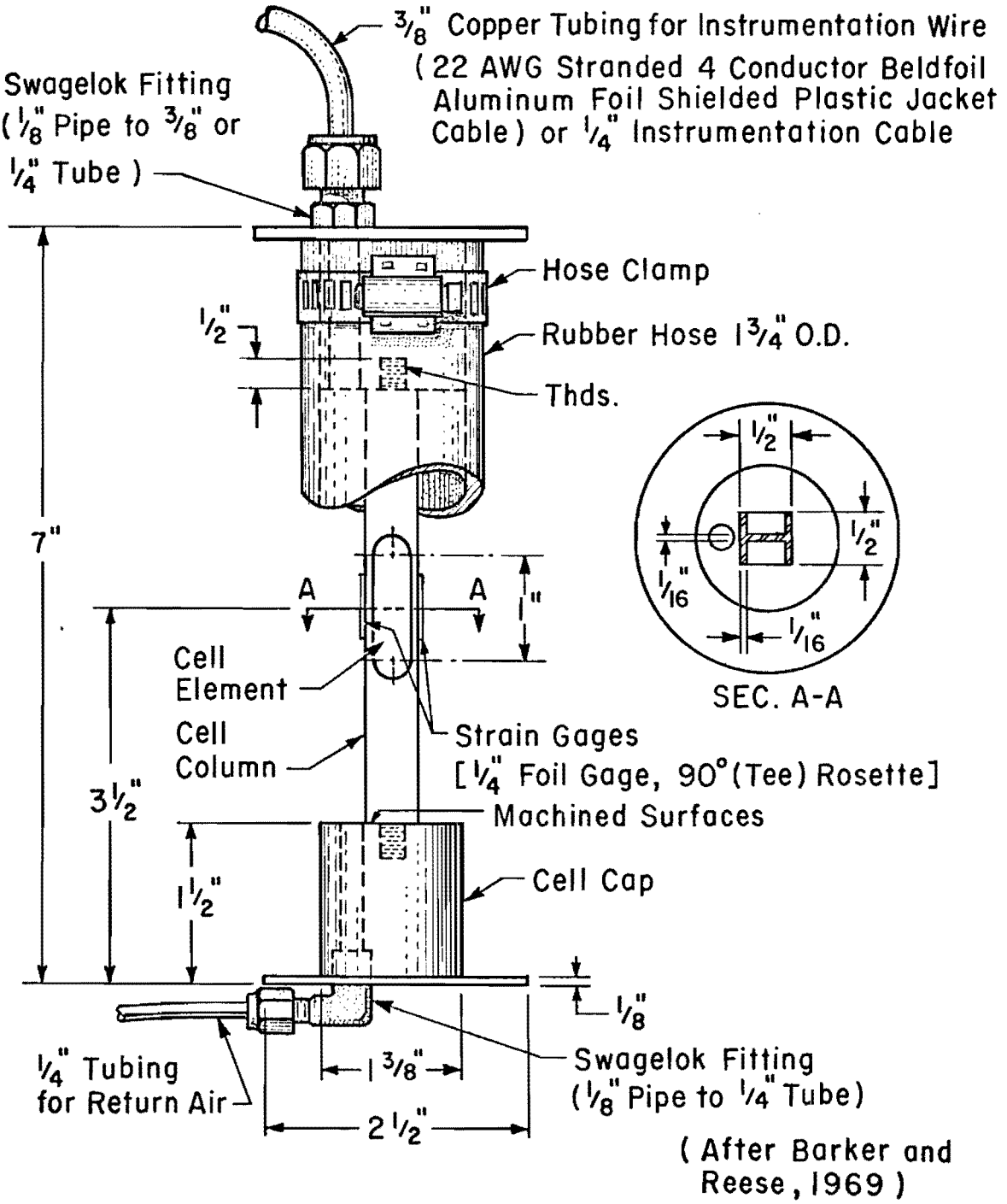

Fig. 9.3. Mustran Cell, Type 1

The Mustran cell is composed of a gaged mild steel bar connected by tight threaded joints between two caps, the ends of which are flanged for embedment in the concrete. Machined bearing surfaces are provided between the caps and bar. The threaded connections are tight enough to allow the cells to act in tension or compression. The gaged bar, or cell element, is enclosed by a rubber sheath composed of a section of radiator hose, which is clamped and sealed securely over both end caps, providing a water-tight chamber around the strain gages. Two 90 degree tee rosette foil-type electrical resistance strain gages are bonded to opposite sides of the bar and waterproofed with a standard commercial compound, as indicated in Fig. 9.3. The rosettes are wired in full bridge configuration to provide maximum gage output under axial load, to cancel bending effects, and to compensate for temperature differences. The bridge is completed inside the chamber, and the two power and two signal leads are brought out from the top cap through a pressure fitting (flare for cells in S1, ferrule for cells in S2, S3, and S4) into a heavy cable jacket (used in S3 and S4) or into a light jacket encased in a protective copper tube (used in S1 and S2) which protects the leads all the way to the surface. The flare fittings were abandoned after the construction of S1 cells because it was felt that they did not provide as good a pressure seal as did the ferrule fittings.

The protruding ends of the lead wires at the surface are installed in a pressure manifold which, in addition to protecting the ends of the lead wires from entrance of external moisture, serves as a device to pressurize the jacket or copper tube with dry nitrogen. Details of manifold designs are described later. Nitrogen pressure from the manifold is transmitted into the cell chamber through the tubing or between the cable jacket and

conductor wires. A second pressure tube returns to the surface from the bottom of the chamber. This return tube is capped at the surface by a pressure fitting. By removing the tube cap, dry nitrogen from the nitrogen source at the surface is allowed to flow through the chamber. This permits the in-place cell to be purged of moisture in case moisture problems are indicated. As an additional precaution against accumulation of moisture on the gage elements, desiccant, in the form of about 30 grams of anhydrous calcium chloride, was placed inside the chamber for the cells used in S3 and S4. The dry nitrogen environment design was chosen over waterproofing by filling the chamber with oil, since the effect of oil on the epoxy used to bond the gages to the bar was uncertain. Use of the gas pressure system also permitted a leaky gage to be located easily.

The gage length of the Mustran cell is the distance between the lips or flanges on the two end caps. Most of the cells used in the field tests had 2 1/2-inch-diameter lips, as shown in Fig. 9.3. However, a few of those used in S4 had 2-inch-diameter lips. Since the cap is machined from a solid piece of mild steel, the use of 2-inch lips significantly reduces machining time. No embedment problems were encountered with the 2-inch lips.

Most of the strain in the Type 1 cell (Fig. 9.3) is concentrated in the bar, in particular, in the thin cut-out section on which the strain gages are mounted. This strain concentration gives the Mustran cell its desired sensitivity. The less sensitive Type 2 cell differs from the Type 1 cell in that it has no cut-out section and has a gaged bar which is 5 1/2 inches long instead of 4 inches long.

Photographs of the Type 1 Mustran cell at various stages of assembly are shown in Figs. 9.4a through 9.4d.

a. Gaged Bar

b. Gaged Bar, End Caps, and Fittings

Fig. 9.4. Mustran Cell at Various Stages of Assembly

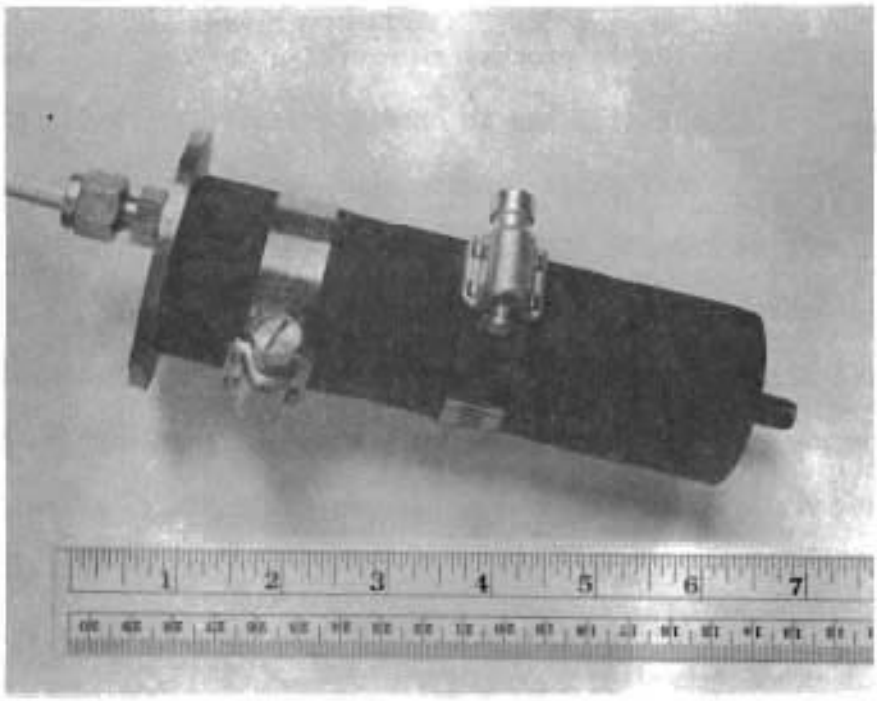

c. Rubber Sheath and Hose Clamps Covering Gaged Bar

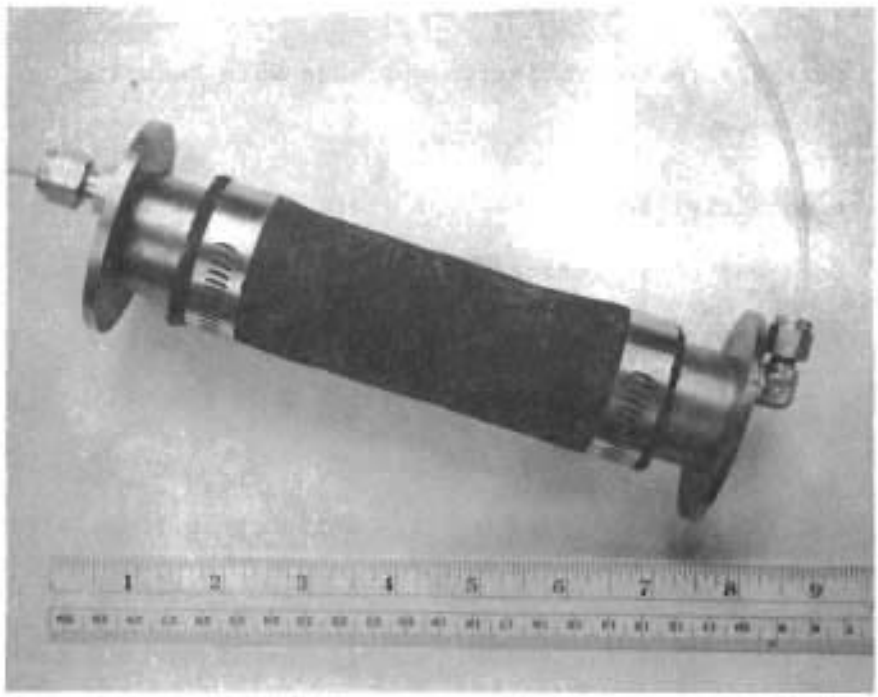

d. Completed Cell

Fig. 9.4. Continued

After each cell to be used in the field study was assembled, it was loaded cyclically in the laboratory to exercise the machined bar, to check electrical continuity, and to obtain a load calibration constant for the cell. The load calibration constant was recorded in terms of output voltage per kip of load applied directly to the cell. The constant provided an indication of linearity and consistency between cells in a given batch. The Type 1 cells used in S1 were precast in 4 1/4-inch by 4 1/4-inch by 11-inch concrete blocks before testing. This was done for the purpose of providing a good bonding surface between the shaft concrete and the cells. This practice was discontinued for S2 through S4 because it was found to be unnecessary. A listing of calibration constants for all cells and other pertinent details concerning cell design are given in Appendix H. Cells with mixed gage factors were used in S4. The resultant sensitivity differences were very small (less than three per cent), and no correction for gage factor variation was made when reducing data for the tests on S4.

Relative sensitivities of the Type 1 and Type 2 cells are shown in Fig. 9.5. Cell output is indicated in terms of microvolts per six volts of direct voltage applied. It is observed that the Type 1 cells are about three times as sensitive as the Type 2 cells when the cells are loaded directly.

Procedures for conversion of voltage output to circuit strain, as indicated on a full-bridge strain indicator, are presented in Appendix I. That appendix also gives factors for conversion of circuit strain to strain in the gage steel and also presents an approximate method for conversion of Mustran gage output to concrete strain.

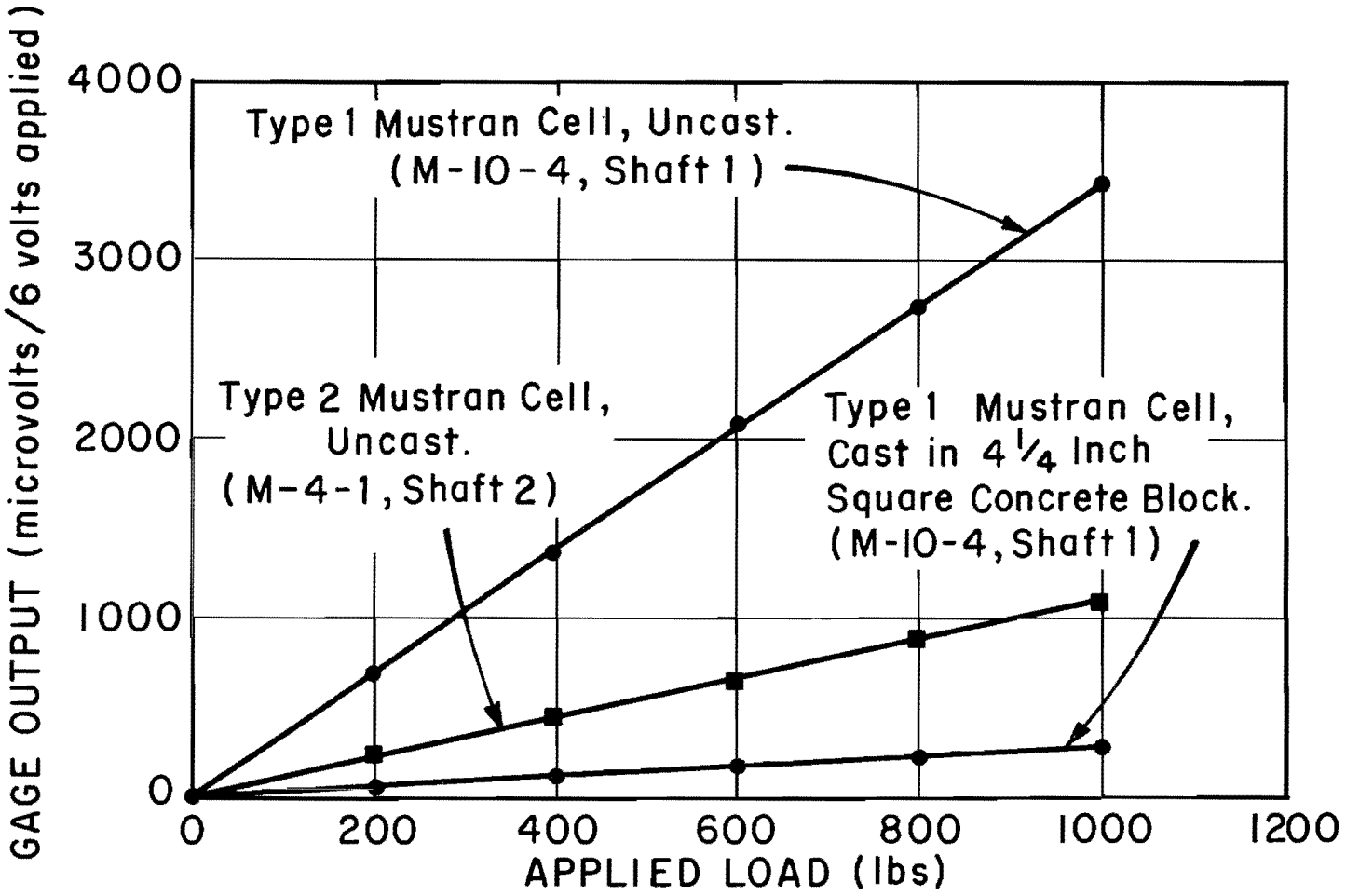

Fig. 9.5. Typical Comparison of Response of Various Types of Mustran Cells Prior to Installation

Temperature and creep sensitivity tests were conducted on two Type 1 cells, denoted V and W, which were gaged with BLH FAET-25C-S6 foil tee rosettes mounted with heat-cured Bean RTC adhesive. Although the Mustran cell is ideally temperature compensated, some changes in reading were indicated with changing temperature, as shown in Fig. 9.6a. This change is quite small for the range in temperature which occurs in a drilled shaft and can be disregarded for all practical purposes.

The same two gages were then directly loaded under a constant compressive force to check creep characteristics. The results of the creep tests, conducted at a stress level of 12 ksi in the steel (1 kip applied load), are displayed in Fig. 9.6b. The small amount of cell creep is apparently caused by bond creep between the foil gages and the steel bar. Most of the creep occurred within the first week after loading. The indicated creep at 73 days is about 3.5 per cent of the original indicated strain.

In the field the cells were installed by tying them securely to horizontal ties on the reinforcing cage as illustrated in Fig. 9.7a. They were placed as far as possible from vertical reinforcement in order to insure good embedment. Before each cage was placed, the cells were carefully aligned vertically. In S1, S3, and S4, Mustran cells were placed two or four at a level in order to permit cancellation of bending effects. In S2, they were placed three at a level equally spaced around the cage, except for the bottom two levels, at which four cells were placed. In S1, the Mustran cells were precast in concrete blocks, which in turn were bolted to the cage. Exact positions for all instrumentation are given later.

Base plates made from 1/4-inch-thick steel were attached to the bottom of the S3 and S4 cages. The Mustran cells in the bottom level were bolted directly to the plate as shown in Fig. 9.7b. Three cells along a diameter

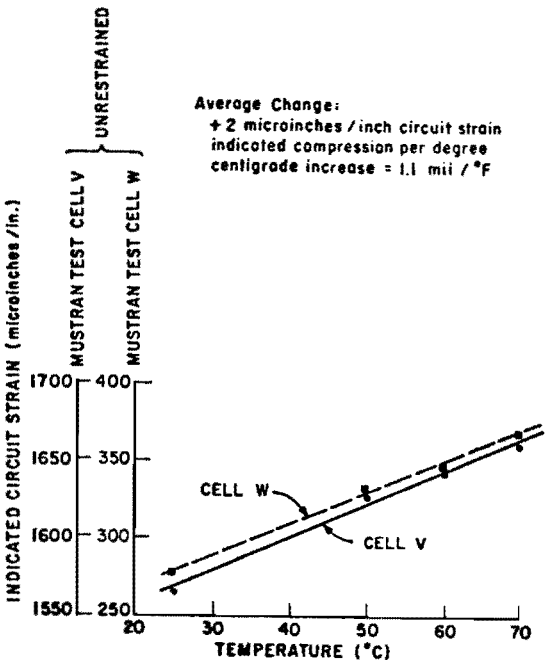

a. Change in Mustran Cell Reading with Change in Temperature

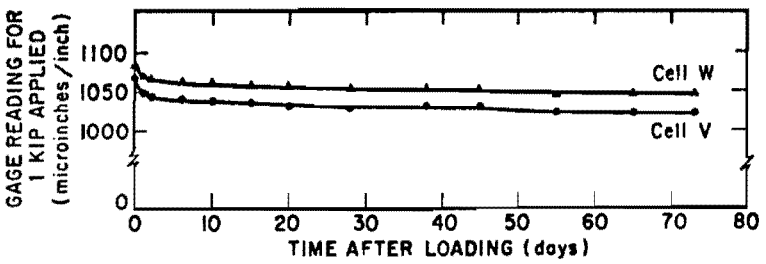

b. Creep of Mustran Cells Under Constant Load

Fig. 9.6. Temperature and Creep Tests - Mustran Cells

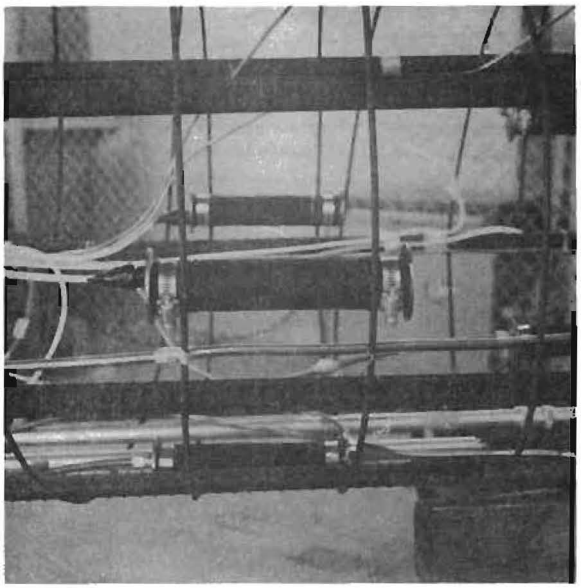

a. Method of Attachment of Cells to Reinforcing Steel (S2) (after Barker and Reese, 1969)

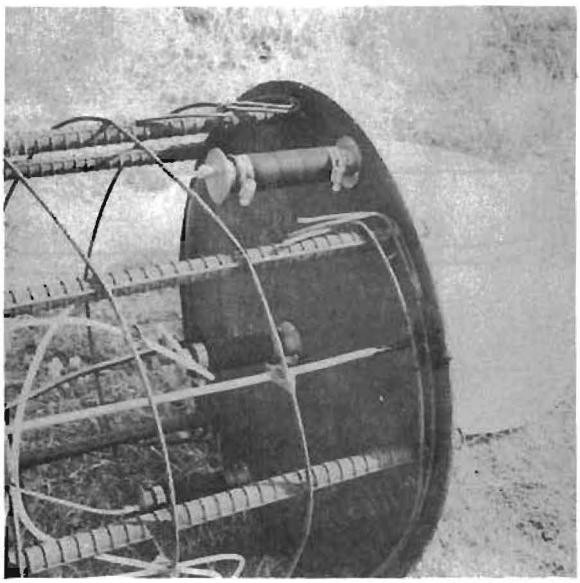

b. Method of Attachment of Cells to Base Plate (S3)

Fig. 9.7. Mustran Cells on Cages

were used in S3; five cells along two perpendicular diameters were used in S4. This arrangement replaced the bottomhole load cell used to measure base load in S1. In S3, the plate served as a bottom form for the concrete. In S4, the plate was embedded in a small amount of concrete placed at the bottom of the borehole before the cage was installed. The instrumentation cables or the copper tubes protecting the lead wires were bundled and brought to the surface. Additionally, bundles of instrumentation cables were taped with heavy cloth tape to assist in preventing abrasion of the cable jackets during the concrete pour. Care was taken during the concrete placement operation to get good embedment of each cell while avoiding cell displacement. Concrete was tremied into the test shafts to provide a free fall of no more than five feet. Concrete was not allowed to fall directly on the gages.

The overall Mustran cell system, as installed, is illustrated schematically in Fig. 9.8. The cells were continuously pressurized (at approximately 10 psi) with dry (oil pumped) nitrogen from compressed gas bottle sources, which remained on the site. Simple manifolds constructed for S1 and S2 are described by Barker and Reese (1969). They were effective but cumbersome to use. The improved manifold used to distribute the pressure to each of the Mustran cells in S3 and S4 is shown in Fig. 9.9. The top and bottom plates, which sealed against the ends of a section of pipe, contained bulkhead pressure fittings for the individual cable jackets and for the pressure inlet. The inside surfaces of the end plates contained plugboards to which the leads were connected. Each set of leads was soldered to a Cinch-Jones eight-pin female plug mounted in the plugboard. A ground wire, which had been grounded to the top ferrule fitting of every cell, was soldered to one pin in each plug. Both signal leads and one

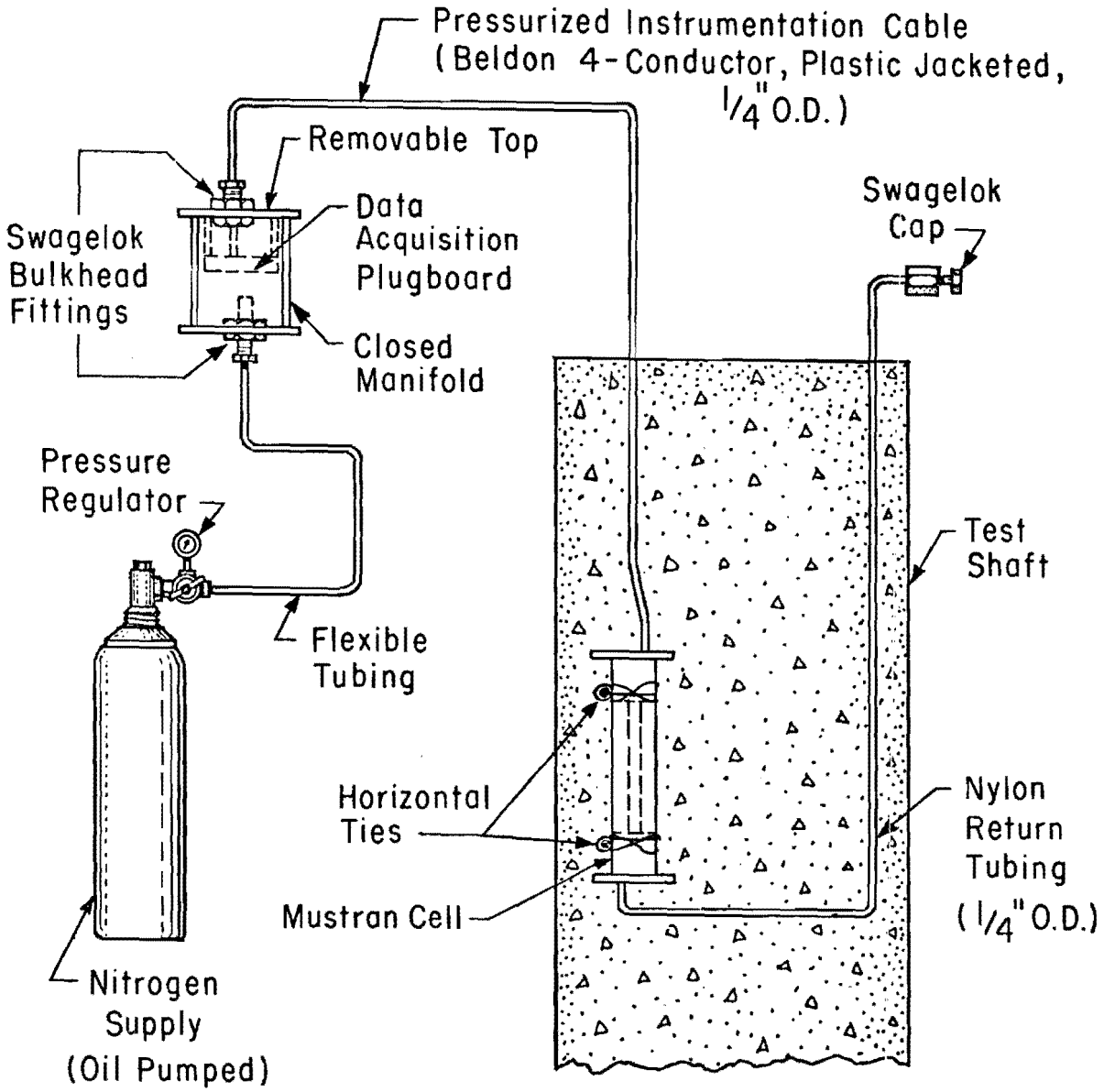

Fig. 9.8. Schematic Diagram of Mustran System

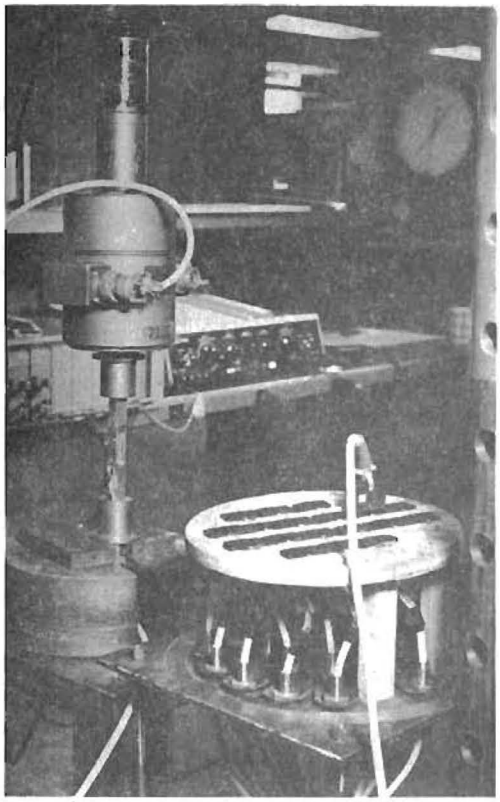

a. Plugboard in Use During Calibration

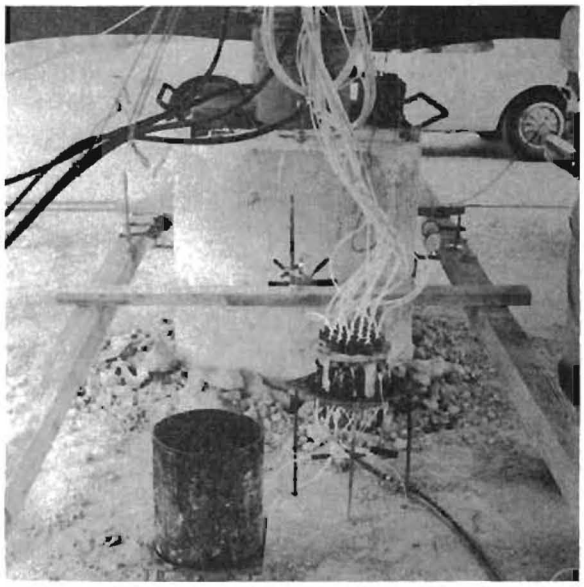

b. Plugboard in Use During Load Test

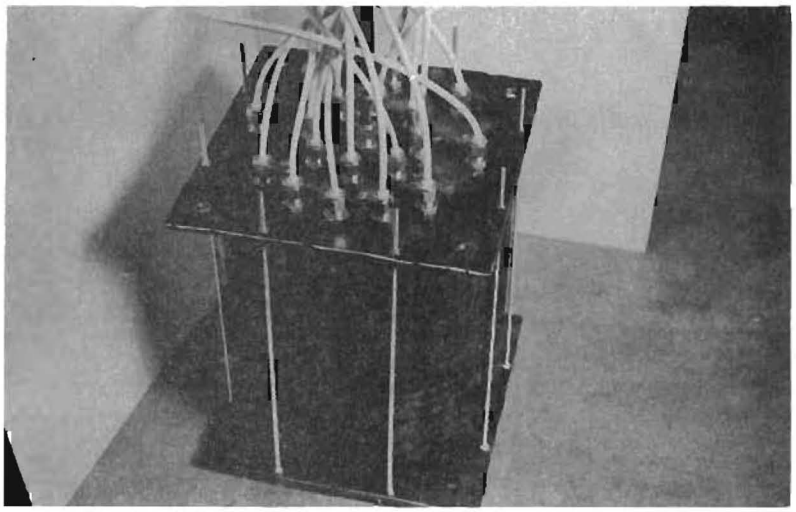

c. Closed Manifold

Fig. 9.9. Mustran Pressure Manifold

power lead were double-pinned for added connector integrity. A matching male plug was used to complete the connection with the data acquisition instruments. Strain indicator or voltmeter readings were taken by plugging into the appropriate cell plug while the manifold was disassembled. Each manifold-cell system was pressurized as soon as the cage was set in the borehole and remained pressurized except during the periods that Mustran cells were being read. Pressure was taken off the system following the last load test in each case.

Once a cell is installed in a shaft, an indication of its reliability is its resistance to ground, which is a measure of the electrical resistance between the gage grid and the bar on which the gage is mounted. Changing resistance to ground serves as a warning that moisture is bridging between the bar and the gage grid and, more importantly, between the lines of the grid. Such moisture accumulation, which is a major problem in drilled shaft instrumentation, causes improper output voltage registration, with resultant incorrect strain indicator or voltmeter readings. Ground resistance readings were taken with a high impedence ohmmeter each time the cell strain readings were obtained throughout the curing period. Two cells in S1 indicated low ground resistance shortly after installation, suggesting that moisture had penetrated the cells either before installation or immediately thereafter. These cells were then flushed with dry nitrogen, and the ground resistance was increased to an acceptable value. Most cells, particularly those in S3 and S4 with desiccant in the chamber, had ground resistances of 5000 megohms or greater throughout the several months of testing. Cells with desiccant in the chamber gave constant values of ground resistance with time, indicating that they were producing stable strain readings throughout the entire period of the field study. Cells

without desiccant gave generally good, but variable, ground resistance. This fact suggests wetting and drying of the gage grid over a period of time, causing the long-term cell readings to be invalid. The short-term reliability is unaffected, however. A few cells in S1 and S2 had somewhat low ground resistance, but in all cases except one (cell M-18-U, S2), ground resistance exceeded 100 megohms, the minimum acceptable value that had been established for good reliability. The one cell which showed low ground resistance was mechanically damaged during placement but was otherwise in good working condition. That cell did not drift under no-load conditions; hence, despite low ground resistance, short-term readings were accepted as correct.

Concrete Embedment Gage System. A second load-measuring system was composed of commercially available concrete embedment strain gages: Type PML-60 concrete embedment gages manufactured by Tokyo Sokki Kekyujo Co., Ltd., of Japan (Vijayvergiya, Hudson, and Reese, 1969; Barker and Reese, 1969). The PML-60 gage is composed of a wire element bonded between two wafers of polyester, whose outer faces are roughened to enhance bonding. The gage leads are vinyl coated, and the point of entrance into the gage is waterproofed with an epoxy compound. Nominal specifications are:

Gage length - 60 mm,

Gage width - 1 mm,

Resistance - 120 ± 0.5 ohms,

Gage factor - 2.12,

Overall dimensions of polyester wafer mold -

125 mm X 13 mm X 5 mm.

A photograph of the PML-60 gage is shown in Fig. 9.10.

Fig. 9.10. PML-60 Embedment Gage

Embedment gages are less sensitive than Mustran cells. However, unlike the Mustran cells, embedment gages directly measure strain in the concrete. That strain can be converted into load if the elastic modulus and cross-sectional area of the concrete are known. In actual practice, however, load at depth was obtained using the same in-shaft calibration method employed for the Mustran system.

Circuits for embedment gages were constructed as shown in Fig. 9.11. Each circuit was a bridge consisting of two opposite arms containing vertically aligned embedment gages and two opposite arms containing unstrained dummy gages. The dummy gages, used to provide temperature compensation, were of the same type as the active gages. They were located inside a waterproof junction box. Active arm gages were precast in small blocks of concrete mortar to enhance bonding with shaft concrete. The leads, encased in plastic tubing for protection, were carried into the junction box, where the bridge was completed. All solder joints were chemically waterproofed and covered with heat-shrinkable spaghetti. The four lead wires for the bridge were then brought to the surface inside a copper tube, which was connected to the junction box through a flare fitting. No attempt was made to pressurize the system or to protect the ends of the leads from moisture, although the junction box and leads were thoroughly flushed with dry nitrogen prior to installation to dry off moisture which had accumulated.

Active gages were placed on the reinforcing cage at opposite ends of a diameter to cancel the effects of bending. They were secured to horizontal ties away from the vertical reinforcement with tie wire in much the same manner as the Mustran cells. The junction box was also tied to the cage

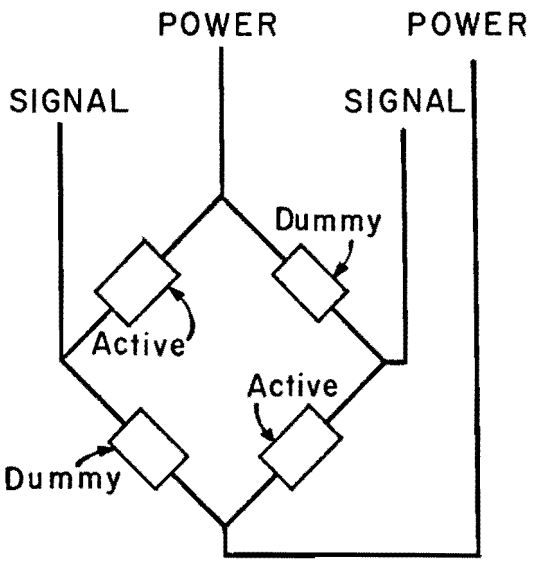

ALL GAGES TOKYO SOKKI KENKYUJO CO. TYPE PML-60 CONCRETE EMBEDMENT STRAIN GAGES

WIRING DIAGRAM-EMBEDMENT GAGE CIRCUIT

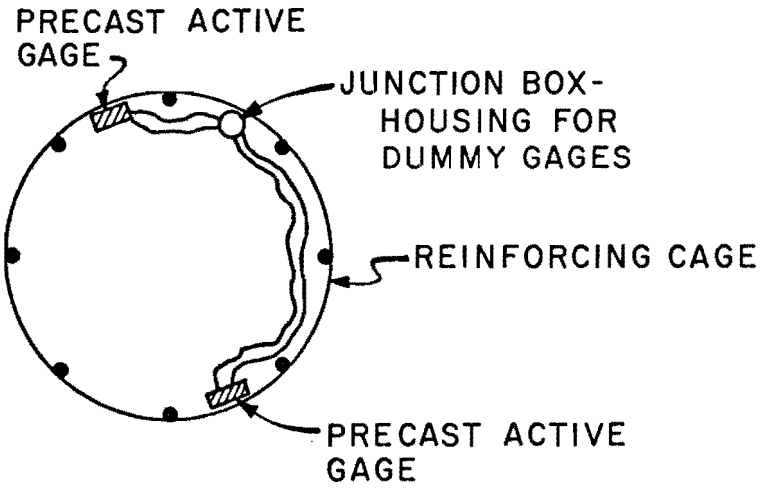

SCHEMATIC-PHYSICAL ARRANGEMENT OF EMBEDMENT GAGE CIRCUIT

Fig. 9.11. Schematic Diagram of Embedment Gage Circuit Used in S1 and S2

at the same depth as the active gages. Two embedment gage bridges were placed at each instrumentation level to provide a degree of redundancy in the event one of the bridges failed. To simplify installation, each junction box accommodated both embedment gage circuits. A photograph of a pair of embedment gage circuits, partially assembled, is shown in Fig. 9.12.

Laboratory studies conducted by Vijayvergiya, Hudson, and Reese (1969) indicated that accurate concrete strain measurements can be secured from the PML-60 embedment gage. The stress-strain relationships measured by the embedment gages at the tops of S1 and S2 (Fig. I.1, Appendix I) yield a modulus value very close to that obtained in cylinder tests on concrete from the batches from which the test shafts were poured.

However, during the curing period for the test shafts, the ground resistance of the embedment gages varied considerably. Although only a few circuits indicated dead shorts, an overall drop in ground resistance was measured in every circuit. Because of this variation, readings taken during curing were both erratic and invalid, although most circuits were usable for the short-term load tests.

In S1, five of the twelve embedment gage circuits gave acceptable ground resistance readings (greater than 100 megohms) one year after casting. In S2, four of the six embedment gage circuits indicated acceptable ground resistance five months after installation, and five showed acceptable values after an additional ten months, with no action being taken in the interim to improve the characteristics of any of the gages.

The procedure used to read all electrical gage circuits during load tests was to power all circuits continuously with a constant voltage power supply and to sample the output voltage at discrete intervals in time

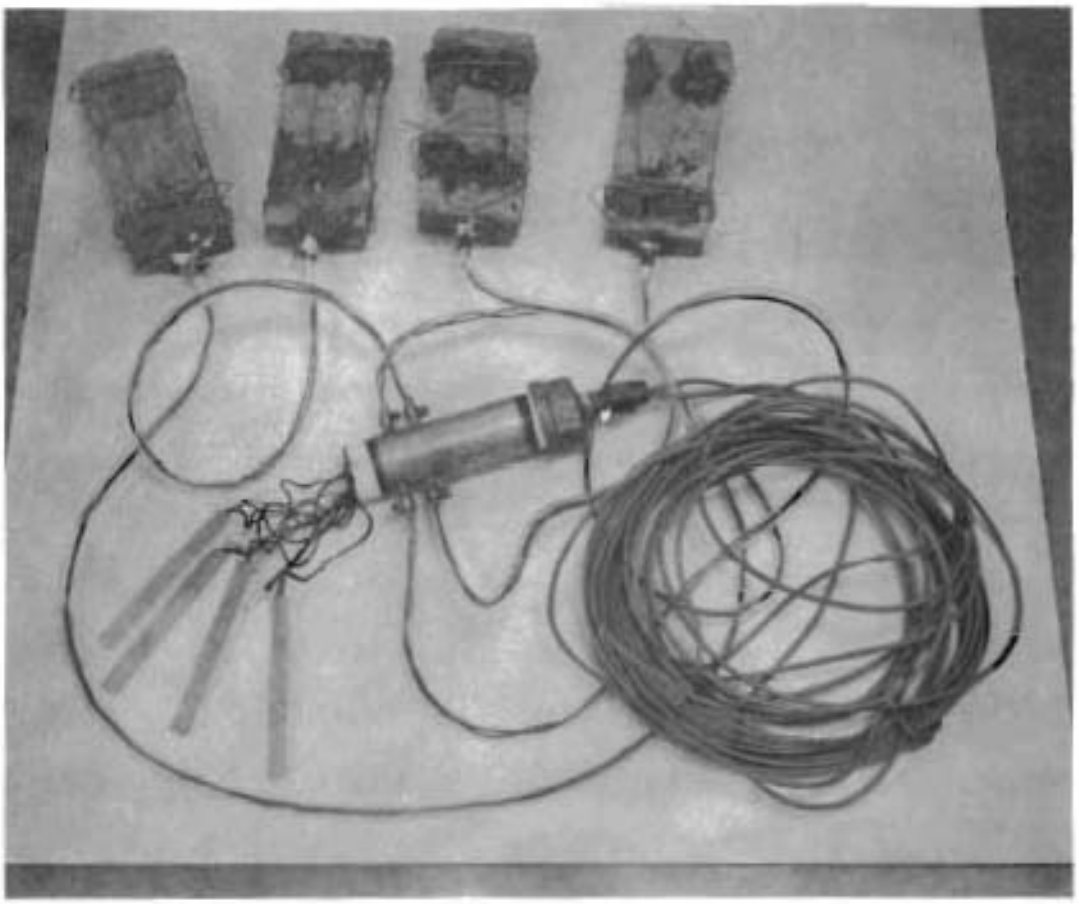

Fig. 9.12. Partially Assembled Pair of Embedment Gage Circuits Prior to Installation in S2

as the applied load changed. The primary problem encountered with the embedment gage circuit was its tendency to drift when continuously powered. Drift was checked on unstrained, continuously-powered gages in the laboratory and on gages embedded in test shafts. In either circumstance, the no-load drift was significant. It appeared to be somewhat cyclic, displaying an approximately diurnal variation. Drift readings taken for in-place circuits for several hours before load testing revealed maximum drift in output voltage as high as 100 microvolts per hour for surface circuits and 5 to 50 microvolts per hour for circuits below ground. By comparison, maximum gage output for the greatest load on S1 was about 400 microvolts. Therefore, the drift was quite significant, since, for a test requiring two hours, the gage zero could drift up to 200 microvolts, or one-half the indicated applied load. The in-shaft drift was minimum in the early morning and late afternoon; hence, load tests involving embedment gages were run at those times of the day.

It was necessary to power and read each gage under no-load conditions for a period of time prior to testing to ascertain a numerical value of drift rate and to stabilize power-induced temperature variations in the gages. Assuming that the drift continued at the same rate throughout the period required to conduct the test as occurred during the final part of the monitor period, a drift correction was made for each gage reading taken during the load test to improve its accuracy.

Because of zero drift, the reliability of the embedment gage system is diminished, since it is not known whether the drift is constant during testing. Drift correction extrapolations of more than one or two hours are undependable. For this reason, the embedment gage system became a

secondary load-measuring system, and the Mustran cells, which were quite stable, were relied upon as the primary instrumentation scheme.

Much of the drift was believed to be due to unequal heating of the active and dummy gages. The heat was provided by the electrical current flowing in the powered unbalanced bridge and by temperature changes in the concrete.

A second embedment gage circuit design was used experimentally in S3. It was wired and attached as shown in Fig. 9.13. The bridge was composed of four active arms, two horizontal and two vertical. All four gages were precast. The leads from each gage were brought through plastic tubing into a small junction box, where the bridge was completed. The bridge leads were brought to the surface through a copper tube. The junction box was potted with an RTV compound, and both the tubes connecting the gages with the junction box and the tube carrying the bridge leads to the surface were filled with lightweight, nondetergent oil.

In principle, the improved tee embedment gage circuit did not permit the concrete strains to be measured as reliably as with the original design, since the horizontal gages were present as active elements in the circuit. However, long-term, no-load strain indicator readings appeared much more stable, ground resistance remained practically constant at 1000 megohms, and the circuit did not drift measurably during the continuously-powered monitoring phase prior to the load test on S3. Furthermore, the experimental circuit, placed just below the ground surface, gave reliable readings during the load test with drift corrections being unnecessary even though the gage was continuously powered. A concrete modulus of 6.5×10^6 psi (assuming Poisson's ratio of concrete to be 0.15) was indicated, compared

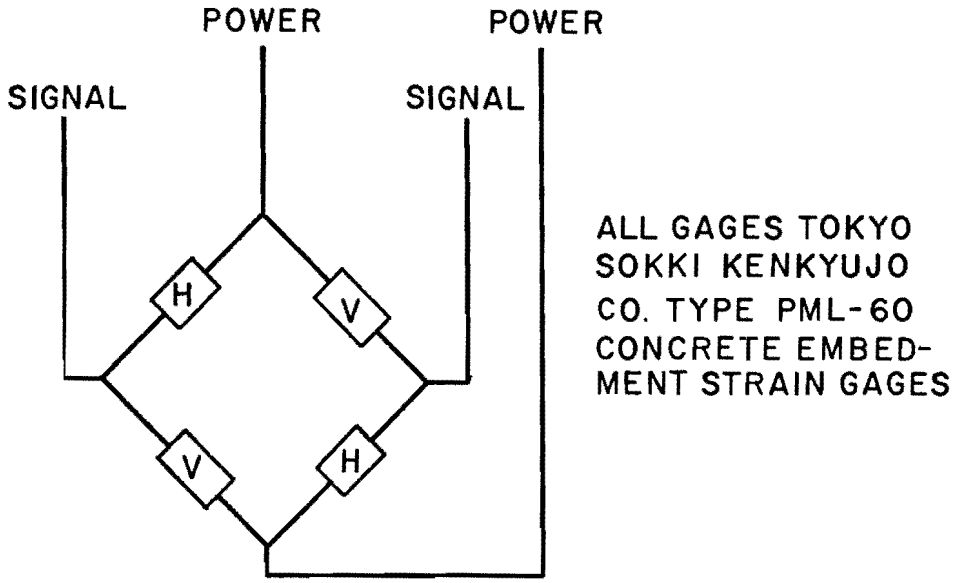

WIRING DIAGRAM-EMBEDMENT GAGE CIRCUIT FOR BRIDGE USED IN SHAFT 3.

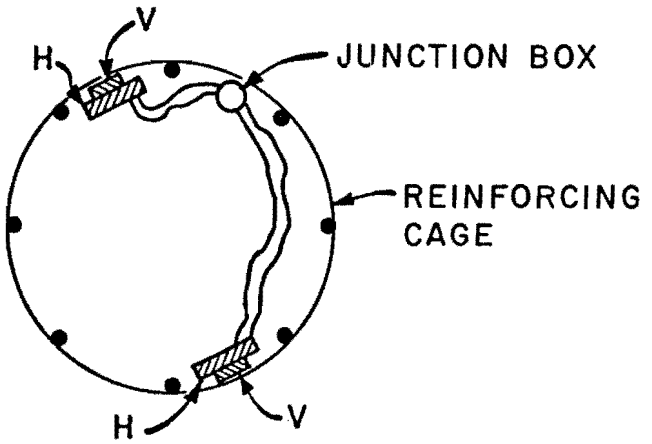

SCHEMATIC-PHYSICAL ARRANGEMENT OF EMBEDMENT GAGE CIRCUIT FOR BRIDGE USED IN SHAFT 3.

Fig. 9.13. Schematic Diagram of Embedment Gage Circuit Used in S3

to 6.4×10^6 psi measured in cylinder tests. This design appears to be superior to the original design in spite of the fact that the Poisson's effect exists. No further evaluations of the new system were made in this study. The installed bridge costs about half as much as one Mustran cell. Its chief disadvantage is that it is only about one-fourth as sensitive as the Type 1 Mustran cell. Its sensitivity is slightly greater than the original embedment gage circuit, however.

Bottomhole Load Cell. A load cell designed and built by the Center for Highway Research was placed at the bottom of S1 in order to obtain an accurate evaluation of base load. The load-measuring elements in the cell were case-hardened steel diaphragms gaged with bonded foil diaphragm-type full bridge strain gages (BLH Type FAES-4-150-12S6), as shown in Fig. 9.14. Each foil gage was waterproofed by coating it with a standard gage coating compound and by potting the diaphragm cup with RTV. Three such diaphragms were placed between two 1 1/2-inch steel plates, 29 inches in diameter. A single circuit was formed, as shown in Fig. 9.15. The diaphragms were centralized and spaced equally around the cell by using a centering template, seen in Fig. 9.16a. The bridge was completed inside the cell, as pictured in Fig. 9.16b. Three connecting bolts, which acted to oppose tension but not compression, were used to center the template and to attach the top plate to the bottom plate, as seen in Fig. 9.16c. The bolts were loosened after the cell was constructed to prevent any preloading of the diaphragms. The leads were brought to the surface through a copper tube connected to the cell by a flare fitting, shown in Fig. 9.17a. The periphery of the cell was sealed with a rubber and neoprene jacket, as shown in Fig. 9.17b.

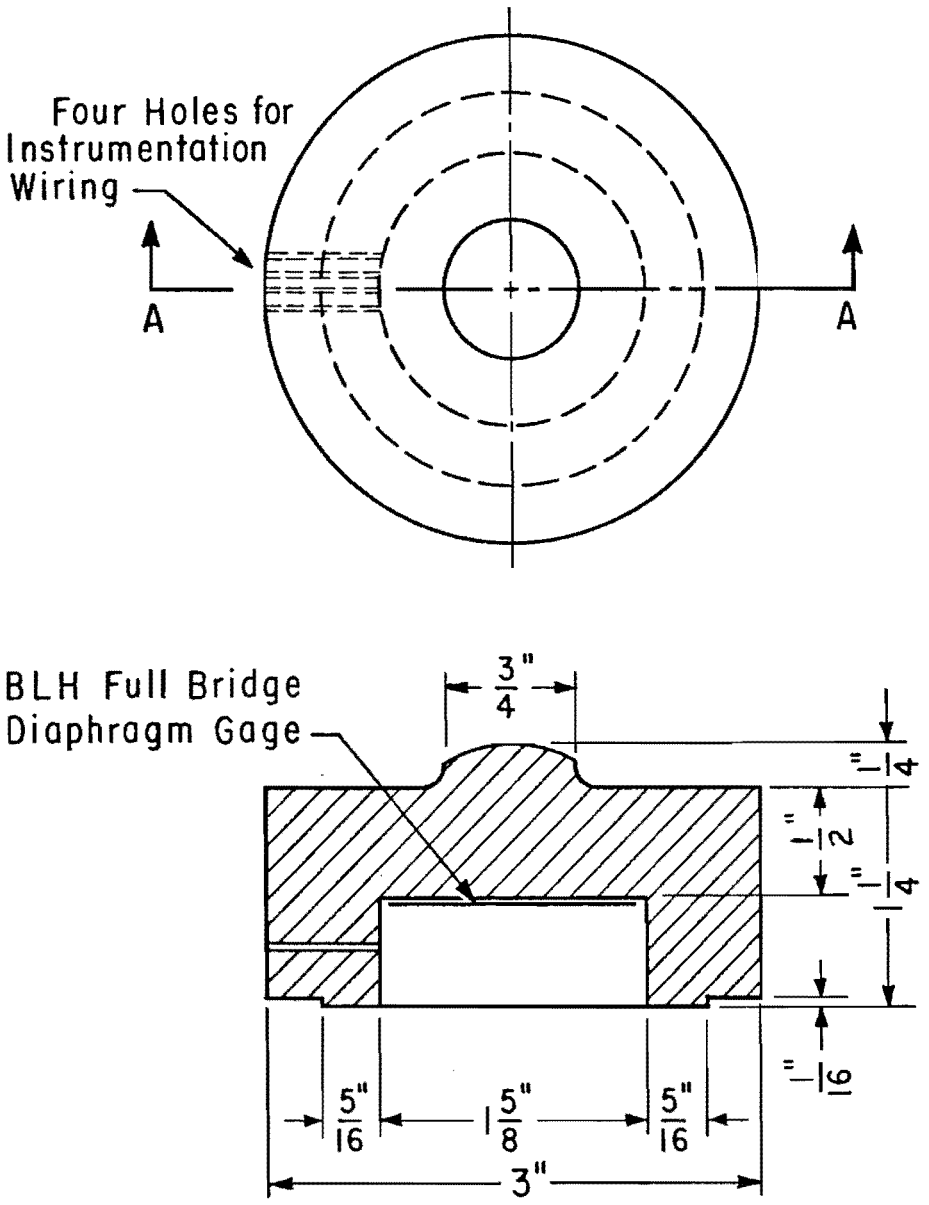

SECTION A-A

Note: Machined from a High Carbon Cold Rolled Steel. Case Hardened.

(After Barker and Reese, 1969)

Fig. 9.14. Load-Measuring Element for Bottomhole Load Cell

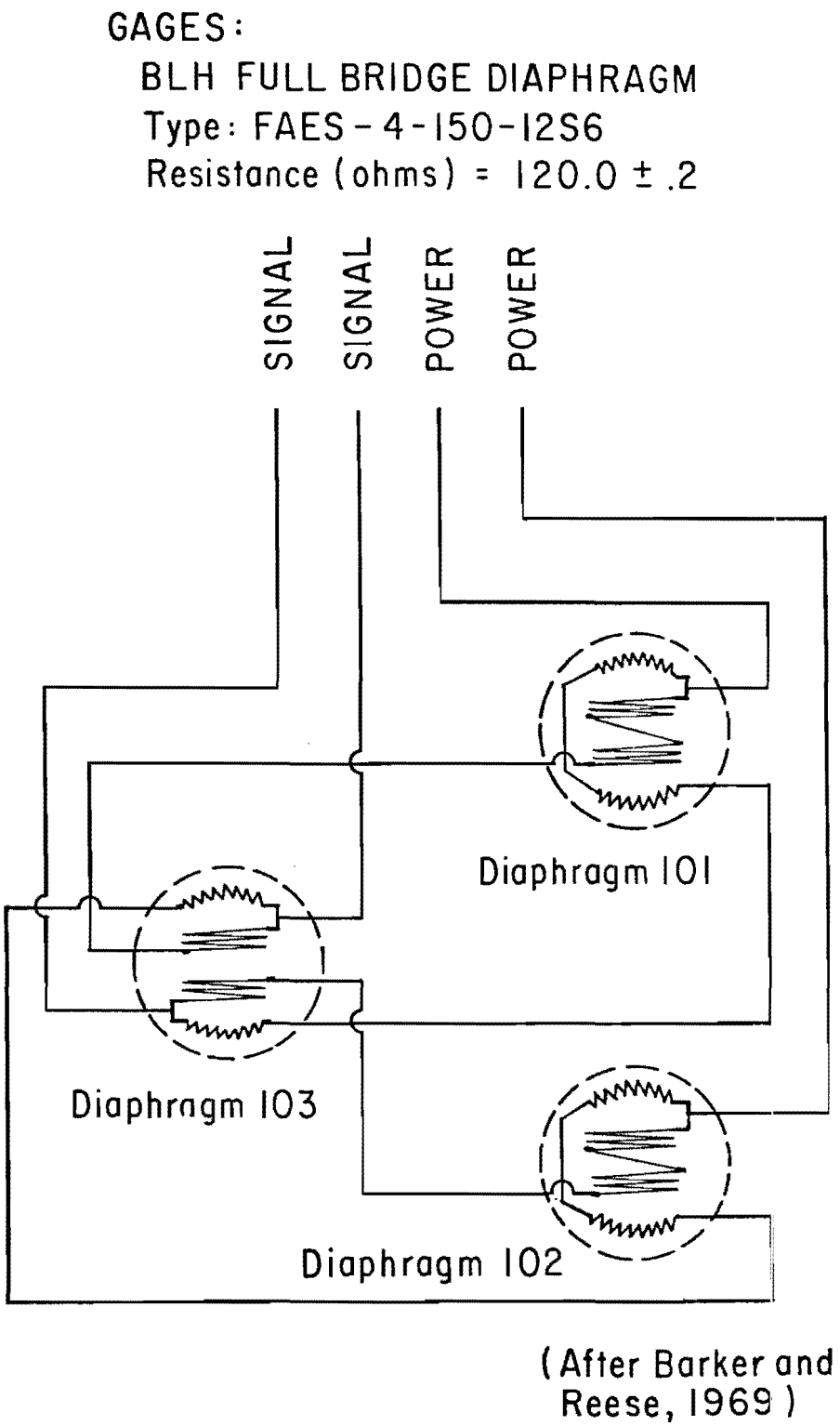

Fig. 9.15. Wiring Diagram for Bottomhole Load Cell

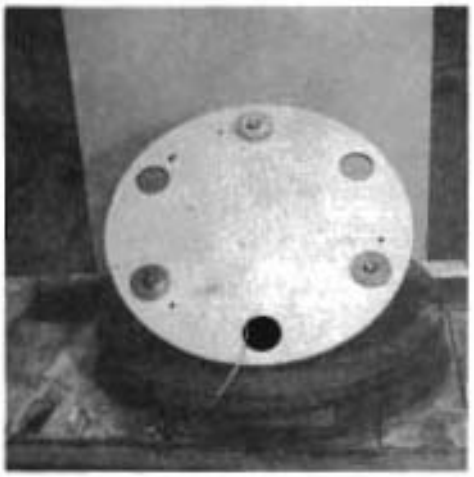

a. Centering Template with Diaphragms

b. Wiring of Bridge

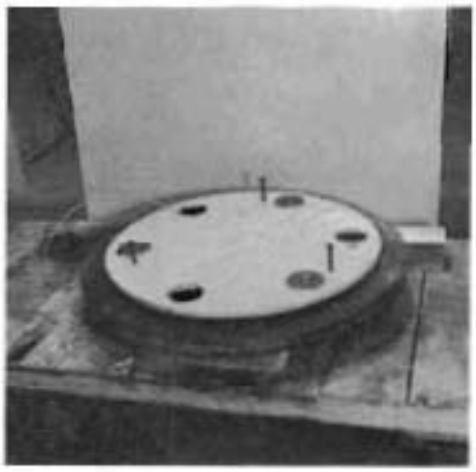

c. Centering Template, Bottom Plate, and Connecting Bolts

Fig. 9.16. Partially Assembled Bottomhole Load Cell

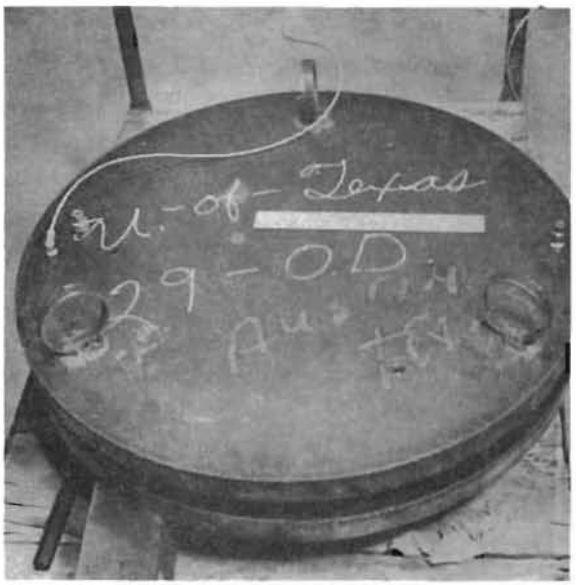

a. Cell with Top Plate in Place

b. Completed Cell

Fig. 9.17. Final Assembly of Bottomhole Cell

The bottomhole cell was designed for the entire central space to be pressurized in the manner described for the Mustran cells. A return tube, seen in Fig. 9.17b, was provided to allow circulation of nitrogen. The cell was to be kept under constant positive pressure during concrete placement to prevent concrete from flowing between the cell and borehole wall and to insure that concrete did not force its way between the two plates.

The cell was installed by lowering it into the hole with a hoist. Three rings for attachment of hoist lines were tack welded onto the top plate, as shown in Fig. 9.17b. The cell was placed on a thin blanket of sand, which had been previously tamped and leveled, at the bottom of the borehole. The rings were then removed, and the instrumented cage was set directly on the cell.

Unfortunately, the jacket seal was apparently broken accidently during installation. Shortly after the cell was installed and pressurized to 10 psi, a leak was detected. Gas pressure was allowed to remain on the cell for about 18 hours, after which the pressure was removed, and lightweight, nondetergent transformer oil was pumped into the cell to provide waterproofing for the diaphragms. The central space and copper tubes were completely filled. Approximately one quart of the oil leaked out of the cell and tubes during the period between installation and the first load test.

Ground resistance remained adequate until after the first load test. However, a short circuit was indicated later, and the cell was rendered ineffective thereafter. Recovery of the load cell fourteen months after placement revealed that the oil had partially dissolved the inner rubber

liner of the sealing jacket. The terminal strip in the cell appeared to be the point at which the short occurred.

Individual diaphragms were calibrated before installation and again after recovery. Diaphragm No. 103 was damaged on removal and could not be calibrated after recovery. No changes in the calibration constants in the other two diaphragms were observed. Strain indicator readings are plotted against applied load in Fig. 9.18 for Diaphragm No. 101 for pre-installation and post-recovery tests. After the final calibration loading, the diaphragms were loaded to failure. An individual capacity of about 60 kips was indicated, with the diaphragm output being linear until just before yielding occurred.

The entire load cell was also calibrated before installation. The results of the calibration are shown in Fig. 9.19. A calibration constant of 2.14 tons per millivolt for 24 volts applied was obtained. The calibration constant did not appear to depend significantly on whether the top plate was loaded by a point load in the center or by a uniformly distributed load. The calibration load was 60 tons, which was ten tons in excess of the predicted base load for S1. Based on the individual diaphragm tests, the total concentric load capacity of the cell was about 90 tons. The calibration loading allowed the loading buttons on the case-hardened diaphragms to form seats in the untreated mild steel top plate.

Since the cell and hydraulic lines connecting the cell to the surface were filled with oil, a small static oil pressure correction was made to the measured calibration constant when reducing load test data.

Load cells were not used in S2, S3, or S4 because the bottomhole cell was bulky and difficult to install and because the scheme of placing

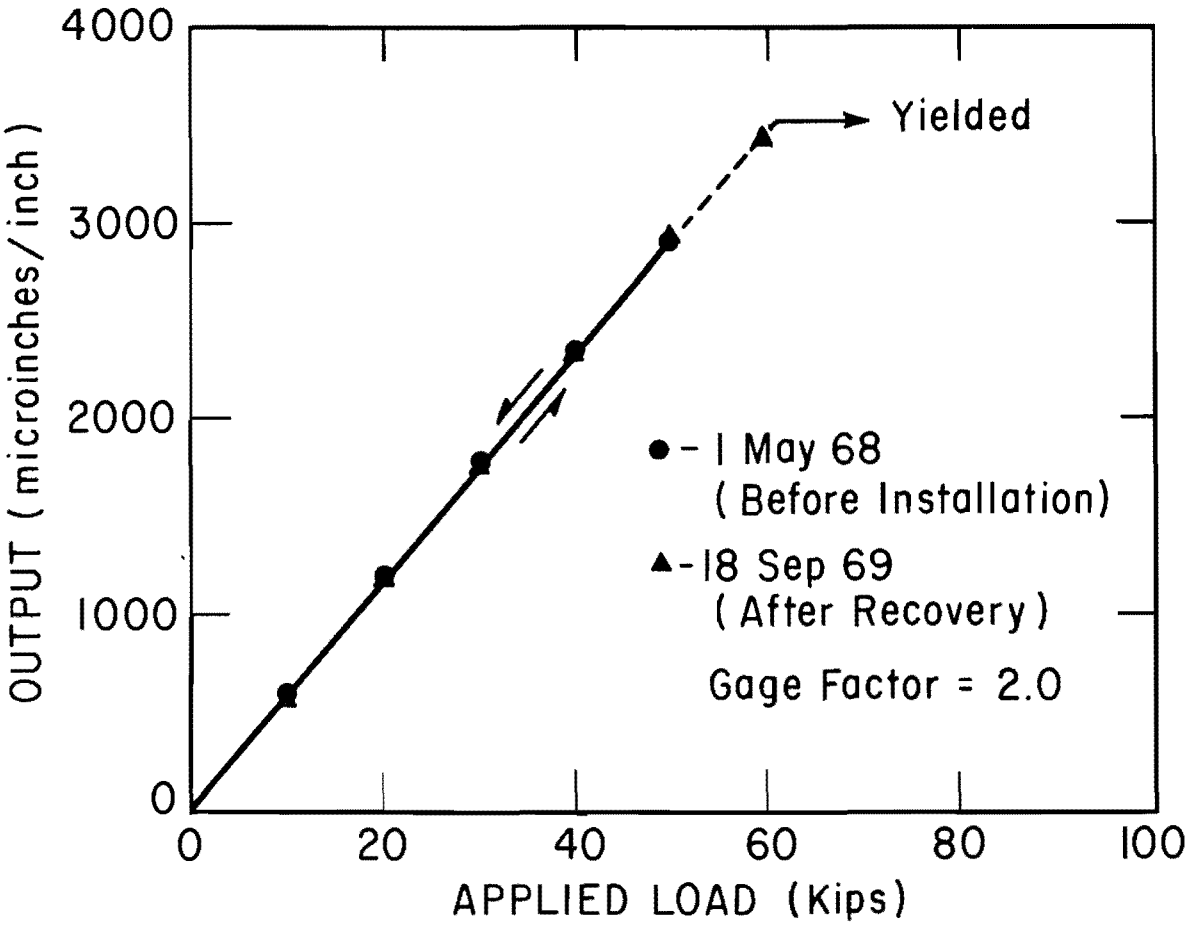

Fig. 9.18. Calibration Curve for Diaphragm No. 101

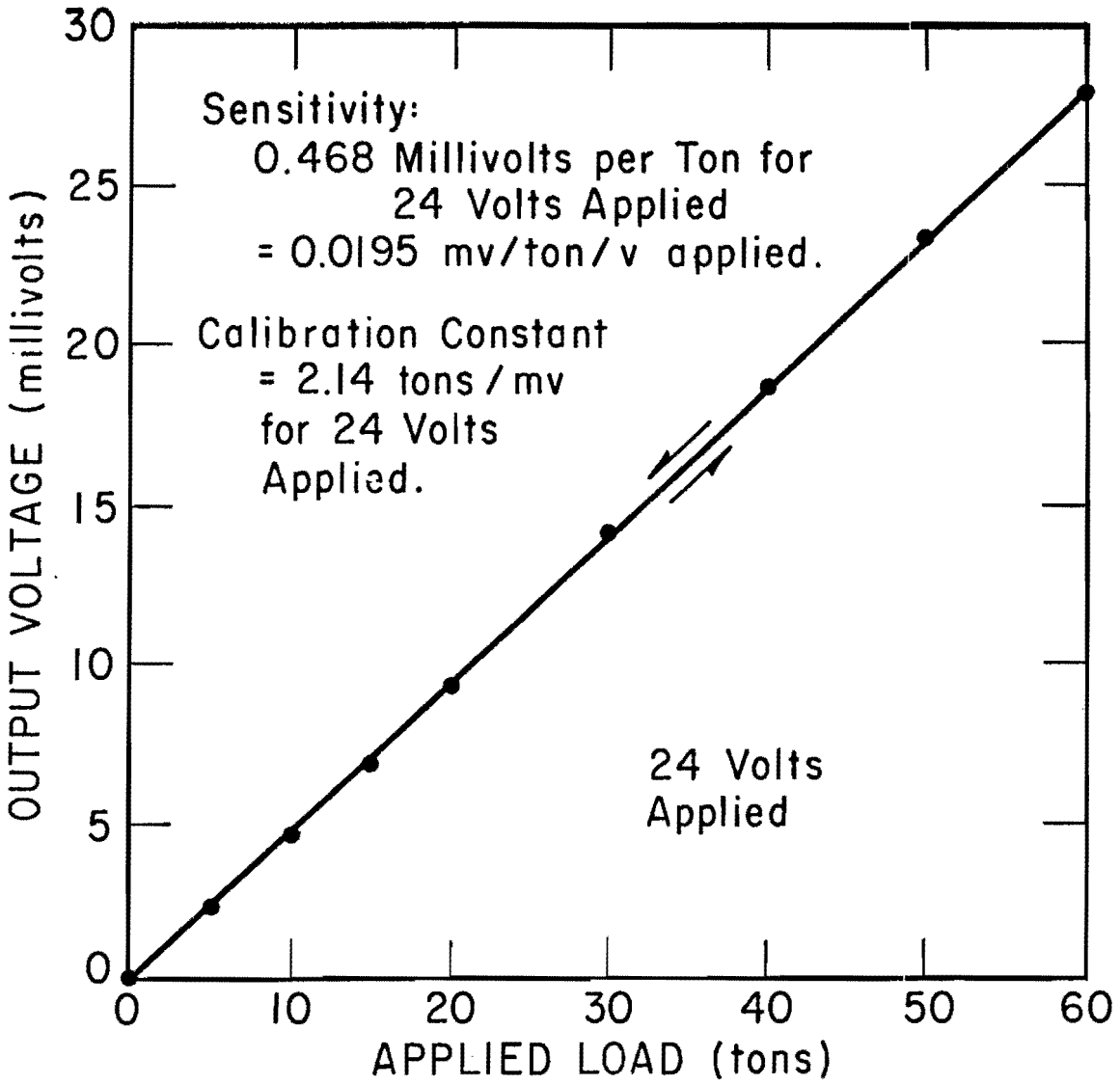

Fig. 9.19. Calibration Curve for Bottomhole Cell

several Mustran cells on a base plate proved to be a satisfactory method of measuring base load.

Strain Rods. Elementary mechanical devices called strain rods, or telltales, can be used to measure compression in concrete and, therefore, can be used to measure load distribution in a drilled shaft (Snow, 1965; Vijayvergiya, Hudson, and Reese, 1969; Barker and Reese, 1969). The feasibility of using strain rods in floating drilled shafts in stiff clay was investigated by installing several in S1 and S2. Strain rods have the desirable advantage of long-term stability not found with most electrical devices. They also provide a means of directly measuring the compression in the shaft. The strain rod design used in the SH225 tests is illustrated in Fig. 9.20. The device consists of a 1/2-inch-diameter hollow steel rod connected to a 3-inch-diameter foot, which is embedded in the concrete at some depth beneath the surface. The rod is encased in a 3/4-inch-diameter steel outer tube, made from electrical conduit, which prevents the rod from bonding to the concrete. A dial indicator, whose stem rests on the top surface of the rod, is mounted on the butt of the test shaft, as shown in Fig. 9.20. As the shaft is loaded, compression occurs between the indicator mount base and the telltale foot. Since the inner rod remains unstrained, the value of this compression is registered directly by the dial indicator.

A strain rod instrumentation system consists of several strain rods with feet embedded at different depths. Load distribution can be measured by taking the difference in compression between two strain rods at adjacent levels and dividing the result by the vertical distance between the respective feet. The value obtained is the average vertical strain in the concrete between the two telltale feet, from which the load at the

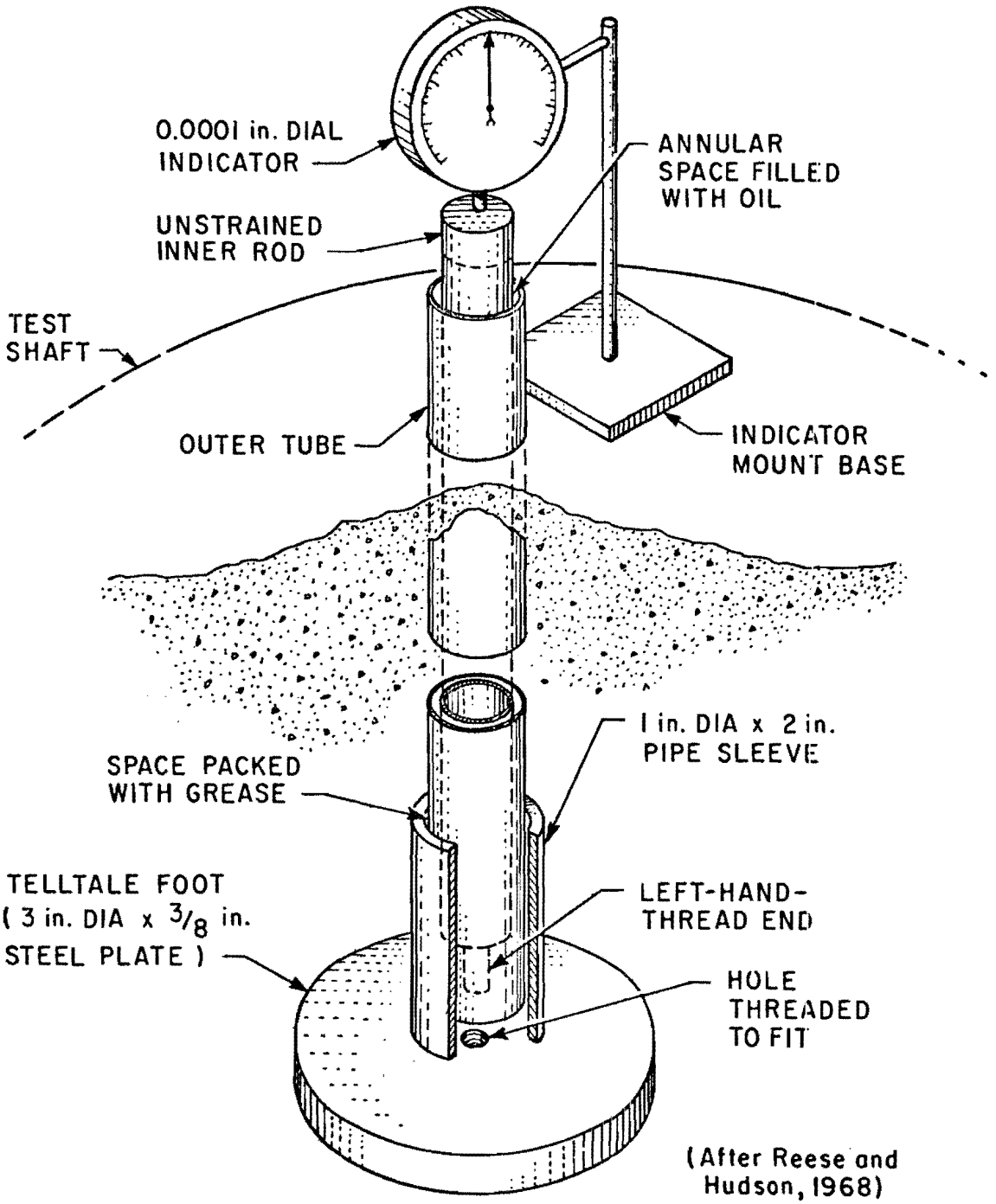

Fig. 9.20. Design of Strain Rods Used in Field Tests

mid-distance can be calculated. Repeated application of this procedure for each vertical interval between telltale feet gives a set of points defining the load distribution relationship.

Vijayvergiya, Hudson, and Reese (1969) present an alternative method for calculating load distribution. They suggest, as a rational smoothing operation, that indicated shaft compression be plotted against depth and a least-squares curve be fitted to the points. The load distribution then may be computed from the equation of the regression curve.

In addition to fitting a regression curve to the telltale compression data, it can be assumed that the rate of change of compression at the top is determinate from the elastic properties of the shaft. In other words, the slope of the compression-versus-depth curve at the top of the shaft is given approximately by:

$$\frac{\Delta L}{L} = \frac{Q_T}{A_c E_c} = Q_T (5.7 \times 10^{-6}) \text{ in./ft.} \quad \ldots\ldots\ldots\ldots (9.1)$$

in which

ΔL = compression occurring in a unit length L, in inches

L = unit length along the shaft, in feet

Q_T = applied load in tons

$A_c E_c$ = product of the transformed area of the concrete and the concrete modulus, taken as 4.22×10^9 pounds for the numerical computation.

The expression given in Eq. 9.1 is a boundary condition used in establishing the equation of the regression curve.

Details of the strain rod design include a protective sleeve, welded to the foot, that surrounds the bottom two inches of the outer tube. The annular space between the outer tube and the sleeve contains an O-ring seal and is packed with heavy grease. The outer tube does not contact the foot, but is held approximately 1/2 inch above the foot by a pin connection between the inner rod, which is screwed into the foot, and outer tube at the top. The inner rod is capped with a plug having a machined surface, on which the stem of the dial indicator rests. The space between the inner rod and protective tube was filled with oil after installation to minimize friction.

The strain rod assemblies were made up in five-foot sections, with one shorter section being added to produce the exact desired length, where appropriate. The inner rod sections were joined by threaded connections, while the outer tubes were connected by conduit couplings. All threaded connections for the inner rods were right-handed, except for that with the foot, which was left-handed. This allowed the inner rods to be recovered for reuse. The inner rods were about one inch longer than the outer tubes. Each completed assembly was attached to the inside of the reinforcing cage at several places with tie wire.

Only one strain rod was provided for each level in S1. Since stem bending was expected to be a problem in S2, pairs of strain rods, mounted diametrically opposite each other on the cage, were provided in that shaft.

In practice, strain rod readings are influenced by the temperature changes in the steel telltale rods and in the surrounding concrete, as well as by temperature changes in the indicator mount, as the load test progresses. Thermal strains due to temperature changes along the rods and

within the concrete are difficult to assess, although thermocouples which were embedded in the concrete at various levels in the present study gave some indication of temperature distributions in the concrete. Consideration of thermal strains is necessitated by the fact that the coefficients of thermal expansion of steel and concrete are different (concrete: 5.5×10^{-6} inches per inch per degree Fahrenheit; steel: 6.5×10^{-6} inches per inch per degree Fahrenheit). Since the dial gages used to measure telltale movements are mounted to the top of the concrete, only relative differences in thermal straining between concrete shaft and steel rod are indicated as errors. Temperature changes can be suffered by the rod throughout much of its length, whereas the concrete temperature is nearly constant along the shaft below a depth of a few feet during a short-term test. Tendencies for expansion and contraction in the concrete below ground level are also resisted by the surrounding soil; however, the steel rod is free to expand or contract (except for frictional binding). Therefore, even if the temperature changes occur at the same rate in the inner rod and in the concrete, the rod will expand (or contract) a greater amount, producing an erroneous indication of compression (or extension) in the reading obtained on the dial indicator. Thermal straining is expected to cause the greatest errors in the shorter strain rods, in which the apparent strain readings due to thermal effects compose a greater proportion of the total indicated compression. During testing, the indicator mounts as well as the entire top of the test shaft were shielded from the sun by covering the immediate test site with a large tarpaulin.

No-load readings taken on the telltales over a period of several hours (reported in Chapter X) indicated that, in reality, almost negligible

drift was produced by changing temperature. For example, the largest change in dial indicator reading was on TT8W in S2 (foot embedded at four foot depth). That change was 0.0004 inches indicated relative concrete extension in 6 1/2 hours, corresponding to an air temperature rise of 17 degrees Fahrenheit. By comparison, a load of 500 tons produced an average telltale reading of about 0.009 inches in the first load test at that level. Since the period of time required to increase the load from zero to 500 tons was much less than six hours, and the corresponding temperature changes less than 17 degrees, the temperature drift in the QL load tests was probably less than 0.0004 inches. Thus, the error in indicated load at a given level due to temperature changes probably did not exceed four or five per cent for the telltales in S2, and was probably considerably less, assuming a linear variation of telltale reading with temperature change and assuming the temperature varied at a constant rate during the test.

Additional theoretical considerations concerning the effect of thermal strains on strain rods are given by Vijayvergiya, Hudson, and Reese (1969).

Frictional binding between the inner rod and the outer tube, possibly produced by improperly aligned strain rod assemblies, produces an indicated compression in the rod as the shaft is loaded. This compression is reflected as an error in the telltale reading. Binding occurs as a consequence of bending of the strain rod assembly during installation. In retrospect, it appears that the rather flexible telltales, which were tied to the cage prior to installation, were probably bent somewhat at the joints as the cages were picked up and set in the boreholes. This lack of proper technique probably caused most of the errors mentioned in Chapter XII. Presumably,

binding could have been minimized by placing telltales on the cage after the cage had been set in the borehole, or by using single-piece rods and tubes, or by a combination of these two procedures.

It should be noted that frictional binding always causes less concrete compression (greater load transfer) to be indicated than actually exists because it forces the inner strain rods to compress instead of remaining unstrained. For example, if the inner rod, which has a cross-sectional area of 0.0705 square inches, is 20 feet long and has a binding force of only one pound per foot of length, an indicated error in shaft compression of 0.0012 inches would occur. Furthermore, strain rods with bent joints could have considerably more binding force than one pound per foot.

As is indicated in Chapter XII, test results from strain rods were generally discouraging. Therefore, strain rods were omitted from S3 and S4. It was concluded that excessive binding was the cause of the poor results. Better installation procedures presumably would have permitted better performance.

Hydraulic Pressure Cell. A Gloetzl hydraulic pressure cell, manufactured in Europe and distributed in the United States by Terrametrics, Inc., was embedded in the concrete in S1 in the center of the shaft just above the ground surface. The Gloetzl cell is described by Barker and Reese (1969). Hydraulic cells ideally provide a direct indication of concrete stress, unencumbered by electrical problems and not requiring knowledge of the concrete modulus. Unfortunately, the method of data readout, which involves measuring the pressure required to activate a differential pressure valve in the cell, requires a relatively long period of time. Hence, a comprehensive instrumentation system composed of these cells may not be compatible

with the QL procedure, but in principle, it could be applied to long-term testing.

The one cell tested did not perform in a satisfactory manner. When an average stress of 375 psi was applied to the butt of S1, the Gloetzl cell indicated only 26 psi. The reason for such a low underregistration is unclear, but it is thought that either the differential pressure valve was damaged during placement or that the embedded cell was not in intimate contact with the concrete, perhaps as a result of concrete shrinkage. No further attempts were made to use the Gloetzl cell.

Weldable Gages. Microdot, Inc., Model SG 189-6 weldable strain gages were installed on short sections of No. 6 rebar embedded in the top four feet of S4. Four such gages, with integral leads extending out of the concrete, were placed. No attempt was made to provide any special water-proofing. The exposed ends of the leads were taped to minimize entrance of water.

The principal advantage of the weldable gages is ease in placement, since the gage is simply spot welded to the reinforcing steel with a miniature arc welder. The individual gage, which costs about twenty-five dollars, has approximately the same average gage factor as the embedment gage; however, a wide tolerance of plus or minus three per cent was observed in laboratory calibration studies. Based on the average measured concrete modulus value for S4, the in-place gage factor was calculated. This gage factor was about ten per cent smaller than that indicated in the laboratory.

The weldable gages were read during testing with a strain indicator using a quarter bridge circuit. Throughout the time between installation and initial testing (five months), the ground resistance remained

acceptable, but varied, in each gage. No problems were noticed during testing, except that load resolution was very low, primarily due to the quarter-bridge circuit configuration. With the present design, gages would be somewhat difficult to wire in full-bridge configuration because of wide tolerances in filament resistance and gage factor.

In general, the reliability of the weldable gages in short-term tests appears comparable to that of the embedment gage system.

Thermocouples. Thermocouples ("Quicktip" thermocouples, Leeds and Northrup Co.) were affixed to the S1, S2, and S4 cages prior to installation. Their primary purpose was to provide a means of measuring temperature changes at various levels in a shaft during curing and during load testing. Data on temperature permitted recognition of potential sources of error in indicated strain due to temperature changes in both telltale and electrical gages.

Overall Instrumentation. Plan and elevation schematics are given for S1 through S4 in Figs. 9.21 through 9.28. These figures show the location of all instruments installed in each test shaft.

Site Instrumentation. Additional geotechnical instrumentation at the SH225 test site included a nuclear moisture probe access hole and an open piezometer.

The probe hole was hand-augered to 20 feet on September 20, 1968. It was then lined with a seamless aluminum tube, which was sealed at the bottom and covered at the top. Moisture content was obtained at various depths at several times during the field test program by lowering a Troxler Electronic Laboratories Model 104 depth moisture probe down the access tube and measuring the tendency of the hydrogen ions in the soil

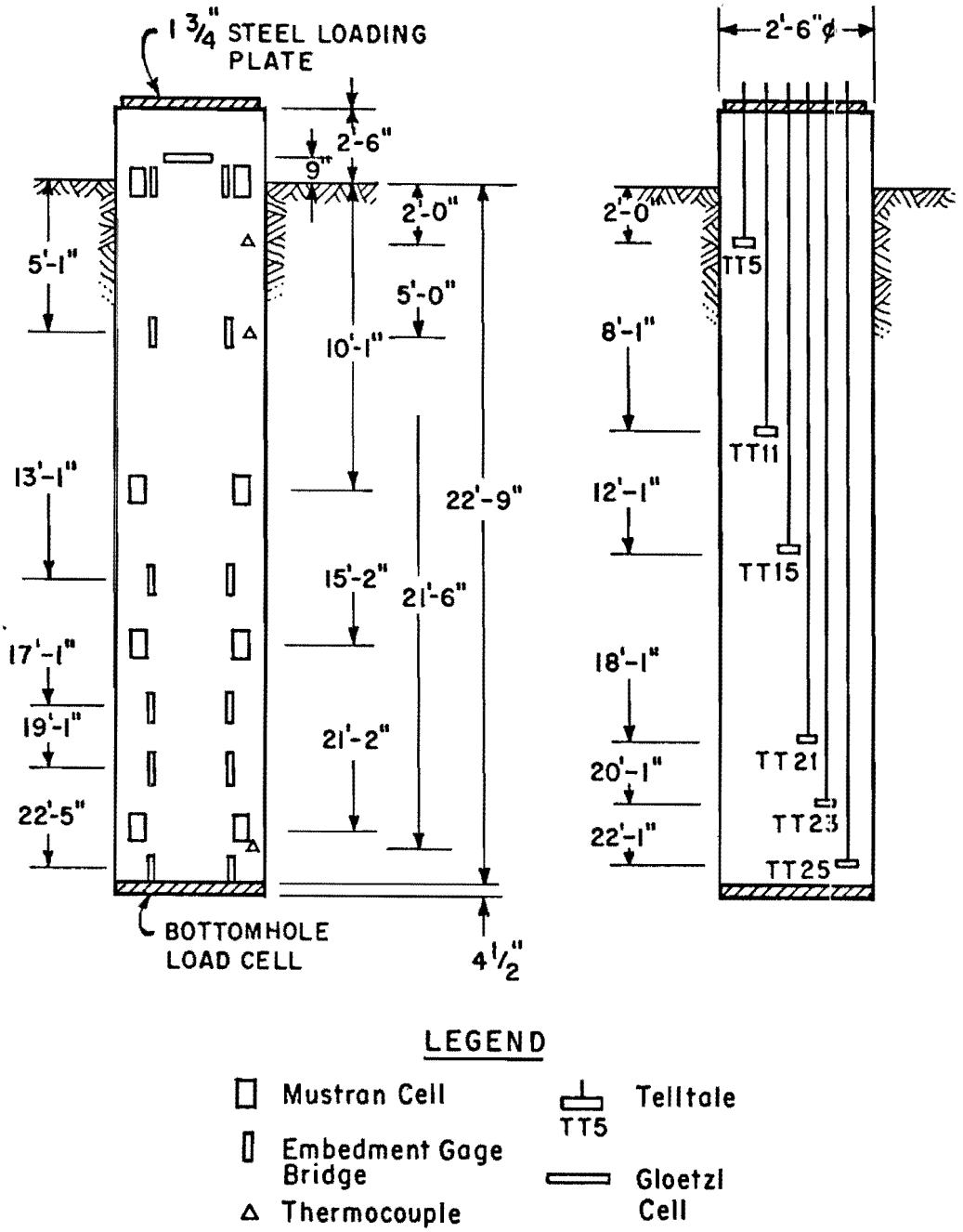

Fig. 9.21. Location of Instruments, S1 - Elevation

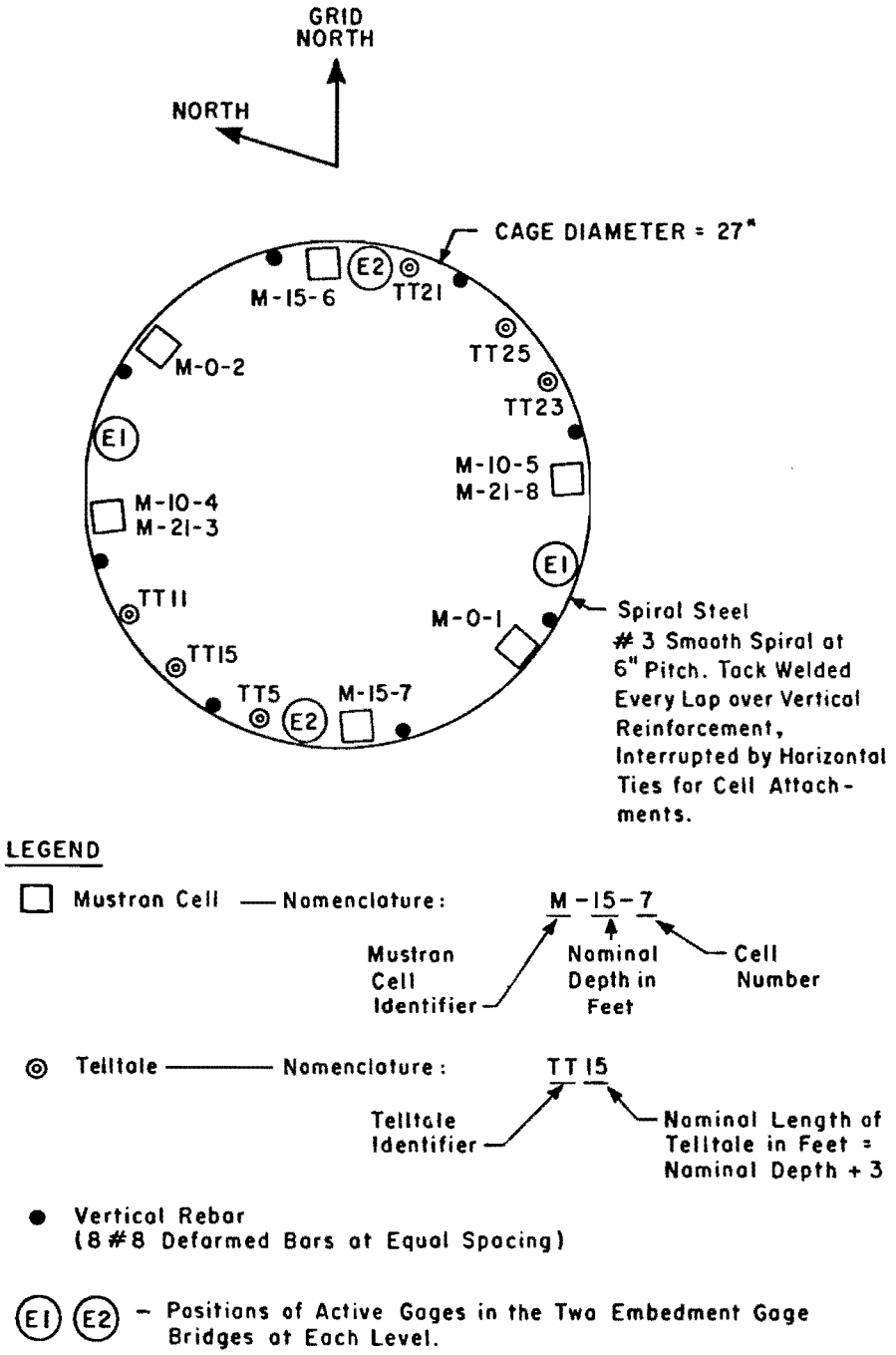

Fig. 9.22. Location of Instruments, S1 - Plan

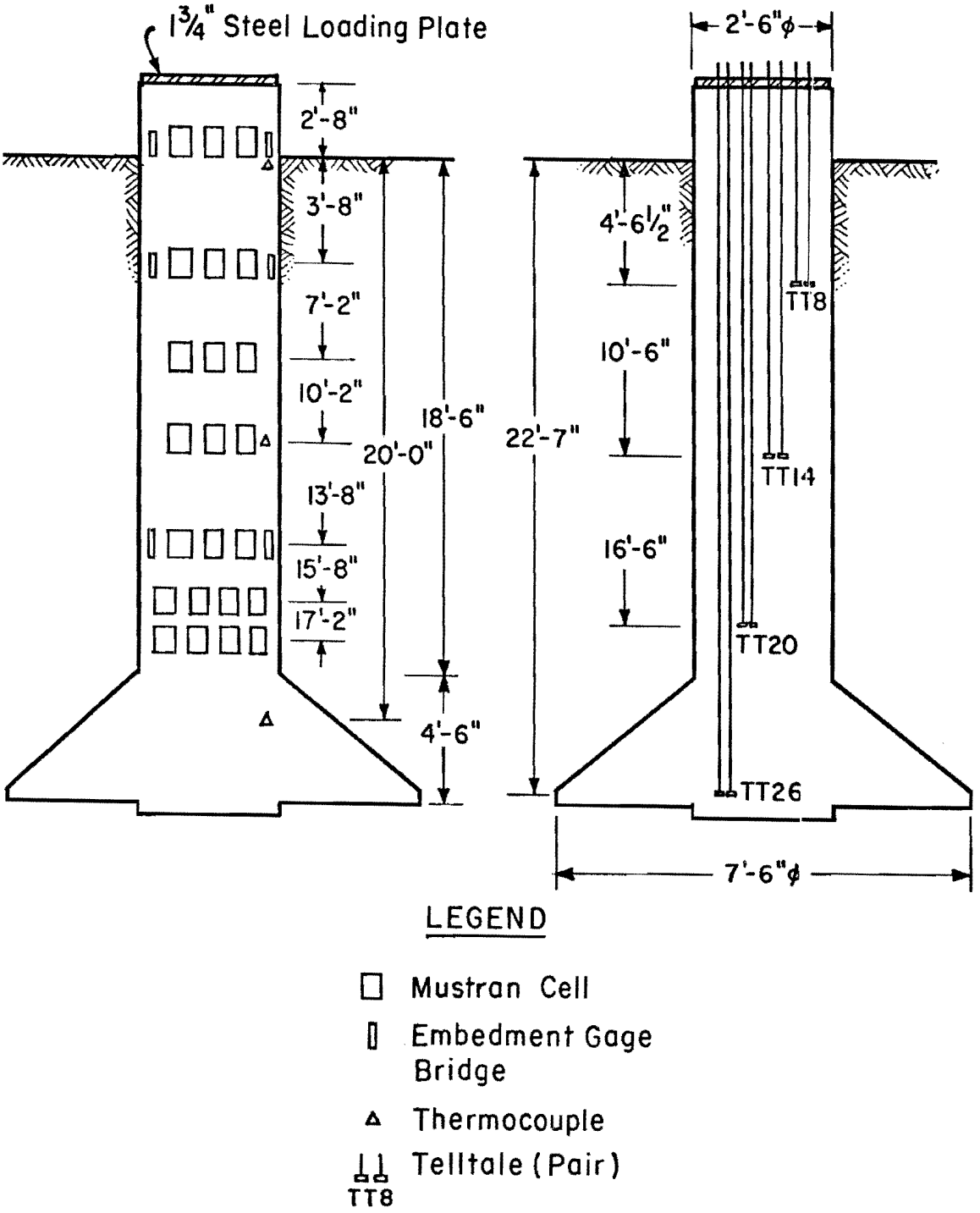

Fig. 9.23. Location of Instruments, S2 - Elevation

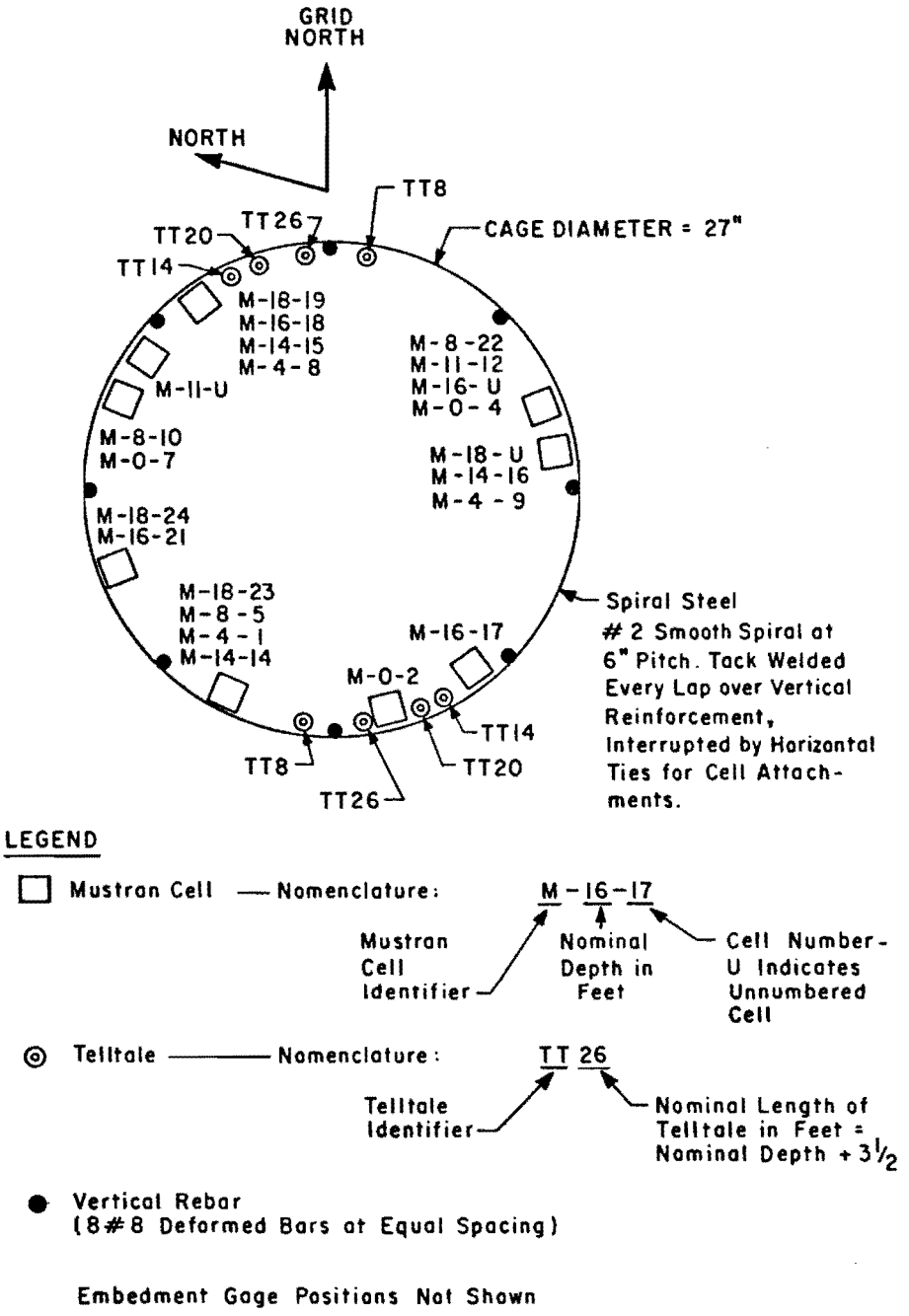

Fig. 9.24. Location of Instruments, S2 - Plan

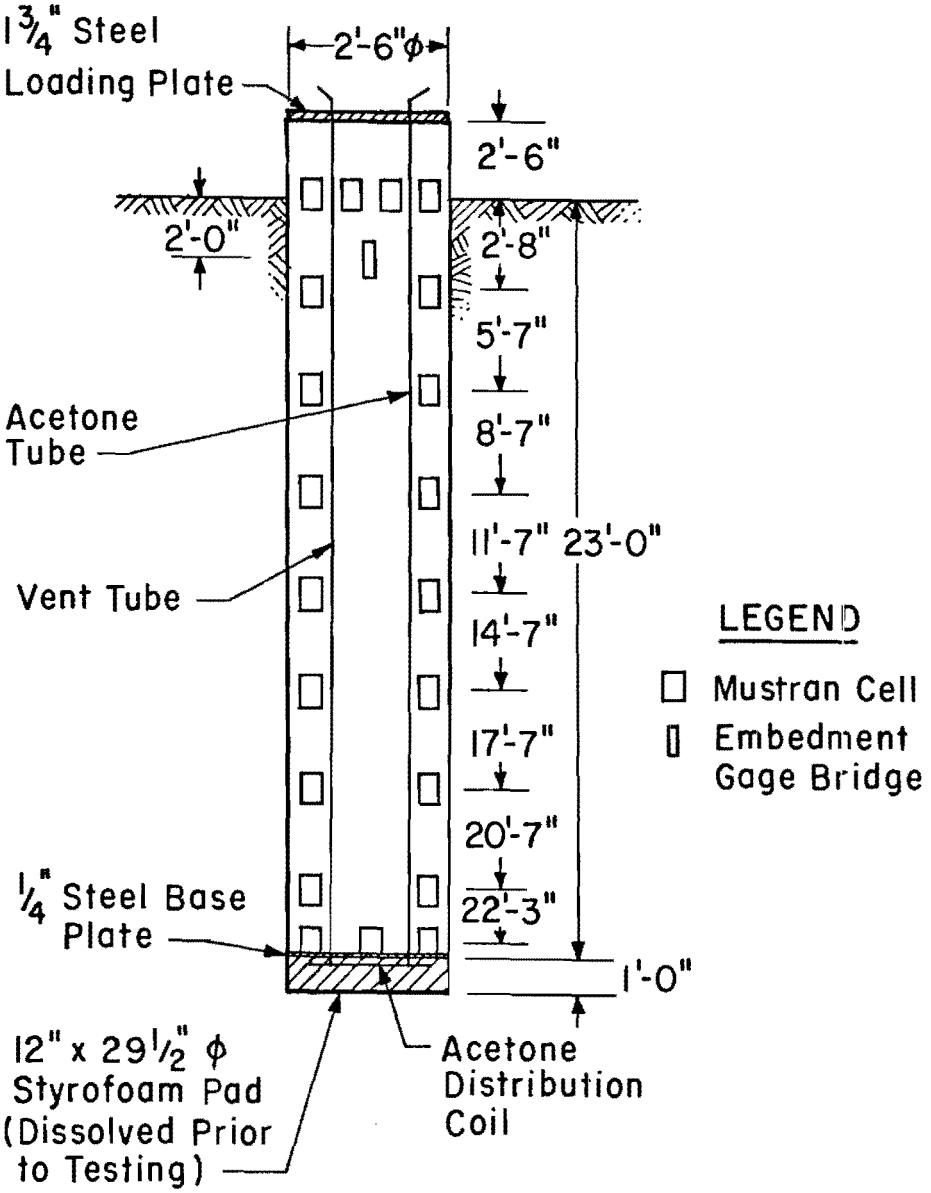

Fig. 9.25. Location of Instruments, S3 - Elevation

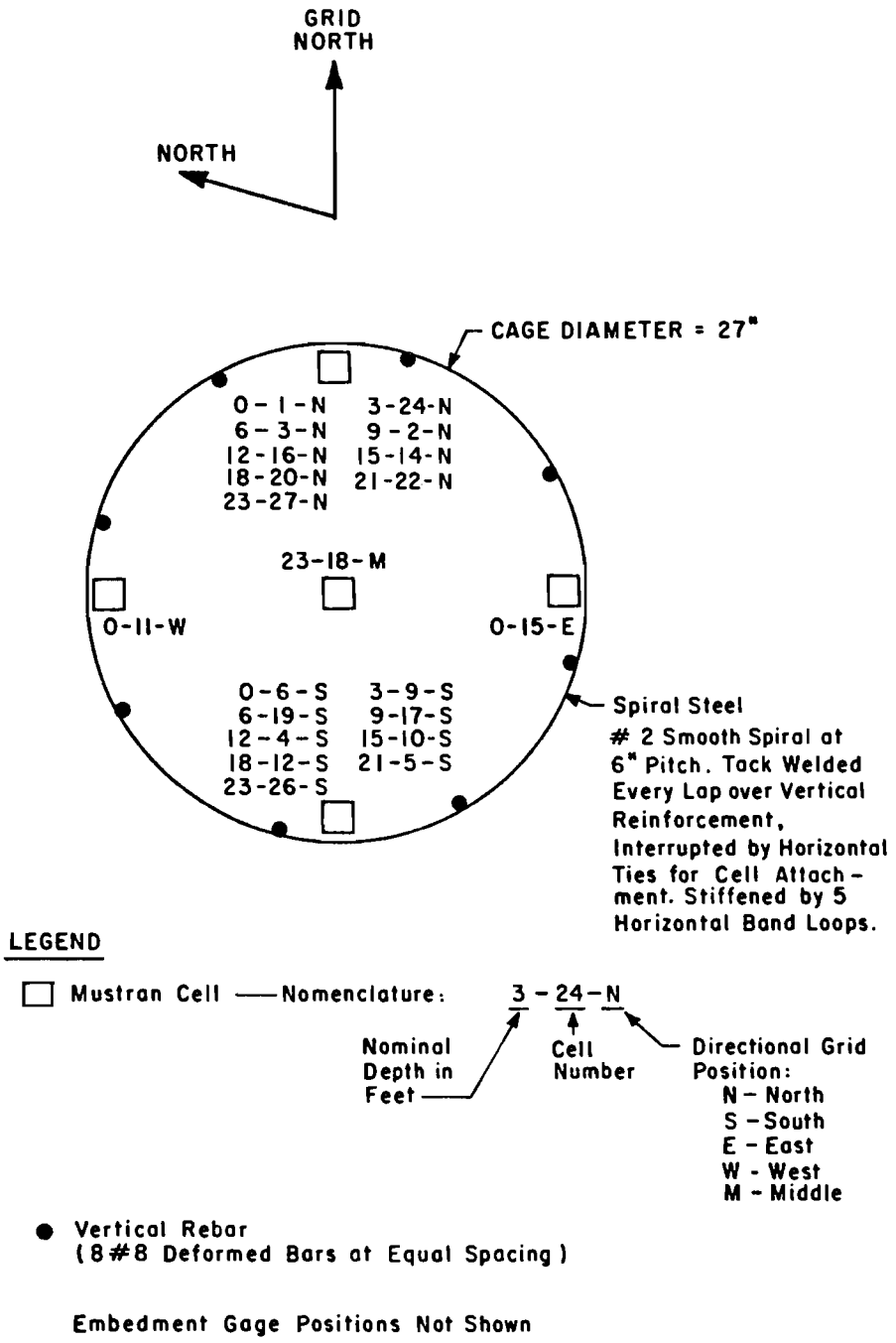

Fig. 9.26. Location of Instruments, S3 - Plan

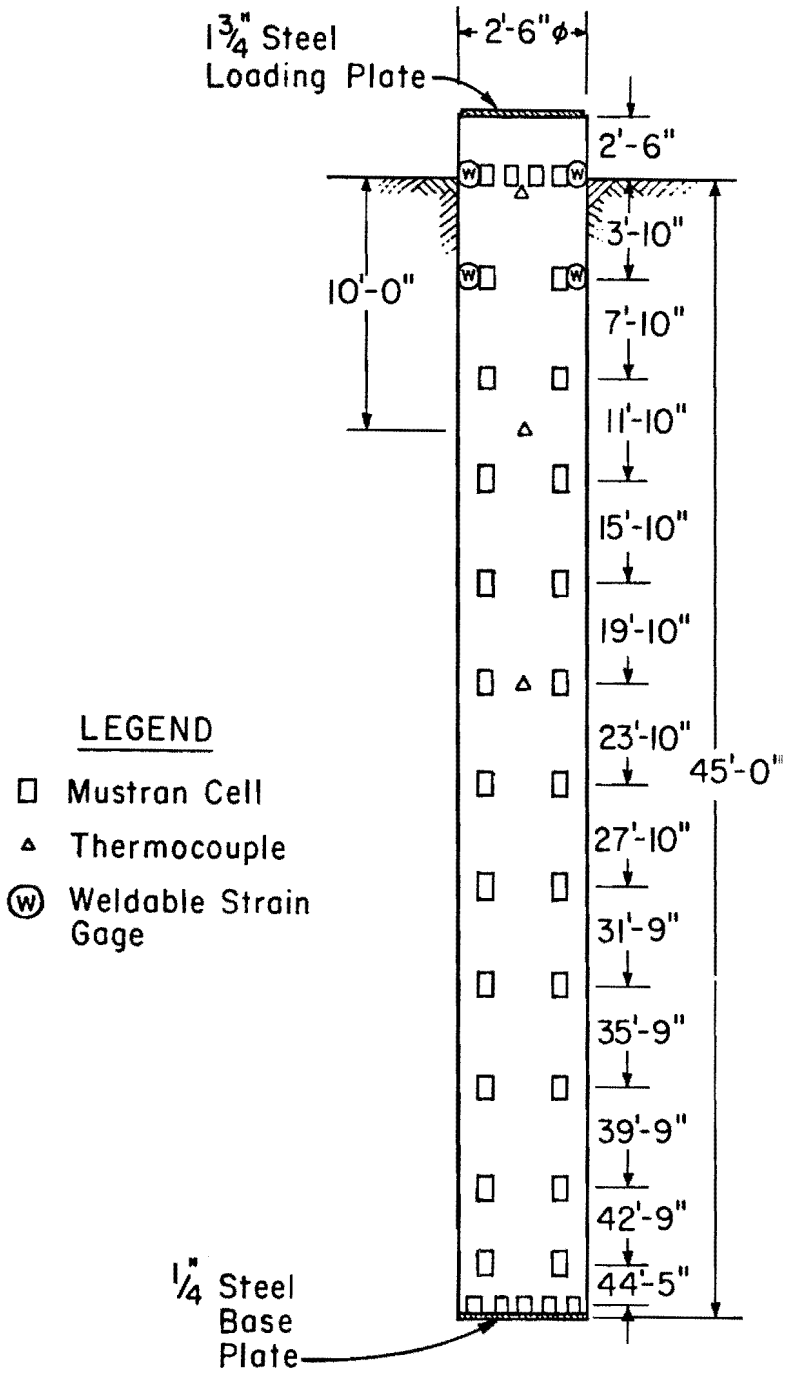

Fig. 9.27. Location of Instruments, S4 - Elevation

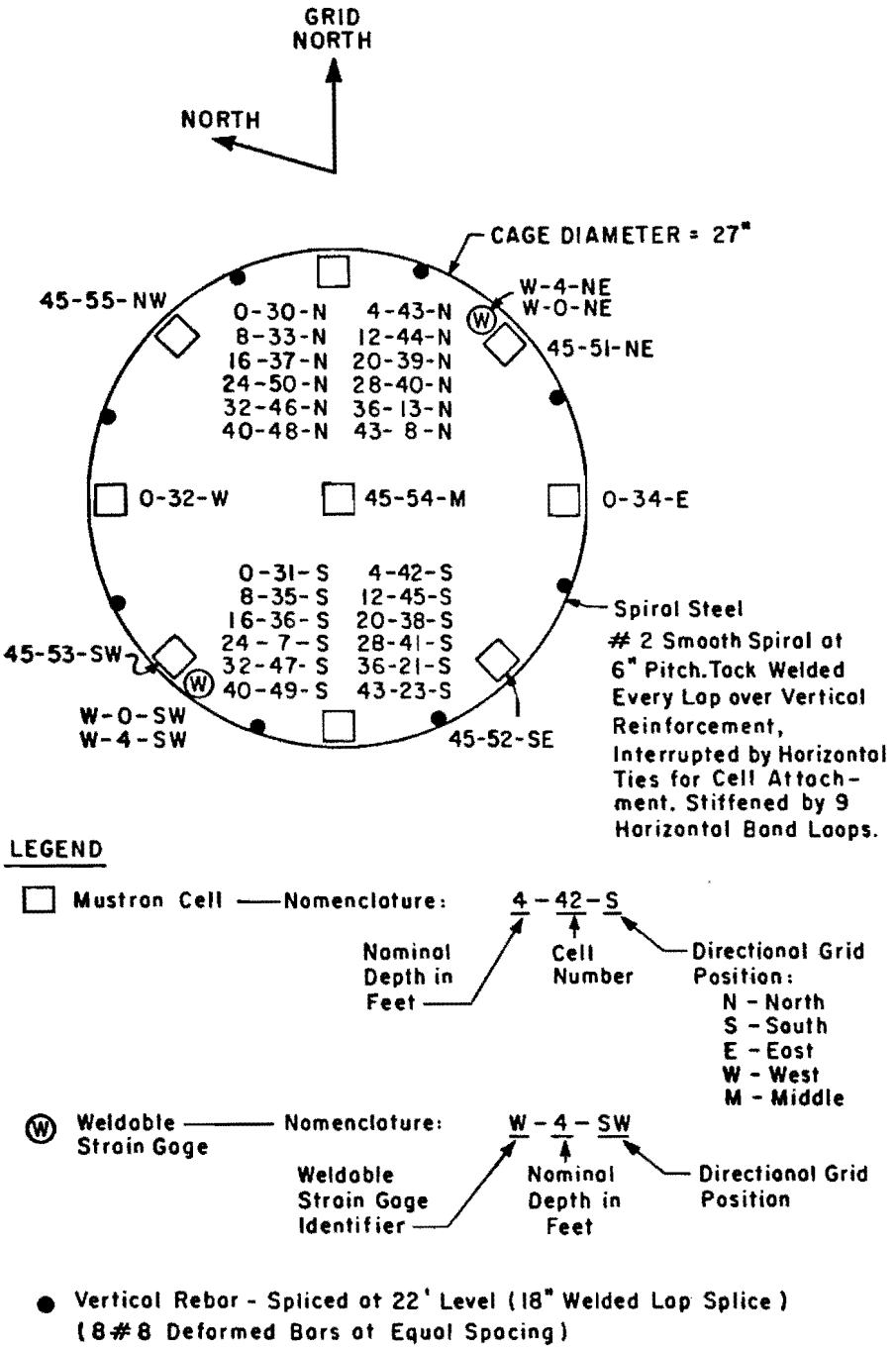

Fig. 9.28. Location of Instruments, S4 - Plan

water at a given level to backscatter low energy neutrons from a high energy neutron source. Neutron counts were read on a Troxler Model 200B portable scalar. The procedure for obtaining moisture content profiles by this method is given by Ehlers, Reese, and Anagnos (1969). The nuclear moisture probe was calibrated against a soil standard at Oklahoma State University, and that calibration was used to obtain numerical values of moisture content at the test site. Use of such a standard to obtain in situ moisture contents in terms of per cent of dry weight requires the assumption that no volume change occurs in the soil.

Results of the nuclear moisture content determinations are given in Fig. 9.29. They are generally good, although some variations in moisture content with time larger than those believed to exist in reality are indicated at every level, possibly due to volume changes in the soil, presence of free water between the access tube and soil, or inconsistencies in positioning of the nuclear probe. The agreement between the February 4, 1969, and June 18, 1969, readings is good. Readings for both dates show a significant moisture content increase over the September 20, 1968, readings, which is thought to be an indication of migration of water into spaces between the access tube and soil. No conclusions, other than the fact that the moisture content appeared to remain reasonably constant above the water table, were drawn from the nuclear moisture probe readings. After the June 18, 1969, readings, groundwater began entering the tube from the bottom. Later attempts to measure the moisture profile were unsuccessful because of the presence of this water.

An open piezometer, terminated at a depth of 30 feet, was installed 15 feet grid West of S4 on November 4, 1969. The piezometer hole was

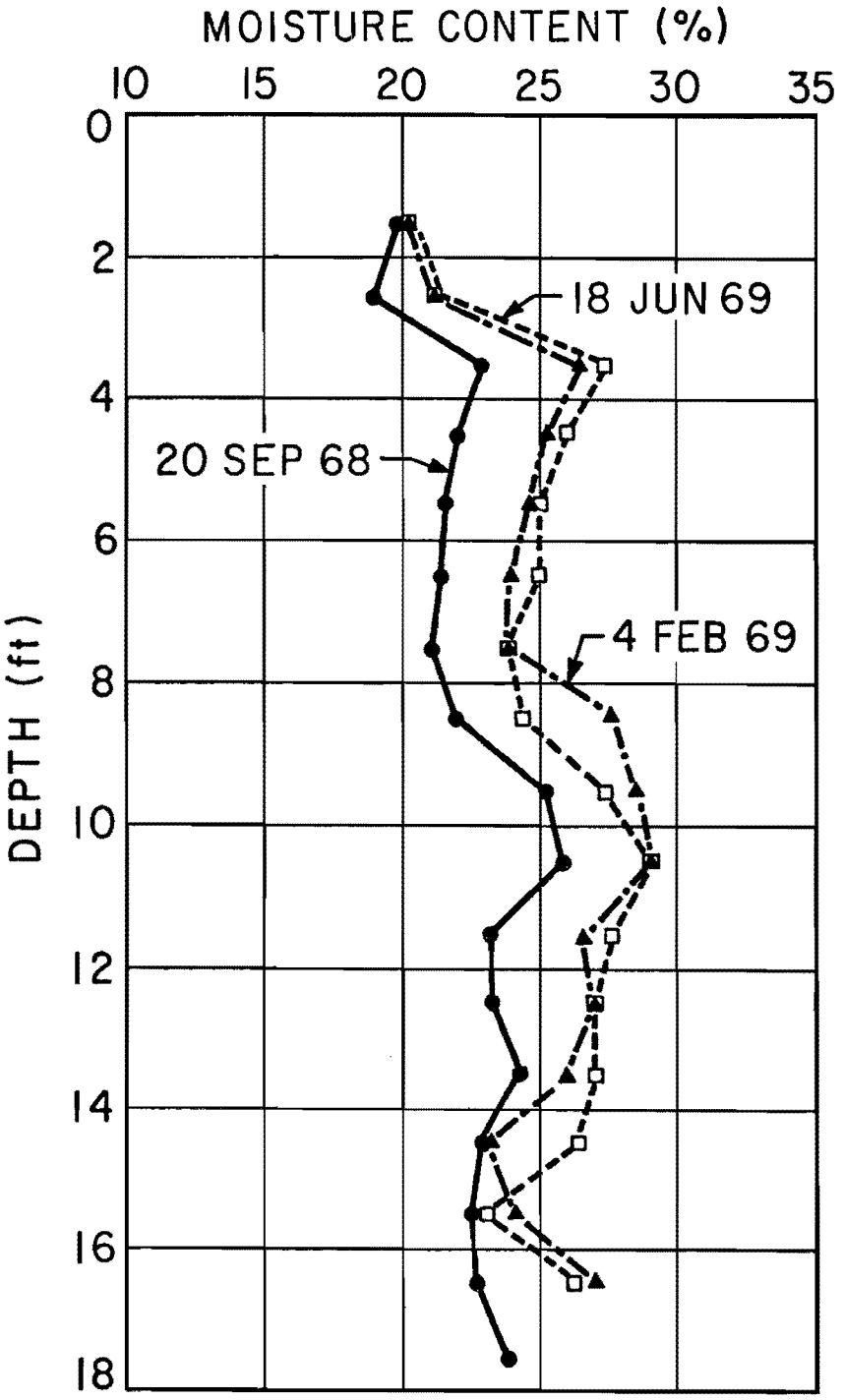

Fig. 9.29. Variation of Soil Moisture Indicated by Nuclear Probe

unlined. It filled with water from the bottom and indicated a stable free groundwater level at a depth of 15 feet after three days. No readings could be taken after November 7, 1969, because the sides of the piezometer hole began sloughing severely on that date.

CHAPTER X

NO-LOAD PERFORMANCE OF TEST SHAFTS

During the period of time between casting and load testing, every gage in each shaft was monitored to evaluate its potential load test reliability and to provide information concerning the curing of the concrete. The electrical gages were read with a Budd Model P-350 portable strain indicator, which had a resolution of ±1 microinch per inch. Ground resistance was read with either an Altec Manufacturing Company Model 102 Megohmmeter or Freed Transformer Company Model 2030-C Megohmmeter. Thermocouples and air temperature were monitored with a Thermo Electric Company Portable Multi-Mite Pyrometer Indicator, Model 80210.

Each time the electrical gages were read, the strain indicator was first balanced to zero against a reference bridge of known resistance. The reference bridge was a standard four-arm bridge mounted on an unstrained steel member with large mass. The circuit, mass, and wiring were enclosed in an electronic chassis for protection. The gages were always read with the connections in normal configuration and again with the power leads reversed. By following this procedure, effects of electrical drift in the strain indicator were minimized, giving a valid long-term reference for the no-load gage readings.

Performance of Mustran Cells

The Mustran cells were read by attaching the strain indicator or megohmmeter directly to the cell leads (S1) or by using an intermediate length of electrical, four conductor cable to connect the instrument (S2, S3, S4). A clip connector was used to attach the intermediate cable to

the leads in S2, while a male Cinch-Jones eight-pin plug was used to read the cells through the manifold plugboards in S3 and S4.

The cells in S1 and S2 indicated generally good ground resistance. Two cells in S1 registered low ground resistance shortly after installation, but circulation of dry nitrogen through the cell chambers brought the ground resistances up to acceptable values. The cell readings themselves fluctuated due to changing ground resistance, possibly brought on by minor intrusions of moisture. For this reason, no significance in terms of concrete performance is attached to the changes in Mustran cell readings in S1 and S2 during the curing periods. The cells did, however, indicate the same trends in the concrete as will be described for S3 and S4.

The Mustran cells in S3 and S4 registered high and stable ground resistance between casting and testing. This fact is thought to be a consequence of using better sealing methods and placing desiccant in the cell chambers. Cell readings taken during the curing period are, therefore, accepted as valid indications of strains occurring in the curing concrete.

Graphs of the circuit strain indicated by the Mustran cells at various depths are shown for S3 and S4 in Figs. 10.1 and 10.2. The values plotted are the average cell circuit strains for each level. A part of the indicated strains are probably false indications due to temperature changes in the cells as curing progressed. Thermocouples registered temperature changes of approximately 30 degrees Fahrenheit, which, according to Fig. 9.6a, cause apparent circuit strains of about 30 microinches per inch (apparent compression with increasing temperature). Observing the magnitudes of indicated strains from Figs. 10.1 and 10.2, it appears that thermal strains in the cells account for only a minor portion of the indicated strains. Gage creep is negligibly small for the readings obtained.

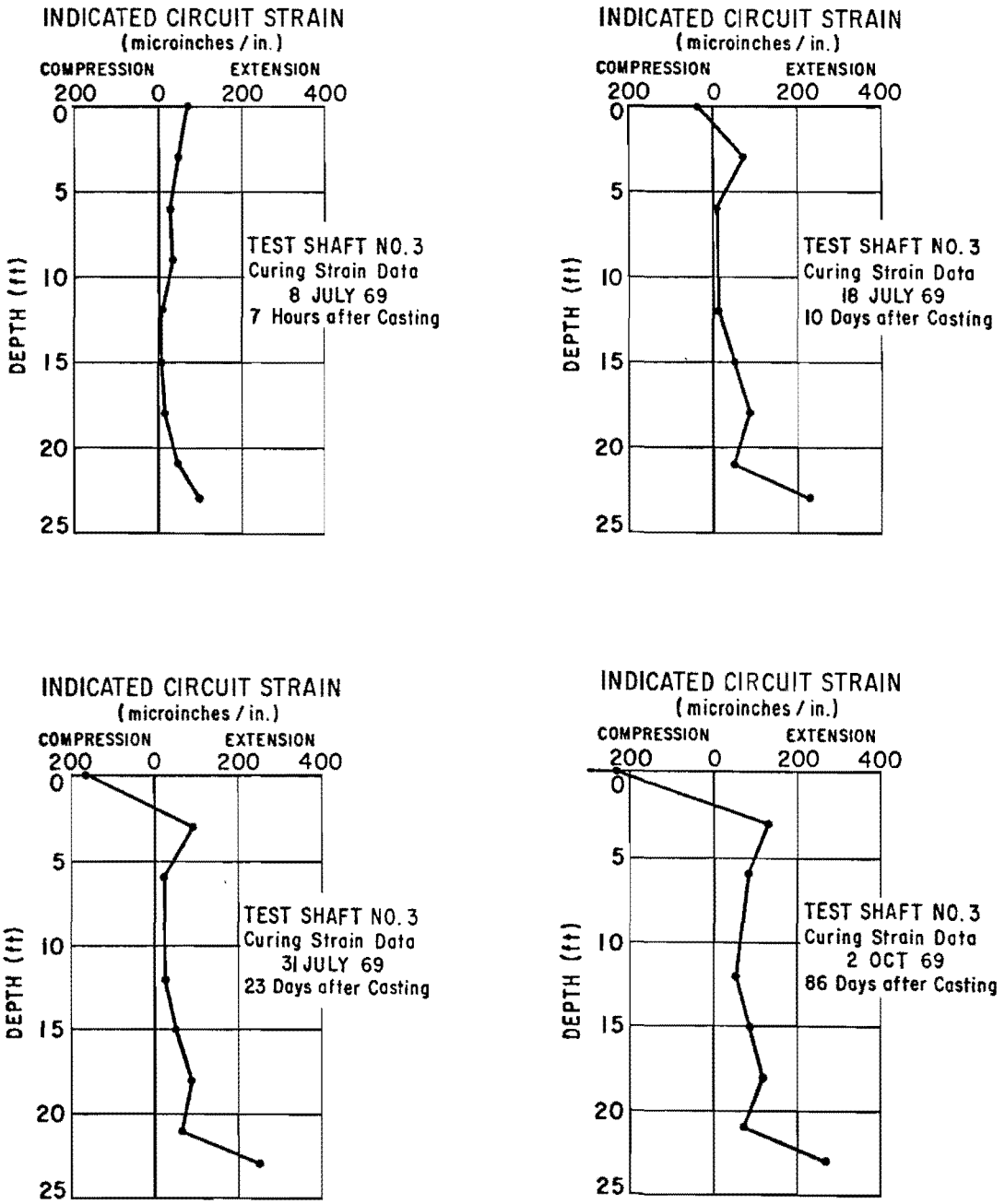

Note: Indicated Circuit Strain Approximately 7.3 Times Concrete Strain.

Fig. 10.1. Curing Strains for Test Shaft 3

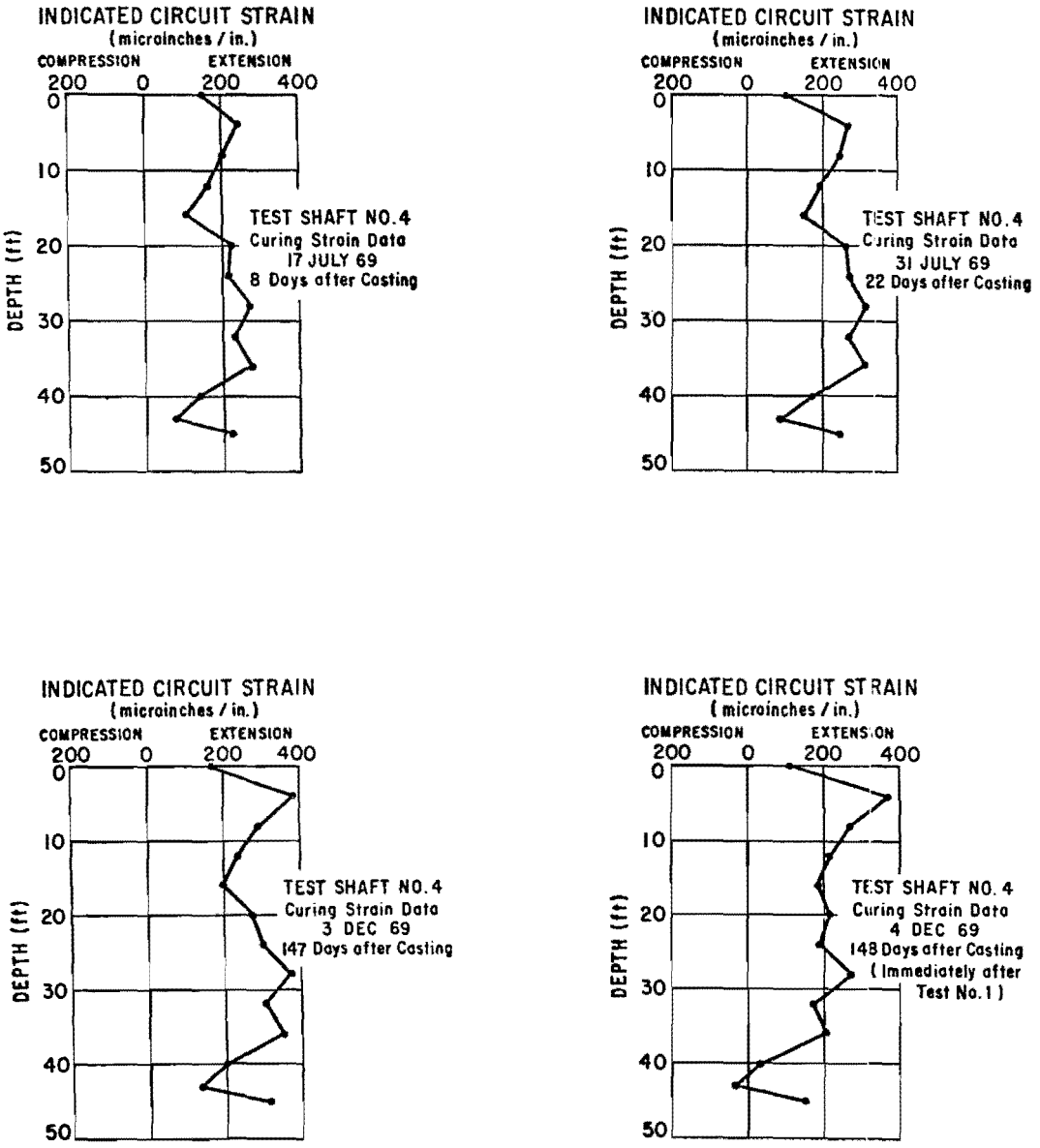

Note: Indicated Circuit Strain Approximately 7.3 Times Concrete Strain.

Fig. 10.2. Curing Strains for Test Shaft 4

Figures 10.1 and 10.2 clearly show that extension occurred in the concrete as curing progressed. In S3, the extension was greatest near the bottom, where the support had been removed nine days after casting. The nine-foot level was not read between two days after casting and just prior to load testing because of a broken lead. The average indicated extension in S3 below ground at 54 days (one day prior to the first load test) was about 80 microinches per inch circuit strain (approximately 11 microinches per inch extension in the concrete).

The behavior of S4 parallelled that of S3, except that the indicated extensions were greater. At 147 days after casting (just prior to the first load test), the average indicated extension was about 270 microinches per inch circuit strain (approximately 37 microinches per inch extension in the concrete). The level of cells at the ground surface indicated extension, presumably because the area around the top of the shaft remained wet for much of the time. After the first load test was concluded, the strain-depth curve shifted toward compression, indicating that residual compressive stresses remained in the shaft after removal of the load.

From the standpoint of rates of extension, Figs. 10.3 and 10.4 were drawn to show average cell readings versus time for several typical levels in S3 and S4. Those figures indicate that most of the extension occurred in the first month after casting.

Extension strains in the concrete are not surprising. Neville (1963) states that "cement paste or concrete cured continuously in water from the time of casting exhibits a net increase in volume and an increase in weight ...due to the absorption of water by the cement gel." He further states that concrete cured continuously under water can exhibit extension strains

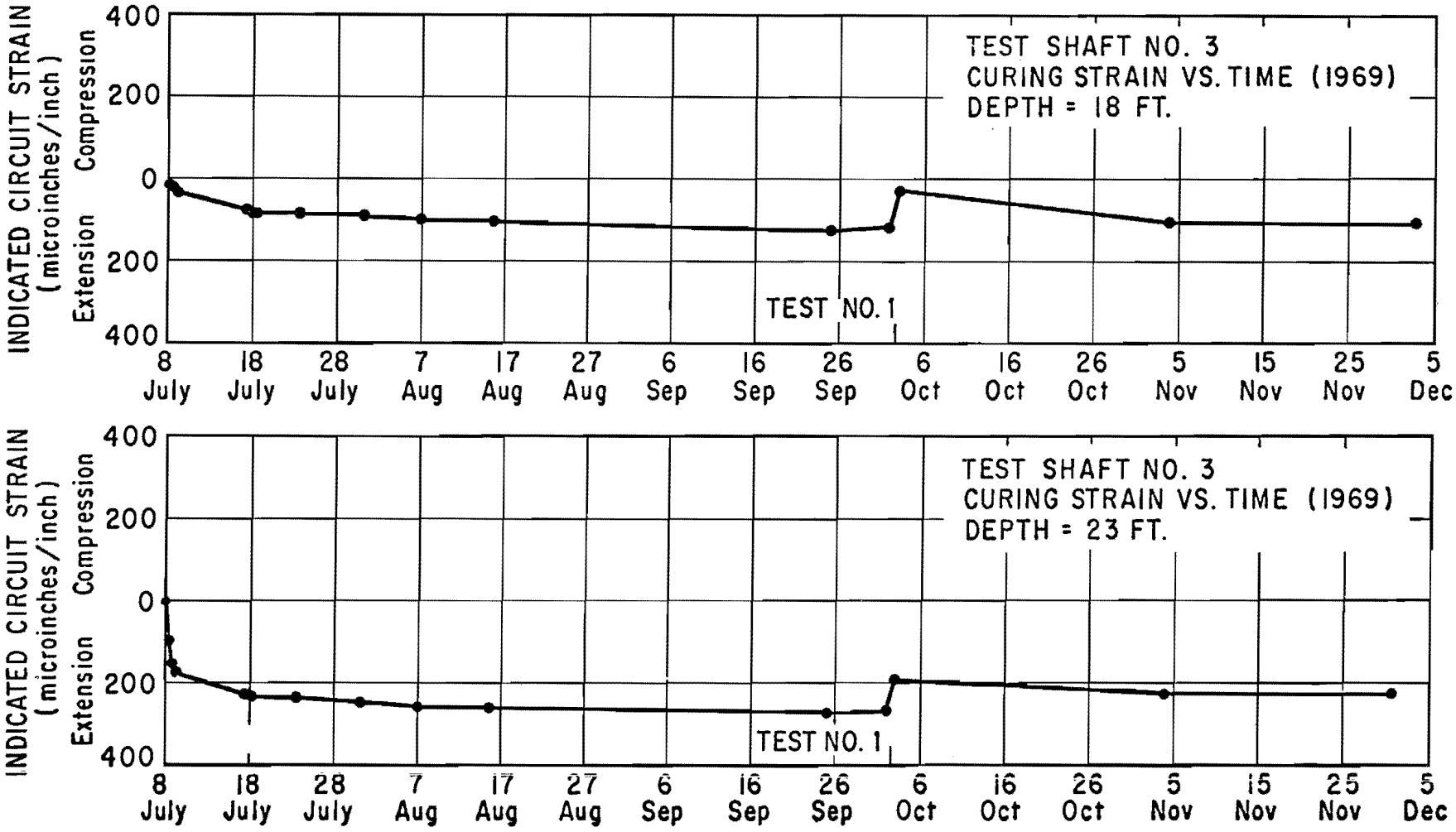

Fig. 10.3. Curing Strain Versus Time - Test Shaft 3

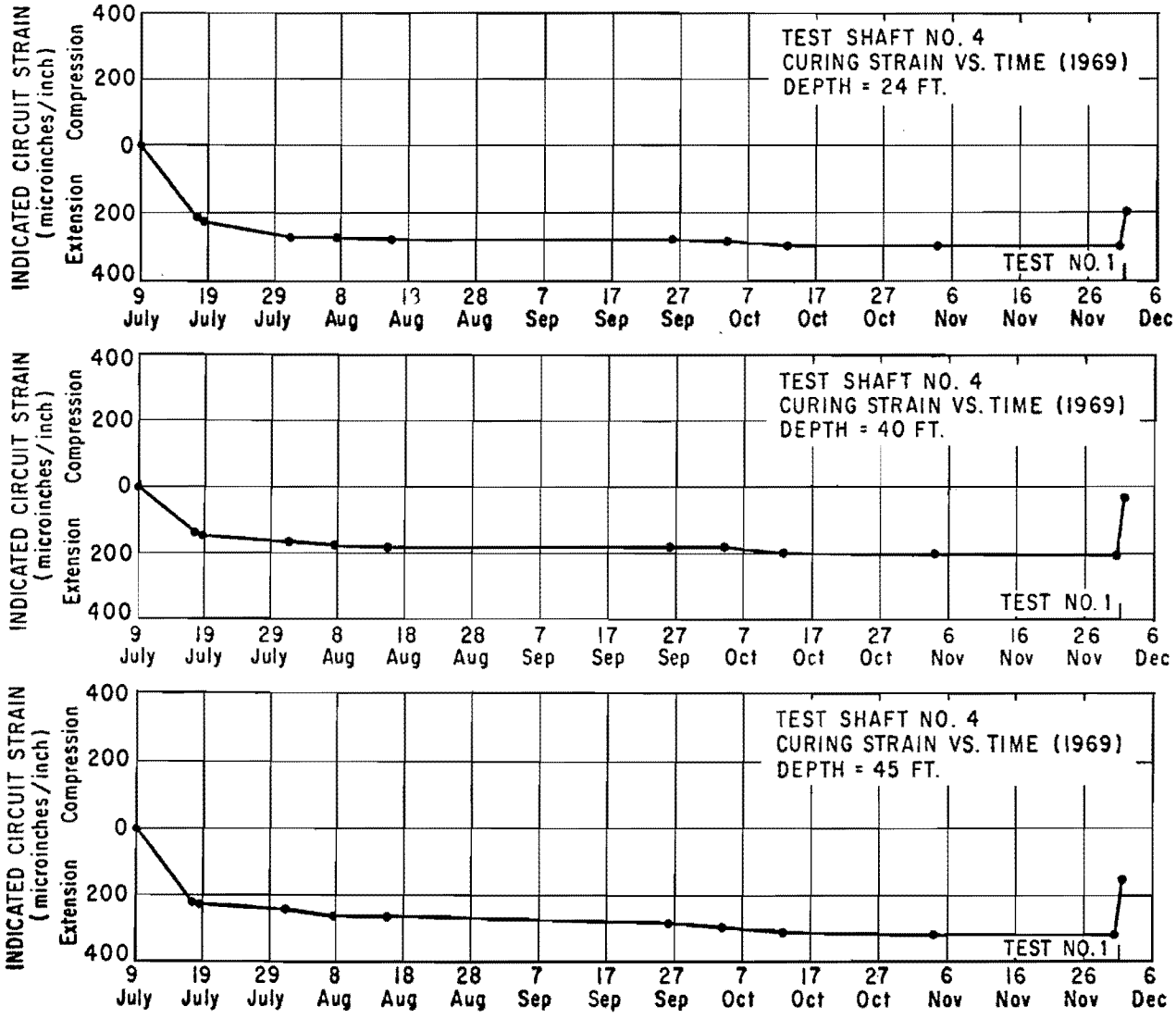

Fig. 10.4. Curing Strain Versus Time - Test Shaft 4

of 100 to 150 microinches per inch. Apparently, curing the concrete composing the drilled shafts in moist soil, with a portion of the shafts extending below the static water table, causes much the same phenomenon to occur. The extension was greater in S4, presumably because the shaft penetrated Layer II, which gave it access to essentially free water. Furthermore, pockets of trapped drilling fluid could have provided an additional water source for charging the concrete.

The extension strains were measured in the vertical direction, which was the direction of alignment for the Mustran cells. It is assumed that extension curing strains of the same magnitude existed in the horizontal direction. The consequence of this fact is that the concrete in the shafts expanded laterally very slightly against the soil. The average indicated concrete strain in the two shafts, S3 and S4, was about 25 microinches per inch. Hence, the increase in diameter in a 30-inch shaft would be slightly less than one-thousandth of an inch. The lateral expansion is too small to cause significant consolidation of the clay around the concrete, but it may be sufficient to enhance the bond somewhat between the soil and the concrete.

The electrical drift in the Mustran cells was quite minimal. Stability readings taken under conditions of continuous powering prior to each test revealed that no drift corrections needed to be applied to cell outputs for tests of a few hours duration, where the test shaft was shielded from direct sunlight. Barker and Reese (1970) report results of continuous strain indicator monitoring of Mustran cells in the test shaft at the HB&T test site. The top level of cells indicated a maximum difference in apparent circuit strain of about 75 microinches per inch in a 24-hour period, with a 20-degree temperature variation. This apparent circuit strain

translates into a concrete strain difference of about 10 microinches per inch and an apparent load of about 28 tons for that shaft. The concrete strains were thermally induced by the action of the sun's rays striking the concrete directly and were not false indications caused by electrical problems. Those studies show that thermal strains in the concrete must be considered in a test requiring more than a few hours to complete. They also indicate that no-load readings can be expected to vary in the top few feet of the shaft with time of day of reading. The readings represented in Figs. 10.1 and 10.2 were taken under different atmospheric conditions. Therefore, the variations in the top one or two levels of cells reflect somewhat random concrete thermal strains.

The nitrogen pressure remained on the Mustran system in S1 through S4 for the first six, five, four, and five months after casting, respectively. The ground resistance of all cells was acceptable at the time pressure was removed. After respective total elapsed times of 12 and 15 months after casting, the ground resistance of cells in S1 and S2 dropped to values ranging from a few thousand ohms to 500 megohms. Seven of the eight cells in S1 registered acceptable ground resistance at the end of that time, while none of the cells in S2 were acceptable. However, the cells in S3 and S4 showed no signs of deterioration nine months after installation.

Performance of Embedment Gages

Embedment gage output was generally erratic during curing, except for the improved circuit installed in S3. Typical results obtained during curing are given in Table 10.1.

The embedment gage circuits experienced considerable drift when continuously powered and read with a digital voltmeter. One circuit was tested by continuously powering the circuit with six volts regulated

TABLE 10.1. NO-LOAD DATA, REPRESENTATIVE EMBEDMENT GAGE CIRCUITS

Shaft No.	Circuit No. and Nominal Depth	Date/Time	Strain Indicator Reading * (microinches/inch)	Resistance to Ground (megohms)	Remarks
1	E-0-2 (0')	27 Jun 68 / 1300	+0222	>1000	Cage in hole before pour
		27 Jun 68 / 1830	+1463	>1000	4 hours after pour
		28 Jun 68 / 1430	+1476	>1000	
		5 Jul 68 / 1330	-0219	>1000	
		15 Jul 68 / 1415	+0271	>1000	
		7 Aug 68 / 0900	+0666	>1000	
	E-17-1 (17')	27 Jun 68 / 1300	+0428	>1000	Cage in hole before pour
		27 Jun 68 / 1830	+1167	>1000	4 hours after pour
		28 Jun 68 / 1430	+1449	>1000	
		5 Jul 68 / 1330	+0474	>1000	
		15 Jul 68 / 1415	+0391	>1000	
		7 Aug 68 / 0900	+0974	>1000	
2	E-0-1 (0')	7 Jan 69 / 0900	-1094	7000	18 hours after pour
		14 Jan 69 / 1000	-2742	5000	
		4 Feb 69 / 1030	-2295	5000	
		25 Feb 69 / 1300	-1342	4000	
		4 Mar 69 / 0730	-2188	8000	Just prior to S2T1
	E-14-2 (14')	7 Jan 69 / 0900	-1552	500	18 hours after pour
		14 Jan 69 / 1000	-0858	500	
		4 Feb 69 / 1030	+0120	500	
		25 Feb 69 / 1300	+0864	700	
		4 Mar 69 / 0730	+1012	600	Just prior to S2T1
3	Improved Tee Design (2')	17 Jul 69 / 1200	-2421	1000	8 days after pour
		31 Jul 69 / 1730	-2354	5000	
		1 Aug 69 / 0700	-2355	5000	
		1 Aug 69 / 1200	-2356	5000	
		7 Aug 69 / 1200	-2389	1000	
		25 Sep 69 / 1200	-2486	3000	
		2 Oct 69 / 1630	-2467	3000	Just prior to S3T1L1

* Compression indicated by algebraically increasing reading.

direct current in the laboratory before installation. Considerable electrical zero drift was evidenced in this test, which was conducted under essentially constant ambient temperature. The bridge was initially balanced, but once it became unbalanced, it was allowed to remain so throughout the several days of the test. This is the procedure followed during load testing when data are acquired using the automatic data logging system described in Chapter XI. Results of the test are tabulated in Table 10.2. A cyclic variation in output was observed, generally following a diurnal pattern. The drift was significant during the first few hours of powering. A general increasing trend in output voltage was evident over the several days of the test.

As mentioned previously, the zero drift was apparently induced by temperature changes in the gages, which were brought about by the presence of an electrical current. The two uncast dummies evidently dissipated heat at a different rate than the two active arms cast in mortar blocks, producing drift and differential resistance changes in the various gages. The magnitude of the current was thereby changed, which, in turn, changed the drift. This process is evidently self-correcting after a period of time, since cyclic reversals were observed. "On-off" reading caused an improvement in drift characteristics.

Similar drift was observed in gages embedded in S1 and S2 during pretest no-load monitoring. Typical drift readings, obtained during continuous powering (6 volts d.c.) are shown for two pairs of bridges in S1 in Fig. 10.5. (Also see Barker and Reese, 1969.) The apparent load (calculated by multiplying the strain corresponding to the output times the product of the concrete modulus and the transformed area of the shaft) is also shown.

TABLE 10.2. LABORATORY DRIFT READINGS FOR CONTINUOUSLY-POWERED EMBEDMENT GAGE BRIDGE (E-17-2, S1)

Date	Time	Bridge Output (microvolts)*	Apparent Circuit Strain (microinches/inch)
16 Apr 68	2003	1270	200
	2006	1620	255
	2026	2020	318
	2100	2340	368
	2130	2390	374
	2145	2400	378
17 Apr 68	0816	2450	386
	0930	2440	384
	1405	2520	397
	1740	2510	395
18 Apr 68	0815	2300	362
	1015	2530	399
	1315	2520	397
	1430	2550	403
	1650	2540	401
	1805	2520	397
	1900	2490	392
	2005	2460	387
	2100	2450	386
	2220	2440	384
19 Apr 68	0800	2390	374
	0915	2430	382
	1020	2490	392
	1100	2500	394
	1315	2450	386
	1500	2440	384
	1600	2440	384
20 Apr 68	1300	2640	416
22 Apr 68	0835	2555	403
	0940	2585	407
	1040	2620	413
	1310	2590	407
	1535	2620	412
	2150	2700	425
23 Apr 68	0830	2680	422
	1340	2730	430
	1640	2750	433
	1740	2730	430
24 Apr 68	0900	2850	448
	1115	2820	444
	1155	2790	439
	1310	2815	443
	1425	2755	433
	1615	2760	434
25 Apr 68	0830	2730	430
	1120	2805	441
	1415	2795	440
	1520	2790	439

*Power applied equals 6 volts. Temperature constant at 75°F throughout test.

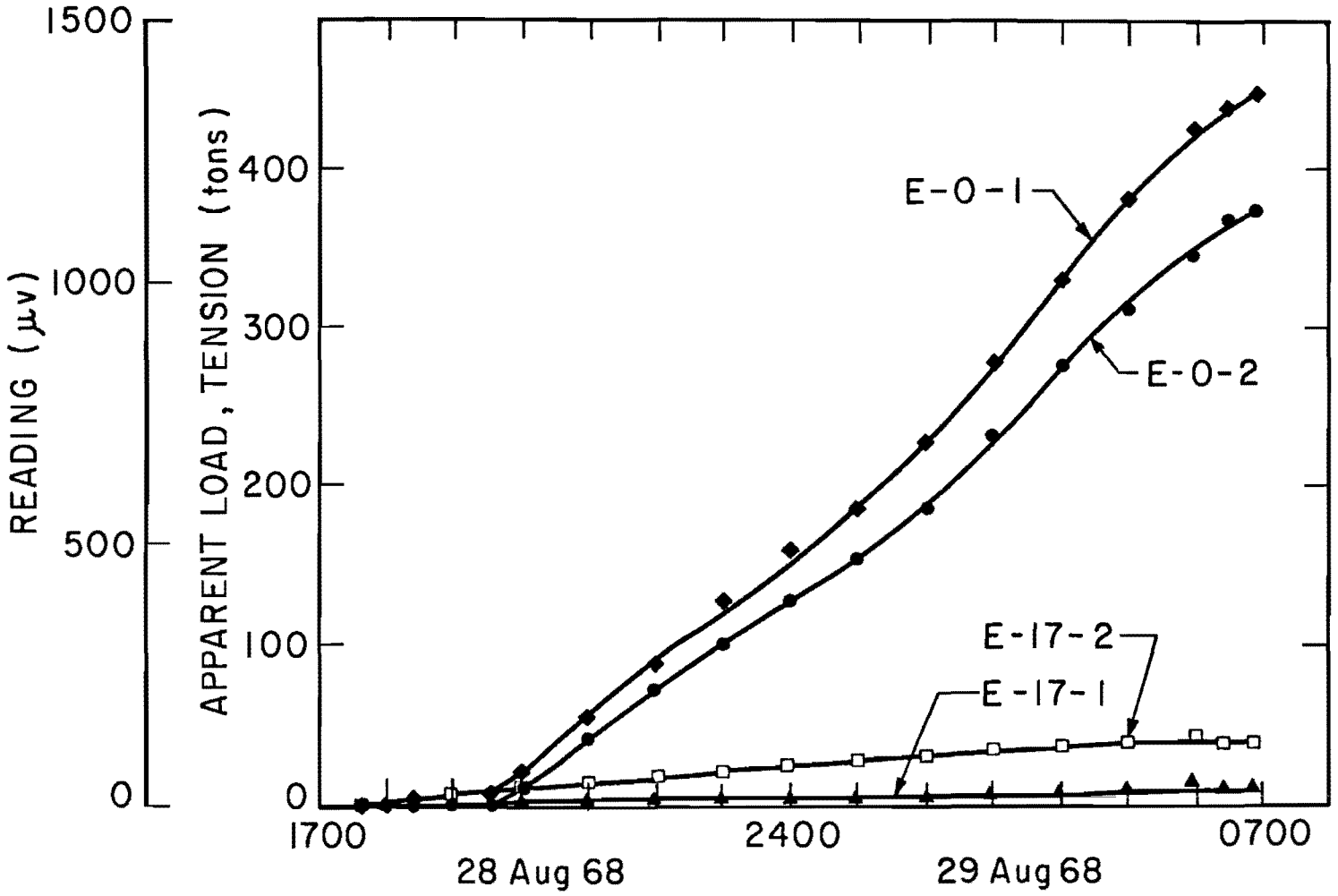

Fig. 10.5. Drift Readings for Four Embedment Gage Bridges, Test Shaft 1, Test No. 1

The greatest embedment circuit drift in both S1 and S2 occurred in the circuits at the top, presumably due to thermal strains in the concrete and to an effect similar to that observed in the laboratory. The zero drift was large enough that drift corrections had to be made to the test readings before the embedment gage data were reduced. This was done by assuming each circuit drifted during the load test at the same rate at which it was drifting just prior to the beginning of the test. Each test on S1 and S2 lasted one to two hours, so the drift correction was significant. Apparent drift after test termination may be due to stress changes in the concrete; therefore, post-test drift cannot be obtained reliably.

The top levels, at which the greatest drift occurred, unfortunately, are the calibration levels. Inaccurate drift corrections for the calibration circuits cause indicated loads to be incorrect at all other embedment gage levels, using the load distribution determination procedure described earlier. The method of correcting for drift apparently was reasonably valid, however, since concrete modulus values calculated from drift corrected embedment gage results at the calibration level and the applied concrete stress agreed closely with values measured or computed from cylinder tests on samples of concrete taken from the batches used to construct the shafts.

Bridges E-0-1, E-13-2, E-19-2, and both E-22.5 circuits showed unacceptable ground resistance before the first load test on S1. The test results from these gages were excluded from consideration in the final load test data reduction (as was E-19-1, which drifted excessively). Reiterating, five of the original twelve embedment gage circuits showed acceptable ground resistance one year after casting.

All bridges in S2 and S3 registered acceptable ground resistance before the initial load test. Five of the six circuits in S2 showed acceptable ground resistance after 15 months in place. The single circuit in S3 was registering a high ground resistance after nine months.

Strain Rods

No-load readings were taken over a 24-hour period on the telltales in S2 five months after the shaft was cast. Air and concrete temperatures (as indicated by embedded thermocouples) were also obtained at the same time telltales were read. A condensation of results is given in Table 10.3. As stated in Chapter IX, thermal drift of the magnitudes tabulated in Table 10.3 produces only minor false indications of load during a test, especially in the longer rods.

It is interesting to observe that rising temperature produced an indicated relative concrete extension in TT8W, which suggests that, for this rod, thermal strains in the indicator mount were more significant than the difference in thermal strain between the steel rod and concrete shaft. This trend was observed in five of the eight telltales monitored, while two others showed the opposite effect (indicated relative telltale extension), and one remained essentially unchanged.

Bottomhole Load Cell

The bottomhole load cell registered an initial vertical compression of 19 psi due to the weight of the wet concrete on the cell immediately after S1 was cast. This value corresponds closely to that computed from the ACI formwork expression for lateral stresses against the borehole wall at that level (American Concrete Institute, 1963). Further readings during curing

TABLE 10.3. TELLTALE DRIFTS AND THERMOCOUPLE READINGS, S2

Time/Date	Temperature (Degrees F)*				Telltale Readings (Inches)**							
	Air	0'	10'	20'	TT8E	TT8W	TT14E	TT14W	TT20E	TT20W	TT26E	TT26W
2025/17 Jun 69	85	88	73	74	.0153	.0250	.1747	.0092	.0405	.0099	.1102	.0340
0730/18 Jun 69	74	78	71	71	.0157	.0268	.1770	.0102	.0426	.0122	.1120	.0346
0900/18 Jun 69	80	79	71	72	.0156	.0265	.1771	.0105	.0427	.0123	.1122	.0347
1100/18 Jun 69	86	80	70	72	.0156	.0264	.1771	.0106	.0428	.0123	.1122	.0346
1300/18 Jun 69	89	82	71	72	.0155	.0264	.1771	.0100	.0427	.0115	.1122	.0346
1400/18 Jun 69	91	83	70	72	.0156	.0264	.1770	.0100	.0427	.0115	.1122	.0345
1700/18 Jun 69	96	86	72	73	----	----	----	----	----	----	----	----

* As read from thermocouples in air or embedded at indicated depth in shaft.

** Direct dial indicator readings, initial settings arbitrary.
Telltale nomenclature: "TT"--telltale designator;
"8"--length of telltale (equals nominal depth plus 4');
"E"--location of telltale, grid East (E), or grid West (W).

were somewhat erratic because of the leak which developed during placement. As curing progressed, the indicated vertical stress tended to decrease with time (Barker and Reese, 1969). Two days after casting, the indicated stress was only about 7 psi.

Thermocouples

Long-term temperature variations as registered by the thermocouples are given in Tables 10.4 through 10.6. Hydration temperatures as high as 109 degrees were measured in the bell of S2. The curing temperatures were generally greater with depth except in S1, where they were somewhat lower at the 21.5 foot level. This fact is possibly due to the presence of extraneous water in the borehole in S1, which may have diluted the mix, and the presence of the steel load cell, which may have acted as a heat sink. Typical 24-hour variations in temperature in S2 five months after casting have been shown in Table 10.3.

TABLE 10.4. THERMOCOUPLE READINGS DURING CURING, S1

Time After Casting*	Temperature from Thermocouples (Degrees F) Air	Shaft 2' Depth	Shaft 5' Depth	Shaft 21.5' Depth
2 Hours	90	100	100	89
4 Hours	83	105	106	92
1 Day	95	105	103	95
6 Days	90	93	93	94
19 Days	90	80	79	77

*S1 cast June 27, 1968.

TABLE 10.5. THERMOCOUPLE READINGS DURING CURING, S2

Time After Casting*	Temperature from Thermocouples (Degrees F) Air	Shaft 0' Depth	Shaft 10' Depth	Shaft 20' Depth (in Bell)
1 Day	55	87	92	109
8 Days	59	57	78	87
50 Days	68	59	63	73
57 Days	55	49	51	72
162 Days	85	88	73	74

*S2 cast January 6, 1969.

TABLE 10.6. THERMOCOUPLE READINGS DURING CURING, S4

Time After Casting*	Temperature from Thermocouples (Degrees F) Air	Shaft 0' Depth	Shaft 10' Depth	Shaft 20' Depth
2 Hours	99	113	106	106
78 Days	94	74	75	72
148 Days	63	59	71	71

*S4 cast July 9, 1969.